UNIVERSITY OF BRISTOL

DEPARTMENT OF
AEROSPACE ENGINEERING

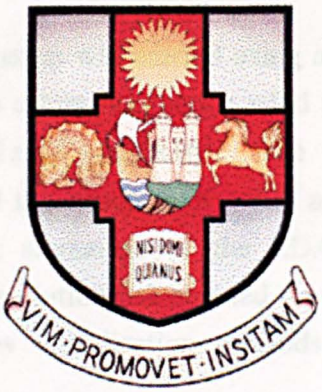

The Thin Aerofoil Leading Edge Separation Bubble

Matthew John Crompton B.Eng. (Hons)

A thesis submitted to the University of Bristol in accordance with the requirements of the degree of Doctor of Philosophy in the Faculty of Engineering

June 2001

ABSTRACT

An investigation into the separation bubble formed behind a sharp leading edge has been undertaken. Commonly found on thin sections, such as flexible sail sections and turbomachine blades, the thin aerofoil bubble generally leads to poor aerodynamic performance. To improve performance, there is a desire to minimise the bubble, but at present the understanding of such bubbles is incomplete. Computational methods are increasingly being used to model such flows and therefore accurate experimental data is required to supplement the development of the models.

The main experimental investigation was carried using a two-dimensional flat plate with sharp leading edge, mounted in a low turbulence wind tunnel, over a Reynolds number range, based on chord, of $0.1 \times 10^5 - 5.5 \times 10^5$. The application of a laser Doppler anemometer (LDA) has enabled the structure of a thin aerofoil bubble to be investigated in detail and taking particular advantage of the LDA's directional sensitivity, non-intrusiveness and high spatial resolution has enabled previously unexplored flow features to be detailed. Enhanced flow visualisation methods were used to complement the numerical results.

The thin aerofoil bubble is characterised by separation from a sharp leading edge followed by rapid transition of the shear layer and delayed reattachment (the bubble length increasing with incidence). The high rate of entrainment of the shear layer drives a recirculating region, which bends the shear layer towards the surface. The reverse flow boundary layer in the bubble exhibited signs of periodic stabilisation before separating close to the leading edge, forming a previously undiscovered secondary separation bubble rotating in the opposite direction to the primary separation bubble. The length of the primary separation bubble was found to be proportional to the square of the plate incidence, once corrections are made for the effects of tunnel constraint. There is also a small variation with Reynolds number because of its influence on the rate of entrainment and growth of the shear layer. Above about 10^5, this Reynolds number effect was no longer evident. Different length bubbles, formed by a change of incidence, have been shown to be similar to one another, with respect to their shape, the static pressure distribution and intermittency of the reverse flow region. The LDA derived velocity profiles, have enabled an inviscid computational model of the thin aerofoil bubble to be applied which successfully predicts the static pressure distribution.

As well as shedding new light on the mechanisms involved in bubble development and behaviour, this research provides a well defined set of test cases to aid the development of computational models.

I dedicate this thesis to

Mum and Henry

ACKNOWLEDGEMENTS

I would like to thank Dr Rod Barrett for his considerable advice, support and guidance whilst acting as Adviser on this research. His support has now extended through my undergraduate and postgraduate years and I wish him well for the future. I would also like to thank all members of the Aerospace Engineering Department Academic and Support Staff whose assistance was very much appreciated. My thanks also go to Dr Chris Allen for his help with the computational aspect of this research.

Special thanks go to Dr Chris Swales for his early assistance in mastering LDA techniques and recent support through the completion of this work.

Thanks also go to the Alan Bishop and all the workshop staff for fabricating the test rig and for their continuous good humour.

Finally I am indebted to Mum and Henry for their continual support and encouragement.

AUTHOR'S DECLARATION

The work presented herein was carried out solely by the author, under the supervision of Dr R. V. Barrett, in the Department of Aerospace Engineering at the University of Bristol, in partial fulfilment of the requirements for the degree of Doctor of Philosophy.

The ideas and results are original except where otherwise acknowledged or referenced, and no part of this work has been submitted previously to any university, college or other institute for examination either in the United Kingdom or overseas.

Note that the views expressed in this dissertation are those of the author and are not necessarily those of the University of Bristol.

Signed: M. J. Crompton

Date: 30/6/01

PERMISSION TO COPY

M. J. Crompton

"The Thin Aerofoil Leading Edge Separation Bubble"

Advisor: Dr. R. V. Barrett

Department of Aerospace Engineering,
University of Bristol.

I, the undersigned, am willing that this thesis should be made available for consultation in Bristiol University Library, for inter-lending, for use in another library or for photocopy in part or in full - at the discretion of the Librarian - on the understanding that the users are made aware of their obligations under copyright.

Signed: M. J. Crompton

Date: 30/6/01

TABLE OF CONTENTS

LIST OF FIGURES

LIST OF TABLES

NOMENCLATURE AND ABBREVIATIONS

Nomenclature

c	Chord Length
C_f	Skin Friction Coefficient
C_L	Lift Coefficient
C_P	Pressure Coefficient = $\frac{p - p_\infty}{1/2 \rho U_\infty^2}$
f_b	Beat Frequency
H	Shape Factor
l	Characteristic Length
p	Static Pressure
Re	Reynolds Number
Re_c	Reynolds Number based on Chord Length
Re_{δ^*}	Reynolds Number based on Displacement Thickness
Re_θ	Reynolds Number based on Momentum Thickness
S	Plate Span
u	Local Chordwise Fluid Velocity
U_∞	Freestream Fluid Velocity
U_{max}	Maximum local Chordwise Velocity
u_{rms}	Root Mean Square Component of Chordwise Fluid Velocity
v	Local Spanwise Fluid Velocity
w	Local Fluid Velocity Perpendicular to Surface
x	Chordwise Distance from Leading Edge
x_R	Separation Bubble Length (Reattachment Length)
y	Spanwise Distance
z	Distance Perpendicular to Surface

α	Angle of Incidence
δ	Boundary Layer Thickness
δ^*	Displacement Thickness
λ	Wavelength of Coherent Light
μ	Dynamic Viscosity
ν	Kinematic Viscosity
π	Pi
θ	Momentum Thickness
ϕ	Beam Separation Angle
ρ	Density
σ	Pressure Recovery Factor

Indices

∞	Freestream Conditions
R	Reattachment
S	Separation

Abbreviations

APG	**Adverse Pressure Gradient**
BSA	**Burst Spectrum Analyser**
CFD	**Computational Fluid Dynamics**
DNS	**Direct Numerical Simulation**
LES	**Large Eddy Simulation**
LDA	**Laser Doppler Anemometer**
O-K	**Owen-Klanfer**
RANS	**Reynolds-Averaged Navier-Stokes**
rms	**root mean square**

CHAPTER 1
INTRODUCTION

This research details a study of the thin aerofoil type separation bubble formed behind the sharp leading edge of a flat plate at incidence. The main objectives are to further the understanding of the thin aerofoil separation bubble which was seen as being incomplete from previous work. A physical and quantitative description of the two-dimensional bubble is required to clarify the mechanisms associated with the process of bubble development and behaviour to a change of variables including incidence, Reynolds number and chord length. Accurate experimental data, particularly velocity and pressure measurements are required to help support in the development of computational methods.

A separation bubble may occur on the rounded surfaces of conventional aerofoils and also, in a different form, off the sharp leading edges of thin aerofoils and membranes. Most previous research has concentrated on the short separation bubble which occurs in the former case. This type of bubble is characterised by laminar separation followed by rapid transition and reattachment and is typically 1-2% chord in length. Under normal conditions such a bubble occurs near the leading edge but at certain regimes it may be situated well aft on the aerofoil. The presence of this bubble will inevitably influence aerofoil performance, leading to increased drag and, on bursting of the bubble premature stall. In certain circumstances this burst bubble will reattach further along the aerofoil, taking on the long bubble form which is the subject of this thesis.

More typically, a long bubble forms as a result of separation on thin aerofoils at a sharp leading edge and this will be referred to as a "thin aerofoil bubble", a term introduced by Gault (1957). This type of bubble has traditionally received less attention than the short bubble, though since the 1950s interest has grown due to the move towards higher aircraft speeds and the consequent need for thin aerofoils to reduce compressibility effects. Interest was heightened further by

developments in turbomachinery towards thinner, more efficient, blading and by the increasing drive to understand the characteristics of thin flexible aerofoils in sailing and in low Reynolds number aviation activities. The separation bubble from a sharp or small radius leading edge is characterised by both a fixed separation process, resulting from the unsustainable pressure gradient at the leading edge, and delayed reattachment (the bubble length increasing with incidence). The nature of the bubble bears closer relation to the separation behind steps, fences and similar obstacles than to the short laminar separation bubble on a rounded aerofoil. This is in line with the findings of Castro & Haque (1987) who argued that for a wide range of complex turbulent flows, in which an extensive recirculation region is bounded by a shear layer, the general features are likely to be similar.

In general, the short bubble only has a small effect on the external potential flow whereas the thin aerofoil bubble (or long bubble) completely alters the overall pressure distribution around the aerofoil.

Although a separation bubble is generally to be avoided, resulting as it does in aerofoil inefficiency, it can in some situations be advantageous. At low Reynolds number the presence of the bubble can delay stall as it induces a turbulent reattached boundary layer which is resistant to separation. The same effect can be obtained by inducing transition without separation, for example with the use of turbulators to reduce drag.

Computational fluid dynamics (CFD) methods have become widespread in the aerospace industry. With rapid increases in processing speed, numerical methods to solve the Euler and Navier-Stokes equations have become practical design tools, both for design and performance evaluation. Some prediction methods require the entire flow domain to be meshed. For example, Direct Numerical Simulation (DNS) methods resolve the entire spectrum of scales and provide results equivalent to experimental data, but are generally limited by the high demands on processing power. Turbulence modelling methods such as

Large Eddy Simulation (LES), which resolves large eddies and models smaller ones, and Reynolds-Averaged Navier-Stokes (RANS) equations, which requires modelling of scales that are averaged out, are all limited by their requirement to simulate or model some scale of turbulence and are unable to predict transition. Alternative methods which do not explicitly capture the boundary layer variation on a computational mesh include viscous-inviscid coupling, where the inviscid flow is first calculated and the results used as a starting point for viscous boundary layer calculations. These methods are limited by the accurate model required for the inviscid calculation and the difficulty in modelling boundary layers. However, it is only recently that the experiments of the 1950s and 1960s have been complemented with data from computational modelling.

One example is the development of turbomachine blades where the flow around the leading edge region is critical in determining the stalling behaviour of the blade. At high altitudes and low flight speeds, the Reynolds number of the flow through the inlet stages of a compressor becomes so low that its performance is often impaired (Johnsen & Bullock 1965). The very thin profiles and small leading edge curvature, typical of these blades, can lead to the formation of both short and long separation bubbles. Although correlation between the CFD and experimental results is generally good for the case of the short bubble, it is not uncommon for the efficiency to be 1-2% in error, hence justifying the continued use of experimental testing (Walraevens & Cumpsty 1993). Furthermore, when considering the effects of increasing incidence, the viscous-inviscid model, proposed by Calvert (1994), does not take proper account of the comparatively thick turbulent boundary layer that exists downstream of the separation bubble. Improving the modelling and understanding the characteristics of separation bubbles is therefore of paramount importance if overall blade efficiency is to be increased.

For the case of modelling the thin aerofoil bubble, the problem is compounded by the increased size of the separated viscous region and the steep velocity and pressure gradients close to the leading edge. Computational models are either

limited by computing power or the empirical constants required for many modelling techniques. Schmidt & Mueller (1989) commented that in order to achieve satisfactory modelling of the separation bubble, the boundary layer characteristics must be accurately determined.

Flow around flexible membranes (sails) is of interest because the thin geometry leaves the membrane susceptible to separation at both the leading and trailing edges. The problem is complicated by the membrane changing shape under load and an equilibrium therefore exists between the shape of the membrane and the pressure distribution on the surface. Jackson (1983) developed a simple sail model to predict the membrane shape and showed that the results are only representative if the camber and incidence are assumed to be small i.e. any effect of separation is negligible. However, modelling the separation that may occur either at the leading edge or trailing edge or both requires a fully-coupled viscous-inviscid model. In a continuing study, Jackson & Fiddes (1995) stated that experimental data from rigid thin sections is required for thorough evaluation of such models.

The predominant reason for there being so few detailed studies of thin aerofoil bubbles has been a lack of instrumentation capable of measuring within a recirculating flow, the previous methods used being both intrusive to the flow and directionally ambiguous. For example, a pitot-static probe must be aligned in the direction of the flow to record accurate measurements and a single hot-wire probe is unable to determine flow direction; both these instruments therefore produce misleading results in a recirculating region. In addition, recirculating flow will, at some stage, be affected by the physical presence of the probe and probe holder and even the hot-wire itself has been shown to affect the location of boundary layer separation (Nash 1996). The difficulties in measuring within recirculating regions and the ensuing risk of significant measurement uncertainties has led to most effort being traditionally directed towards regions where the flow is relaxing following reattachment. With modern instrumentation

such as laser Doppler anemometry, the possibilities for measuring within separation bubbles have opened up.

The investigation described within this thesis considers the most basic case of the leading edge bubble, i.e. that formed over a two-dimensional thin flat plate at incidence with a sharp leading edge in incompressible flow. Imposing two-dimensionality is, of course, intended to reduce the complexity without losing the essential features of the separation bubble. As well as providing detailed velocity data, the objective was to gain further understanding of the flow phenomena which from previous work was seen to be not completely understood. Laser Doppler anemometry was employed, thereby eliminating the problems of directional ambiguity and probe interference that had previously been a limitation when measuring in the separation bubble. With the laser Doppler anemometer (LDA), detailed measurements of mean and fluctuating components of velocity were obtained within, and downstream of, the bubble. The LDA's high spatial resolution and small measurement volume enabled for the first time, the steep velocity gradients and intricate flow details contained within the bubble to be fully defined.

From the results of this extensive investigation and from applying some conclusions from similar work, previously performed, has enabled a detailed analysis of the thin aerofoil bubble to be formed. This has shed new light on the mechanisms associated with the process of bubble development and behaviour to a change of variables including incidence, Reynolds number and chord length. The results also reveal previously unexplored flow features and provide data which is of value in the development and validation of numerical simulations for thin aerofoil bubbles. The illustrative data provides explanations of the flow phenomena encountered and clarifies the mechanisms controlling the separation bubble, whilst further ascertaining the differences between the thin aerofoil bubble and the short separation bubble.

The velocity data is used to create a solid surface to represent the thin aerofoil bubble and the predicted pressures from the inviscid solution show excellent agreement with the experimental data.

It is proposed that future work should investigate a three-dimensional thin aerofoil bubble. This would more closely represent real flow situations, for example a yacht sail which has sweep and varying curvature. Therefore, an introductory study into the effects of sweep was undertaken to provide a qualitative description of how the thin aerofoil bubble structure changes as sweep and incidence are increased for the flat plate test case.

CHAPTER 2
LITERATURE REVIEW AND BACKGROUND

2.1 Introduction

The objectives of this research were to provide further insight into the flow phenomena associated with separation bubbles and velocity and surface pressure data for the development of numerical models. This chapter presents a review of previous investigations, outlining the most important findings and detailing the relevant background information most pertinent to the subject of this thesis. Although there are very few investigations which examine the subject of the separation bubble formed behind the sharp leading edge of a flat plate at incidence specifically, there are many which relate to aspects of separation, transition and reattachment both in short bubbles and flows containing a separated turbulent shear layer. An understanding of these related flow situations is therefore essential for the development of this subject. Alving & Fernholz (1996) make a distinction between separation caused by sharp changes in surface geometry, referred to as geometry-induced separation, and separation from smooth surfaces caused by adverse pressure gradients, denoted adverse-pressure-gradient-induced separation (APG-induced separation). The initial part of the chapter covers the more general background, the review of related research then follows. The chapter concludes by outlining the main objectives of the current investigation determined from the literature review.

2.2 Boundary Layers

2.2.1 Introduction to Flow Parameters

A large component of this research is based on the interaction of boundary layers, both attached and separated, with the solid surface of an aerofoil. In order to explain the similarities and propose mechanisms for the development and behaviour of all separated flows, it is first necessary to include a brief description of attached boundary layer theory.

Consider a real flow past a slender body, then in all regions except those close to the body surface, the effects of viscosity are negligible. However, in the so called "boundary layers" between the freestream and the body surface viscous actions predominate. Prandtl (1904) first conceived the idea of the boundary layer and stated that a no-slip condition must exist at the boundary between the solid and fluid. Therefore, the relative velocity of fluid tangential to the surface is everywhere zero. He also stated that the velocity parallel to the surface must vary continuously from zero at the body to that of freestream velocity away from the body. The edge of the boundary layer is difficult to define as the velocity approaches freestream asymptotically, however commonly the distance from the surface at which the velocity reaches 99% of the main stream velocity is used. Since the freestream velocity at a small distance from the surface may be considerable, it is evident that appreciable shearing velocity gradients may exist in the boundary layer. The fluids internal resistance to the shearing velocity is known as the viscosity and this causes the boundary layer. For a body moving through a fluid, the shearing stresses at the surface give rise to a "skin friction" drag force, one of the various types of drag which act upon the body.

Prandtl pointed out that the boundary layers are usually very thin and can, as a first approximation, be ignored for the purpose of calculating the pressure produced around the body. For aerofoil shapes, the pressure field is only slightly modified by the presence of the boundary layer and since almost all the lifting

force is produced by normal pressures at the aerofoil surface, it is possible to develop theories to determine the lift force by consideration of the flow outside of the boundary layers, where the flow behaviour is essentially inviscid. This simplification, ensuring that equations of viscous motion need only be considered in the limited regions of the boundary layer led to the advance in aerodynamic theory in the first half of the twentieth century.

The boundary layer which forms on an infinitely wide flat plate with zero pressure gradient (no acceleration in the streamwise direction) is one of the simplest to analyse as it may be considered two-dimensional, with fluid only moving in a streamwise direction and perpendicular to the surface. Figure 2.1 shows a simplified diagram of a flat plate boundary layer, showing the main features which include the laminar, transitional and turbulent regions.

2.2.2 Laminar Boundary Layer

As described above, when the freestream flow initially meets a solid surface a boundary layer will be initiated due to the no-slip condition at the surface. As the fluid proceeds downstream, there will be more fluid entrained in the boundary layer and it will thicken.

Initially, the flow will be "laminar" with the layers of fluid sliding over one another, parallel to the surface, with little interchange of mass between the layers. In an ideal laminar flow, the velocity fluctuations at any given point are zero, although in practice there will be some small fluctuations in velocity. Blasius (1908) developed an analytical solution for laminar boundary layer flows over a flat plate with zero pressure gradient. Figure 2.2 shows a "Blasius" laminar boundary layer profile compared to that of a velocity profile in the turbulent region of the boundary layer.

The shear stress in a fluid due to viscosity is connected by Newton's Law; it is the product of the dynamic viscosity and the rate of shearing of the fluid (rate of change in velocity perpendicular to the flow direction). Therefore, the shear stress at the surface, τ_0, which is equal in magnitude, but of opposite sign, to the skin friction drag per unit area is given by

$$\tau_0 = \mu\left(\frac{\partial u}{\partial y}\right)_{y=0}$$

where μ is the dynamic viscosity of the fluid, u is the local fluid velocity parallel to the surface and y is the normal distance from the solid surface.

2.2.3 Turbulent Boundary Layer

As the laminar boundary layer continues to develop along the surface, small disturbances can grow in the flow. The disturbances arise from a variety of sources including freestream turbulence, sound waves, surface roughness and vibration. The stimuli create low amplitude waves in the boundary layer which move downstream and, depending on local conditions, will either grow or decay. If they grow, the whole boundary layer will become involved in the process, eventually forming eddies; the flow now being referred to as "turbulent". The region in which disturbances grow and turbulent flow is formed is called the transition region and is of limited extent.

In turbulent flow, a seemingly random motion of fluid exists with velocity fluctuations both along and perpendicular to the mean flow direction. As a result of the perpendicular velocity fluctuations, there is appreciable mass transport between the adjacent layers of fluid. If a mean velocity gradient exists, then there will be significant streamwise momentum transport between layers, resulting in shear stresses. These stresses are of much greater magnitude than

those caused by viscous actions alone and the shape of the velocity profile is controlled by these "Reynolds stresses" as they are termed. The turbulent boundary layer profile is much "fuller" with higher velocity being maintained much closer to the surface than for a comparable laminar boundary layer (Figure 2.2). The penalty for this high perpendicular momentum transfer is an increased rate of thickening of the boundary layer and a much higher skin-friction drag caused by the steeper velocity gradient at the surface. However, close to the surface, this velocity component must decrease to zero because of the impermeability boundary condition that exists there (i.e at the surface, there can be no velocity component perpendicular to it). This suppression of perpendicular motion close to the surface gives rise to a thin laminar region ($\approx$1% of the boundary layer thickness). In this region, the flow is similar to a laminar boundary layer with purely viscous forces generating shear. This region is called the "laminar sub-layer" and has an almost linear velocity gradient.

2.2.4 Physical Similarities of Fluid Flows

To allow quantitative comparison between two fluid flows under different conditions, e.g. a model in a wind tunnel and the real aircraft, the flows must be physically similar. Physical similarity is a general term covering several different types of similarity including, "dynamic" (a similarity of forces), "kinematic" (a similarity of motion) and "geometric" (a similarity of shape). For fluid flows, there are many potential causes of force in a system including viscosity, gravitational effects, pressure differences, surface tension and elasticity and so on.

For dynamic similarity, the magnitude ratio of any two of the forces must be the same at corresponding points of the two systems, but typically some forces do not apply or are negligible in magnitude and can be ignored. For most low speed wind tunnel testing involving boundary layer flows, only the viscous, pressure and inertia forces are important. Conventionally, the ratio of |Inertia force| to

|Net viscous force| are used and the non-dimensional parameter is termed Reynolds number, Re, as developed by Reynolds (1895).

$$\mathrm{Re} = \frac{|InertiaForce|}{|NetViscousForce|} \text{ is proportional to } \frac{\rho l^2 U_\infty^2}{\mu U_\infty l} = \frac{\rho U_\infty l}{\mu} = \frac{U_\infty l}{\upsilon}$$

where ρ is the density, U_∞ is the freestream velocity, l is the characteristic length (specific to each type of flow), μ is the dynamic viscosity and ν is the kinematic viscosity (μ/ρ).

Many other similarity conditions exist for different types of flow, e.g. Froude number (inertia/gravitational), Weber number (inertia/surface tension) and Mach number (inertia/elastic). Therefore, when testing scale models, provided both the geometric and dynamic similarity are met, the full scale flows will behave in an identical manner. In some cases it is not possible to match all the similarity conditions but to minimise inaccuracies in the testing, at least the most important must be matched. In the current research, the Reynolds number is used as the most important similarity criterion with the characteristic length, l, being defined as the plate chord length.

Assuming dynamic similarity exists, one important parameter which is comparable between investigations is the "coefficient of pressure", a non-dimensional aerodynamic pressure term. This is defined as:

$$C_P = \frac{p - p_\infty}{\frac{1}{2}\rho_\infty U_\infty^2}$$

where p is the static pressure at some point in the flow and p_∞ is the static pressure of the freestream. For incompressible flow, Cp can be expressed in terms of a velocity variation only. From Bernoulli's equation, assuming constant density,

$$p_\infty + \tfrac{1}{2}\rho U_\infty^2 = p + \tfrac{1}{2}\rho U^2$$

$$p - p_\infty = \tfrac{1}{2}\rho\left(U_\infty^2 - U^2\right)$$

substituting into the equation for Cp, gives

$$C_p = \frac{p - p_\infty}{\tfrac{1}{2}\rho_\infty U_\infty^2} = \frac{\tfrac{1}{2}\rho\left(U_\infty^2 - U^2\right)}{\tfrac{1}{2}\rho U_\infty^2}$$

or

$$C_p = 1 - \left(\frac{U}{U_\infty}\right)^2$$

Hence, the pressure coefficient at a stagnation point (where U=0) in an incompressible flow is always equal to 1.
It can also be seen that,

(i) If Cp is positive, $p>p_\infty$ and $U<U_\infty$

(ii) If Cp is zero, $p=p_\infty$ and $U=U_\infty$

(iii) If Cp is negative, $p<p_\infty$ and $U>U_\infty$

Assuming the boundary layer to be very thin, the streamlines on a scale of the boundary layer thickness are virtually parallel to the surface and it is therefore a good approximation that the static pressure is constant across the boundary layer. This assumption, for a known static pressure at the surface, enables the velocity of the flow at the edge of the boundary layer to be calculated. The validity of this assumption across a separated region, will be covered in more detail later.

2.2.5 Effects of an External Pressure Gradient

The change in freestream velocity and pressure in the streamwise direction has a profound effect on the development of the boundary layer. When the pressure decreases and the corresponding velocity along the edge of the boundary layer increases, then the external pressure gradient is said to be "favourable" with gradient $\partial p/\partial x<0$. The consequence of the favourable pressure gradient is to alleviate the effects of the shearing in the boundary layer. The boundary layer velocity profile becomes much fuller and in particular the flow is decelerated less markedly near the wall. The boundary layer thus grows more slowly than for the corresponding zero pressure gradient condition. This effect is illustrated in Figure 2.3.

Conversely, when the pressure increases and the freestream velocity decreases in a streamwise direction, the external pressure gradient is said to be "adverse". The pressure change now adds to the shearing actions and the flow decelerates more markedly near the wall. In this case, the boundary layer velocity profile is much less full than for a zero pressure gradient and a point of inflection develops (see Figure 2.3). If the adverse pressure gradient is sustained, then the flow near the wall will decelerate so much that it will begin to reverse its direction near the wall. When this happens, the boundary layer has separated from the surface, as will be discussed later, having profound effects on the whole flow-field. Pressure gradients are therefore one of the most important parameters in determining the behaviour of a boundary layer.

2.2.6 Boundary Layer Integral Properties

The velocity across a boundary layer rises asymptotically towards the value of the freestream and therefore some convention is needed to define the outer edge of the boundary layer. The most common definition is to define the edge of the boundary layer as the point at which the velocity reaches 99% of the local stream

value (U_{max}). Hence the boundary layer thickness, δ, is the perpendicular distance from the solid surface to the position where $u=0.99U_{max}$. Other boundary layer thickness parameters are outlined below and are applicable to any flow with an attached boundary layer.

The "displacement thickness" is a measure of the deficit in the mass flow associated with the boundary layer because of the reduced velocity. As the boundary layer develops, the mass flow per unit volume decreases within it relative to the freestream. To satisfy continuity, in for example the two-dimensional case, a streamtube within the boundary layer must increase in width (normal to the surface) to balance this reduction in mass flow. To the freestream flow, this is equivalent to an inviscid region in which the surface is displaced into the flow. The displacement thickness is therefore defined as:

$$\delta^* = \int_0^{\delta} \left(1 - \frac{u}{U_{max}}\right) dy$$

where u is the local velocity, y is the normal distance from the surface, U_{max} is the local stream velocity and δ is the boundary layer thickness.

Also associated with the developing boundary layer is a decrease in momentum. The streamwise momentum flux in the boundary layer is less than that occurring in the freestream. A measure of this deficit is given by the momentum thickness, the distance that a surface would have to be displaced into the freestream so that, with no boundary layer, the total flow momentum would be the same as that which is actually occurring for the actual mass flux of the boundary layer. Momentum thickness is defined as:

$$\theta = \int_0^{\delta} \frac{u}{U_{max}} \left(1 - \frac{u}{U_{max}}\right) dy$$

The ratio of momentum thickness to the displacement thickness is called the Shape Factor, H and is given by,

$$H = \frac{\delta^*}{\theta}$$

This is a measure of the "fullness" of the boundary layer profile and gives an indication of the state of the boundary layer. A low shape factor indicates a fuller profile and a higher velocity gradient near the surface. Generally,

Laminar boundary layers	$2.3 < H < 3.5$
Turbulent boundary layers	$1.3 < H < 2.2$

2.3 The Laminar Separation Bubble (Short Bubble)

2.3.1 Overview

Although the basics of the laminar separation bubble are simple to explain, each element requires more detailed discussion and this can be found in the next section. At low Reynolds number, conventional aerofoils tend to lose performance significantly due to the forward progression of flow separation commencing at the trailing edge. Leading edge stall, where the flow suddenly breaks completely away from the surface, causes a dramatic loss of lift and can be a very undesirable behavioural characteristic. It is therefore common to design aerofoils to stall from the trailing edge progressively, but with the flow separation being delayed as rearward as possible on the aerofoil to minimise losses.

The laminar separation bubble will form prior to stall under conditions determined primarily by the Reynolds number and the aerofoil geometry. The attached laminar boundary layer is subjected to an adverse pressure gradient as it passes the minimum pressure location on the leading edge of the aerofoil. The boundary layer is decelerated under the influence of the pressure gradient, causing the fluid close to the surface, where velocity is already low, to begin moving in the opposite direction. The flow separates and if the Reynolds number is high enough, the shear layer formed will undergo transition to turbulence and may, with its higher kinetic energy and increased rate of thickening, reattach back to the surface further downstream as a turbulent boundary layer. Otherwise, the flow will remain separated from the surface. The chordwise pressure rise under the shear layer drives the flow reversal, aided by the entrainment on the low-velocity edge of the shear layer. It is important to note that under the reverse flow region, the skin friction becomes negative. Figure 2.4 is a schematic showing the structure of a laminar separation bubble. It is important to note that because the bubble typically has a length of approximately 1% chord, the diagrams are often drawn not to scale.

As the Reynolds number increases, the extent of such a bubble is reduced until the momentum of the flow is high enough to overcome the pressure rise and the flow remains attached. i.e. the bubble shortens in length and disappears.

If the Reynolds number is decreased low enough, the flow may not be able to reattach resulting in a "burst" bubble. This bursting is defined as a sudden breakdown of the bubble structure leading to fully detached flow. Bursting can also be achieved by an increase in incidence, this first contracts the bubble but then at some incidence the flow breakaway occurs. This is generally referred to as leading edge stall. The contraction of the bubble is caused by the adverse pressure gradient becoming steeper as incidence increases.

The size and location of the separation bubble is also affected by the aerofoil geometry and the freestream turbulence level. The presence of the bubble has little effect on the pressure distribution over the aerofoil until bursting occurs. Subsequent to this, there is a significant pressure redistribution with the new distribution bearing little resemblance to the attached flow profile. Consequently, bubble bursting is usually accompanied by a sudden loss of lift, increase in drag and an undesirable change in pitching moment. Following the bursting of a laminar separation bubble, if the incidence is low enough the flow may reattach further downstream forming a "long" bubble which increases in length with further increases in incidence.

Although the formation of a laminar separation bubble should more often than not be avoided, it can be beneficial. At high Reynolds number, the separation bubble can lead to a deterioration of the lift and drag coefficients prior to stall. However, at low Reynolds number, the presence of the separation bubble will allow downstream flow to stay attached to an aerofoil longer than if it were absent. Stall may therefore occur at higher incidences or lower velocities.

The separation bubble can be eliminated completely by enforcing transition upstream of the separation point. However, in many applications this is not

desirable since the turbulent boundary layer, present over a larger portion of the aerofoil, leads to increased skin friction and an even larger total drag. Therefore, the separation is often controlled by careful design of the aerofoil shape or by placing roughness on the surface to promote transition close to the separation point (Häggmark 2000). This is to avoid the situation when the shear layer fails to reattach leading to a severe loss of lift.

The occurrence of laminar separation bubbles is not just restricted to conventional aerofoils. They can also be found:

- On thicker aerofoil sections (20% thickness to chord ratio) at low Reynolds numbers. Assuming that transition of the attached boundary layer does not occur before the separation point, the bubble can be found well aft on the aerofoil.
- In supersonic flow, the bubble appears near the leading edge and the reattachment mechanism is due to an expansion fan forcing the flow to reattach, sometimes maintaining laminar flow.
- On flat plates at zero incidence where an adverse pressure gradient has been imposed from outside. In this case, the laminar boundary layer formed at the leading edge of the plate separates in the presence of the pressure gradient before it undergoes transition and then reattaches in the manner described above.

2.3.2 Literature Review on the Laminar Separation Bubble

The whole subject of laminar separation bubbles on rounded aerofoils is well documented and consequently fairly well understood. The earliest observations of the phenomenon were made by Jones (1934). However, it was not until McGregor (1954) measured velocity distributions and turbulence intensities for a range of Reynolds numbers and incidences, that the structure of the "short" bubble with its "dead air" and reverse flow regions was revealed. This is shown in Figure 2.5. There is a dividing streamline which marks the limit between the

outer flow and that within the bubble, and rejoins the surface at the reattachment point.

Crabtree (1957) proposed from his experiments involving short bubbles that they consistently had the same principal features:

- Constant pressure over the front portion of the bubble with a laminar shear layer over this region. This implies that the air in the front part of the bubble is at rest (dead air region) and the shear layer is quite thin without any turbulent mixing. The external stream is curved in a manner appropriate to the constant pressure.
- A pronounced region of pressure rise, both on the surface and along the dividing streamline (this was shown by Gault (1955) to be the onset of fully developed turbulent flow). Crabtree showed that the external stream then straightened out after the region of pressure rise, which displayed intense turbulent mixing.
- An eddy forming in the rear part of the bubble, necessary for continuity of mass flow (providing flow to the aerofoil side of the turbulent mixing region).

Crabtree (1957) and Ward (1963) amongst others, showed that the pressure distribution over the aerofoil surface downstream of the bubble is approximately that which would occur if there were no bubble present (providing the bubble length is small). This implies that the bubble only slightly modifies the pressure distribution, and hence the boundary layer aft of the bubble is not greatly affected. The boundary layer is slightly thicker, but normal boundary layer assumptions can be applied. Figure 2.6 shows the effect of a typical laminar separation bubble on the pressure distribution. In contrast, the long bubble strongly alters the pressure distribution and the suction peak does not appear.

Early studies by McCullough & Gault (1951) first revealed the occurrence of two types of bubbles formed near the leading edge, short and long, characterised by the ratio of the chordwise length of the separated region, s, to the

displacement thickness at the point of separation. Typically for a short bubble, $s/(\delta^*_s) = 10^2$ and for a long bubble, $s/(\delta^*_s) = 10^3$-10^4.

Since the flow phenomenon involves a fully attached laminar boundary layer just prior to separation, the location of the separation point is very dependent on the condition of the laminar boundary layer. Therefore, various characteristic length scales of the separation bubble appear in the literature, usually relating to the local flow conditions at the separation point or the bubble length. The most common parameter used is a Reynolds number based on the displacement thickness at the separation point, δ^*_s and the velocity just outside the boundary layer at separation U_s and hence $Re(\delta^*_s) = (U\delta^*/\nu)_s$.

Owen & Klanfer (1953) produced a criterion to determine which type of bubble would form. They based this on the separation displacement thickness Reynolds number, $Re(\delta^*_s)$, and dependent on whether this was greater or less than a critical value would determine whether the bubble was short or long respectively. From their analysis of previous two-dimensional tests, they set this critical value at 400-500 (O-K Criterion). Below this range only long bubbles occur and above only short bubbles are formed. Tani (1964) claimed to have first revealed the existence of this critical Reynolds number, but with limited test data, his estimation of 780 was too high.

When the laminar boundary layer separates the shear layer is generally so thin that early measurements of the velocity profiles proved both difficult to obtain and inaccurate, with the limited measuring equipment available. Therefore, it was necessary to calculate the displacement thickness at the separation point using the pressure distribution instead, which was easily measured with pressure tappings. The growth of the boundary layer was calculated for this purpose by Crabtree and Tani amongst others by using the "quadrature formula" developed by Thwaites (1949).

Their results led to the important result that $Re(\delta^*_s) \propto Re_\infty^{1/2}$ which implied that both types of bubble *should* be able to exist on an aerofoil at a given incidence depending on the freestream Reynolds number, Re_∞. i.e. it should be possible for an aerofoil to attain values both greater than and less than the critical Reynolds number, defined by the O-K criterion, simply by a change in the freestream Reynolds number. This was confirmed by the experiments of Crabtree who showed the existence of both bubble types on a single aerofoil, as shown on Figure 2.7.

The bursting of a short bubble is generally associated with no reattachment downstream and with aerofoil stall. However, in many cases the bursting may be a sudden transition to a long bubble following the O-K criterion. The long bubble may only be a few percent of the chord length on formation, but may soon grow with increasing incidence and eventually stall. i.e. it extends beyond the trailing edge and into the wake downstream of the aerofoil. Although the O-K criterion successfully distinguishes between long and short bubbles, Gault (1955), Gaster (1966) and Horton (1969) all pointed out that there was no universal critical value of $Re(\delta^*_s)$ for the breakdown of a short bubble and hence the O-K criterion does not help in determining the conditions under which bursting occurs. Further information about the flow was required and it was Crabtree who found that the pressure gradient that the bubble is subjected to was an important parameter.

Another theory for bursting was put forward by McGregor (1954) who examined the balance of energy in the standing eddy of the separation bubble. He argued that the supply of kinetic energy from the shear layer to the bubble must balance the loss through viscous dissipation and bursting was due to the bubble expanding to achieve equilibrium, but disintegrating instead. Young & Horton (1969) considered that this disintegration might be due to the vortex attempting to entrain more air than it was able to accommodate. However, it is most likely that the circulatory flow in the bubble is in some kind of equilibrium.

2.3.2.1 Pressure Recovery

In some cases, leading edge stall on a rounded aerofoil may be due to the value of $Re(\delta^*_s)$ reaching a critical value and causing the bubble to burst. However, if the adverse pressure gradient is very steep, for example behind the kink in a droop nosed aerofoil, or if the leading edge is of high curvature, the short bubble may be insufficiently small to provide the required pressure recovery. Therefore, the bubble may burst causing stall even though $Re(\delta^*_s)$ is greater than the critical value.

Crabtree (1957) proposed that the chordwise length of the separated flow was related to the pressure recovery which is required to take place through the turbulent mixing process as the shear layer reattaches to the aerofoil. Thus the criterion for bursting of a short bubble may be that at a given Reynolds number the change to a long bubble will occur at such an incidence that the pressure recovery is unattainable in the turbulent reattachment process. That is to say the change in pressure required to bring the pressure back to its value in the absence of the bubble cannot be sustained solely through the process of turbulent mixing. The pressure gradient aft of the suction peak is the determining factor that decides whether the pressure recovery can be achieved within the confines of the bubble, the pressure gradient getting steeper with increasing incidence.

The parameter defined by Crabtree for this process is the pressure recovery factor σ, where

$$\sigma = \frac{P_R - P_S}{1/2\rho U_\infty^2} = \frac{\left(C_{P_R} - C_{P_S}\right)}{\left(1 - C_{P_S}\right)}$$

subscripts $_R$ and $_S$ refer to the conditions of reattachment and separation and C_P is the normal pressure coefficient, defined in Section 2.2.4.

Analysis of results from Gault (1955) and McGregor (1954) showed that there was a maximum value of the pressure recovery factor that could be obtained in the turbulent mixing process preceding reattachment. The experiments concluded that as the bursting point was approached, the pressure recovery tends to a maximum value of σ=0.35. Results from McGregor are shown in Figure 2.8. This value of pressure recovery was confirmed by Savage (1960) and Tani (1964).

Tani (1964) suggested that the maximum value of pressure recovery represents the maximum possible turbulent shear stress that is able to exist in the reattaching turbulent shear layer. This was confirmed by Tani's own experiments over plane mixing layers, steps and grooves where a similar maximum turbulent shear stress existed.

The basic cause of breakdown of short bubbles is therefore either an increase in incidence, or a decrease in Reynolds number. The latter directly controls the length of the laminar region of the separated shear layer and hence the distance the turbulent shear layer must travel before reattachment can occur, and the maximum pressure recovery that will be attainable.

Gaster (1966) described the correlation of Crabtree's bursting criterion as being incomplete and developed a non-dimensional parameter describing the pressure distribution in the region of the bubble, $(\theta_s^2/\nu)\Delta u/\Delta x$. Δu is the rise in velocity along the length of the separation Δx. He suggested that the structure of the bubble was dependent upon the two parameters, $(\theta_s^2/\nu)\Delta u/\Delta x$ and $Re(\delta^*_s)$. Conditions for bursting then showed a strong correlation between the two quantities, as shown in Figure 2.9.

Crabtree concluded that if σ is less than the maximum attainable value, then the suction peaks are maintained and the bubble remains short. As the incidence is increased, the suction peaks grow higher, but the pressure gradient following the

peaks steepens. Although the bubble contracts slightly, the pressure recovery occurring over the rear of the bubble still rises until a maximum value of σ is reached. Similarly, if the Reynolds number falls for a given incidence, σ rises (see Figure 2.8) and since $Re(\delta^*_s) \propto Re_\infty^{1/2}$ the laminar portion of the shear layer increases. Therefore, although the suction peak is lower (for lower Reynolds number), the pressure recovery may still reach its maximum. Once the flow has broken down, the pressure distribution becomes totally redistributed and it may be possible for a long bubble to form with a reattachment point further downstream. This will define a new value of pressure recovery factor (possibly less than that when the short bubble burst), but as of yet, no analysis of the pressure recovery has been attempted on the long bubble.

2.3.2.2 Effect of Changes in Reynolds Number and Incidence

MacGregor (1954), Gault (1955) and Crabtree (1957) were the first to show that the length of the short bubble decreases with an increase in incidence or Reynolds number, whereas the height increases with increase in incidence or reduction in Reynolds number.

O'Meara & Mueller (1987) and Liebeck (1992) show the separation point to move forward with increasing Reynolds number (due to the steepening pressure gradient, the same pressure recovery can occur over a shorter chordwise distance and hence the bubble will also contract as Reynolds number increases.) The limiting factor is when the Reynolds number is sufficiently high to cause transition from laminar to turbulent flow ahead of the "theoretical laminar separation point", that point where separation would have occurred if the flow had remained laminar. Under these circumstances, the bubble formation will be precluded. Alternatively, the forward movement of the separation point causes the value of $Re(\delta^*_s)$ to decrease and eventually the value will drop below the critical value for transition to the long bubble. Figure 2.10 shows the effect of Reynolds number and incidence on the length of the short separation bubble.

At low freestream Reynolds number, it is possible for a long bubble to collapse into a short bubble. As the freestream Reynolds number is increased, the length of the separated region decreases simply because transition in the shear layer can occur sooner at a higher freestream Reynolds number (O'Meara & Mueller (1987), Tan & Auld (1992)). An increase in the freestream turbulent level has a similar effect. As the freestream Reynolds number increases, so does $Re(\delta^*_s)$, because of the relationship $Re(\delta^*_s) \propto Re_\infty^{1/2}$, so at some stage the critical value of $Re(\delta^*_s)$ is reached and the bubble becomes short.

Thus in terms of aerofoil performance, the greatest lift coefficient ($C_{L\,max}$) occurs on aerofoils that first form a long bubble at low Reynolds number and switch to a short bubble as lift increases (Crabtree). This is because $Re(\delta^*_s) \propto Re_\infty^{1/2}$, and any increase in Reynolds number means that a higher incidence will be reached before $Re(\delta^*_s)$ drops below the critical value. Consequently, an increase in Reynolds number can be associated with an increase in $C_{L\,max}$.

The behaviour of the long bubble differs considerably from that of a short bubble. Owen & Klanfer (1953), Gault (1957) and Crabtree (1957) showed the length of a long bubble is only a few percent of the chord when formed at low incidence, but lengthens considerably with increase in incidence. The reason for the growth of long bubbles with increased incidence at a constant Reynolds number may at first seem to be simply due to the geometry. If the height of the dividing streamline is assumed to be proportional to the incidence and then a constant spreading angle assumed for the turbulent region of the shear layer, then it follows that the bubble length must increase with incidence. In addition since $Re(\delta^*_s)$ decreases with increased incidence, then the laminar portion of the shear layer will lengthen further delaying reattachment. Unlike the short bubble, the presence of the long bubble greatly changes the form of the pressure distribution and causes a collapse of the leading edge suction peak, Figure 2.6.

The long bubble was termed "thin aerofoil bubble" by Gault (1957) because its behaviour is strongly related to separation bubbles behind sharp leading edges and will be discussed in more detail in Section 2.4.

2.3.2.3 Stability of the Laminar Separation Bubble

The location of transition in the shear layer, subsequent to separation, is an important parameter in the behaviour of the separation bubble. For attached boundary layers, the location of transition can be easily predicted, but without the solid surface bounding the lower limit, it has been argued that the transition may commence immediately subsequent to separation. Crabtree (1957) proposed the phenomenon to be controlled by the freestream Reynolds number but with the transition of the laminar shear layer at the "surface of discontinuity" playing an important role. Gaster (1966) concluded that the transition occurred due to instability waves in the laminar shear layer and O'Meara & Mueller (1987) showed the length of the laminar portion to be controlled by the disturbance amplification process, directly affected by the Reynolds number (based on chord length), incidence and the freestream turbulence level. More recently Häggmark (2000) observed an exponential disturbance growth in the separated shear layer associated with a highly two-dimensional flow. A local maximum in the disturbance amplitude developed at the inflection point in the mean velocity profile and he associated this with an inviscid type of instability.

Liebeck (1992) and Dovgal et al. (1994) detailed the spectral distributions of the fluctuation velocities which describe the mechanism of transition (Figure 2.11). Within the laminar part of the shear layer there exists little or no activity of fluctuation velocities over the entire spectrum. At the onset of transition, a narrow band of frequencies begins to grow with a distinct peak at the fundamental frequency, whilst the remainder of the spectrum is quiet, as shown in Figure 2.12. Growth of this fundamental frequency proceeds rapidly until a peak level is reached when the entire spectrum amplifies dramatically, signifying

transition. Dovgal et al. showed the fundamental frequency to agree well with linear stability theory and the dynamics of the bubble were shown to be independent of the aerofoil shape, the incidence and the Reynolds number. In addition, Liebeck (1992) confirmed the two-dimensional nature of the laminar separation bubble in terms of mean flow and transitional instabilities.

The effect that the reverse flow region has on the separation itself has not yet been fully explained, but Gaster was the first author to suggest that the upstream flow must affect the feedback cycle and thus have a controlling influence on the bubble as a whole, although Gaster was unclear about exactly which parameters were important.

Recently, most interest has been shown in the unsteady aspect of the entire separation bubble. Traditionally, the flow was perceived as "steady", certainly when time averaged, however, low frequency oscillations have been observed in the wake of separation bubbles. Pauley et al. (1990) conducted a numerical study into the influence of an imposed external adverse pressure gradient on the separation bubble, finding that a strong adverse gradient caused periodic vortex shedding after separation of the shear layer. Comparisons with the work by Gaster showed that his phenomenon of "bursting" occurred at the same conditions as the periodic shedding, implying that the bursting was simply periodic shedding that had been time averaged. Furthermore, Pauley et al. suggested that Gaster's long and short bubble were in fact respectively steady and unsteady separation bubbles with the low pressure gradient of the long bubble producing no periodic shedding. The shedding frequency was found to be independent of Reynolds number and a further study by Ripley & Pauley (1993) indicated that this frequency varied with pressure distribution. They concluded that large-scale two-dimensional structures control the reattachment and small-scale turbulence contributes a secondary role.

2.3.2.4 Prediction Methods

Horton (1969) developed a semi-empirical prediction method for the length of a separation bubble up to bursting. By using previous results from many of the authors mentioned above, he based his method on a pressure gradient criterion and a correlation between the length of the laminar portion of the shear layer and the momentum thickness Reynolds number at separation ($Re\theta_s$). Roberts (1980) modified Horton's method, which was found to produce a delayed prediction of bursting and neglected the effect of freestream turbulence. He included the effect of freestream turbulence and the results showed reasonable prediction of growth and bursting of the laminar separation bubble. Schmidt & Mueller (1989) cited the major deficiency in the methods of Horton and Roberts by stating that the integral boundary layer type methods they had used were useful for defining some of the characteristics of separation bubbles, but relied heavily on experimental data. Therefore they argued that they cannot easily be applied to new situations.

As more experimental data became available, the models proposed were again assessed for their validity. Weibust et al (1987) found the methods to be generally confirmed. O'Meara & Mueller (1987) though finding some consistency with the available results, showed a high level of scatter when comparing predictions at reattachment.

Schmidt & Mueller were not able to verify Horton's universal reattachment profile, shown in Figure 2.13. Horton proposed a single non-dimensional profile, based on nine measured velocity profiles, existing for all separation bubbles at reattachment which had a shape factor of 3.5, but the range of values measured experimentally was 1.54 - 4.37. Tan & Auld (1992) who completed the most detailed comparisons of previous semi-empirical theories found agreement to be generally poor. They cited possible reasons for discrepancies as being different techniques for determining the separation and transition locations, and different wind tunnel conditions.

Calvert (1994) set up a coupled viscous-inviscid computational method to model the separation bubble. This was applied to a range of test cases and was found to show good agreement when the transition point was chosen to match the test case. A study of previous transition correlations showed that none of them were capable of predicting the position of transition within the leading edge separation bubble. A new correlation was proposed, based solely on the results of Walraevens & Cumpsty (1993), which modelled the trends reasonably well, but still with a large amount of scatter. Ripley & Pauley (1993) and Lin & Pauley (1996) were able to successfully model parts of the separation bubble, but a complete solution required greater computing power. Alam & Sandham (2000) defined the complete solution to be the successful resolution of the reattached turbulent boundary layer and the prediction of transition in the shear layer. The computational aspect of predicting separation bubbles is covered in more detail in Chapter 6.

2.3.3 Conclusions from the Literature Review on the Laminar Separation Bubble

The previous work has shown there to be two types of separation bubble that can form near the rounded leading edge of an aerofoil:

- The short bubble, with a typical chordwise extent of ≈1%. This bubble contracts with increasing incidence and freestream Reynolds number and has little effect on the pressure distribution of the aerofoil. As incidence increases, the peak suction continues to rise despite the presence of the bubble.

- The long bubble, which on formation at low incidence covers 2-3% of the chord and grows rapidly with increasing incidence until the separated shear layer fails to reattach to the surface of the aerofoil. Pressure distribution is

very much affected by the presence of the bubble and the leading edge suction peak collapses.

- Both types of bubble are formed by the separation of the laminar boundary layer with a subsequent reattachment which is thought to be accomplished by the entrainment process of the turbulence initiated in the separated flow.

- Analysis based on experimental results shows that a short bubble will only form when the Reynolds number based on boundary layer displacement thickness at separation is above a critical value (O-K criterion). In addition, there exists a maximum limit to the pressure recovery coefficient across the turbulent mixing region in order for reattachment to occur. Just prior to short bubble breakdown, the first criterion must be fulfilled and the second criterion must be about to be violated.

- The violation of either criterion forces a breakdown of the short bubble and a consequent redistribution of the pressure distribution which may enable a new longer bubble to form, reattaching further downstream.

- The long bubble, formed on a rounded aerofoil is strongly related to the thin aerofoil bubble, which exists exclusively on aerofoils with sharp leading edges, where the boundary layer separation is fixed, regardless of Reynolds number.

2.4 The Thin Aerofoil Bubble

2.4.1 Overview

The behaviour of a long bubble is very different to that of a short bubble. Crabtree (1957) stated that it is better to differentiate between long and short bubbles by their effect on the pressure distribution than by their length. As previously mentioned, the long bubble has been termed "thin aerofoil bubble" by Gault (1957) and "nose separation" by Wallis (1960), with the former term being used in the current work.

The lift produced by a flat plate with a separation bubble is generated in a different manner to that produced by a conventional aerofoil. It is not only the section shape that causes flow acceleration along the aerofoil and creates the pressure distribution, the condition of the boundary layer and the effect it exerts on the external flow is also more significant than for a rounded aerofoil.

The flow around a flat plate with a sharp leading edge results in a very different behaviour to that for the laminar separation bubble, discussed in the previous section. At zero incidence, the flow can be expected to be laminar and attached on both sides, producing zero lift (assuming identical surface profiles). If an incidence is introduced to the plate, the stagnation point might be expected to move to the lower surface. The boundary layer driven around the leading edge by the pressure difference must be very thin and is expected to separate immediately with such a direction change. The fixed separation point leads to the hypothesis that the flow will be insensitive to a change in Reynolds number, and transition will occur soon after separation.

The thin aerofoil bubble formed on an aerofoil with a sharp leading edge is therefore characterised by a flow separation at the leading edge with a subsequent reattachment to the top (leeward) surface at a position which moves progressively rearward with increasing incidence. The flow will reattach if the

angle of incidence is sufficiently low (typically <7 degrees), however above this the bubble can extend downstream into the wake. Figure 2.14 shows typical geometries on which thin aerofoil bubbles have been studied. The classical model is of a bubble which, when time averaged, is assumed to be two-dimensional. Because of the requirement for continuity within the flow, there is a dividing streamline which demarcates the bubble from the outer flow and which rejoins the surface at the reattachment point, as shown in Figure 2.15.

The geometry of the leading edge is of paramount importance when determining the flow over the remainder of the aerofoil. For the ideal flat plate, the flow will always separate at the leading edge on departure from zero incidence. However, by increasing the radius of curvature at the leading edge, the flow may negotiate the leading edge and remain attached. A laminar boundary layer can then form leading to the possibility that a laminar separation bubble may exist further downstream.

The thin aerofoil bubble at the leading edge leads to strong interaction between the viscous and inviscid parts of the flow. Without a separation bubble forming, the pressure gradient at the leading edge would go to infinity. The viscous part of the flow responds by separating and forming the separation bubble, so removing the singularity. This results in pressure distributions which are of very different form to those on common rounded nose aerofoils, see Figure 2.6. The inviscid pressure distribution around a sharp leading edge separation bubble therefore does not resemble that over a rounded nose aerofoil.

After separation, a lack of viscous damping at the wall means that the shear layer is likely to undergo transition very close to the leading edge. The turbulent shear layer thickens at an accelerated pace and has a high entrainment rate; it then reattaches further downstream and bifurcates. Some flow is directed upstream to feed the shear layer and the resultant backflow reduces the pressure at the surface and in turn helps to bend the shear layer back to the reattachment point. The remainder of the flow is directed downstream where it gradually reverts to

an attached turbulent boundary layer before reaching the trailing edge (assuming there to be sufficient length left after reattachment).

2.4.2 Literature Review on the Thin Aerofoil Bubble

There have been very few detailed experimental studies of the flow near a sharp leading edge. Gault (1957) performed a thorough investigation of the thin aerofoil bubble formed on a flat plate aerofoil. When compared to the short bubble he described the long bubble as having "vastly different characteristics" yet in the same paper he commented that "the physical significance, if any, of this difference between the two types of separated flow is not readily apparent".

One of the major differences between the sharp and rounded leading edge is the mechanism for flow separation. With a rounded leading edge, the primary mechanism is an external adverse pressure gradient which decelerates the attached laminar boundary layer and causes it to separate. With the sharp leading edge, the detachment of the flow is forced by the inability of the flow to make the sharp change in direction around the leading edge and not simply by the adverse pressure gradient (the two mechanisms were termed APG-induced and Geometry-induced separation by Alving & Fernholz (1996)). Consequently, the O-K criterion cannot be applied since this relies on empirical values from an attached boundary layer at the separation point.

The geometry of the leading edge, even when nominally sharp, is of paramount importance when determining the initial conditions for separation. Gault stated that the incidence required for separation is primarily due to the roundness of the leading edge and McCullough & Gault (1951) showed that even the thinnest rounded aerofoil displayed properties of separation parallel to those of thicker aerofoils up to 4.5-5 degrees incidence. After that, the flow changed abruptly to that found on the double-wedge shaped aerofoil with a sharp leading edge. They tested a family of symmetrical aerofoils with different thickness and compared

them to the double-wedge aerofoil. The aerofoil profiles are shown in Figure 2.16 and the resulting lift curves in Figure 2.17. They characterised the curves as being a result of three types of stall phenomena:

- Trailing edge stall where there is a gradual loss of lift at high lift coefficient as the turbulent separation point moves forward from the trailing edge.
- Leading edge stall where there is a sudden loss of lift due to the breakdown of a short bubble near the leading edge.
- Thin aerofoil stall with gradual loss of lift at low lift coefficient due to the lengthening of the long bubble.

The discontinuity in the lift curve for the NACA 64A006, the thinnest of the rounded aerofoils, is due to a transition from a short to a long bubble as the incidence is increased.

The failure to obtain a high leading edge suction peak accounts for a rapid rise in pressure drag experienced by these aerofoils (Ward 1963). As the incidence is increased, a region of constant pressure forms over the separation bubble and this increases in chordwise extent as incidence increases. After the constant pressure region, there is a marked pressure rise around reattachment before the pressure settles and the trailing edge is reached. This pressure rise has been attributed to intense turbulent mixing with the start of this region being due to transition of the shear layer.

The flow separates as a laminar shear layer, however Newman & Tse (1992) stated that transition to a turbulent shear layer occurs at fairly low Reynolds numbers, in the order of 100 when based on the overall width of the shear layer. Thus the shear layer becomes turbulent close to the leading edge. Gault (1957) showed that the extent of the laminar flow close to the leading edge is virtually zero which is in marked contrast to the rounded leading edge separation where up to 80% of the free shear layer was shown to be laminar. If the Reynolds number for transition is defined as,

$$Re_f = \frac{U_\infty f}{\nu}$$

where U_∞ is the velocity of the outer flow and, f, is the extent of the laminar flow in the shear layer, then for a sharp leading edge, $Re_f \approx 5000$ and for a rounded leading edge there is a tenfold difference i.e. $Re_f \approx 50000$.

The turbulent shear layer entrains much more fluid than it would have done if it had remained laminar. The entrainment on the aerofoil side is provided by backflow along the wall which in turn reduces the pressure there and causes the mixing layer to curve back towards the surface. The growth of the mixing layer is decreased slightly by its curvature, but increased by the backflow and the adverse pressure gradient over the reattachment region.

McCullough & Gault (1951) showed the shear layer to be "a region of intense turbulence", with the turbulence level reducing near the trailing edge. They found that the separated region increased in size with increasing incidence until it covered the entire surface. Maximum lift was achieved in this condition i.e. just before the bubble detached from the aerofoil. This produced an enclosed bubble which started at the leading edge and finished in a reattachment region of highly turbulent flow. Also at the higher incidences, a strong reverse flow was shown to exist underlying the detached flow. McCullough & Gault also observed a variation in static pressure normal to the surface across the bubble. The pressure first decreases and then increases with distance from the surface as shown in Figure 2.18. This variation diminishes after reattachment when turbulent mixing dampens out the effect. Before this the steepest static pressure gradients, perpendicular to the plate, exist across the shear layer. Therefore, the assumption of constant static pressure across an attached boundary layer, described in Section 2.2.4, is not valid for a separation bubble. The coupling of the strong reverse flow and the variation in static pressure is a strong indication of a vortex type flow forming after separation. This was confirmed by Rose & Altman (1950) who conducted flow studies on a double-wedge aerofoil.

Gault (1957) was the first author to take velocity measurements from within the reverse flow region of a thin aerofoil bubble. He showed that the magnitude of velocity in this region was generally $>0.2U_\infty$ and reached a maximum of 0.35-$0.4U_\infty$. The magnitude of the velocity in this reverse flow region is another major difference between the short bubble and the separation bubble from a sharp leading edge. The maximum reverse flow velocity in a short bubble was shown by Gaster (1966) to be around $0.2U_\infty$. This difference may be due to the fact that the sharp leading edge bubble is generally much larger than the short bubble, but it is an important result showing the large quantity of reverse flow that is entrained into the separated shear layer in the thin aerofoil bubble. The effect of this is discussed in Section 2.5.

The location of the reattachment point was shown by Gault to be approximately at the termination of the rapid pressure rise that succeeds the region of constant pressure. He compared the flow to a jet mixing in still air with the expanding mixing region downstream of the leading edge separation. The intensity of the turbulent mixing on one side of the shear layer bends the flow towards the surface. After reattachment, the intensity and distribution of the turbulence becomes similar to that of a turbulent boundary layer which is not surprising as a zero pressure gradient exists after reattachment, until close to the trailing edge.

2.4.2.1 Thin Flexible Sail Sections

Flexible sail sections are particularly prone to thin aerofoil bubbles and have been the subject of much research. Jackson & Fiddes (1995) reviewed early measurements made on thin sections, both rigid and flexible and developed a weakly coupled viscous-inviscid method to model the separation bubble on a flexible section. However, comparisons with experiment results were limited by a lack of available data on sharp edged rigid sections.

Previous attempts to compare the theoretical solutions to experimental data for flexible sections have not proved successful due to a number of factors. Experimentally, this has been due to the failure to produce a two-dimensional flow, and theoretically, the basic cause of discrepancies has been due to neglecting viscous effects in the model which become dominant when the flow separates at the leading edge. The membrane supports at the leading and trailing edges also influence the flow. They have to be strong enough to resist bending yet of small enough diameter not to interfere with the flow. In practice, the supports generally tend to bow under load thus inducing three-dimensional flow effects.

Newman & Low (1984) tested quasi two-dimensional sails of small camber and at small incidences at a Reynolds number of 1.3×10^5. They found that their measurements disagreed with linearised inviscid theory when the excess length exceeded 0.03 (where excess length is defined as the fractional excess of arc length over chord length). The lift coefficient, C_L, was found to be less than that predicted by theory. They attributed this to a boundary layer separation bubble at the leading edge and boundary layer effects near the trailing edge, identified by means of supplementary flow-visualisation. Greenhalgh et al (1984) found good agreement between theoretical and experimental results, but only for the angles of incidences where there was no flow separation. Theoretical and experimental values for C_L were found to be within 5% in an incidence range of -5 degrees to 8 degrees (tested at a Reynolds number of 1.3×10^6). The best comparison was found by Sugimoto & Sato (1991) who concluded that the linearised inviscid theory can predict the essential properties of the flow around membranes providing the excess length was <3%. When the excess length exceeded the chord by 5%, viscous effects dominated and the experimental results showed poor agreement with theory at a Reynolds number of 1.3×10^5. They used rounded supports which again showed good agreement, but only within the attached flow regime.

2.4.2.2 Attempts to Model the Thin Aerofoil Bubble

On a rounded aerofoil, the thickness of the boundary layer must be modelled because of the effect it has on the distribution of effective aerofoil thickness and camber. The existence of a separation bubble has a more pronounced effect which must be simulated in any model used. The flat plate creates its own aerodynamic shape in conjunction with the separation bubble. Hence, lift can be produced from this effective thickness and camber as well as from the pressure difference between the upper and lower surface.

Norbury & Crabtree (1955) attempted to model the pressure distribution over a flat plate aerofoil at incidence by tackling the inviscid and viscous regions individually and then combining one with the other to produce a unique solution. For the cases when the bubble reattached well forward of the trailing edge, an expression was derived for the rise in the coefficient of pressure at the reattachment end of the bubble. Combining this with a consideration purely of the external flow, enabled the complete pressure distribution to be found for this type of flow. Several simplifying assumptions were made in the analysis and several empirical constants used, based on unpublished experimental results. The assumption of constant static pressure across the separation bubble allowed forces to be calculated based on the external flow, however McCullough & Gault (1951) and Gault (1957) showed that the pressure was not constant and varied considerably across the bubble.

The computational model for the flow-field proposed by Jackson & Fiddes (1995) was for a membrane of fixed length supported at its leading and trailing edges. The membrane takes up an equilibrium shape under the influence of pressure and skin friction for a given incidence. The viscous models are confined to a separation bubble at the leading edge and to thin boundary layers which remain attached all the way to the trailing edge. This limits the model to small values of camber and incidence. The primary effect of the viscous areas is to alter the inviscid pressure distribution in much the same way as for a rigid

surface. The membrane will then alter its shape and provide another mechanism for the interaction of inviscid and boundary layer solutions. The numerical results of Jackson & Fiddes agreed well with experimental results of Rose & Altman (1950) and Newman & Tse (1992), both obtained on a thin double-wedge aerofoil with 4.2% thickness to chord. However Jackson & Fiddes state that the double-wedge section is not a good shape for comparison between numerical models and experimental results as it is prone to laminar separation near the trailing edge at low Reynolds numbers. The model predicted a laminar separation near the underside trailing edge, which had the effect of increasing the lift slope at higher incidences. This could not be represented by the methods used and they regarded the results as qualitative. At the higher Reynolds number used, the model predicted a bubble soon becoming turbulent and reattaching. The model was also found to be unsuitable for predicting the pressure under the leading edge separation bubble. Results for pressure drag rise were compared to those of McCullough & Gault (1951) and found to be higher than the experiment suggested. Similarly, the predicted pressure coefficients under the bubble are less negative than those measured. In conclusion, Jackson & Fiddes said that they required more data to evaluate the model thoroughly and this would be best obtained on rigid thin sections to avoid the problems of edge supports on membranes.

Newman & Tse (1992) used a simple theoretical model to predict the length of the separation bubble formed at the sharp leading edge of a flat plate at Reynolds number $>2.5 \times 10^5$. It was based on irrotational and incompressible flow and used a uniform array of sources under the bubble to represent the entrainment in the outer part of the shear layer. Thus the displacement thickness and momentum loss in the far wake were determined and were equated to the loss of leading edge suction due to the bubble.

They showed the length of the bubble to be:

$$\frac{x_R}{c} = \frac{U_\infty}{n} \pi \alpha^2$$

where x_R is the length of the separation bubble, n is the strength of the sources per unit length x, α is the plate incidence and c is the plate chord length.

The length of the bubble was shown to be proportional to the square of the incidence, Figure 2.19, and they confirmed this with experimental results on a thin sharp section (a scale model of that first used by Rose & Altman (1949)). However, Jackson & Fiddes commented that the results of Newman & Tse showed no calculated pressure distributions and so it is unclear how well their model represents the pressures needed for further boundary layer calculations. Newman & Tse assumed U_∞/m to be constant and bubbles of different lengths to be kinematically similar when time-averaged.

2.4.3 Conclusions from the Literature Review on the Thin Aerofoil Bubble

- The separation bubble formed behind a sharp leading edge has a reattachment point which moves progressively rearward with increased incidence. The initial formation of the bubble is at a much lower incidence than for a short separation bubble because the development of the local flow is not a factor. The only determining factor is the geometry of the sharp edge.

- Transition was shown to occur close to the leading edge and so almost the entire shear layer is turbulent. This differs from the short separation bubble, where the onset of the adverse pressure gradient coincides with transition in the shear layer.

- The low-velocity edge of the shear layer bounding the upper region of the thin aerofoil bubble exhibits strong entrainment inducing maximum reverse flow velocities of the order of $0.4U_\infty$ at certain chordwise locations (Gault 1957).

- Recent empirical models show reasonable agreement with sparse experimental data for double-wedge aerofoils and show the length of the bubble to be proportional to the square of the angle of incidence (Newman & Tse). Also, the length of the separation bubble was shown to be independent of a change in Reynolds number over a limited range.

- No investigations have looked at the effect of a broad range of freestream Reynolds number on the separation bubble characteristics.

- Work done on flexible sail sections shows limited agreement with experimental results. This is due to a combination of inadequacies in the model and in the experimental set-up.

2.5 The Turbulent Shear Layer Bounding a Recirculating Region.

2.5.1 Overview

The occurrence of a separated turbulent shear layer bounding a recirculating region is common and there have been many detailed studies behind steps, fences and similar obstacles where such flow conditions exist. Figure 2.20 shows some typical geometries where this type of flow may occur. Castro & Haque (1987) argued in a wide range of complex turbulent flows which are dominated by a shear layer bounding a large recirculating region that the key features will be similar. This is important to the present study because all separation bubbles are partly composed of a separated turbulent shear layer which reattaches to the surface. Without suitable instrumentation, taking measurements inside the recirculating region has been difficult. Indeed, only with recent advances in pulsed hot-wire and laser Doppler anemometry have accurate measurements been possible.

2.5.2 Literature Review on the Turbulent Shear Layer Bounding a Recirculating Region

Attempts to view the shear layer development and reattachment as a boundary layer problem has led to comparisons being drawn between the separated shear layer and a plane mixing layer between two streams. Most authors consider the separated shear layer to be a modified version of the plane mixing layer (Castro & Haque 1987).

Bradshaw & Wong (1972) investigating the flow from a backward facing step noted three main differences between the shear layer and plane mixing layer.

1. The curvature of the shear layer has a stabilising effect and tends to reduce the shear stress and turbulence intensity (Wyngaard et al 1968).
2. The reverse flow region increases the velocity difference across the shear layer and increases the shear stress and turbulence intensity.
3. The recirculating turbulent fluid is entrained in the shear layer. Arie & Rouse (1956) showed there to be significant shear stress in the reverse flow.

Chandrsuda & Bradshaw (1981) confirmed the earlier results and stated that reattaching shear layers have factors similar to plane mixing layers, but distorted by curvature, approach to a solid wall and entrainment of turbulent fluid on the low-velocity edge. More recently, Hancock (2000) proposed the shear layer to be a mixing layer subjected to an extra rate of mean strain arising from the curvature of the streamlines, and to fluctuating rates of strain imposed on the low velocity edge by entrainment of fluid from the recirculating region. The shear layer was shown to grow linearly until close to reattachment (similar to a plane mixing layer), with the differences arising from the feedback of turbulent fluid.

A common theme of the turbulent shear layer bounding a recirculating region is a low-frequency motion with a timescale much longer than that associated with large eddies in the shear layer. This low energy component of the flow has been linked to a quasi-periodic bursting of the separation bubble and has been seen on step flows, blunt-plate flows (Kiya & Sasaki 1983), flat plates normal to the airflow (Castro & Haque 1987) and flows over surface mounted fences (Castro 1981). Experiments carried out by Kiya & Sasaki found that large scale vortices were shed with a frequency of about $0.6U_\infty/x_R$. In addition to these regularly shed vortices, large scale unsteadiness was found to exist at a frequency of <0.2 U_∞/x_R. The authors proposed that the regular vortex shedding was being hindered by a still unknown mechanism, causing a large amount of vorticity to be accumulated in the separation bubble. This would tend to increase the bubble length until the accumulated vorticity is suddenly shed downstream as an extremely large vortex; this then immediately reduces the separation bubble

length by a large extent. The large scale unsteadiness is associated with a flapping of the shear layer near the separation line. It is most noticeable where the spectral peak is well separated from those associated with the shear layer turbulence (Castro (1981) and Kiya & Sasaki (1983)).

On reattachment, a portion of the shear layer is deflected upstream to form part of the entrainment flow. Bradshaw & Wong (1972) showed that the fraction of the shear layer mass flow deflected upstream depended on the initial thickness of the boundary layer before separation. If this is small, then at least half the shear layer may be deflected upstream to provide entrainment. The dividing streamline is not too far from the line of maximum shear stress or of turbulence intensity. Therefore, when the large eddies created in the shear layer reach the solid surface they are torn in two. The result is a rapid decrease in the turbulent shear stress and eddy length scale downstream of reattachment. The reattached shear layer then exhibits a slow non-monotonic return to a conventional turbulent boundary layer.

There is insufficient experimental data at present to determine the Reynolds number dependency of these flows. The free shear layer can be expected to become turbulent very soon after separation as discussed in a previous section and therefore the reattachment process can be assumed to always be a turbulent one. Consequently, the separation bubble length is only likely to be weakly dependent on Reynolds number. The reattachment length is the single most important length scale that describes the flow pattern and Newman & Tse (1992) found this to be independent of Reynolds number at a value based on chord of 2.5×10^5. Castro & Haque (1987) showed that except for the region very close to the wall below the separated shear layer, the flow was very nearly Reynolds number independent. This result was based on reattachment length and static pressure measurements at a freestream Reynolds number of 2.3×10^4. Tests carried out at various Reynolds numbers showed a decrease in skin-friction coefficient as the Reynolds number rose. However the static pressure and reattachment length showed very slight variation and at further increases in

Reynolds number showed undetectable changes. This indicated that bubble length was only dependent on Reynolds number below a critical value. Ruderich & Fernholz (1986) found the same insensitivity of bubble length above a value of $1.4x10^4$. The near wall region is the only part of the flow likely to be significantly influenced by viscous effects, and the changes in skin-friction coefficient occur there even when the Reynolds number is high enough to ensure insensitivity in the overall flow. Figure 2.21 shows flow visualisation results, for three different Reynolds numbers, taken over a normal plate to the flow with a downstream central splitter plate. As Reynolds number is increased, the pairing process of the spanwise vortices can be seen to become finer as the transition moves closer to the leading edge. At the highest Reynolds number, no defined vortex shedding can be seen. Westphal et al (1984) found that although the separating boundary layer was very thin, there was a surprisingly strong dependence of the separation bubble length on the boundary layer thickness. This agreed with the results of Bradshaw & Wong (1972).

Skin-friction measurements from the wall underneath the shear layer indicate that the thin boundary layer developing there has some "laminar-like" features. Castro & Haque (1987) have compared the skin-friction data from various experiments and found that the change in the value of C_f in the reattachment region is consistent with a laminar boundary layer. In addition they compared the data to a Faulkner-Skan laminar boundary layer solution for an imposed favourable pressure gradient appropriate to the freestream velocity variation. Experimental data showed evidence of a slightly stronger pressure gradient, but the computed results showed consistent features.

However, over the reattachment region of the shear layer the instantaneous skin-friction could have either sign. Data from Ruderich & Fernholz (1986) and Westphal et al (1984) showed that nowhere in the reverse flow region does the intermittency exceed 95%, where the intermittency is defined as the fraction of time during which the wall flow is in the upstream direction. A simple laminar boundary layer description is therefore too simple. Westphal et al. were also

able to collapse the intermittency data from a variety of reattachment lengths onto a single trend lending further evidence to the hypothesis that all separation bubbles are dynamically similar.

The energy added to the shear layer by the reverse flow region was suggested by Castro & Haque (1987) to be a form of "positive feedback". The fluid that passes upstream after reattachment will have increased energy levels when compared to the fluid forming the shear layer initially. Therefore, any fluid entrained in the shear layer will enhance the energy levels there. The limit to the amplification of the vertical component in this process is provided by the presence of the surface. The transverse velocity fluctuations can continue to rise but are prevented from rising too high relative to other components by the viscous interactions between all components. The implication of this feedback process is that it might force transition in the shear layer to always initiate close to the separation point. The turbulent fluid will cause this by either becoming entrained in the laminar shear layer or by simply disturbing it.

Simpson (1987) proposed that the fluid forming the backflow did not come from as far downstream as the mean streamlines suggest and that in fact the backflow is supplied locally. A thin separation bubble (low height to length ratio) will have a component of the backflow provided by the transport of large eddies from the shear layer and not from far downstream. As the bubble gets thicker and the shear layer moves away from the surface, more backflow comes from downstream and less from the large scale structures. These structures also transport the turbulence energy to the backflow from the outer flow by means of turbulent diffusion. This theory of large scale structures providing the backflow was supported by the inflections in the profiles for v_{rms} and u_{rms} in the backflow region. At the surface, because of the impermeability of the wall, $w_{rms} = 0$. To satisfy continuity, the fluid motions towards the wall must be deflected and contribute to streamwise and transverse motions. This would not be the case if the flow had come from far downstream. These inflections were not seen downstream of reattachment where the boundary layer relaxes.

2.5.3 Conclusions from the Literature Review on the Turbulent Shear Layer Bounding a Recirculating Region

- The stabilising effect of streamline curvature is weak compared to the effect of entrainment at the low-velocity edge of the shear layer of turbulent fluid returned there after reattachment. Streamline curvature tends to reduce the shear stress and turbulence intensity. In contrast, the reverse flow region effectively increases the velocity difference across the shear layer which has the effect of increasing both shear stress and turbulence intensity.

- A feedback process has been proposed for the entrainment of turbulent fluid in the shear layer. This feedback may cause transition in the shear layer to always initiate close to the separation point.

- A common feature in this type of flow is a low frequency component thought to be associated with a flapping of the shear layer bounding the recirculating region and the associated periodic shedding of a vortex downstream.

- Large eddies created in the shear layer have been shown to break apart upon reattachment, resulting in a decrease in turbulent shear stress downstream.

- There is evidence that the external flow (including the reattachment distance) is only sensitive to a change in Reynolds number below a certain limit. In contrast, the reverse flow region shows a dependency across the full range of Reynolds number tested.

- Wall skin friction measurements have shown the reverse flow boundary layer to demonstrate "laminar like features" (Castro & Haque 1987).

2.6 Conclusions from Previous Work and Objectives of Present Study

The literature review has revealed several unanswered questions regarding the features of different types of separation bubble. The objective of this thesis is to provide further understanding of the thin aerofoil bubble, formed behind the sharp leading edge at incidence, which was seen to be incomplete from previous work. A physical and quantitative description of this two-dimensional thin aerofoil bubble is required to clarify the mechanisms controlling the bubble and aid in the development of computational modelling. The most pertinent features related to the present study are outlined below including the objectives of the present work.

- Current computational models have only recently modelled short separation bubbles successfully. The development of models for the thin aerofoil bubble have been hindered by the limited experimental data available for correlation.

Accurate experimental data, particularly velocity and pressure measurements, is provided to support the development of computational models.

- The generally accepted definition for the length of the separated region, x_R, for two-dimensional flow is the location of either the zero time-averaged skin friction coefficient or the zero time-averaged streamwise velocity close to the surface. There have been a large variety of methods used to locate x_R (including qualitative flow visualisation), but it is not clear how well they correlate with each other.

The present study aims to define an unambiguous and repeatable measure of reattachment length, correlate this with other more common techniques (e.g. flow visualisation) and also to compare the results with previous relevant experiments.

- There is very limited data showing the effect of certain variables on the length of the thin aerofoil bubble. These variables include freestream Reynolds number, plate incidence and chord length. More specifically, in step flows and normal plate flows, the external shear layer bounding a recirculating region was observed to be independent of Reynolds number above a certain value. At the same time, the reverse flow region displayed a dependency on Reynolds number over the entire range measured and also exhibited laminar like features. It is not clear whether this dependency on Reynolds number occurs for a thin aerofoil bubble.

The effect of changes in incidence, chord length and Reynolds number on the structure of the thin aerofoil bubble is investigated. A wide range of Reynolds number is used to determine the behaviour of the thin aerofoil bubble. In addition, the reverse flow region is explored for any signs of laminar like flow to help establish the state of the reverse flow boundary layer.

- A low frequency component of the flow in reattaching turbulent shear layers has been measured and tentatively linked to the bursting of the separation bubble. It is not clear whether this component occurs in a thin aerofoil bubble flow.

Using the laser Doppler anemometer a full time history of the flow is measured and therefore, any periodic behaviour in the flow can be detected.

- Due to the previous lack of suitable instrumentation, little reliable data has been taken from within the reverse flow region of any separated flow. Consequently, little is known about the nature of the reverse flow boundary layer or the dead-air region near the leading edge.

With the use of laser Doppler anemometry, detailed velocity and turbulence information is gained within the reverse flow region with a high spatial resolution.

- To date, the effect of sweep on the behaviour and structure of the thin aerofoil bubble is not fully understood. In real flows, for example sails on

yachts, sweep exists and therefore future research should focus on a three-dimensional bubble.

A qualitative study is undertaken to isolate the main effects on the bubble structure caused by sweep in combination with changes of incidence. This provides a starting point for future investigations into sweep effects.

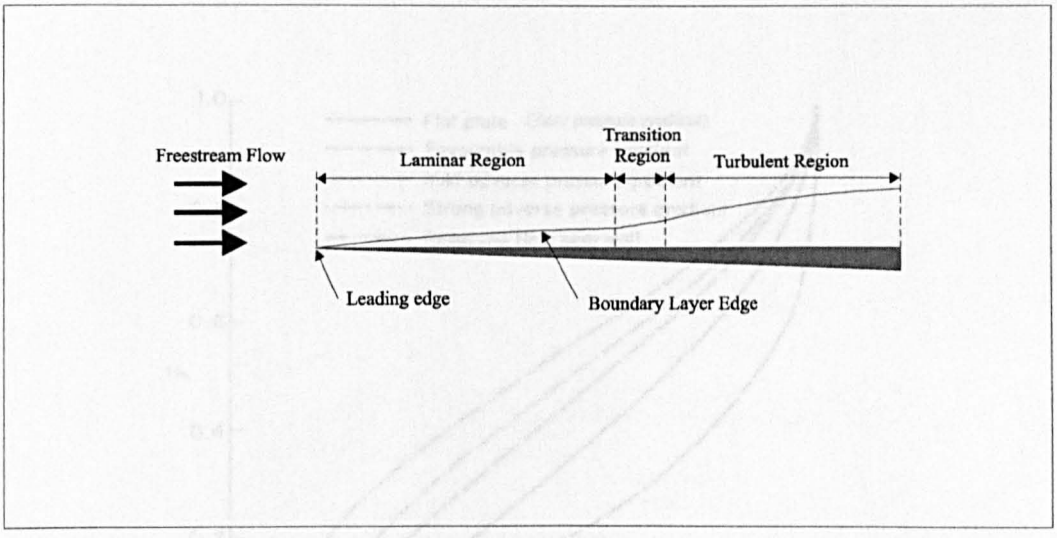

Figure 2.1 Main features of the boundary layer formed on a flat plate with zero pressure gradient.

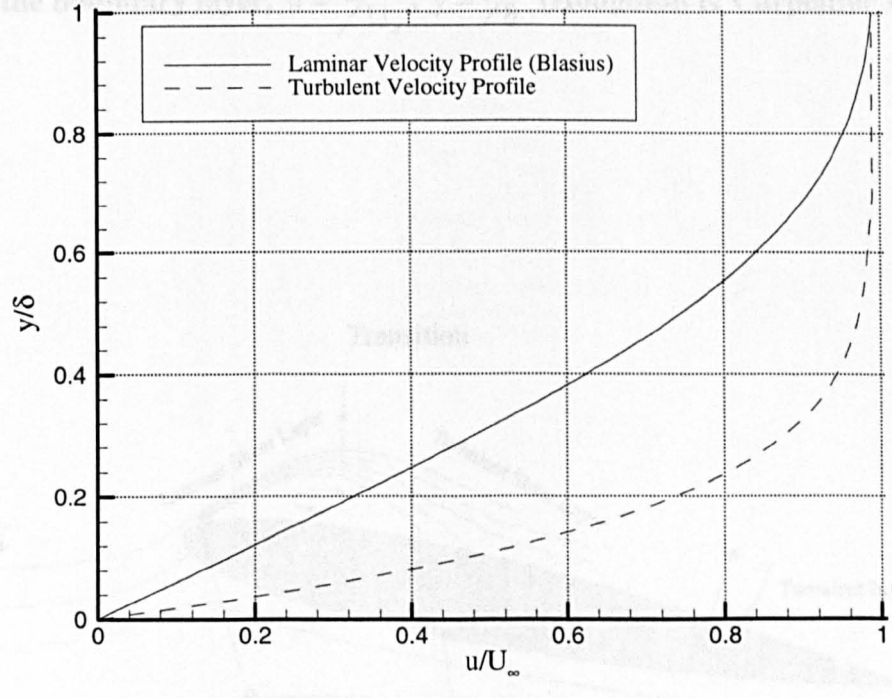

Figure 2.2 Typical velocity profiles in laminar and turbulent boundary layers.

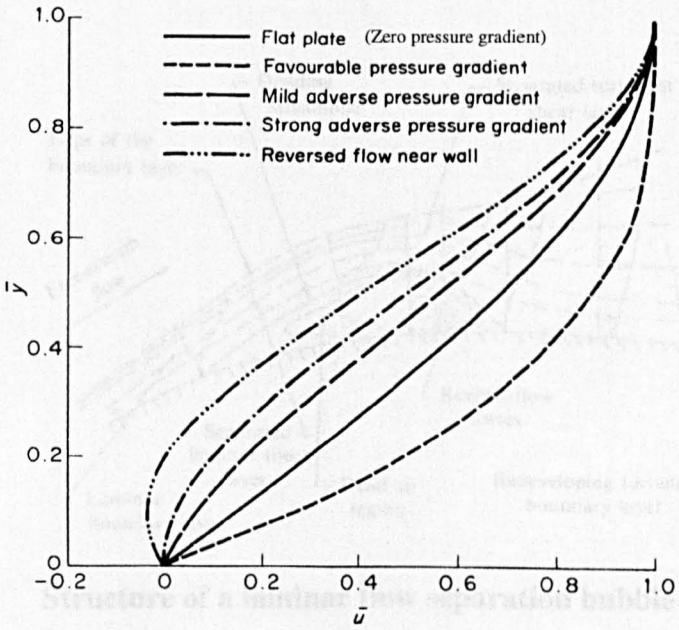

Figure 2.3 Effect of external pressure gradient on the velocity profile in the boundary layer, $\bar{u} = u/U_e$, $\bar{y} = y/\delta$ (Houghton & Carpenter 1993).

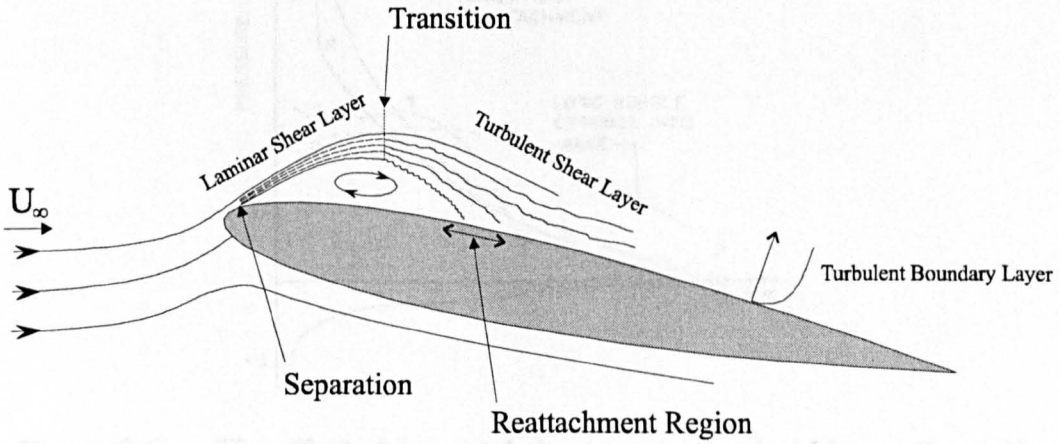

Figure 2.4 Simplified model of a laminar flow separation bubble on a rounded nose aerofoil (not to scale).

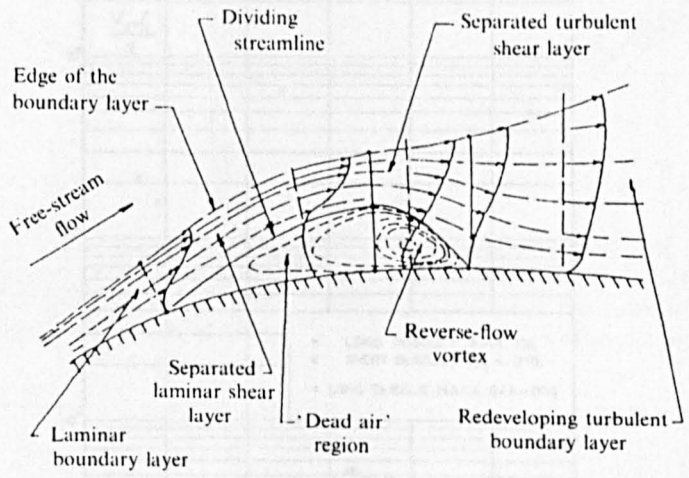

Figure 2.5 Structure of a laminar flow separation bubble (Horton 1969).

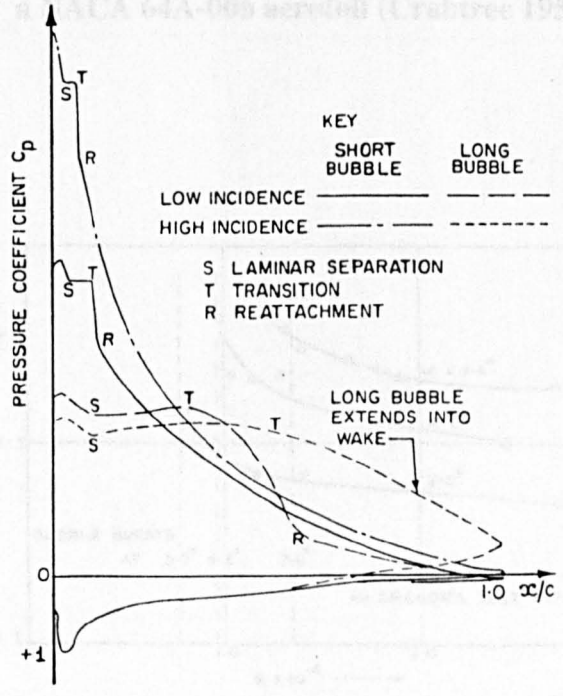

Figure 2.6 The effect of long and short separation bubbles on the static pressure distribution of an aerofoil (Ward 1963).

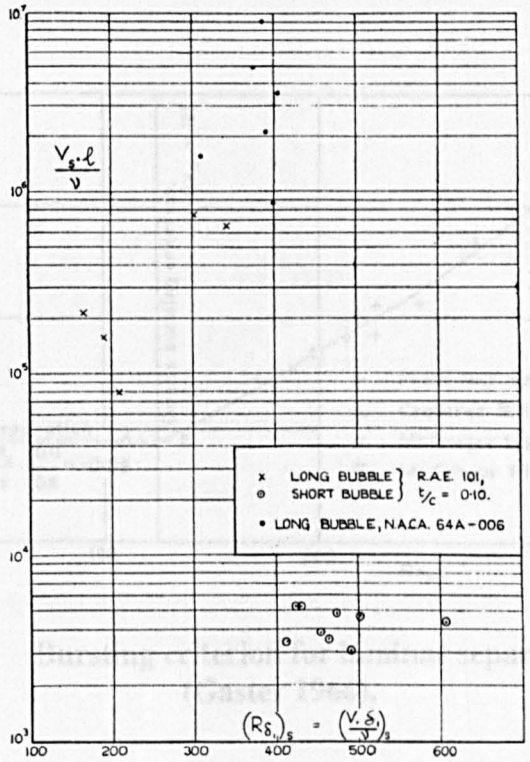

Figure 2.7 The two regimes of separation bubbles on a NACA 64A-006 aerofoil (Crabtree 1957).

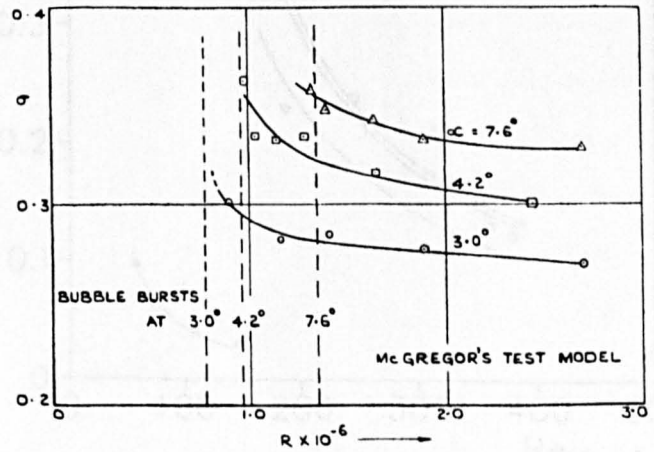

Figure 2.8 Variation of pressure recovery factor in short bubbles (McGregor 1954)

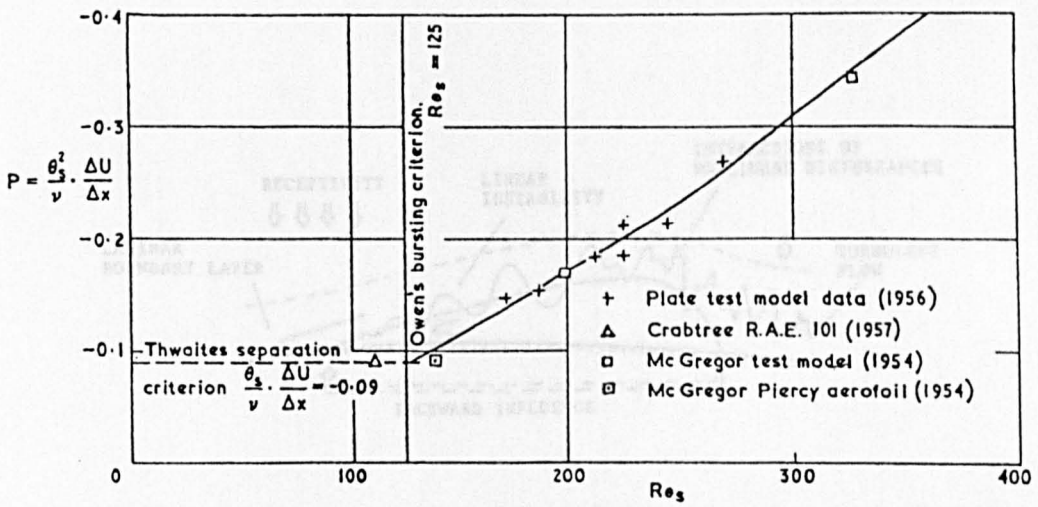

Figure 2.9 Bursting criterion for laminar separation bubbles (Gaster 1966).

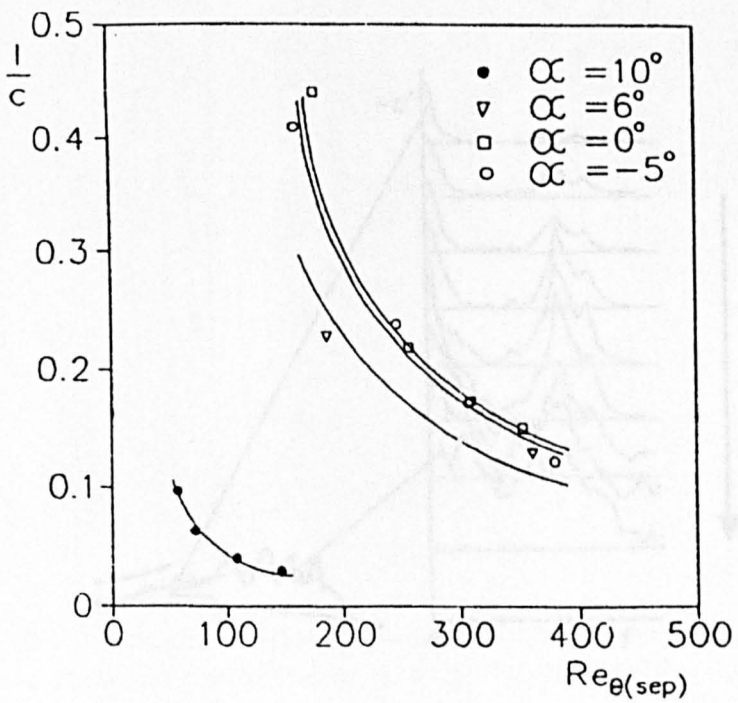

Figure 2.10 Relationship between laminar separation bubble length and Reynolds number at separation (Tan & Auld 1991).

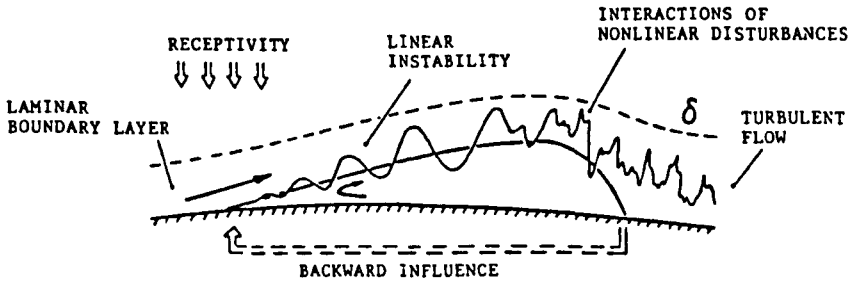

Figure 2.11 Instability and transition in a laminar separation bubble (Dovgal et al. 1994).

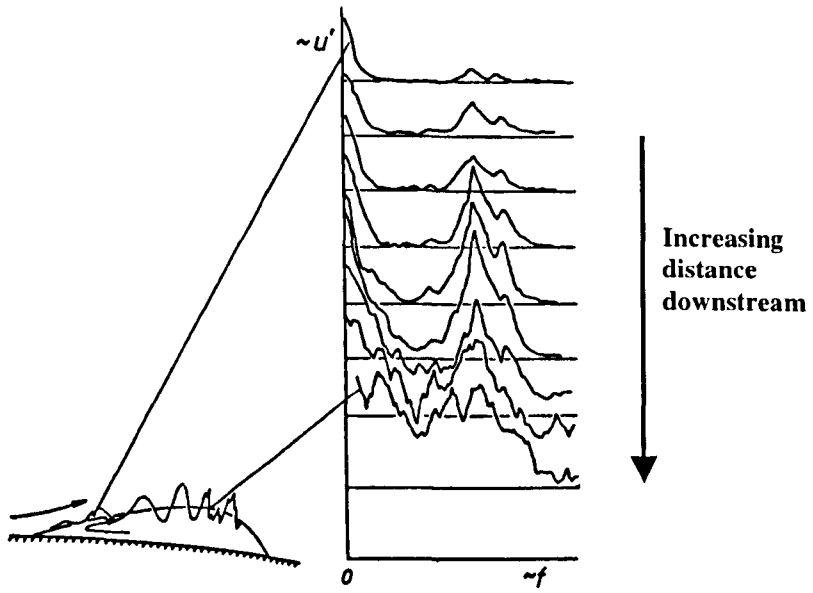

Figure 2.12 Spectra of disturbances in a laminar separation bubble (Dovgal et al. 1994).

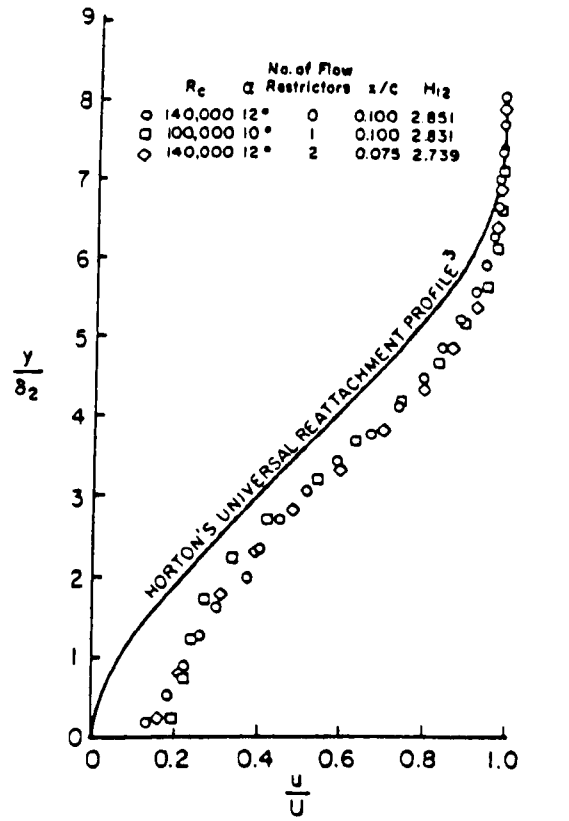

Figure 2.13 Examples of velocity profiles at reattachment compared to Horton's universal reattachment profile (Schmidt & Mueller 1989).

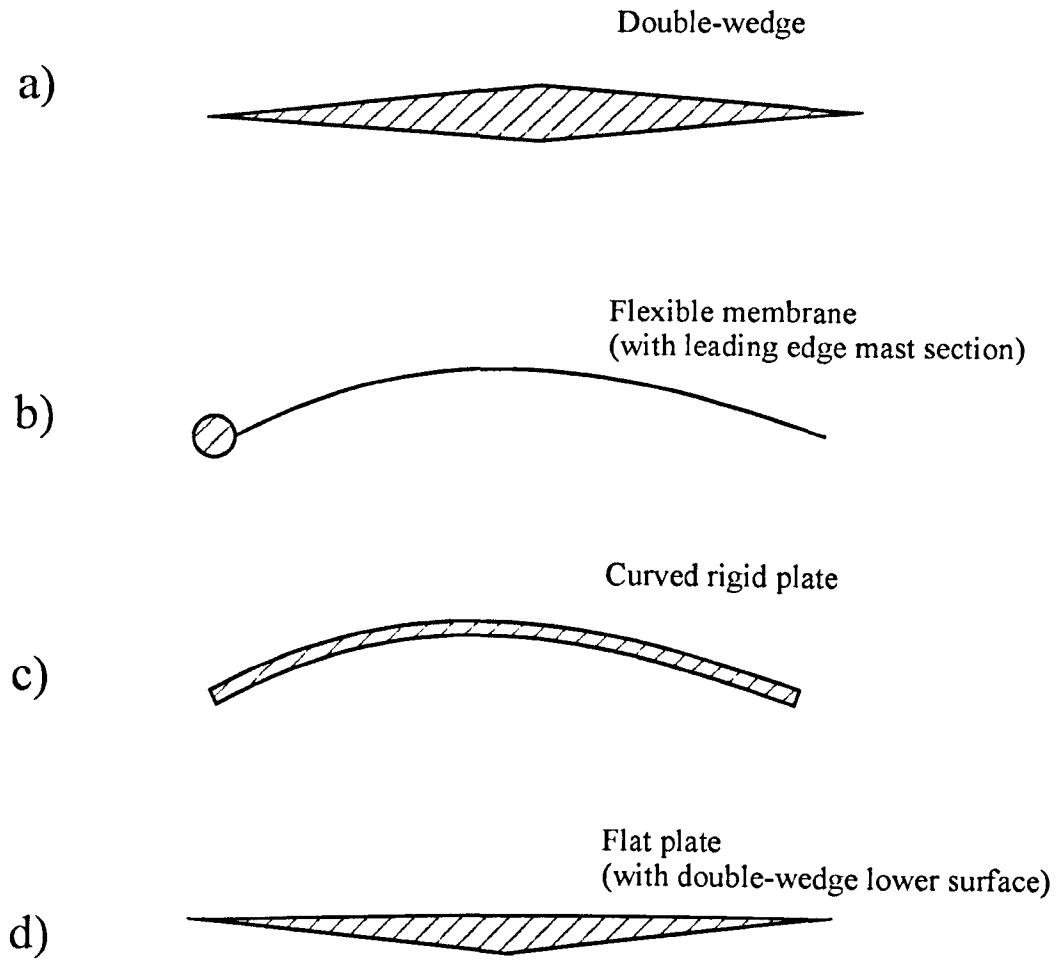

Figure 2.14 Typical section profiles which produce thin aerofoil separation bubbles.

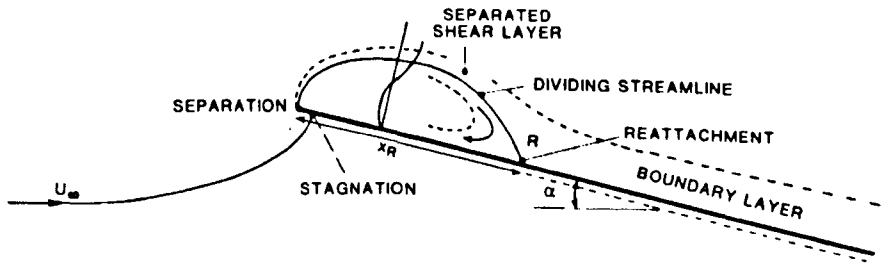

Figure 2.15 Simplified model of a thin aerofoil separation bubble (Newman & Tse 1992).

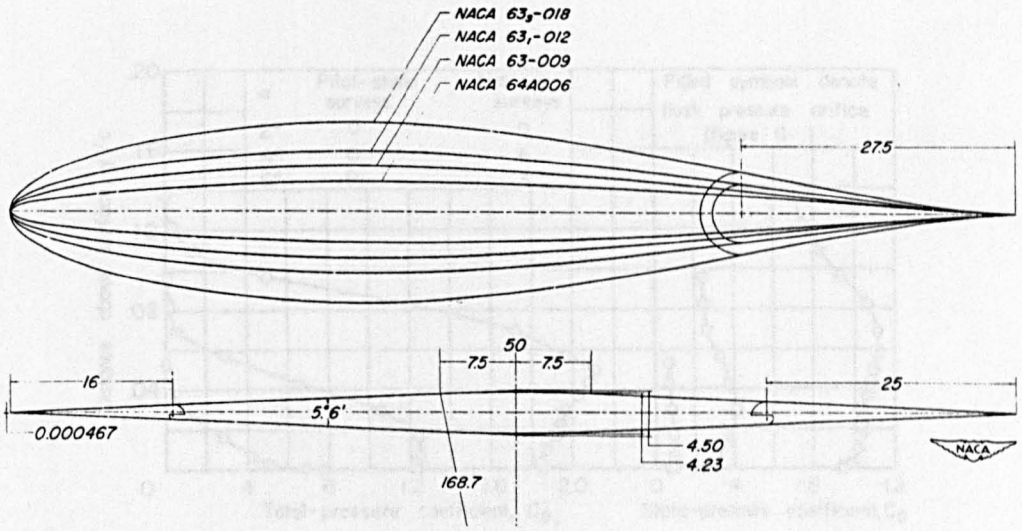

Figure 2.16 Profiles of the five aerofoil sections (McCullough & Gault 1951).

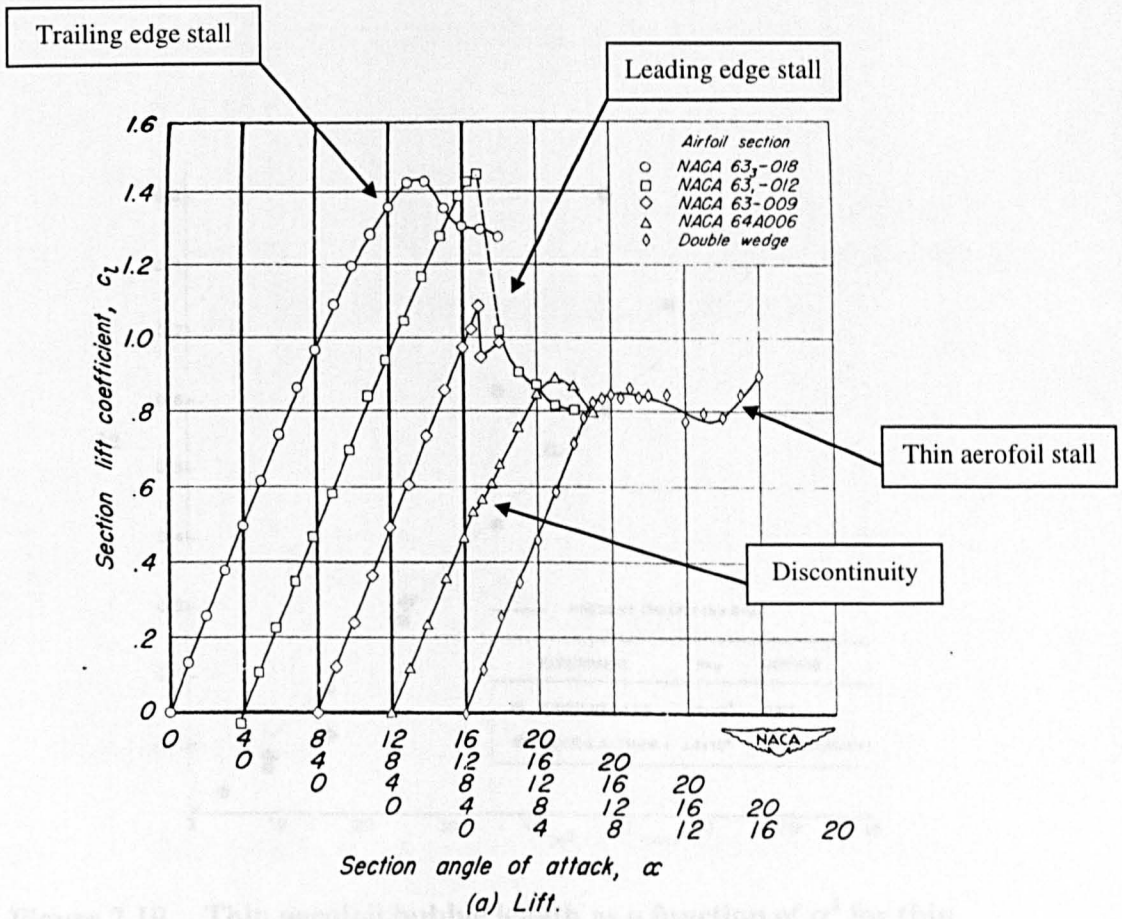

Figure 2.17 Lift curves for the five aerofoil sections above. Reynolds number=5.8x10^6. (McCullough & Gault 1951).

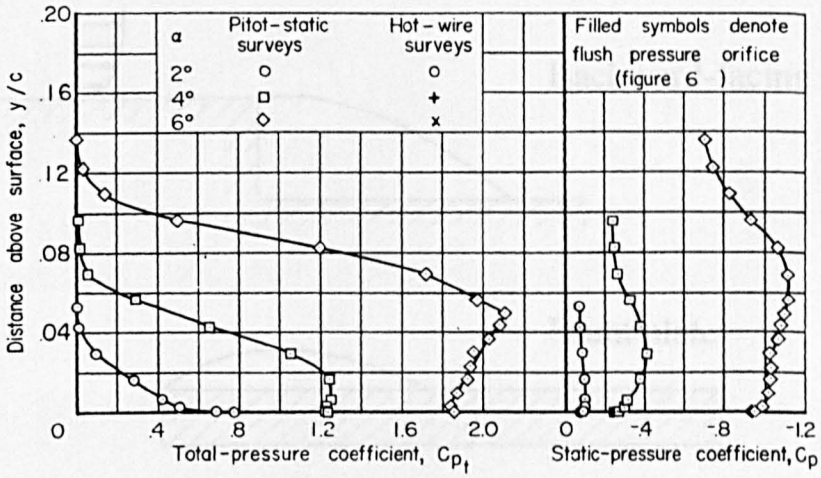

Figure 2.18 Pitot-static pressure profiles perpendicular to the surface through the thin aerofoil bubble. Chordwise location, x/c=0.3 (Gault 1957).

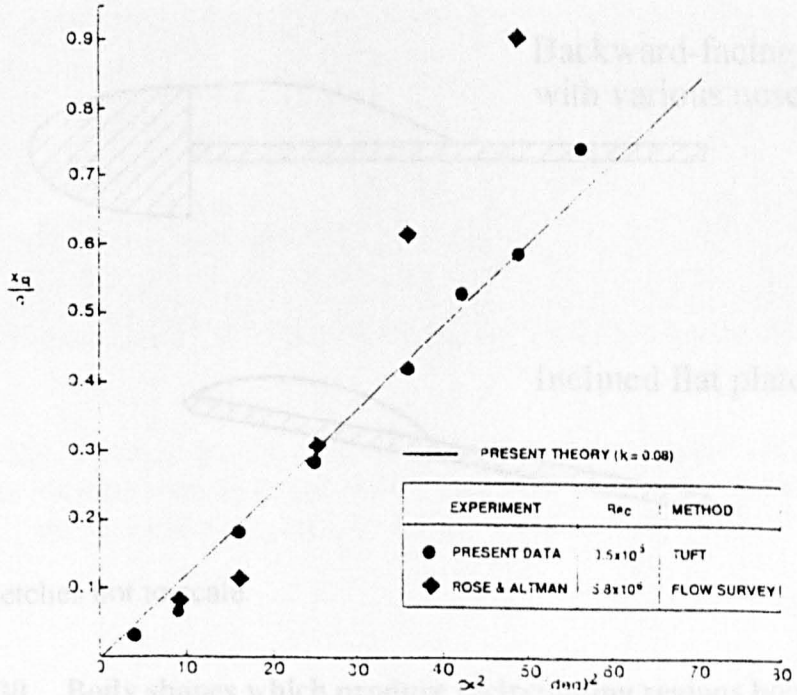

Figure 2.19 Thin aerofoil bubble length as a function of α^2 for thin double-wedge aerofoils (Newman & Tse 1992).

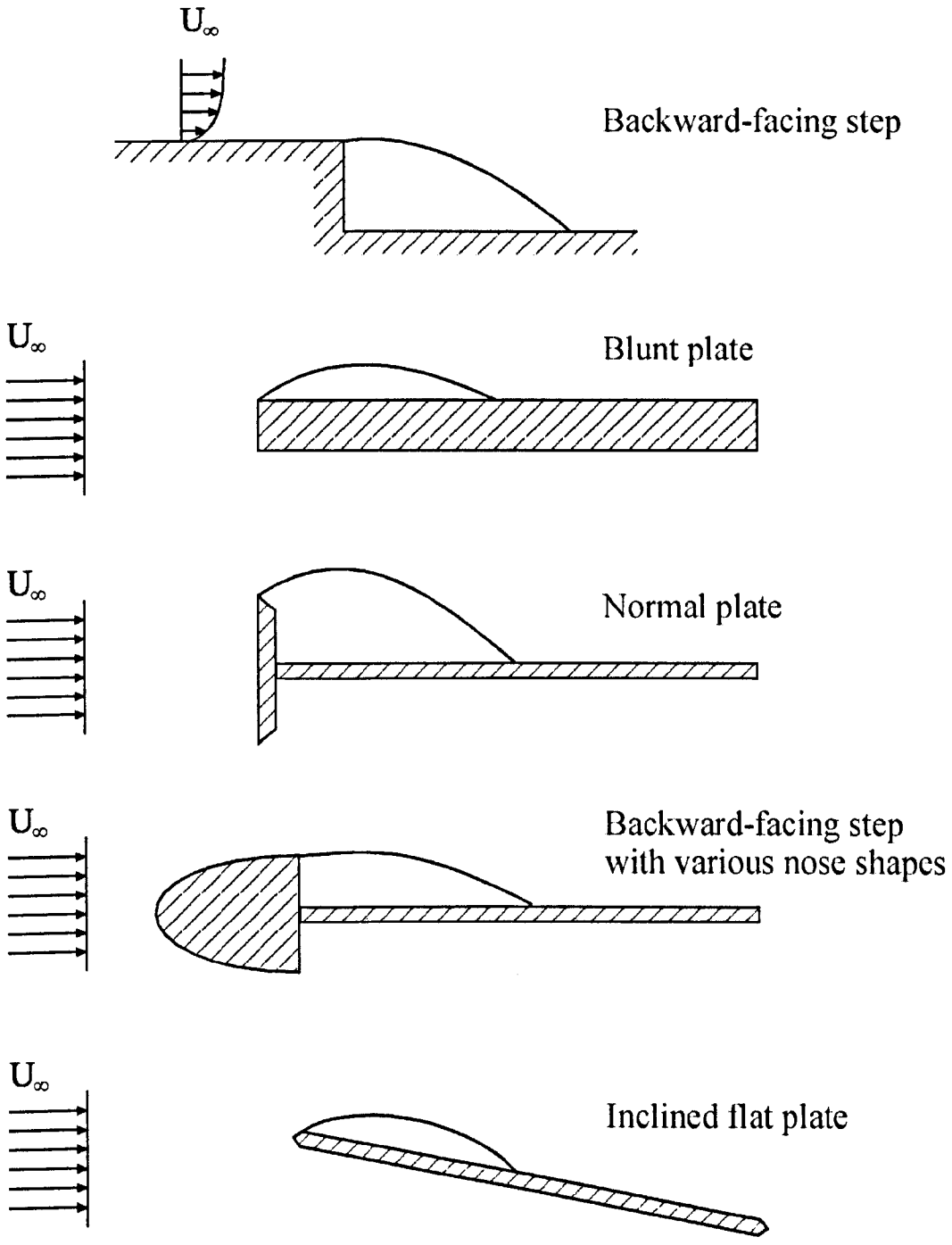

Sketches not to scale

Figure 2.20 Body shapes which produce recirculating regions bounded by a turbulent shear layer.

a)

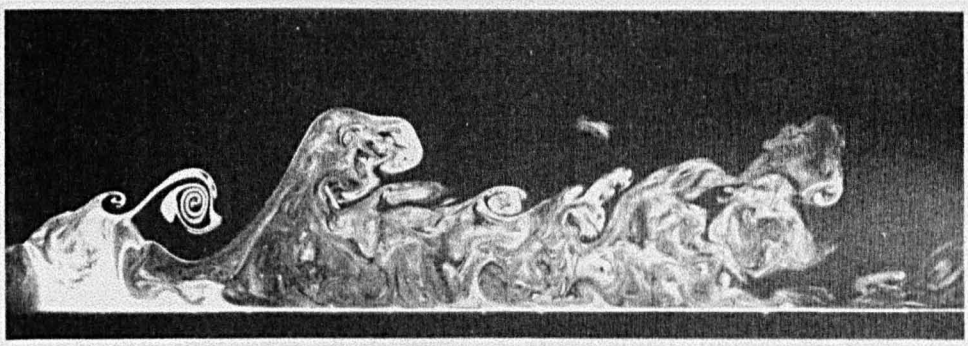

(a)

b)

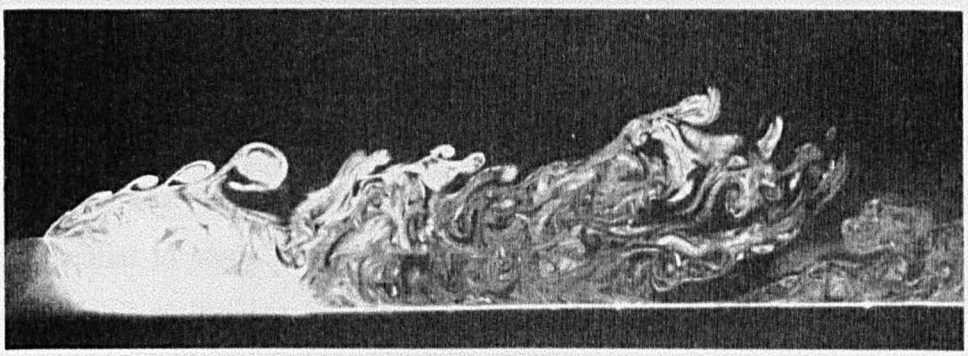

(b)

c)

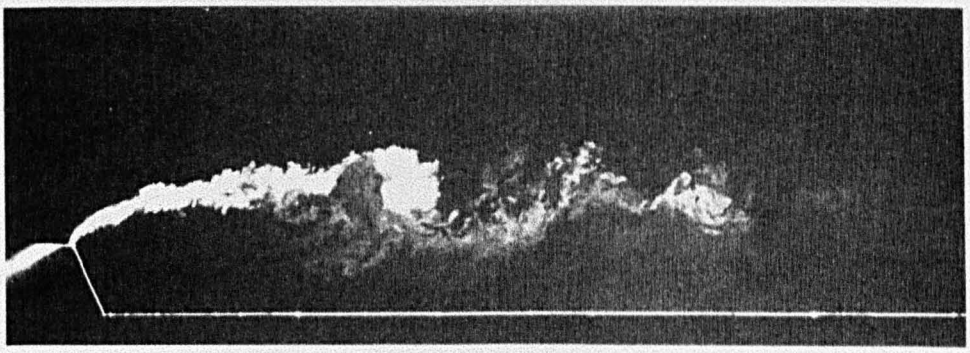

(c)

Figure 2.21 Smoke photographs of a separated shear layer at various Reynolds numbers: a) Re_{hf} $1.5x10^3$; b) $2.2x10^3$; c) $2.1x10^4$, h_f, half normal plate height. (Ruderich & Fernholtz 1986).

CHAPTER 3
PRELIMINARY INVESTIGATION

3.1 Introduction

The literature described in Chapter 2 highlighted important gaps in the understanding of thin aerofoil separation bubbles, opening up a number of avenues for further research. This chapter describes a preliminary test rig which was configured with the objective of establishing the important trends associated with the thin aerofoil bubble and developing appropriate experimental techniques. Due to a lack of existing data on separation bubbles of this type, it was essential to study a wide range of variables at an early stage. From the results of this preliminary investigation, the direction and focus of the continuing research, described in the main investigation, was formed.

3.1.1 Introduction to Experimental Configuration

The criteria for the initial plate design were based upon several conclusions from previous investigations, as highlighted in Chapter 2. The literature review revealed that most importantly, in order to form a thin aerofoil bubble a separation of the boundary layer at the leading edge is required. By ensuring a sharp radius at the leading edge this separation point is then fixed. Following recommendations by Jackson & Fiddes (1995), a rigid thin section was therefore chosen for the preliminary investigation described in this chapter. The formation of the bubble had been shown to first occur at very low incidences and typically, the bubble length, which increases with increasing plate incidence, to reach the trailing edge at an incidence of <7 degrees. With the absolute bubble length increasing with chord length, a 700mm chord length was therefore chosen to produce a bubble length which would allow a detailed investigation. At this

early stage it was not clear whether a small bubble would prove to be inhibitive for detailed study.

The tests were carried out in the University of Bristol low turbulence wind tunnel, which is described in detail in Section 4.2.1. The flat plate used was made from rolled aluminium plate and had dimensions 0.8m x 0.7m (span x chord). The leading edge was chamfered on the lower surface at 20 degrees to the horizontal to produce a sharp leading edge. The plate had a thickness to chord ratio of 1.9% which was sufficient to allow a set of pressure tapping lines to be run internally. The plate contained 35 pressure tappings (0.9mm internal diameter brass tube) in a chordwise line located at a quarter span, exiting at the trailing edge where silicone tubing connected the individual tubes to a scanivalve and pressure transducer system. Details of the plate design and support brackets used in the preliminary investigation are shown in Figure 3.1. The coordinates of the pressure tappings are shown in Appendix A and the details of the scanivalve and associated software are described by Eustace (1999).

The plate was mounted in the working section of the wind tunnel with the spanwise axis horizontal; the plate support brackets were attached, via a support pin passing through the tunnel walls, to a mounting bracket on the outside of the working section. The external mounting bracket and support pins system was common to the main investigation and this is therefore described in more detailed in Section 4.4.3. The rear central mounting consisted of a vertical lead screw which passed through a hole in the plate, fixing to the tunnel floor, thereby enabling a change of incidence to be applied through turning of the lead screw. The general layout, with key dimensions, of the experimental set-up is shown in Figure 3.2.

3.1.2 Introduction to Preliminary Investigation

All velocity measurements were taken using a Dantec 3-component laser Doppler anemometer (LDA); this technique is described fully in Section 4.3. In simple terms, the LDA is an optical measuring device capable of accurately measuring velocity at a single point in space. The measuring point is defined by the intersection of laser beams which are projected through a window into the wind tunnel. The optic heads, which project the laser beams are located on a traverse mechanism outside the tunnel and can therefore move the location of the measuring point. The output format of the LDA is based on statistical velocity information (mean, root mean square etc.) which can be presented directly or further processed depending on the requirement of the user. Tests were carried out at Reynolds numbers, based on chord, of between 0.6×10^6 and 1.0×10^6.

The preliminary investigation, described in this chapter, consisted of four main sections. Firstly, the overall structure of the separation bubble was investigated in order to establish the main flow regimes present; this included a detailed study of the flow close to the leading edge. Secondly, the effect of changes in incidence and Reynolds number on the separation bubble length was investigated. Thirdly, the suitability of the experimental set-up was assessed, concentrating on the suitability of the experimental measurement techniques for the main investigation, but also including a consideration of tunnel wall boundary layer interference. Finally, the integral boundary layer properties were determined for both the separation bubble and the region downstream of reattachment.

From this preliminary investigation a modified plate and support rig was designed, enabling the main investigation, described in Chapter 5, to develop and concentrate on the key areas of interest highlighted by the results from this chapter.

3.2 General Bubble Structure

The initial objective was to survey the mean and fluctuating velocity components in a chordwise plane of data points perpendicular to the plate, encompassing an entire separation bubble. The plate was set to an incidence of 2 degrees, an angle chosen, and confirmed by basic flow visualisation with a wool tuft, to give a bubble length terminating at around a quarter chord.

At this stage the main structural features of the separation bubble were undefined. Consequently, a coarse grid of data points was used to gain an overview of the flow (typically >20mm chordwise increments and >1mm increments normal to plate). The objective was to use the LDA to identify the bubble length, areas of reverse flow and regions where steep velocity gradients existed. This necessitated a higher density of data points perpendicular to the plate. Figure 3.3 and 3.4 show the contour plots of the mean and root mean square (rms) chordwise velocity components respectively. The data plane was taken at 3/8 span where the flow was assumed to be planar. Several main features of the separation bubble structure were clearly revealed by these plots:

- The length of the separation bubble was approximately $x_R/c=0.17$ (non-dimensionalised with respect to the plate chord length). The reattachment point was defined as being "the chordwise location at which the velocity gradient perpendicular to the plate at the surface is zero". This was interpreted for practical purposes as the chordwise position with zero mean chordwise velocity at the closest measurement location to the surface (typically around 0.05mm).
- A region of very steep velocity gradient, identified by the close spacing of the velocity contour lines, was found close to the leading edge with the contour lines diverging downstream.
- A reverse flow region was found within the bubble, extending from the leading edge to the reattachment point, reaching a maximum height of 4.2%

of x_R, the separation bubble length. The peak velocity in the reverse flow region was found to be $u/U_\infty = -0.35$. It is important to note that the contour plots do not show the features in full detail but rather formed a preliminary survey. The detailed individual velocity profiles seen later in Figure 3.5 show better the steepness of the velocity gradient across the shear layer.

- Transition in the shear layer was shown to occur at some distance downstream of the leading edge, identifiable by a marked increase in the rms component of velocity. Figure 3.4 shows evidence of high chordwise rms in the shear layer starting in the region 1-4% chord length from the leading edge and this indicated the transition region (the exact location of transition is shown more clearly in Figure 3.9). A region of stable flow with low chordwise rms, close to the surface in the front portion of the bubble was also identified.

The initial contour plots contained "jagged" contour lines in regions of steep velocity gradients, predominantly close to the leading edge. It became clear that measurements needed to be taken at a greater spatial resolution, particularly perpendicular to the plate, in order to describe the velocity gradients more accurately. Therefore, to refine the number of data points most efficiently, a graduated mesh spacing of data points was required to be generated, providing a higher density of data points in areas of high velocity gradient.

Figure 3.5 shows the velocity profiles (perpendicular to plate) of the mean chordwise velocity component at various chordwise distances from the leading edge. A much reduced increment of 0.2mm perpendicular to the plate was used resulting in smooth velocity gradient data. The profiles show how the separation bubble acts as an effective camber to the outer inviscid flow, with the maximum velocity occurring just above the viscous region corresponding to the separation bubble. Further away from the surface, the velocities approach that of the freestream value asymptotically. The maximum velocity gradient, measured

across the shear layer, perpendicular to the plate was shown to be $12ms^{-1}/mm$ at a chordwise location of x/c=0.03.

Static pressures were measured chordwise along the plate for various angles of incidence. The resulting static pressure coefficients are shown in Figure 3.6. The representative distributions for negative angles of incidence are included to provide an indication of the distributions along the lower surface of a flat plate. It can be seen that unlike an aerofoil with a rounded leading edge, where the flow remains attached and a high pressure peak is sustained, the pressure peak at the leading edge collapses because of the separation and a pressure "plateau" of approximately constant pressure forms instead. Downstream of this plateau there exists a steep adverse pressure gradient up to and beyond reattachment followed by a near zero pressure gradient continuing to the trailing edge. Static pressure coefficients very close to the leading edge were unobtainable because of the leading edge chamfer, the nearest pressure tapping being 10mm from the leading edge.

In Chapter 2 it was reported that for a short separation bubble, the transition region was associated with the onset of the adverse pressure gradient (Gault 1955). In Section 3.3, it is shown that transition actually occurs much closer to the leading edge than this (<1% x/c). This result indicates that the constant pressure region for the thin aerofoil bubble is occurring along a turbulent shear layer and the onset of the adverse pressure gradient is not associated with transition. Based on the reattachment length defined earlier for the 2 degrees plate incidence case ($x_R/c=0.17$), it was found that reattachment coincided closely with the inflection point of the adverse pressure gradient. With further increases in incidence, the pressure plateau forms more of a "humped" profile and the adverse pressure gradient becomes less steep. The hump is possibly due to the significant reverse flow velocities close to the surface and to the curvature of the shear layer. Above 5 degrees, the overall pressure gradient flattens and does not increase in magnitude with further increases in incidence. At this point,

the reattachment point has reached the trailing edge and any further increases in incidence will result in a bubble that fails to reattach to the plate.

3.2.1 Suitability of Laser Doppler Anemometry

One aspect of the preliminary investigation was to ascertain the performance of the LDA at measuring in this type of flow. This technique, described fully in Section 4.3, relies on smoke particles (seeding) crossing the measurement point, where essentially each particle corresponds to a velocity sample. In a fluctuating flow, the mean velocity is based on the average of any number of samples, with a higher population size giving a more accurate mean. Previous investigations suggested the presence of dead-air regions within the separation bubble resulting in a considerably reduced density of smoke particles. Without sufficient seeding, the "data rate" (number of samples measured per second) might therefore be too low to provide valid measurements (if the real time response of a flow is to be resolved, a data rate of approximately 2π multiplied by the frequency of interest is required). A sufficient data rate was therefore key to the success of this investigation.

The preliminary study showed, indeed, that data rates were very high (>6kHz) in most parts of the flow with the exception of the recirculating region close to the leading edge. Within this recirculating region a maximum data rate of approximately 600Hz was achieved, this proved adequate for real-time analysis but, in order to maximise the accuracy of the mean and turbulence velocity information, required a longer sampling time. To compensate for this, the sampling time outside of the recirculating region could be reduced. The reason for the data rate being as high as this in the recirculating region is described in Section 4.3, but is essentially down to excellent alignment of the optics. This also ensured a much smaller measurement volume, and this together with the 0.005mm vertical resolution of the traverse ensured that a considerable number

of points could be defined within the bubble. With the additional advantage of directional unambiguity, the LDA proved itself to be ideally suited to this application.

3.2.2 Effect of Tunnel Wall Boundary Layer Interference on the Separation Bubble

From an early stage, it was important to assess the effect of the tunnel walls on the flow. There was likely to be wall interference effects caused by the junction of the plate tips and the wall and the usual boundary constraint effects (discussed in Section 5.5.1). The two-dimensional nature of the flow was therefore investigated using a pseudo-visualisation technique involving the LDA. By taking a survey of velocity very close to and in a plane parallel with the upper surface, a close indication of the surface flow could be examined quantitatively. For this investigation, the plate incidence was set to 3 degrees and data was measured in an XY plane 5mm above the surface. Initially the junctions between the plate and the tunnel wall were not sealed, allowing air to pass from the lower to the upper surface, driven by the pressure difference between the two. With reverse flow close to the surface along the length of the separation bubble, this "blown" air had the effect of reducing the length of the separation bubble near the plate ends. Consequently, the separation bubble length was constant across only the central 40% of the plate span. To improve this, the gaps between plate and tunnel wall were sealed and the result of this change can be seen in Figure 3.7. The separation bubble length was now constant across the central 60% of the span, with a much smaller decrease in its length at the plate ends (in the main investigation, a smaller chord length plate was used and that increased the planar region to 80% of the span for 3 degrees incidence). The presence of the solid surface at the plate ends and the boundary layer on the tunnel walls were responsible for the continued lack of planar flow at the plate ends despite the modification. Although the use of large end plates has been shown previously to

give a greater proportion of planar flow in similar experiments, Newman & Tse (1992), this approach would not have been readily compatible with the use of laser anemometry. Similarly, any form of suction to remove tunnel wall boundary layers would have interfered with the optical access required. Providing a seal between the plate and walls was therefore the preferred solution, and 60% proved more than adequate for a preliminary investigation.

3.3 Structure of Shear Layer Close to the Leading Edge

The area of flow at the front of the short separation bubble, underneath the constant pressure region, had, in previous investigations, often been described as a region of stagnant air. It was, however, unclear how the structure of the short bubble compared with that of the thin aerofoil bubble. In this investigation, significant reverse flow continued all the way to the leading edge. However, the velocity profiles taken near the leading edge, shown in Figure 3.5, revealed a small region of forward chordwise flow close to the leading edge within the recirculating region of the separation bubble. Further investigation showed this to be a separation of the reverse flow boundary layer 8mm from the leading edge creating a rotation of fluid in a direction counter to the main recirculation in the bubble. Figure 3.8 shows this "secondary separation bubble" to be approximately 1-2mm in height and 6mm in length. The cause and effect of this smaller bubble were not immediately apparent but the direction of rotation implies that it is driven by the main recirculation in the separation bubble rather than by the shear layer (the rotation of the secondary bubble counters the flow direction of the shear layer).

The onset of transition in the shear layer is clearly shown in Figure 3.9, illustrated by the rapid increase in chordwise rms velocity. This can be seen to increase rapidly from about 5mm (x/c=0.007) from the leading edge. Upstream of this, within the laminar shear layer, instabilities were displayed in the flow.

This was evident from the double-peaked velocity histograms taken from the laminar region and shown in Figure 3.10. The double peak signifies a periodic behaviour of the flow and this was only present in advance of transition. Downstream of this, the periodic structure broke down implying that the shear layer had become fully turbulent.

The instability of 2D mixing layers is well documented; in the absence of a solid surface, there is a lack of viscous damping, allowing instabilities in the shear layer to be amplified much more readily. This instability is most likely to be related to the classic Kelvin-Helmholtz type, which is discussed in detail by Drazin & Reid (1981). They considered the shear layer to be a simple vortex sheet and showed that by imposing a small disturbance to the sheet so that the displacement is sinusoidal, the induced velocity will tend to cause an amplification of the sinusoidal displacement. This will grow exponentially, maintaining the displaced shape, as long as the initial disturbance is small enough. Eventually, the sinusoidal shape will break down signifying the onset of turbulent flow. With this mechanism present in the shear layer, it is seen intuitively that the distance from the leading edge to the onset of transition will be dependent on the Reynolds number of the flow. Increasing the Reynolds number should move the onset of transition closer to the leading edge, although the effect of this on the separation bubble length is unclear at this stage.

3.4 Effect of Plate Incidence and Reynolds Number on the Separation Bubble Length

The length of the separation bubble is likely to depend on many variables including leading edge geometry, chord length, incidence and Reynolds number. Due to the fact that separation is fixed by the sharp leading edge, it is expected that the influence of the leading edge geometry will be removed as a variable.

For a thin double-wedge aerofoil, Newman & Tse (1992) showed that the bubble length was proportional to the square of the angle of incidence and was independent of changes in Reynolds number. The present plate has a flat upper surface and so the relationship between bubble length and plate incidence is expected to be more linear than for a double-wedge, where the rate of change of bubble length will be affected by the change in gradient at the mid point of the upper surface.

The effect of the two variables, plate incidence and Reynolds number, on the separation bubble length were first investigated, in the case of the latter by varying the freestream tunnel speed. The incidence of the plate was initially set with an inclinometer and, when the tunnel was running at the test speed, checked by using the LDA traverse, which had itself been levelled.

Figure 3.11 shows the separation bubble length against plate incidence for three different tunnel speeds. The separation bubble length increases with an increase of incidence. However, the exact relationship is not clear from the limited sample size. The thickness of the plate and the leading edge chamfer give the plate a slight camber, hence a small bubble is produced at zero incidence (referenced to the upper surface). The incidence at which the bubble first forms is very difficult to determine from Figure 3.11, therefore no correction was made at this stage but the effect is discussed more fully in Section 5.4.

The effect of changes in Reynolds number proved inconclusive, with there being no significant variation of bubble length over the range of Reynolds number measured.

3.5 Boundary Layer Integral Properties

In order to determine the boundary layer integral properties, the standard expressions, defined in Section 2.2.6, were applied to the series of seven detailed velocity profiles, shown in Figure 3.12. These were measured perpendicular to the plate, at various distances downstream of the leading edge, and for a plate incidence of 2 degrees.

Figure 3.13 shows the development along the plate of the displacement thickness, momentum thickness and shape factor. The displacement thickness grows rapidly and reaches a maximum at approximately half the bubble length and then decreases as the flow relaxes along the plate. It is clear from the velocity distributions that the separation bubble has a large displacement effect on the freestream and the profile appears valid. This is confirmed in Chapter 6, using an inviscid solver on a model of the bubble.

Momentum thickness is slightly negative over the front portion of the bubble. It then grows rapidly around reattachment before levelling off as the boundary layer relaxes downstream of the bubble. The significance of this is discussed in more detail in Section 6.3. Finally, the shape factor shows a large variation over the length of the bubble until reattachment, where it drops sharply. As the shear layer reattaches, the boundary layer changes form to that of a conventional turbulent boundary layer and the shape factor responds accordingly reaching a value of approximately 1.3.

3.6 Conclusions from the Preliminary Investigation

The main structure of the separation bubble is composed of a large recirculating region of fluid. This is bounded on the upper edge by a shear layer which is initially laminar but becomes turbulent soon after leaving the leading edge (<1% chord).

A secondary separation bubble was found close to the leading edge rotating in a direction counter to the main bubble. Because the secondary bubble produces velocities on its upper edge which oppose the direction of flow in the shear layer, it will cause additional shear stress within it.

The laminar shear layer showed instabilities prior to transition thought to be of the Kelvin-Helmholtz type. Downstream of this, once the shear layer was fully turbulent, there was no evidence of any periodic instabilities. Similarly, at the reattachment point where the approaching flow bifurcates, there was no evidence of periodic unsteadiness.

Within the limited freestream Reynolds number range tested, the length of the separation bubble was primarily dependent upon the incidence of the plate. The bubble grows from its initial formation, at close to zero incidence, to a length equal to the plate chord at about 6 degrees incidence.

The technique of laser Doppler anemometry was proven to be very successful at measuring within this flow regime. In particular, the steep velocity gradients were measured with high spatial resolution and high sampling rates, resulting in well defined velocity profiles. The directional unambiguity of the LDA was shown to be vital for identifying reverse flow regions and in particular the very small secondary separation bubble.

The adverse pressure gradient over the rear half of the bubble is not established as a direct result of transition, as is the case for short bubbles, but is located over the region where the shear layer attaches to the plate. Transition was shown to occur very close to the leading edge.

A pseudo flow visualisation technique was used to investigate the effect of tunnel wall interference. A plane of velocity data, measured 5mm above the surface at 3 degrees plate incidence, showed that by sealing the plate ends to the tunnel walls, the reattachment length remained constant across 60% of the span, compared to 40% without sealing. This increases the validity of the assumption that the flow is two-dimensional.

3.7 Recommendations for Future Work and Limitations of the Preliminary Investigation

3.7.1 New Plate Design

Based upon the limitations identified in the preliminary investigation, the future plate and support rig design should satisfy the following criteria:

- Static pressure measurements are required closer to the leading edge than the preliminary study allowed, i.e. <10mm.
- Following the discovery of the secondary bubble which is linked to the reverse flow boundary layer, it is important for future measurements that the surface quality of the plate is improved. Steel would offer superior surface quality over the rolled aluminium and in addition would provide a stiffer plate for a given thickness, allowing the plate to be thinner hence reducing wind tunnel constraint effects.

- Two plates, with different chord lengths, would enable a wider range of parameters to be investigated, in particular the effect on bubble length of a variation in chord length and Reynolds number.
- The LDA proved very capable at capturing the flow features of a thin aerofoil bubble with approximate length 120mm. Therefore, a much shorter chord length should be used which would improve the two-dimensionality of the flow and reduce the effects of the tunnel constraint.

3.7.2 Future Investigation

The results from the preliminary work provided an excellent foundation on which to base the continued research. However, in addition to a more detailed investigation of velocity over a full range of plate incidences, the following points would need to be addressed specifically in any future work:

- The parameters which affect the length of the separation bubble must be established. A greater velocity range is therefore needed to determine the effect of Reynolds number and a variation in chord length is also required to provide further comparison.
- The secondary separation bubble requires further investigation. In particular, the mechanism for its formation and the effect that various parameters have on its size and shape should be established.
- To generate an inviscid model of the thin aerofoil bubble for computational analysis, more detailed measurements of the displacement thickness, obtained from accurate velocity profiles, are required.
- Flow visualisation techniques and computational methods should be correlated with the LDA and pressure results where possible.
- The effect of plate sweep on the thin aerofoil bubble structure should be investigated, forming the basis for a study into the three-dimensional separation bubble.

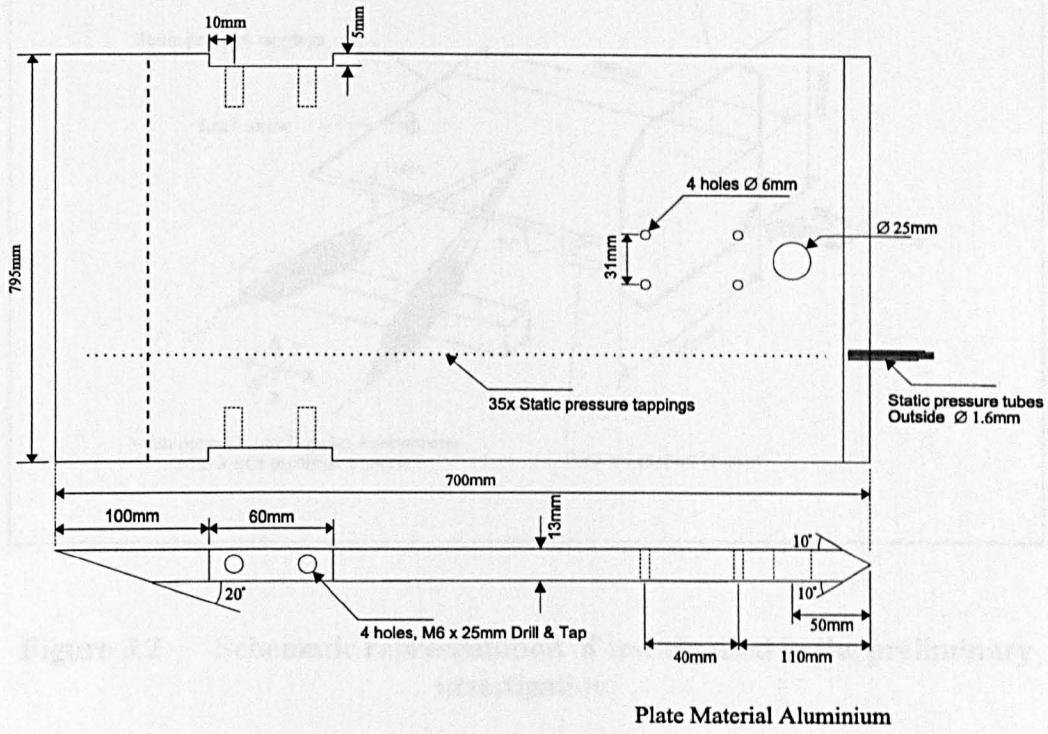

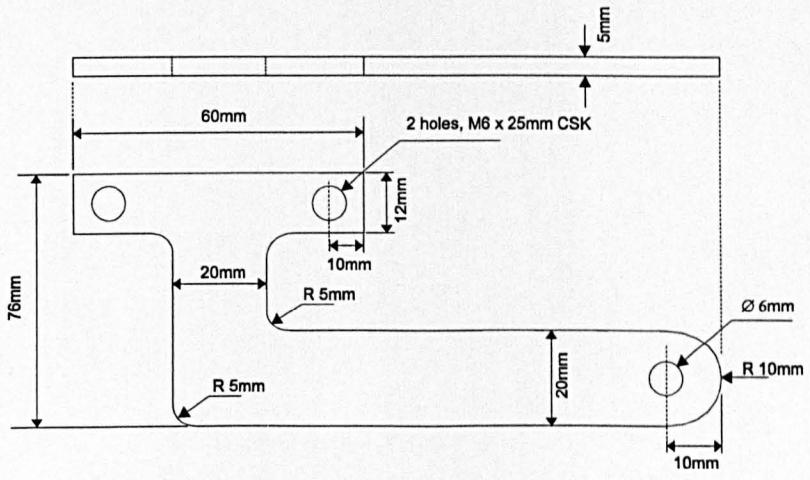

Figure 3.1 Details of plate and plate support bracket design used in the preliminary investigation.

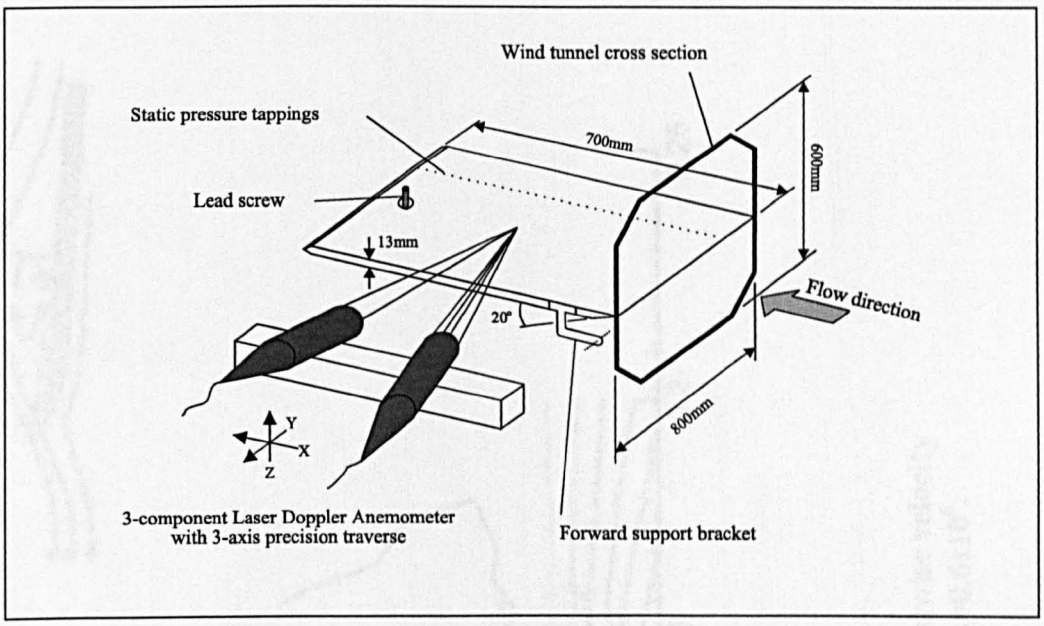

Figure 3.2 Schematic representation of test rig used in the preliminary investigation.

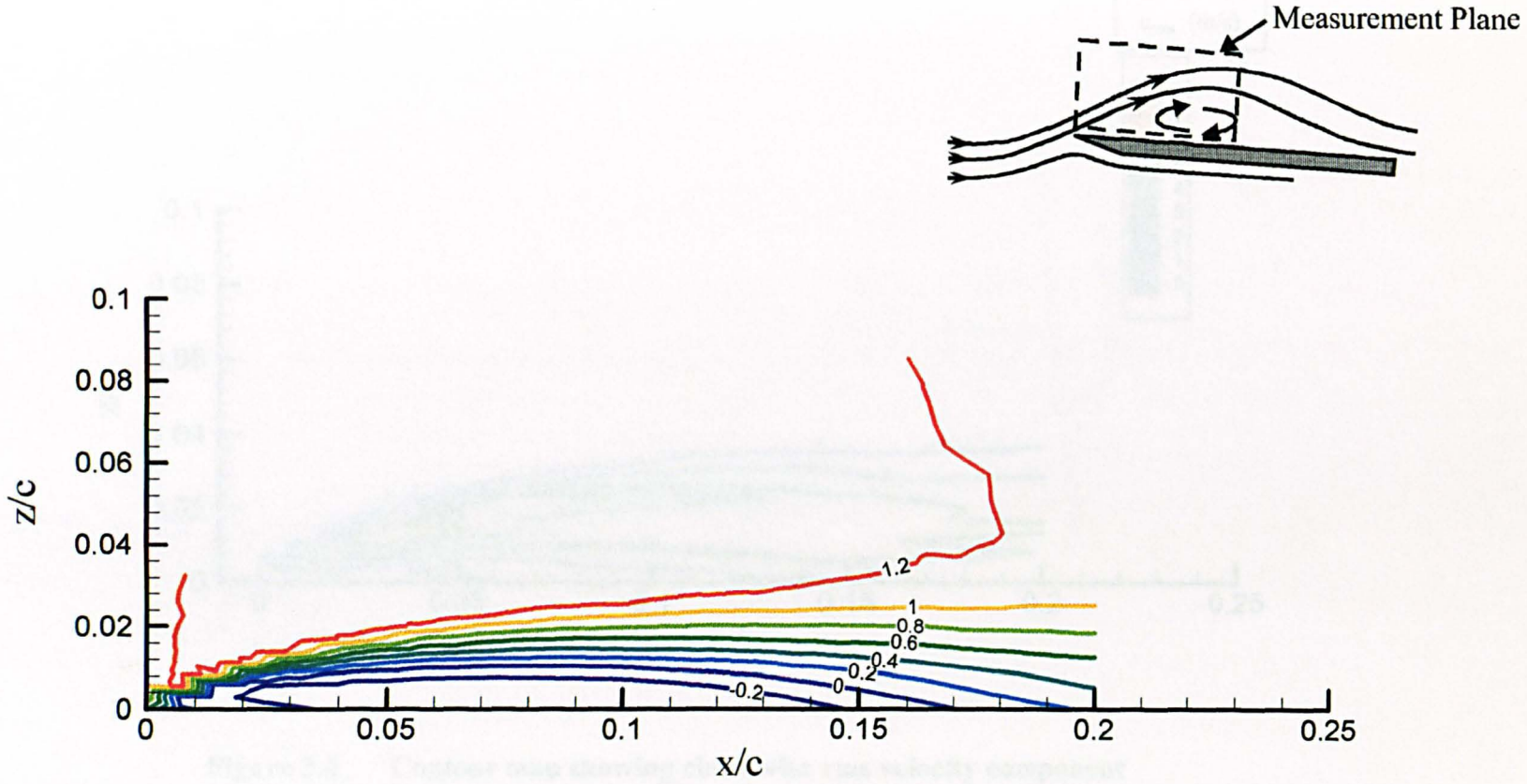

Figure 3.3 Contour map showing mean chordwise velocity component u/U_∞ for $\alpha=2°$, $U_\infty=12.5m/s$, $Re_c=0.6x10^6$.

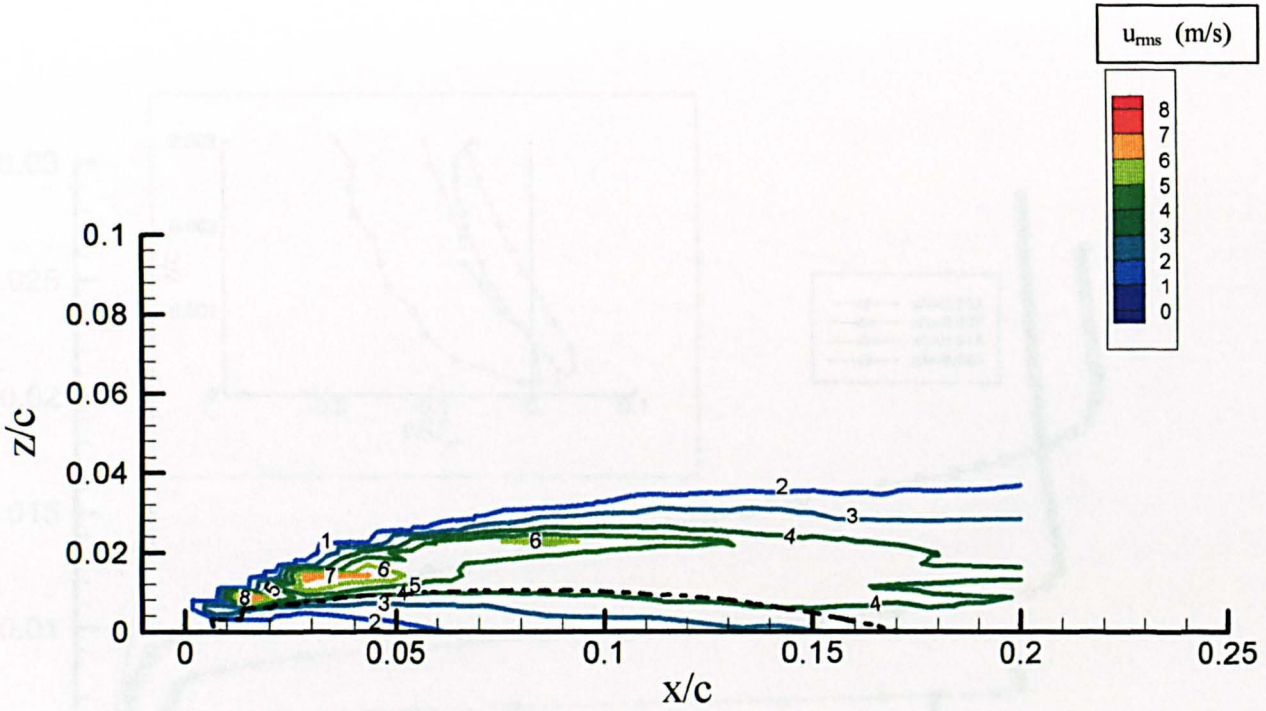

Figure 3.4 Contour map showing chordwise rms velocity component for α=2°, U_∞=12.5m/s, Re_c=0.6x10^6. ----, locus of u/U_∞=0.

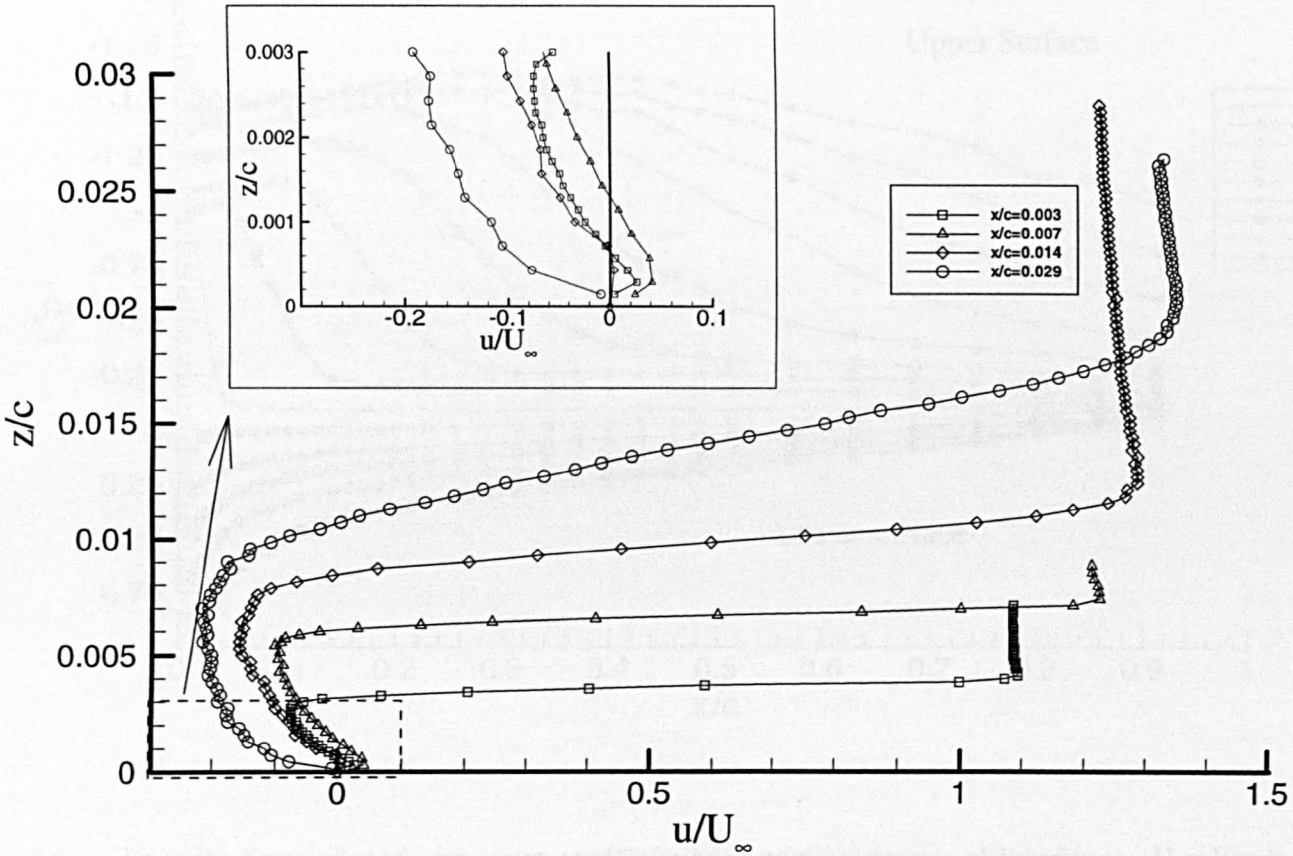

Figure 3.5 Mean chordwise velocity distributions normal to plate for α=2°, U_∞=12.5m/s, Re_c=0.6x10^6.

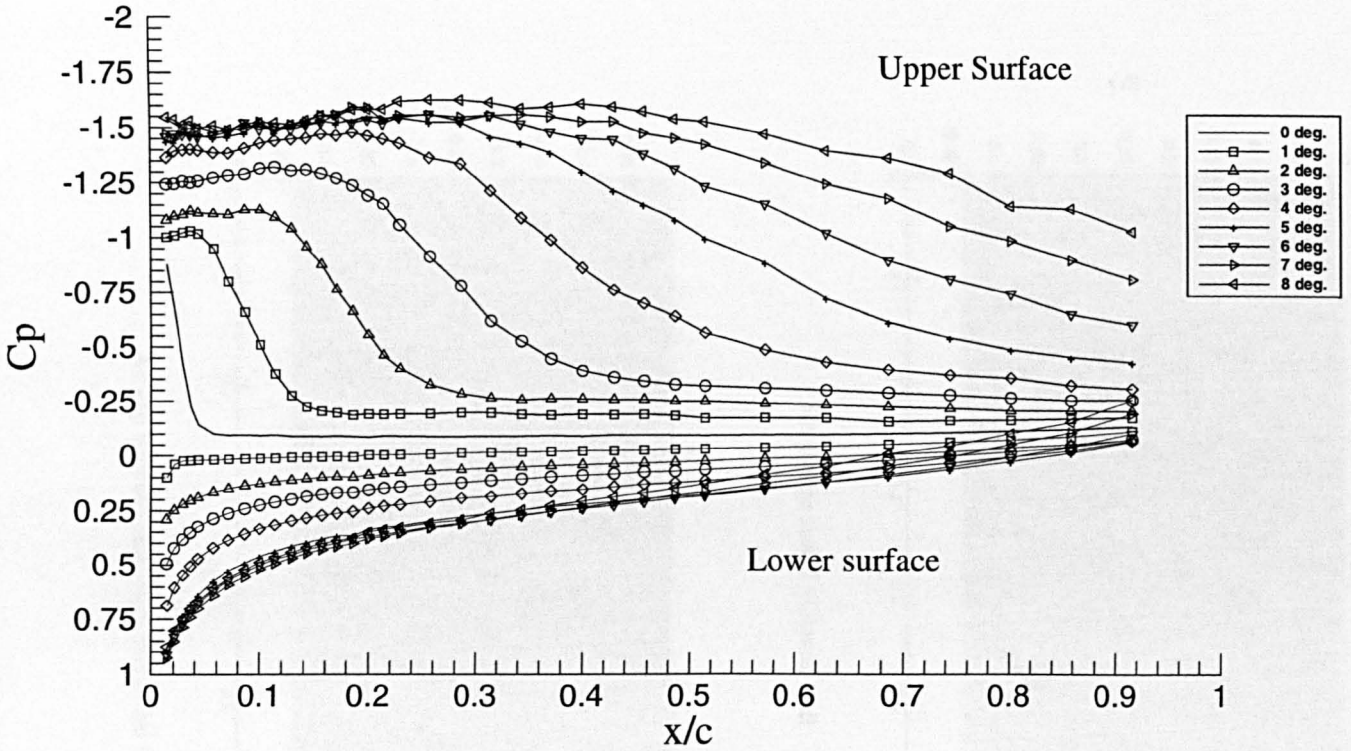

Figure 3.6 Distributions of static pressure coefficient for various angles of incidence. U_∞=20m/s, Re_c=1.0x10^6.

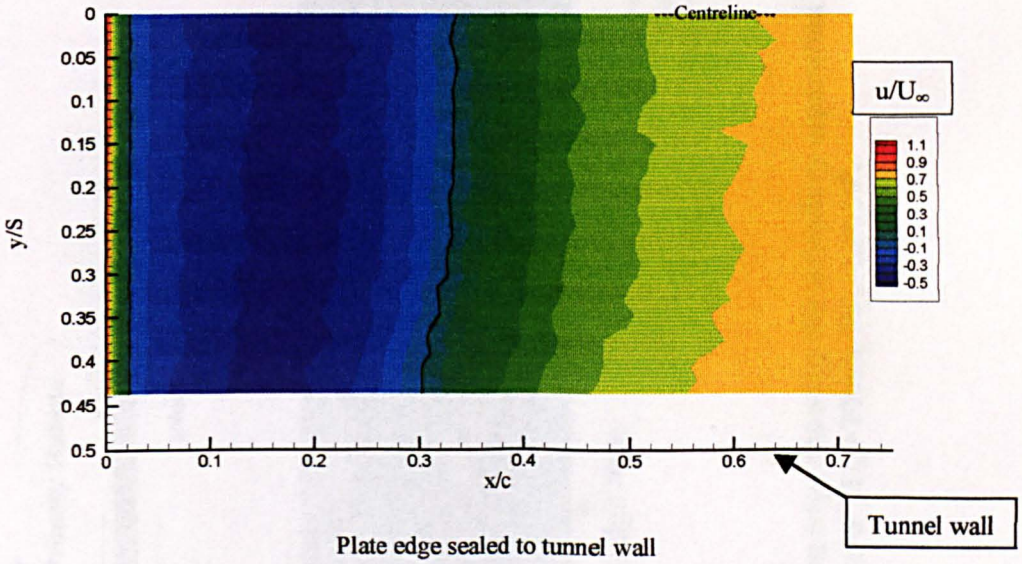

Plate edge sealed to tunnel wall

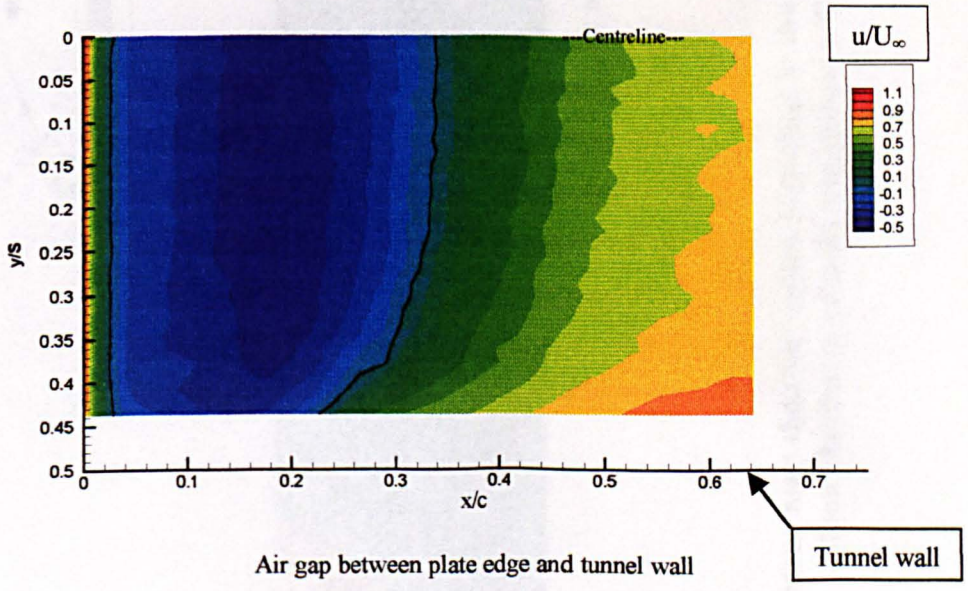

Air gap between plate edge and tunnel wall

Figure 3.7 Contour map showing mean chordwise velocity component u/U_∞, 5mm above plate surface for α=3°, U_∞=20m/s, Re_c=1.0x10^6, z=5mm. ——, locus of u/U_∞=0.

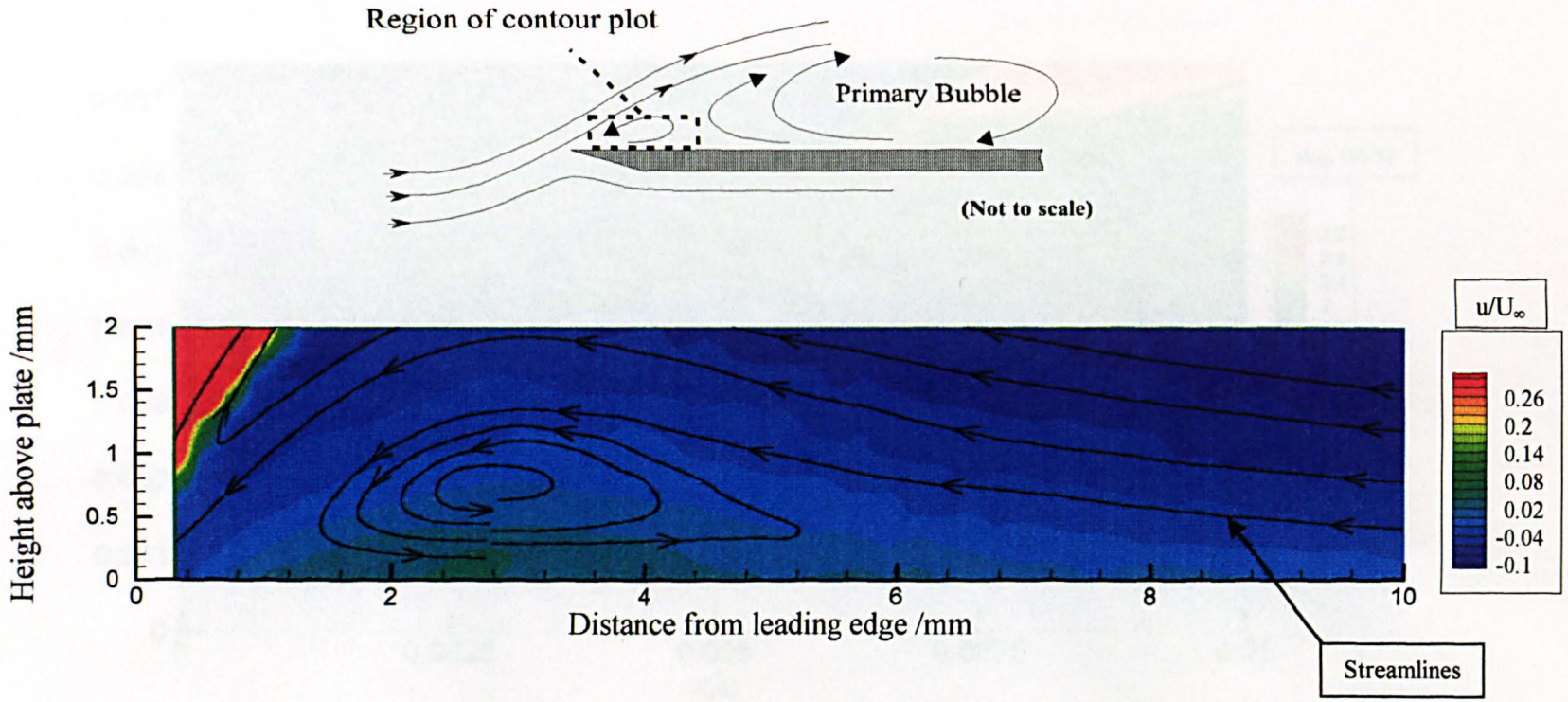

Figure 3.8 **Contour map showing region very close to the leading edge showing the secondary separation bubble. Mean chordwise velocity component u/U_∞ for $\alpha=3°$, $U_\infty=20m/s$, $Re_c=1.0x10^6$.**

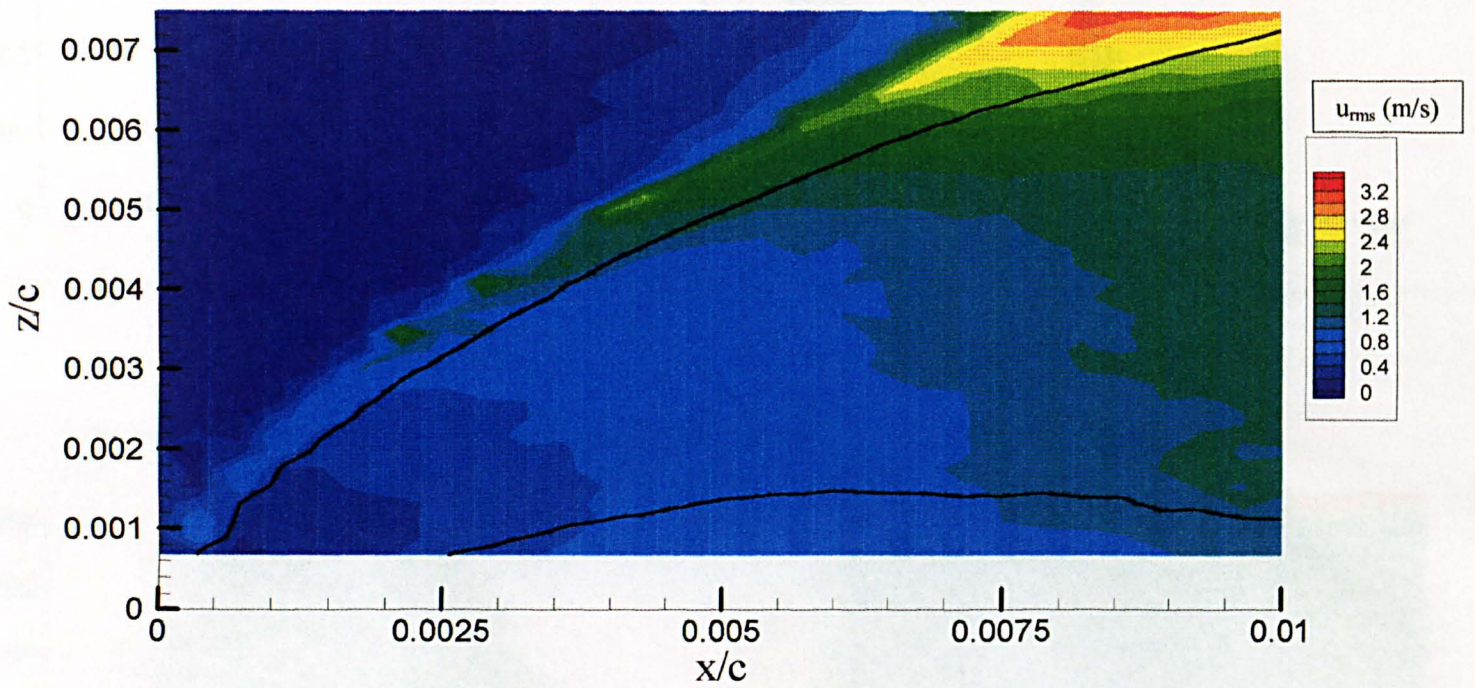

Figure 3.9 **Contour map showing chordwise rms velocity component close to the leading edge for $\alpha=2°$, $U_\infty=12.5$m/s, $Re_c=0.6\times10^6$. ——, locus of $u/U_\infty=0$.**

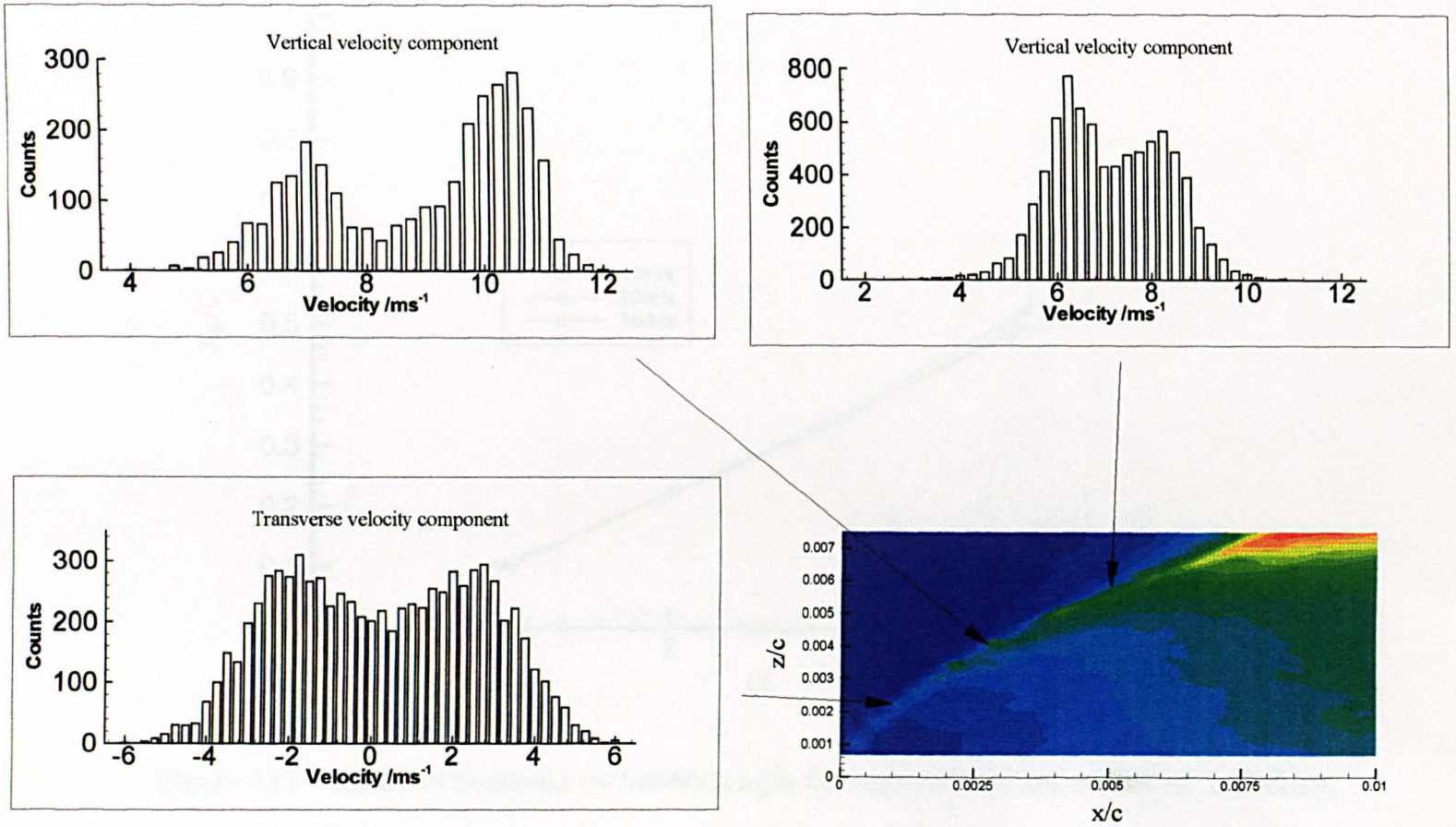

Figure 3.10 Velocity histograms showing location of observed periodic instability in the shear layer. Contour map showing chordwise rms velocity contour for $\alpha=2°$, $U_\infty=12.5m/s$, $Re_c=0.6x10^6$.

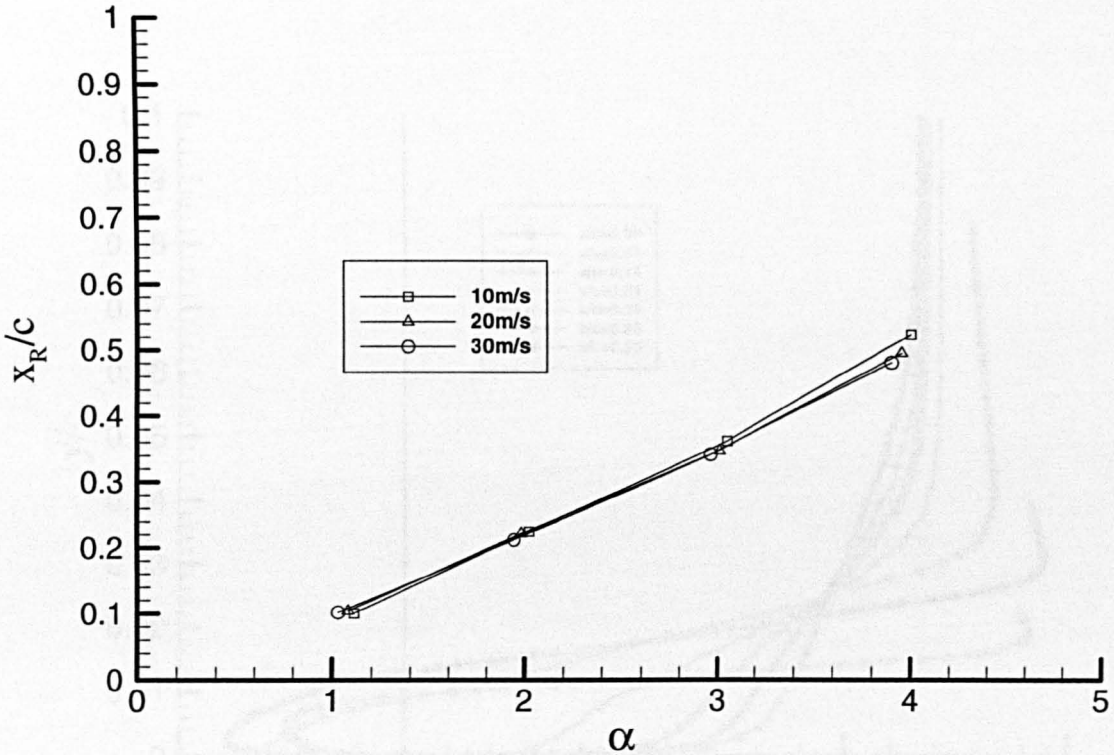

Figure 3.11 Effect of incidence on bubble length for various Reynolds numbers. c=700mm.

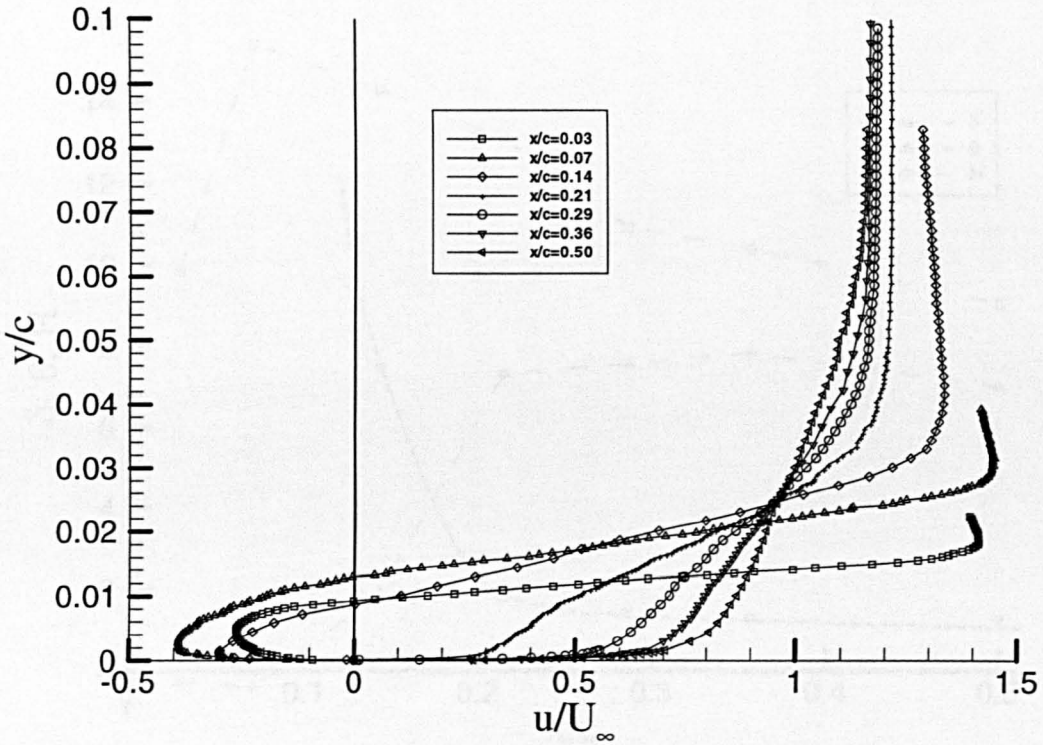

Figure 3.12 Mean chordwise velocity distributions normal to plate for α=2°, U_∞=12.5m/s, Re_c=0.6x10^6.

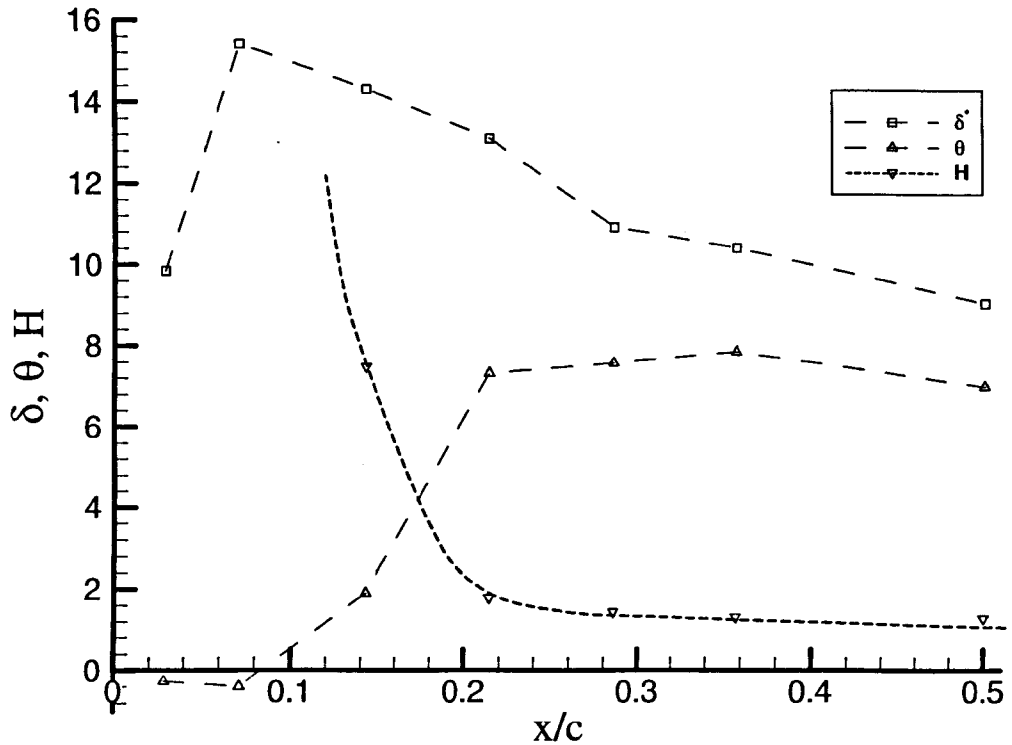

Figure 3.13 Displacement thickness, momentum thickness and shape factor distributions for $\alpha=2°$, $U_\infty=12.5m/s$, $Re_c=0.6x10^6$.

CHAPTER 4
GENERAL EXPERIMENTAL PROCEDURE AND FLAT PLATE RIG DESIGN

4.1 Introduction

As discussed in Chapter 3, a modified flat plate test rig was required in order to best allow the flow details of the thin aerofoil bubble to be investigated. The new plate design had a reduced chord and thickness necessitating the development of an alternative method of measuring static pressure on the plate surface.

This chapter describes the flat plates, support rigs, wind tunnel and subsidiary test equipment used during the investigation. The acquisition of velocity data was obtained solely with the use of the laser Doppler anemometer (LDA) and a description of the system set-up, operation procedure and summary of possible errors is included. The flow visualisation techniques employed in the main investigation are also described.

A summary of the test conditions used in the current work is provided in the final section.

4.2 Subsidiary Equipment Used

4.2.1 Low Turbulence Wind Tunnel

All tests were carried out in the low turbulence wind tunnel at the Department of Aerospace Engineering, University of Bristol. The tunnel, as fully described by Barrett (1984), is of a closed loop design with a contraction area ratio of 12:1

which, in combination with the upstream settling chamber and screens, ensures low turbulence levels. It is powered by a 75kw dc motor which produces a maximum air speed in the working section of approximately 105m/s. The working section has internal dimensions of 0.8m x 0.6m x 1.6m (width x height x length) with tapered corner fillets. A general layout of the wind tunnel is shown in Figure 4.1.

The wind tunnel provides a stable airspeed (typically ±0.01% variation with time) and a consistent velocity across the working section to within 50mm of the tunnel walls. A most important feature with respect to the current investigation was the low freestream turbulence level (freestream turbulence intensity components below 0.05%, measured with a hot-wire anemometer, for the range of speeds used in this investigation, i.e. up to 40m/s). The low turbulence intensity allows the free shear layer to develop in the laminar regime.

The main problem experienced with the tunnel throughout testing was the dissipation of heat. There is no cooling system for the tunnel stream and the heat can therefore only escape through the wooden construction of the tunnel walls. This leads to an increase of air temperature with time, the rate of which is dependent on the freestream air speed. For the current investigation, this was typically a 5°C rise in 60 minutes of testing at 20m/s. As a consequence, the length of a test run was restricted in order that the temperature did not vary >5°C temperature range and if this was exceeded, a cooling down period was applied. The day to day variation in temperature and pressure caused by atmospheric conditions were measured and accounted for in the Reynolds number calculations.

4.2.2 Pressure Measuring Equipment

Two types of pressure measurements were required. Firstly, to determine the freestream velocity of the working section a pitot-static probe was used and secondly, to determine the static pressure distribution over the plate surface pressure tappings mounted in the plate were used.

The pitot-static probe was mounted 500mm upstream of the test rig leading edge, in the freestream flow, and at a quarter working section height to ensure any wake it produced passed well below the test rig. The probe was connected to a Betz manometer from which the dynamic pressure and hence freestream velocity could be determined.

The method for determining static pressures between the preliminary investigation and main investigation varied slightly. The plate used in the preliminary investigation had 35 internally mounted pressure tappings along a single chord line. These were connected using silicone tube to a 48D3-1070 Scanivalve which contained a Setra Systems, Model 237, 0 to ± 0.25 PSI differential pressure transducer to convert pressure signals into voltage. In this set-up, the scanivalve also recorded the freestream total pressure and freestream static pressure from the pitot-static probe. All measured pressures were logged on a PC using an analogue to digital conversion system.

In the main investigation, the scanivalve was removed as the new plate design, described in Section 4.4.2, allowed for only single pressure measurements to be taken at a time. The method developed employed a chordwise slot in the upper surface of the plate covered in thin adhesive tape. A pin prick was then made at the exact chordwise location where the static pressure was required. This enabled measurements to be taken as close as 2mm from the leading edge and a higher density of measurements to be taken in regions of steep pressure gradient. The single brass tube protruding from the trailing edge was connected via plastic

tubing to the pressure transducer mentioned above. The outside diameter of the tube was 1.6mm so as to minimise any disturbance to the flow. The voltages were recorded and values of pressure coefficient calculated after testing was completed.

4.3 The Laser Doppler Anemometer (LDA)

4.3.1 Introduction

The majority of the measurements required were of velocity, and it was necessary for these to be taken throughout the separation bubble (including reverse flow regions) and close to the leading edge. Potential techniques available for this work included laser Doppler anemometry, hot-wire anemometry and pitot pressure probes. The latter two were discounted for the following reasons: firstly, both techniques are intrusive to the flow, secondly, in reverse flow, the pitot-static probe does not work and the hot-wire cannot resolve the flow direction. A three component hot-wire would allow the direction to be resolved, but the spatial resolution is poor and it would not be possible to measure close to the surface.

In support of this, Tan and Auld (1992) and Weibust et al (1987) showed the flow in the vicinity of a separation bubble to be affected by the presence of a single hot-wire probe. Nash (1996) quantified the error related to hot-wire probe interference on a trailing edge separation and the results are shown in Figure 4.2. This shows an extremely good correlation between the hot-wire data and the LDA data, taken close to the hot-wire probe. However, removal of the hot-wire and repeating the LDA measurements leads to a different velocity profile which now includes reverse flow. The hot-wire was shown to modify the flow locally by inducing unsteadiness in the boundary layer, which in this case allowed the

flow to remain attached and laminar instead of separating, as evidenced by the presence of the reverse flow.

Laser Doppler anemometry was therefore chosen as the suitable measurement technique, thus eliminating problems of directional ambiguity and probe interference that had, in previous work, been a limitation when measuring within separation bubbles.

The LDA was invented by Yeh & Cummins in 1964, and is a well-established technique enabling both, mean and time varying velocity data to be resolved in three mutually perpendicular axes in a manner non-intrusive to the flow. The high spatial resolution allows the steep velocity gradients to be fully defined, for example in the boundary layer, it was also possible for data to be taken less than 0.1mm from the surface, thus allowing the separation of a boundary layer to be investigated. The system also enabled the direction of the mean and fluctuating flow components to be resolved, this being essential for studies of separation bubbles.

4.3.2 General Principles of Laser Doppler Anemometry

The measurement of velocity is based on the principle of the "Doppler effect" which states that whenever there is relative motion between a wave source and an observer, there is a frequency shift as perceived by the observer. A full derivation of the frequency shift in this situation is given by Drain (1980).

The basic LDA system is composed of

- A continuous wave laser
- transmitting optics with beam splitter and focusing lens
- receiving optics, including focusing lens and photo-multiplier (or equivalent)
- a signal conditioner and signal processor

The fundamentals of operation are the same for a 1D, 2D or a 3D system. The source laser beam is first split into two, the beams are then brought to a transmitting / receiving optical probe, with or without the use of optical fibres. In the probe, the beams are focused by a lens to intersect at a common point, known as the "measurement volume". The distance of the measurement volume from the probe is determined by the focal length of the lens used.

The process of obtaining velocity information can be explained in two ways, by Doppler theory directly or by a model, known as the Fringe model.

Using the Doppler theory, as a seeding particle (added as a tracer) passes through the measurement volume, light is scattered at two distinct frequencies (Doppler shifts). This is due to the different component of velocity of the seeding particle "seen" by each beam at the measurement point. The two frequencies of the scattered light interfere in a process called "heterodyning" resulting in a single "beat" frequency which is the difference between the two Doppler shift frequencies. The beat frequency is related to the velocity of the particle, perpendicular to the bisector and in the plane of the two beams, by the equation:

$$f_b = \frac{2u}{\lambda} \sin\left(\frac{\phi}{2}\right)$$

where f_b is the beat frequency, u, the velocity of the seeding particle, λ, the wavelength of the coherent light and ϕ, the beam separation angle.

The Fringe model is based upon consideration of the measurement volume, typically a few millimetres long, where the light intensity is modulated by the interference fringes that are created by the intersection of the two coherent laser beams (Young's fringes). The parallel fringes of high light intensity have a

separation distance, defined only by the wavelength of the laser light, λ and the beam separation angle ϕ.

Seeding particles which pass through the measurement volume scatter light which fluctuates in intensity with a frequency proportional to the velocity of the seeding particles, producing a signal "burst". The frequency contained within the burst is the beat frequency as defined above.

This light scattered by each seeding particle passing through the measurement volume is focused by the receiving optics onto a photomultiplier. This converts the light into an electrical signal. The signal conditioner and signal processor remove the noise from the signal and extract the frequency using a series of algorithms. The equation given above for the derivation of the particle velocity shows the important result that the direction of the observer is not important and for a given wavelength of the light source and beam separation, the particle velocity is only related to the beat frequency.

If the intersecting beams were of the same frequency, the measured velocity for two equal speed seeding particles moving in opposite directions would be the same. Therefore in the basic form, the LDA is directionally ambiguous. This problem can be solved by introducing a frequency shift to one of the beams, using for example, a Bragg cell. This is a piezo crystal which vibrates imposing a frequency shift of known value onto one of the beams. The output from the splitter box is therefore two beams of equal intensity with a frequency shift superimposed on one of the beams (typically 40MHz). The frequency shift introduces a velocity offset, chosen to be large enough so that all velocities measured are of the same sign, before the offset is finally removed. It is this frequency shift which makes the LDA unique in its ability to determine direction as well as speed.

A full schematic of the LDA flow measurement process is shown in Figure 4.3 (illustrating the Fringe model).

The seeding particles scatter light in all directions with the highest concentration for translucent particles being in forward scatter i.e. away from the direction of the transmitted beams. Much less light is scattered towards the transmitting beams (backscatter), but direct backscatter is often used because the transmitting and receiving optics can be integrated into a single optic head. This is more practical than several optic heads, which must be carefully aligned with each other.

A single pair of beams will therefore measure a single vector component of velocity. In order to measure two velocity components, two extra beams are added to the transmitting optics in a plane perpendicular to the first pair of beams. The velocity can now be determined for a given plane, i.e the two-dimensional case.

three-dimensional measurements are achieved with a further additional pair of beams from a second optic head, all beams intersecting in the same measurement volume. Different wavelengths are used for each beam pair to separate the measured components. Colour filters are also introduced with each photomultiplier to distinguish between velocity components.

4.3.3 Description of Bristol LDA System

The LDA used for this research was a Dantec 3-component system. The laser light is generated by a Spectra-Physics Stabilite 2016, continuous wave 5 Watt Argon-Ion laser. The three wavelengths used are Green 514.5nm, Blue 488nm and Violet 476.5nm, each measuring a different velocity component in the measurement volume.

The projection optics, of 600mm focal length, were mounted outside the tunnel on a precision three-axis traversing rig with operating dimensions of 0.6m x 0.6m x 0.6m. The two optic heads could be rotated on their respective mountings, allowing them to be dipped and swept to provide the required optical access. In most cases, the traverse was aligned with the wind tunnel so the traverse axes were the same as the wind tunnel (streamwise, spanwise and vertical). The resolution of the traverse was 0.005mm in the vertical direction and 0.01mm in the streamwise and lateral directions.

The "2D optic head" transmitted the green and blue pairs of beams and the "1D optic head" transmitted the violet pair. Both optic heads were capable of receiving light and so the system could be used in on-axis or off-axis mode as described below.

1. On-axis mode: the scattered light from each pair of beams is collected by the same optic head from which it was transmitted.
2. Off-axis mode or "Cross-coupled mode": The green and blue scattered light is collected by the optic head transmitting the violet beams and vice-versa.

The system as described by Barrett & Swales (1998), was configured to run in off-axis backscatter mode in order to achieve the smallest possible measurement volume, this being of the order of 0.05mm in diameter and near spherical in shape. An illustration of this set-up is shown in Figure 4.4. The enhanced alignment methods developed at Bristol made possible the use of off-axis mode throughout, while still maintaining high data rates across the bubble.

The scattered light is converted to an electrical signal by three photomultipliers (type 57X08) containing pre-amplifiers. Each time a particle crosses the measurement volume, a "Doppler burst" is received, an example of which is shown in Figure 4.5. The increase in amplitude of the signal across the burst is

due to the near Gaussian distribution of light intensity across the diameter of the laser beam. These signals are processed using Dantec Enhanced Burst Spectrum Analysers (BSA) which extract the Doppler frequency using fast Fourier transforms. Each BSA processes the signal from one colour only, corresponding to a single velocity component. In order to produce only coincident data in space and time, the BSAs were set up to only record the velocity data from a burst if present on all three channels simultaneously. Software on the PC post-processes the data checking for coincidence and converting the non-orthogonal velocity data from the three beam pairs to orthogonal tunnel axes by the application of a transformation matrix. This matrix is determined by the geometry of these beams and is derived in full by Swales et al. (1992).

Seeding was provided by a Safex 2001 fogger using a glycol based fluid. It produces a uniform distribution of particles with an average diameter of 1μm (Anon). The type of seeding used in air is important because the signal-to-noise ratio (SNR) increases with particle size. However as the size of the particle increases its ability to truly follow the flow deteriorates. A compromise is required and it is generally accepted that a particle size of around 1μm is most suitable. A more complete discussion of seeding is given by Swales (1994). The seeding was drawn into the tunnel downstream of the working section so as not to create turbulence ahead of the test model. This also helped to uniformly disperse the seeding, providing a more continuous data rate.

4.3.4 LDA Measurement Errors

The enhanced alignment method used allows routine operation in the off-axis mode while maintaining high data rates. As a consequence, a minimisation of errors is achieved due to the greatly reduced effective measurement volume. This allows:

- precise 3D measurement in poorly seeded areas whilst maintaining satisfactory data rates.
- increased positional accuracy in defining the location of the surface and for velocity measurements in the boundary layer close to the surface (<0.1mm).
- reduced statistical errors in regions of high velocity gradient.

For the current work, the quasi two-dimensional nature of the flow in which the velocity is predominately in the streamwise direction reduces some error sources considerably. The general accuracy of the system when aligned by the method described and configured to run in off-axis mode was analysed by MacManus et al. (1996), based on tests carried out at Bristol University using the same LDA system.

The main errors associated with the LDA in the present application can be categorised as:

- **Seeding particle behaviour -** For particles with a mean diameter of around 1μm, flow accelerations are shown to cause negligible deviation in particle path relative to the flow direction and therefore small errors in velocity. For example, Melling & Whitelaw (1973) found the largest errors due to the effects in a vortex core to be of the order 0.007m/s in the radial component, equating to an error in total velocity of <0.01%. In the present study the flow contained no vortex regions as strong as this and therefore the centripetal influence will be negligible.
- **Frequency measurement errors -** The processors determine the Doppler frequency by Fourier analysis of the signal, employing a high discretisation resolution, resulting in a maximum error of <0.001m/s for each velocity component measured (Anon).
- **Calibration and Transformation errors -** The frequencies are converted to velocities and transformed into the desired axis system using a velocity transformation matrix. In general, the accuracy in determining this matrix is

of the order of the positional accuracy of the traverse (Rickards et al. 1995), (±0.02mm in the x and y axis). The beam orientations were chosen to minimise the velocity errors in the plane of the two-dimensional flow, which were calculated to be within the range 0.1% to 0.8% depending on the local flow velocities. The out-of-plane errors were greater than this, but were of little consequence to the results presented.

- **Statistical errors** - These occur due to:

  I. **Finite sample size** - Errors occur because of the finite sample size recorded in relation to the overall unsteadiness of the flow. Following the approach of Pfeifer (1991), it was calculated that, for a measurement obtained from 5000 samples, the maximum errors were ±0.007m/s (mean velocity) and ±0.023m/s (rms) in the region of flow with the highest turbulence intensity, for a confidence limit of 95%.

  II. **Velocity bias** - In a fluctuating flow, a greater proportion of particles pass through the measurement volume at times when the velocity is high than when it is low. Therefore a bias of the mean velocity is recorded which is dependent on the turbulence intensity. For the flow under investigation, this was found to be of the order of 0.0002m/s, based on an analysis given by McLaughlin & Tiedermann (1973).

  III. **Gradient bias** - When a velocity gradient exists across the diameter of the measurement volume, more particles pass through the higher velocity region, so biasing the measured mean velocity. In the present study, this effect is most significant in the shear layer close to the leading edge where the highest velocity gradient occurs (40m/s per mm), giving a maximum bias of 0.052m/s.

- **Positional accuracy** - The greatest positional error was in the determination of the location of the surface of the plate. By monitoring the output of the photomultiplier anode current as the measurement volume was traversed

towards the surface, the uncertainty was reduced to the resolution of the traverse, i.e. ±0.005mm in the vertical direction. Based on the same maximum velocity gradient as quoted earlier, this equates to a maximum error of ±0.200m/s. The backlash of the traverse mechanism was in the order of its positional resolution. This error was minimised by ensuring that, whenever possible, the traverse axes moved in a single direction when data of high spatial resolution was required.

Most of the statistical errors are variable over the flow-field and small relative to the freestream velocity and are therefore only important in local regions of steep velocity gradient or high velocity fluctuation. The inter-dependent nature of various errors makes any estimate of the overall error difficult to ascertain. Maximum errors in mean velocity range from the order of 0.5% in the freestream areas to <2% in local regions of steep velocity gradients.

The repeatability of the velocity measurements was ascertained for the short and medium term only. Short term repeatability was determined by repeating the measurement of a velocity profile immediately after it was first taken and also after the wind tunnel had been stopped and re-started. The medium term repeatability, for example after the model had been removed and replaced in the wind tunnel, was determined by measuring the velocity at selected points in a measurement grid and comparing results. Although not presented, the repeatability proved to be excellent with negligible variation over time.

4.4 Flat Plate and Mounting Rig Design.

4.4.1 Requirements of New Plate and Mounting Rig Design

From the Preliminary Investigation (Chapter 3), several limitations were exposed regarding the flat plate rig initially used. The main requirements of the modified

flat plate, as identified from the preliminary investigation, in order of importance were to:

I. Further minimise the tunnel blockage caused by the plate by reducing the chord length and thickness.
II. Change the plate material to steel. This stiffens the plate to compensate for the reduced thickness and improves the surface quality.
III. Enable the effect of chord length to be investigated by having two plates of substantially differing chord lengths.
IV. Reduce flow interference by keeping plate supports, pressure tapping tubes and the trailing edge sting as far from the plate as possible.
V. Ensure the plate fully spans the tunnel working section and is sealed to the wall to reduce tunnel wall interference.
VI. Position the plate in the working section to allow the most efficient LDA access possible.
VII. Develop a new technique to allow the measurement of static pressure very close to the leading edge (<5mm).
VIII. Provide a sharp leading edge by chamfering the lower surface.

4.4.2 General Features of Plate Design

To provide stiffness with reduced thickness, mild steel was chosen for the plate material. The plate thickness required was determined by simple calculations using Euler bending equations and an approximated aerodynamic loading to give a satisfactory deflection. Based on this result, 6mm was chosen for the main plate thickness, giving, for a nominal chord length of 160mm, a thickness to chord ratio of 3.75%. A 20 degree chamfer at the leading edge produced the sharp edge, a shallower angle would leave the leading edge very fragile and therefore prone to damage. A consistently smooth leading edge was essential as it was predicted that a damaged section might induce turbulence locally in the

shear layer and influence the separation bubble behaviour. This chamfer angle also allowed pressure measurements to be taken to less than 5mm from the leading edge.

In the preliminary investigation, pressure tappings tubes were run internally in the plate, exiting at the trailing edge. The reduced thickness meant that this was no longer possible without compromising the stiffness. Therefore a new technique was developed whereby a narrow chordwise slot was cut in the plate upper surface measuring 2mm x 2mm (width x depth). The location of the slot was at a quarter span, extending within 2mm of the leading edge and all the way to the trailing edge. A single brass tube (1.6mm outside diameter) was then mounted parallel to the slot at the trailing edge so that it protruded downstream into the flow. The tube extended 5mm into the slot and was sealed in place leaving a 3mm flat section at the trailing edge upper surface. The detailed design of the flat plates used in the main investigation is shown in Figure 4.6. In use, the slot was closed with thin adhesive tape and a single pressure tapping was introduced by pricking the tape at the required chordwise location.

In order to investigate the effect of chord length on the separation bubble, a second plate was also manufactured, scaled to the first. The chord length was halved to 80mm and the thickness to chord ratio was maintained giving it a thickness of 3mm.

4.4.3 Plate Mounting System.

The plates were mounted horizontally in the low turbulence wind tunnel. To achieve separation bubbles of varying lengths, adjustable plate incidence was required. Spanwise adjustment of the plate angle was also incorporated for setting the plate horizontal across the working section. To simplify the rig used, both plates were designed to be mounted in a similar way on a three point

mounting system. The plates were mounted from outside the tunnel with a complex bracket assembly allowing the height adjustments to be made at each side of the leading edge. These mounting brackets were first used by Eustace (1999) and the design is shown in Figure 4.7. The mounting brackets hold a pin, on clamps connected to the tunnel frame by two screw threads. The pin passes through a small slot in the glass window or tunnel wall into the working section. The pin then supports a simple right angle bracket, mounted under the leading edge of the plate and fixed at the quarter chord point, allowing the plate to rotate around the pin and hence enabling the required angle of incidence adjustment. The design of the support pin and plate support brackets are shown in Figure 4.8. The support bracket held the plate clear of the mounting system and ensured that the leading edge was in undisturbed flow. This set-up also raised the plate high enough above the mounting assembly to give clear optical access for the LDA.

The trailing edge was attached via a sting to a tensioned steel wire strung vertically in the centre of the working section, approximately two chord lengths downstream of the trailing edge. The sting was attached to the underside of the plate and had a tightening bolt clamping it to the wire, enabling easy adjustment to be made to the incidence. The wire was tensioned with weights suspended under the working section.

Figure 4.9 shows the general arrangement of the flat plate rig in the wind tunnel whilst Figure 4.10 is a section view of the mounting system.

It is important to note that the glass window was independent of the mounting system. Any distortion of the glass adversely affects the alignment of the LDA and so this design ensured no loads were transferred to the glass window. In addition, 12mm glass was used to avoid bending under the low static pressures imposed on it at high wind tunnel speeds.

The panels on the opposite side of the window were easily removable to allow access when the plate was fully mounted in the test position. These panels were constructed in wood and painted matt black to reduce laser reflection and were carefully designed to eliminate any risk of beams exiting the far side of the tunnel.

4.5. Flow Visualisation

4.5.1 Introduction

There are many different methods of flow visualisation which can be incorporated as part of an investigation into an unknown flow. The main advantage is that a good insight into a flow can be achieved quickly, without the need for time consuming analysis. Flow visualisation is most powerful when used to validate more complicated fluid measurement techniques and computational predictions at any stage in an investigation. The only drawbacks of this method of investigation is that at best, the results are only qualitative or semi-quantitative and can often be difficult to interpret. The various methods of flow visualisation are broadly categorised into two areas, those that are applied to a surface only and those that describe the flow surrounding an object. The most common methods and those considered for the present investigation are outlined below.

4.5.2 Non-Surface Methods

4.5.2.1 Tufts

Thread tufts (usually connected to the end of a thin probe) can be used to examine the flow direction. Within a laminar or steady region, the tuft remains

steady, but in a region of transition or turbulence, the tuft will flutter visibly. They are also able to identify large areas of reverse flow but are unable to establish accurate separation or reattachment points. Simple flow direction information can be obtained but this is generally used as a very quick familiarisation tool.

4.5.2.2 Smoke Filaments

Smoke particles can be injected into a flow allowing the direction of the flow to be observed. This is often aided by illuminating a section of the flow with a strong light source. The smoke particles are typically generated by vaporising a mineral-based oil by resistive heating of a hot filament or wire. Smoke can be injected into the flow using slight positive pressure through slots or small tubes mounted in or ahead of the object of interest. Alternatively, oil can be vaporised directly from a wire placed in the flow providing a plane of smoke. All these smoke tracer methods are well summarised by Mueller (1983), but they can be time consuming to set up and only work well at low speeds. High speeds and turbulence tends to break the filaments up into an indistinct cloud. Illumination is commonly supplied by a powerful fibre optic lamp or a thin plane of laser light.

A laser light sheet is a powerful plane of light produced to illuminate a section of a flow. The laser light source is spread by a cylindrical lens or by the use of rotating or vibrating mirrors and produces a plane of light typically 2-4mm thick with a divergence angle of 40 degrees. Tracer particles are required in the flow to track the fluid motion and reflect the light. The result shows the behaviour of the flow across a two-dimensional "slice" even if the flow is highly three-dimensional. The scattered light is observed at an oblique angle or normal to the plane of the light.

4.5.3 Surface Methods

4.5.3.1 Minitufts

Minitufts are very fine thread filaments attached to the surface. They can be attached at discrete points, either locally to an area of interest or globally to cover an entire test object. The tufts then become aligned with the flow direction. The main advantage is that once the tufts are applied, a sequence of tests can be run continuously. Dobney et al. (1986) used a large number of nylon filaments (<0.04mm diameter), coated in dye and then photographed whilst illuminated with UV light. They showed that the tufts produce minimal flow disturbance. The main disadvantage is the long preparation time and the limited data obtained from the discrete distribution of the tufts.

4.5.3.2 China Clay

This method utilises the differing evaporation rates of a volatile liquid obtained in laminar and turbulent flow and is described in detail by Moir (1986). A solid coating of white china clay is applied to the test surface in a lacquer form. Methyl salicylate (oil of wintergreen) is usually used as the volatile liquid which is sprayed on causing the solid coating to become transparent. The aerofoil is then run at the required speed and the white coating becomes visible as the evaporation occurs. A disadvantage of this technique is that it requires the aerofoil to be chemically resistant and dark in colour to provide adequate contrast with the white coating with care being taken to maintain the required surface finish. An advantage of the method is that it is not affected by gravity and so can be used for any aerofoil incidence. This method was used successfully by Nash (1996) to identify the short separation bubble present on a NACA 0012 aerofoil.

4.5.3.3 Oil Streakline

This method is reliant on the surface shear stress moving a volatile oil in the direction of the surface streamlines, showing up as streaks once the oil evaporates. It can be used locally or globally over an entire aerofoil surface. The volatile oil (paraffin) is mixed with a fine dyed talc at a ratio of about 5:1. This mix is spread evenly and thinly over the area of interest with a soft brush, ensuring no air bubbles or large deposits build up. The aerofoil is then run at the required speed until all the oil has evaporated leaving a dry powder surface pattern. The main advantage is that it gives a continuous pattern that is easy to interpret. Unlike the china clay method, very little, if any aerofoil preparation is needed and the aerofoil can be removed from the tunnel for analysis as the flow pattern is stable once all the oil has evaporated. The disadvantages are that the oil is affected by gravity and cannot be used with confidence at high incidences (>8 degrees). In addition, it must be re-applied after every run.

If the test surface has porous sections or is pressure tapped, care must be taken with all surface methods so as not to block up the holes.

4.5.4 Methods Used in the Present Investigation

A number of techniques were used for the main investigation with varying degrees of success. A thread tuft was used initially and this gave qualitative information about the flow. Though the results were not recorded it gave a basic insight into flow direction, flow stability and approximate separation bubble dimensions.

Towards the end of the main investigation, the 160mm chord plate was sealed with a black primer in an attempt to utilise the china clay method. However, this method failed to give useful results with anything but low incidences (<1

degree). This method had been shown to work well with attached boundary layers which undergo separation (Nash 1996). However, because the thin aerofoil separation bubble has no boundary layer attachment prior to separation, it was concluded that the large scale turbulence and unsteadiness at the higher incidences did not yield the required variation in evaporation rates for this method to succeed. At the very low incidences, the short bubble length provided ample chordwise distance for the boundary layer to reattach and produce a significant difference in evaporation rates.

The majority of results came from the oil streakline method and a modified smoke filament employing a laser light sheet. The oil streakline was implemented as described in Section 4.5.3.3 and only used at incidences below 5 degrees to avoid gravitational effects. Pressure tappings were covered with a thin strip of adhesive foil tape to avoid becoming blocked.

4.5.4.1 New Smoke Visualisation Technique

The smoke visualisation technique used was based on the single wire method, modified to improve visualisation. Firstly, a vertical wire was strung in tension, vertically across the working section, approximately one chord length upstream of the plate. The wire was two lengths of 12.71 Ohm/yard fuse wire entwined with a hand drill to give a twisted pair finish. This proved to be very advantageous. Whereas a single wire will produce a continuous plane of smoke, the twisted pair finish had the effect of producing regularly spaced filaments of smoke. This gave much clearer representation of the directionality and turbulence in the flow.

The wire was connected to a standard 12 Volt power supply requiring between 2-3 Amps to vaporise the oil. The oil was pumped from a reservoir to the top of the wire using silicon tubing and then ran down the wire under gravity, the

volume flow rate being adjustable. In order to produce intense smoke filaments, a compromise between current and oil volume flow rate was required. If the current was too high, or volume flow rate too low, the oil would vaporise very early on the wire. Conversely, too much oil or too low a current would result in very faint smoke filaments. No optimum values can be quoted because the oil volume flow rate was not easily quantifiable and the settings used also depended on freestream velocity and the length of the wire.

A laser light sheet was also used to enhance the clarity of the smoke filaments over the area of the separation bubble. The light source was generated by a Spectra-Physics He-Ne 20mW laser located on the tunnel roof. The beam passed through a small cylindrical lens to spread the beam into a plane before being reflected by a mirror 45 degrees vertically into the tunnel working section. The adjustable mirror allowed the beams to be steered into the same plane as the smoke wire. A small glass window was installed in the tunnel ceiling to allow the optical access.

All images were captured using a digital camera linked to a PC running Image Pro© software. The camera was located 90 degrees to the plane of the light, mounted outside the tunnel. The apparatus used for this smoke wire method is represented in Figure 4.11 and the exposure time on the camera was 1/10,000 second.

4.6. Summary of Test Conditions

The table below is a summary of the main results presented within this thesis.

a) Velocity and pressure data

Chord Length /mm	Reynolds Number	Incidence /degrees	Data Format	Variable presented
700	$0.6x10^6$	2	Contour	U_{mean}, U_{rms}
700	$0.6x10^6$	2	Velocity profile	U_{mean}
700	$0.6x10^6$	0,1,2,3,4,5,6,7,8	Line	Cp
160	$2.13x10^5$	1,2,3,4,5,8	Contour	U_{mean}
160	$2.13x10^5$	1,2,3,4,5	Contour	U_{rms}
160	$2.13x10^5$	1,2,3,4,5	Line	Cp
160	$2.13x10^5$	1,2,3,4,5	Velocity profile	U_{mean}, U_{rms}
160	$2.13x10^5$	3	Velocity profile	V_{mean}, V_{rms}, W_{mean}, W_{rms}

b) Flow Visualisation

Chord Length /mm	Reynolds Number	Incidence /degrees	Technique
160	$0.3x10^5$	0,1,2,3,4,5	Smoke wire
160	$2.13x10^5$	0,1,2,3,4,5	Oil streakline

Table 4.1 Summary of test conditions used in the experimental investigations

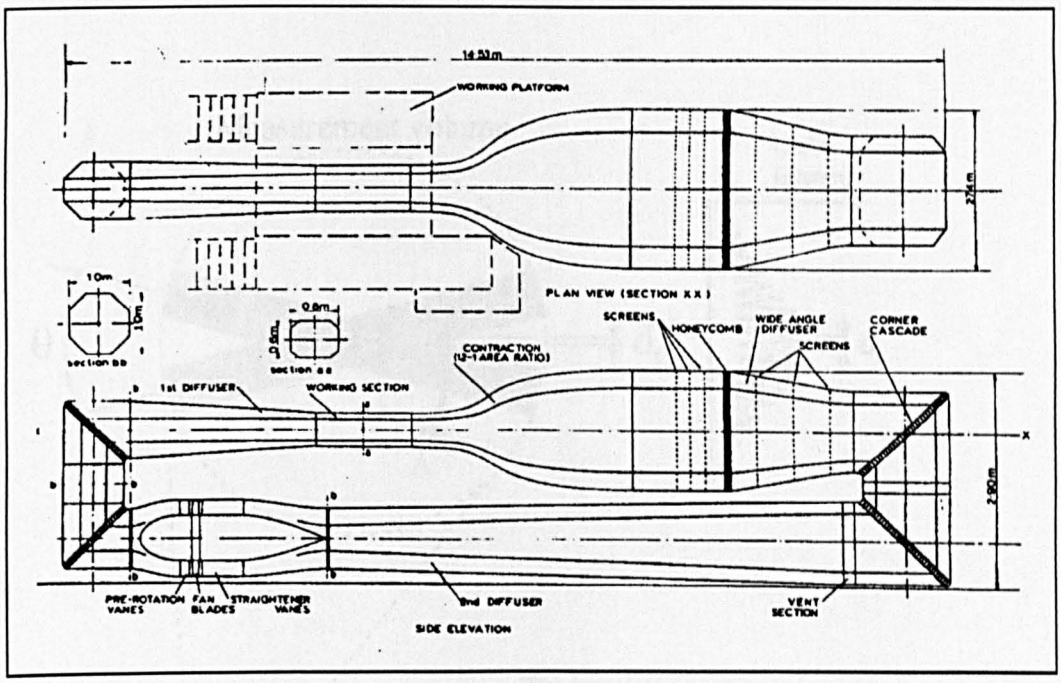

Figure 4.1 Low turbulence wind tunnel (Barrett 1984).

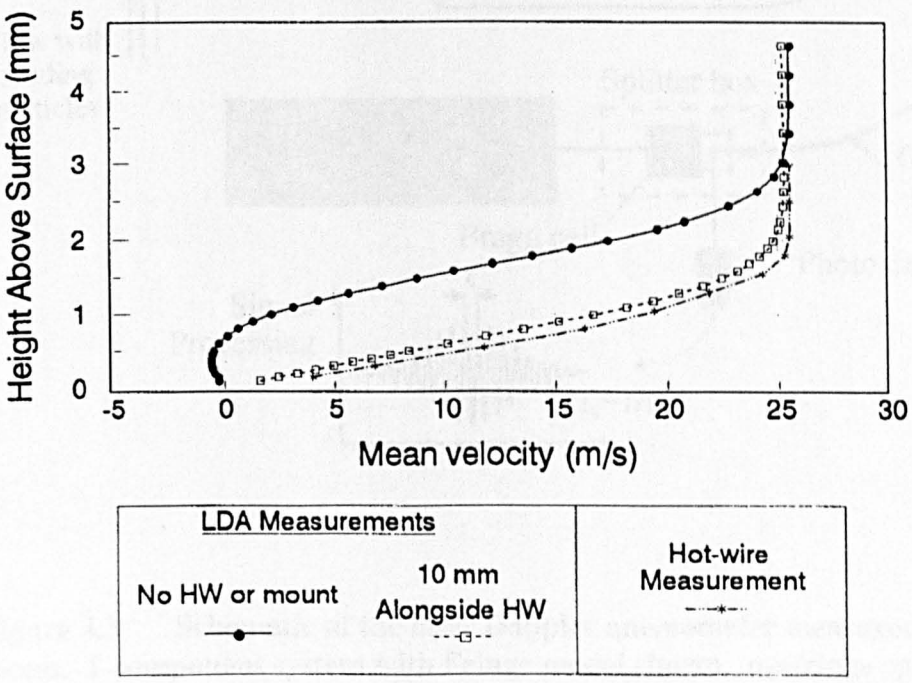

Figure 4.2 The effect of a hot-wire on an aerofoil with trailing edge separation. (Nash 1996).

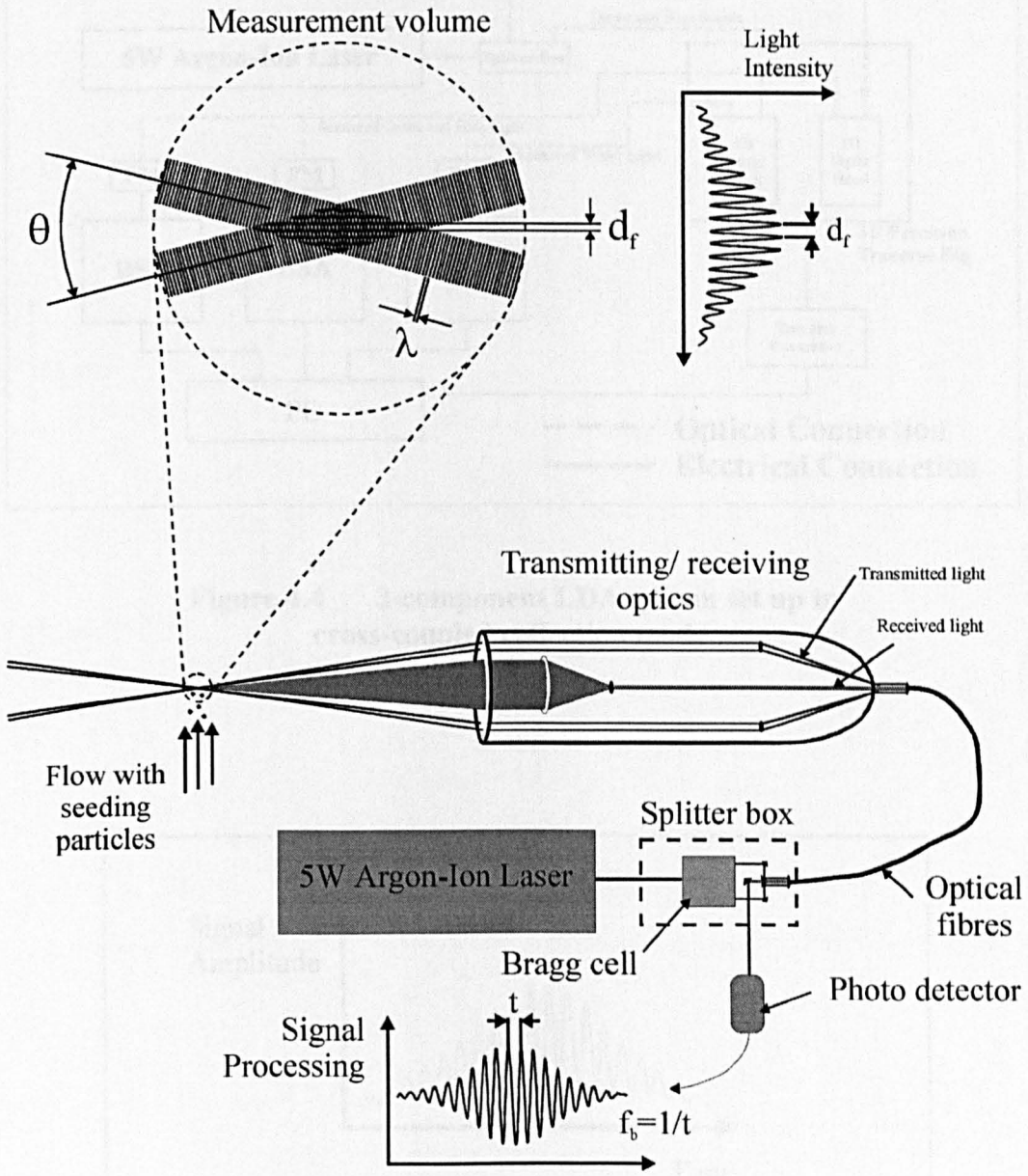

Figure 4.3 Schematic of the laser Doppler anemometer measurement Process. 1-component system with Fringe model shown. d_f=fringe spacing.

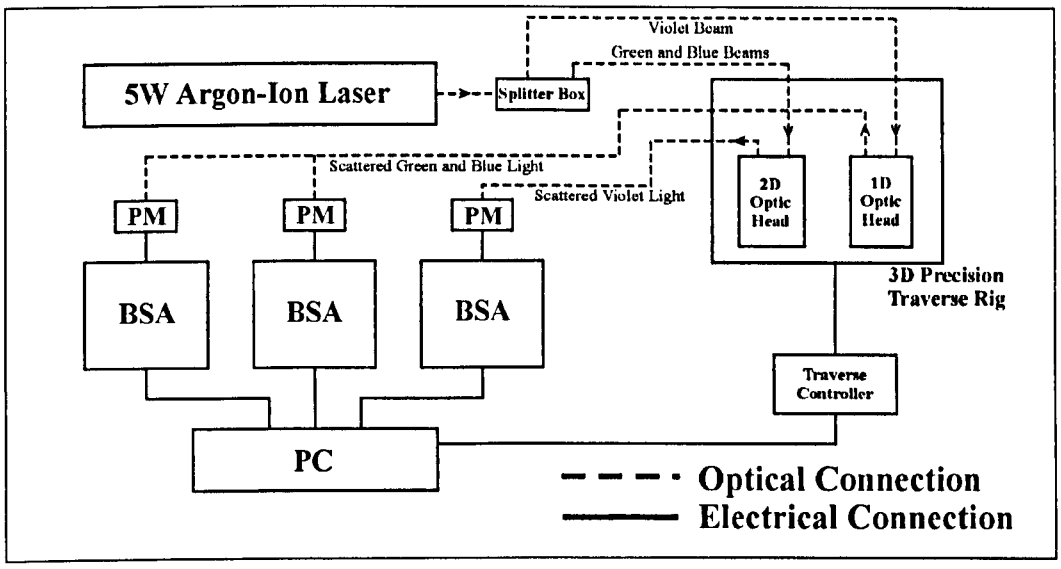

Figure 4.4 3-component LDA system set up in cross-coupled collection mode.

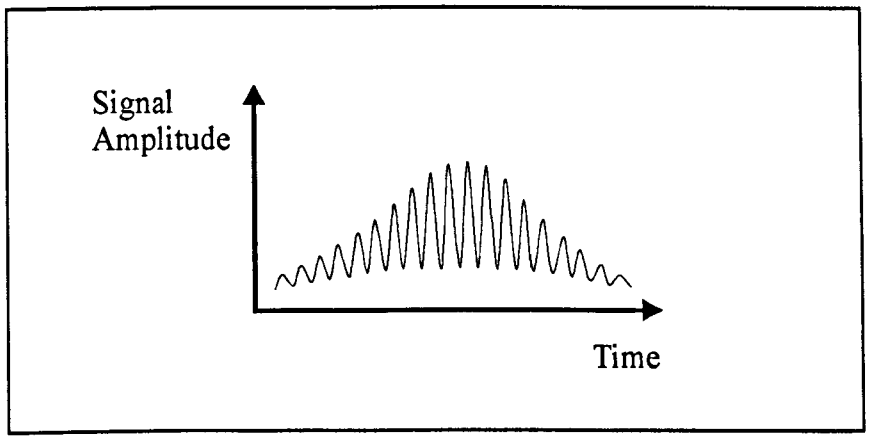

Figure 4.5 An example of a Doppler burst produced as a seeding particle crosses the measurement volume.

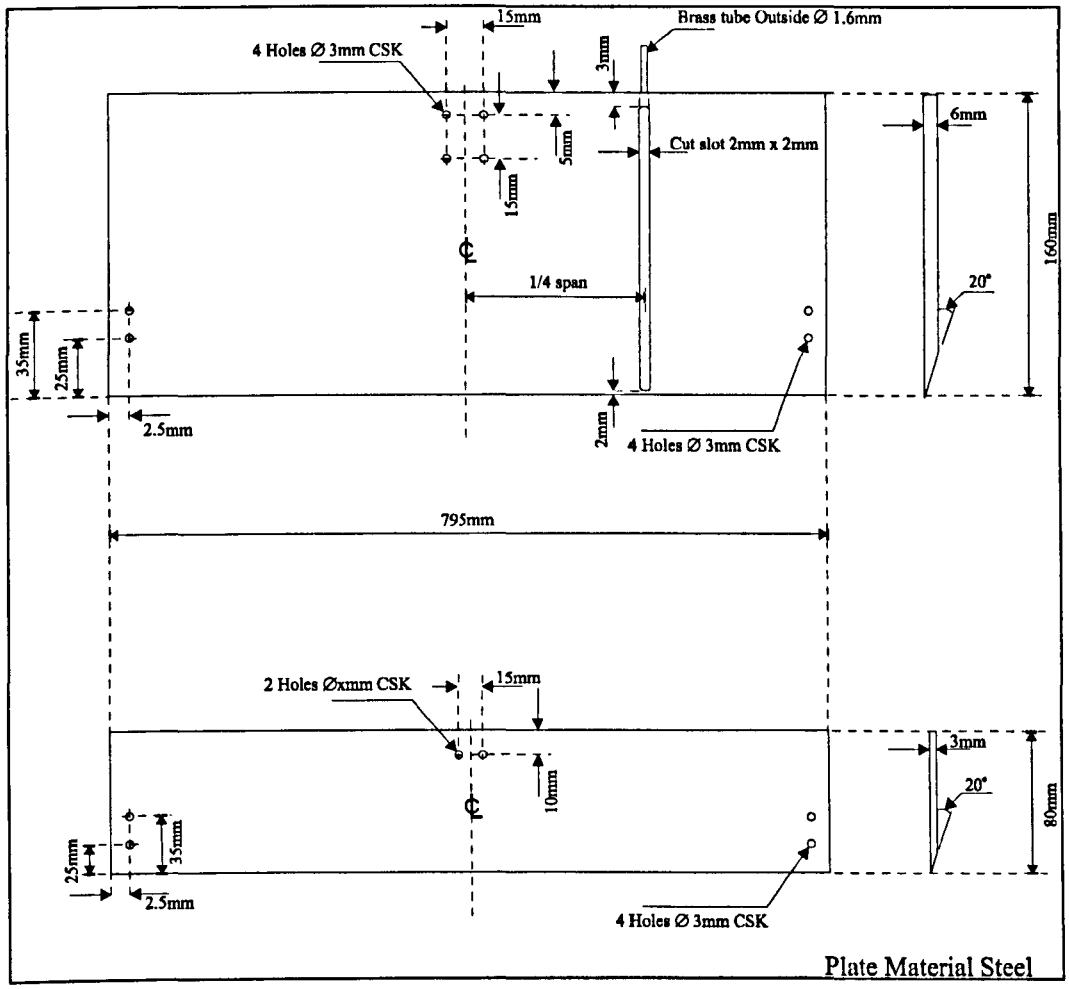

Figure 4.6 Details of flat plate designs used for the main investigation (not to scale).

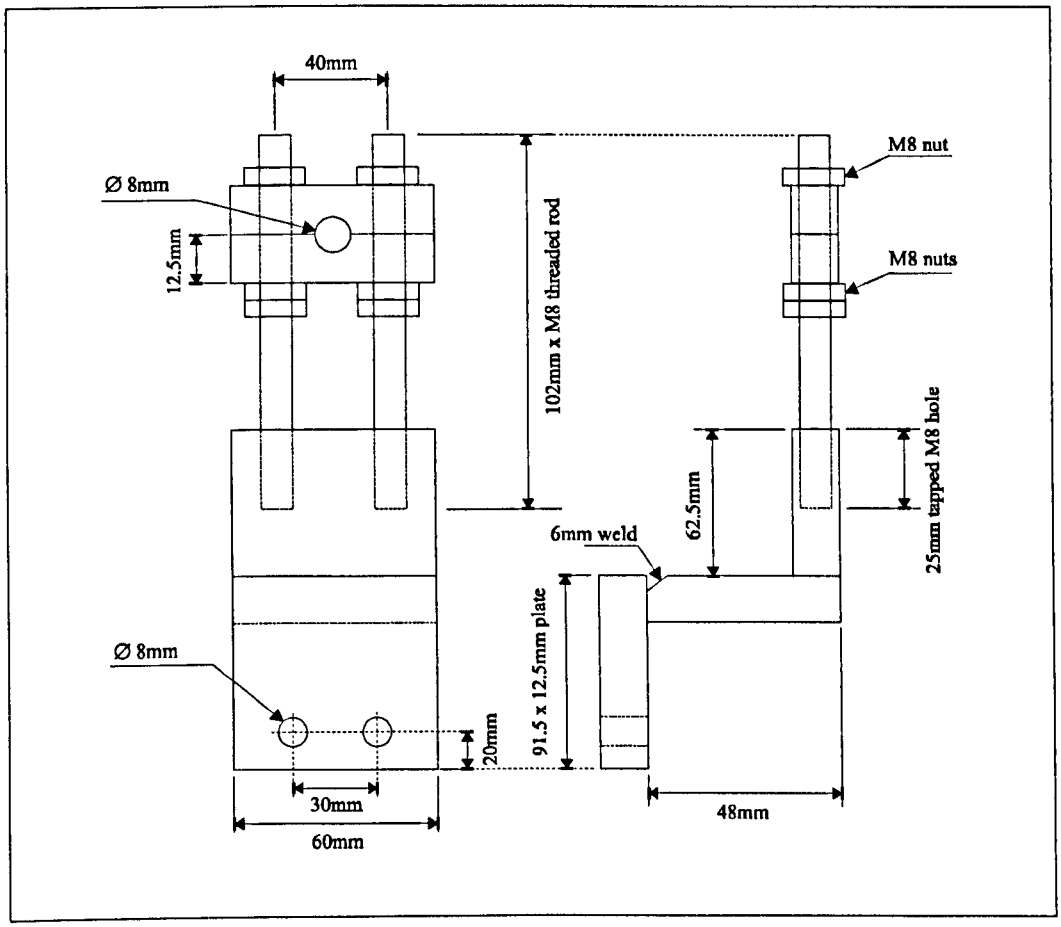

Figure 4.7 Detail of plate mounting bracket design (not to scale).

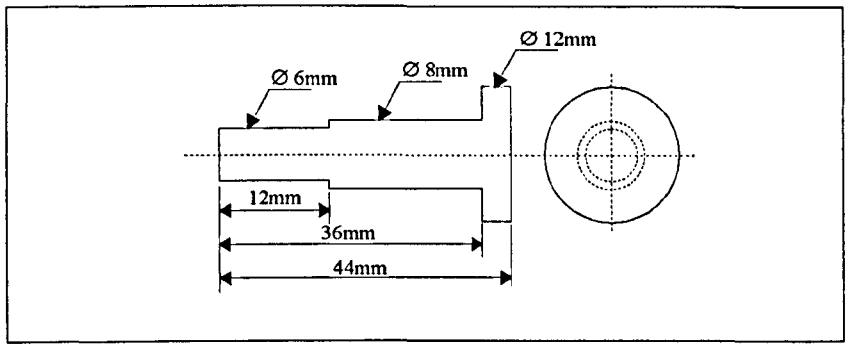

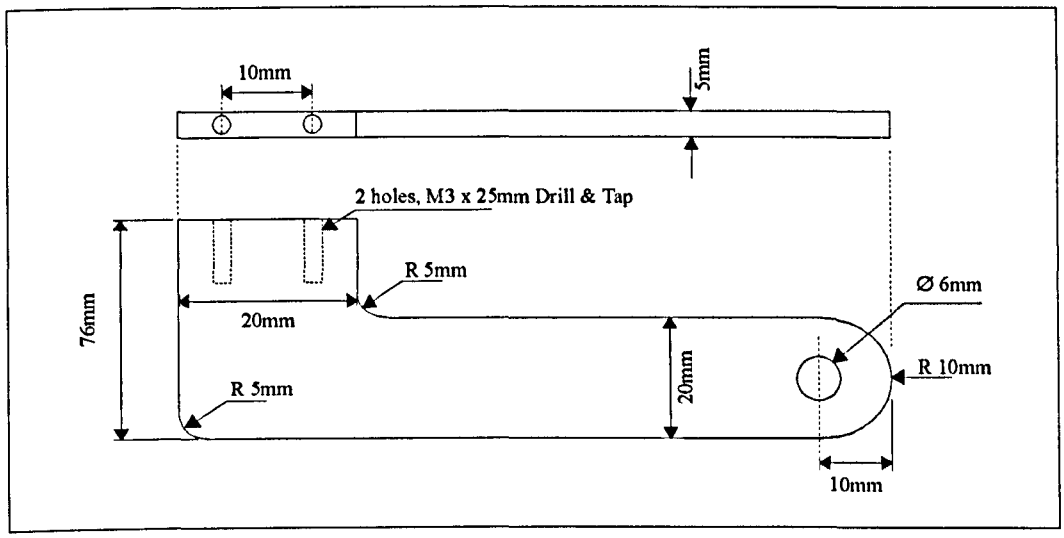

Figure 4.8 **Details of the plate support bracket and support pin design used in the main investigation (not to scale).**

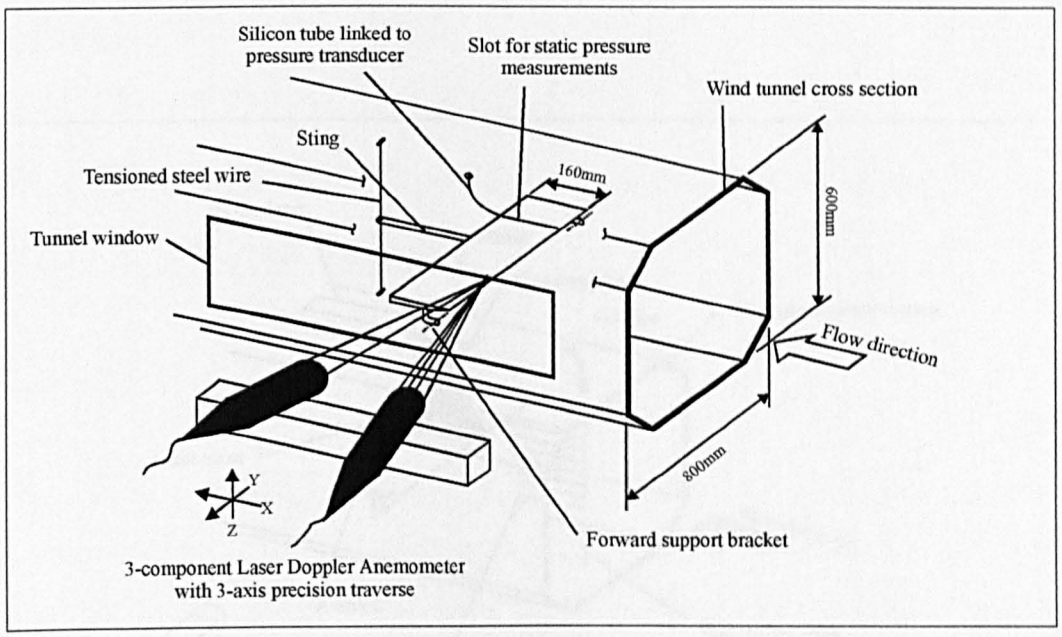

Figure 4.9 Schematic representation of experimental set-up used in the main investigation (not to scale).

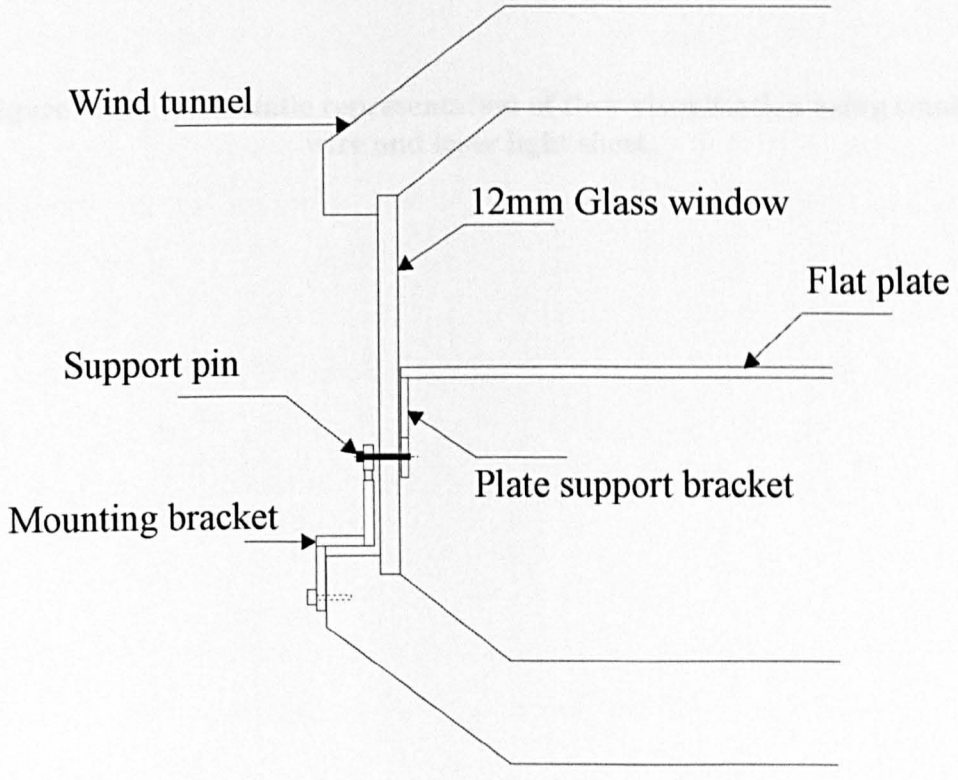

Figure 4.10 Enlarged section showing mounting brackets, support pin and tunnel window (not to scale).

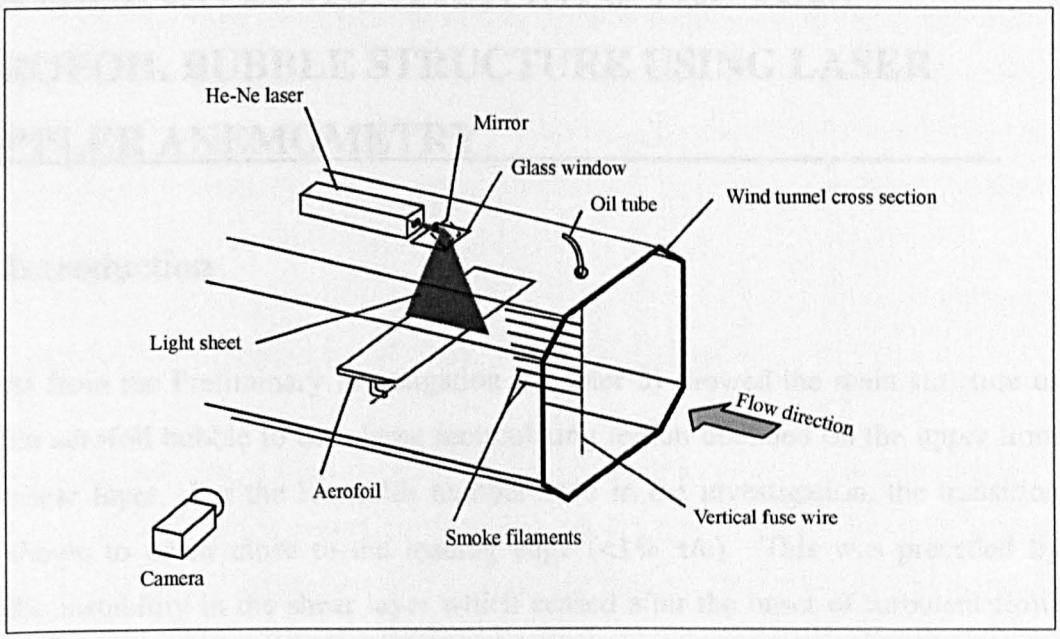

Figure 4.11 Schematic representation of flow visualisation using smoke wire and laser light sheet.

CHAPTER 5
FURTHER INVESTIGATION INTO THE THIN AEROFOIL BUBBLE STRUCTURE USING LASER DOPPLER ANEMOMETRY

5.1 Introduction

Results from the Preliminary Investigation (Chapter 3) showed the main structure of the thin aerofoil bubble to be a large recirculating region bounded on the upper limit by a shear layer. For the Reynolds number used in the investigation, the transition was shown to occur close to the leading edge (<1% x/c). This was preceded by periodic instability in the shear layer which ceased after the onset of turbulent flow. The now turbulent shear layer displayed an increased rate of thickening and had a high entrainment rate of fluid on the low velocity edge. The shear layer then curved back towards the surface and reattached at a point that moved progressively rearward with an increase of incidence. Upon reattachment, the shear layer bifurcated with some fluid being fed upstream, forming the reverse flow region and the rest continuing downstream where it gradually reverted to a conventional attached turbulent boundary layer. The length of the separation bubble was strongly dependent on the plate incidence, with any further dependency of this length on a change in Reynolds number and chord length not being evaluated. A region of separated flow measured close to the leading edge, at the very front of the separation bubble, was identified as a small enclosed region of flow rotating in a direction counter to the main bubble.

The aim of the main investigation, described within this chapter, was to determine the effect, if any, of various parameters on the separation bubble, in particular, Reynolds number, plate incidence and chord length. The mechanisms of the leading edge separation, transition, reattachment and further separation of the attached boundary

layer were also detailed. A complete set of velocity data for a given Reynolds number was measured over a range of incidence where the separation bubble reattaches to the plate surface. To further validate the results, flow visualisation was used and a new technique developed to further enhance the visualisation of the separation bubble. Finally, an introductory investigation into the effects of three-dimensionality on the bubble structure was carried out by introducing sweep angle and a free tip to the plate.

5.2 General Structure of the Thin Aerofoil Bubble

Using the 160mm chord plate, extensive velocity measurements were obtained with the use of laser Doppler anemometry. The spatial resolution of the surveys was refined to give greater resolution over regions of steep velocity gradients. In addition, higher sample sizes (20,000 samples) were used in turbulent regions, giving consistent smooth data for the mean and root-mean square (rms) components of velocity. In freestream regions, a smaller sample size was used (5000), sufficient to give accurate data where there was little velocity fluctuation. This approach maximised the accuracy of the measurements whilst maintaining a realistic total acquisition time.

The general flow structure of a typical thin aerofoil bubble formed on a flat plate with sharp leading edge and its development with increasing incidence can be seen by the velocity contour plots measured in a chordwise plane perpendicular to the plate surface. Figures 5.1a-f show the mean chordwise velocity and Figures 5.2a-e show the corresponding rms chordwise velocity component. Figure 5.2f shows a typical graduated measurement grid used for producing the contour maps. The velocity measurements have been non-dimensionalised to the freestream tunnel speed U_∞ and the chordwise and perpendicular distances relative to the plate are non-dimensionalised with respect to the chord length. The examples are for a Reynolds number of 2.13×10^5, based on chord, and incidences range from 1-5 degrees, the

range for which the separation bubble reattaches to the surface before the trailing edge is reached. An additional plot, Figure 5.1f is shown for mean chordwise velocity at an incidence of 8 degrees by which incidence the separation bubble fails to reattach to the surface and extends into the freestream downstream of the trailing edge. It is important to note that the rms velocity readings are higher when compared to those that would be measured using a hot-wire anemometer for the same flow. This is as a result of the high electrical noise that is present in the LDA signal processing equipment. The settings on the BSA, including signal gain and high voltage affect the background noise and hence rms velocity value. For the present investigation, an rms velocity below 5% (u_{rms}/U_{∞}), measured by the LDA, is considered to be laminar in the range of speeds used, Eustace (1999).

The reattachment point is defined as the location along the chord at which the mean chordwise velocity gradient perpendicular to the surface is zero. This was interpreted for practical purposes as the position with zero mean chordwise velocity at the closest measurement location to the surface attainable, i.e. 0.05mm. The reattachment region is highly unstable and so it is essential that an instrument able properly to resolve flow reversal, such as the LDA, is used.

It is apparent from the close spacing of the velocity contour lines in Figures 5.1a-f that there are steep velocity gradients close to the leading edge of the flat plate. The large change in chordwise velocity over a short perpendicular distance to the plate generates a high level of shear. This high level of shear is common on many bluff body geometries where the flow often separates from a sharp edge generating a shear layer, the region of mixing between the freestream flow and the low velocity region. The shear layer is an important source of turbulence, generated by instabilities that develop between the layers of fluid moving at different velocities. The shear layer thickens at a low rate up to about 5% chord from the leading edge at which point a substantially increased rate of thickening begins. (This will be shown in more detail in Figure 5.8, Section 5.3.1). The increased rate is due to the transition of the shear layer from a laminar to a turbulent state.

In Figure 5.2a-e the associated increase in the turbulence is seen to begin a little closer to the leading edge than 5% chord. Turbulence intensity then reaches a peak (>35% u_{rms}/U_∞) close to the maximum thickness of the bubble, before decreasing as the shear layer bends towards the surface and reattaches. After reattachment, the reduction in turbulence intensity continues to the trailing edge owing to the relaxation of the newly attached boundary layer, as noted previously by Bradshaw & Wong (1972). The reasons that the reduction in turbulence intensity begins prior to reattachment are twofold:

1. In the general downflow near reattachment, eddies approaching the surface will be damped out.
2. The bifurcation of the shear layer will tend to split the large eddies into smaller ones.

Supporting this, Bradshaw & Wong measured a rapid decrease in the turbulent shear stress and eddy length scale just downstream of reattachment.

Over the front portion of the bubble, the outer flow is subject to a large acceleration, similar to that experienced around a conventional rounded aerofoil. For all plate incidences tested, the velocity reaches a maximum value of $1.35U_\infty$ at 20% bubble length and it is this acceleration, and hence low value of static pressure reached, that provides the main source of lift on the flat plate.

The strong reverse flow component of the separation bubble reaches a maximum mean chordwise velocity of $-0.4U_\infty$, the fluid being driven by the entrainment process provided by the shear layer. The magnitude of reverse flow velocity is approximately the same for all angles if. It is particularly energetic because most of the shear layer (at least 95%), is turbulent. This contrasts with short separation bubbles on rounded aerofoils where a considerable portion of the shear layer, sometimes as much as 80% of the length, is laminar (Gault 1955) and the maximum reverse flow velocity is

typically less than $-0.2U_\infty$. The acceleration of low velocity fluid on the lower boundary of the shear layer requires, by continuity, that additional fluid must be injected to replace it. This is provided by entrainment along the shear layer which is present all the way to the leading edge. The high mean velocity of the reverse flow region has the effect of reducing the static pressure under the shear layer and hence increasing its curvature towards the surface.

The similarity of the absolute velocities found across the separation bubbles at different incidences is the first indication that separation bubbles of differing lengths are displaying a degree of comparability for the range of incidence measured on a given aerofoil.

Figure 5.3 shows the static pressure coefficients over the flat plate for angles of incidence at which the separation bubble reattaches to the surface. The distributions are for the unchamfered (upper) surface of the plate for both positive and negative angles of incidence. The representative distributions for negative angles of incidence are included to provide an indication of the distributions along the lower surface of a flat plate, assuming the incidence to be positive. The minimum pressure occurs over the front portion of the bubble where there is a pressure plateau. This is followed by a region of strong pressure recovery up to and beyond reattachment, with zero pressure gradient further downstream. The maximum adverse pressure gradient exists just prior to the reattachment point and the relaxation of the turbulent boundary layer occurs mainly in the zero pressure gradient region. The low values of static pressure under the majority of the bubble length tend to increase the curvature of the shear layer. The separation bubble grows in length as incidence is increased, with the shorter bubbles sustaining stronger adverse pressure gradients. The majority of the pressure recovery occurs over the aft portion of the bubble, a region where the flow is fully turbulent and the chordwise flow is decelerating. The start of transition in the shear layer is not associated with the onset of the adverse pressure gradient, as was shown to be the case for the short separation bubble. Figures 5.2a-e show transition to begin $<0.05x/c$ from the leading edge for all plate incidences. Also, for all

incidences, the location of maximum bubble height and maximum chordwise rms velocity component are both further downstream than the onset of the positive pressure gradient. This indicates that the onset of pressure recovery occurs in the transitional region of the shear layer.

5.3 Detailed Structure of the Thin Aerofoil Bubble

The velocity contour plots, described above, were generated from a grid of approximately 1000 data points for each test case and provided general surveys for the new flat plate. Although some key features of the thin aerofoil bubble have been identified, the contour plots do not show any precise details of the flow parameters and are therefore unsuitable for the detailed investigation of, for example, the boundary layers. Consequently, to fully resolve these features, detailed velocity profiles were taken perpendicular to the plate upper surface at various distances downstream from the leading edge. Figures 5.4a-e show the mean chordwise velocity profiles while Figures 5.5a-e show the chordwise rms velocity for the same measurement locations. The profiles were graduated to provide a greater density of data points close to the surface and across the shear layer and a lesser density in the freestream, where the velocity gradients are small.

5.3.1 Separation and Transition in the Shear Layer

The flow close to the leading edge is important in determining the nature of the flow-field over the rest of the plate. Velocity profiles taken at 3% chord from the leading edge (x/c=0.031) for any angle of incidence (Figures 5.4a-e) display particularly steep velocity gradients across the shear layer. The magnitude is in the order of a change in velocity of $1.5U_\infty$ over a vertical distance of just 1% chord (1.6mm) perpendicular to

the plate. Above this, the velocity reaches a maximum before tailing off gradually in the freestream where it approaches the tunnel speed asymptotically.

The dominant feature in the profile of the rms velocity is the central maximum which coincides with the point of inflection of the mean velocity boundary layer profile, approximately at the mid point of the shear layer. This indicates that the inflection point is associated with the amplification mechanism for instabilities in the shear layer. This rms peak becomes wider further downstream as the shear layer thickens.

The overall rms distribution is comparable in parts to the profiles found after separation of an attached boundary layer, where a triple peak profile was shown to exist, for example, across trailing edge separation bubbles, Nash (1996). However, in this example the presence of the attached boundary layer prior to separation was the cause of the three peak profile. The attached boundary layer was found to be responsible for two peaks whilst the third, formed between the first two, was a result of the separation and was generated by the instabilities of the shear layer.

For the thin aerofoil bubble case, there is no attached boundary layer prior to separation and therefore it is the shear layer which produces the major peak in rms, with the separation of the reverse flow boundary layer responsible for a second peak in some cases.

A remarkable feature is that the rms does not reach a steady value until approximately twice the local height of the bubble, or twice the boundary layer thickness downstream of reattachment. The peak values of unsteadiness are very high with rms values reaching 5.5-7.5m/s (27.5-37.5% u_{rms}/U_{∞}), in most cases. The mean and rms spanwise velocity components, Figure 5.6, are shown for profiles perpendicular to the plate at 3 degrees incidence. The mean velocity is negligible indicating no spanwise flow being sustained over time and the assumption of mean planar flow is valid. However the peak in the shear layer of the spanwise rms component is similar to the corresponding chordwise component. This suggests that the process of transition in

the shear layer is a three-dimensional process. Bandyopadhyay (1989) conducted careful flow visualisation of a reattaching shear layer and showed that eddy structures are not easily identifiable but are more clearly three-dimensional near reattachment.

Figure 5.5d includes insets of velocity histograms for various points across the shear layer for x/c=0.375. A large scale fluctuation of ±5m/s can be seen, at a height of z/c=0.05, where the mean velocity is near zero. The double peak velocity distribution is located in the mid point of the shear layer. Both above and below this point in the shear layer, the velocity histogram is asymmetric as one of the two peaks collapses. This distribution signifies a periodic behaviour of the shear layer. An identical behaviour was found to exist in the Preliminary Investigation, but only prior to transition.

This result suggests that the highly ordered periodic structure, formed prior to transition in the shear layer, propagates downstream, beyond transition, but with the increasing levels of background turbulence becomes less distinct as it is absorbed in the overall turbulence present within the widening shear layer.

This behaviour is apparent from the flow visualisation pictures from Ruderich & Fernholtz (1986) shown in Figure 2.21 (Chapter 2). At low Reynolds number, the periodic formation of vortices occurs close to the leading edge and the structure is maintained far downstream. Conversely, at high Reynolds number, this periodic structure breaks down very soon after separation and is absorbed in the turbulence. This is proposed to be the mechanism for this case investigated at a Reynolds number of 2.13×10^5.

The separation of the flow will always initiate a laminar shear layer, which both Gault (1957) and Newman & Tse (1992) showed to undergo rapid transition. Newman & Tse found that transition occurred at a Reynolds number based on shear layer width of the order of 100 which was very close to the leading edge. Similarly, Gault found that the extent of the laminar flow was virtually zero in tests at a chord Reynolds number

of $4x10^6$. The early transition, compared to that of a short bubble, suggests that some form of initial instability is affecting the shear layer closer to the leading edge in the flat plate case. This must be linked to the severe shear generated by the sharp edge separation.

A second possible reason for early transition is that the shear layer entrains highly turbulent fluid on its lower velocity edge. Castro & Haque (1987), in an experiment where separation was induced by a small plate normal to the flow with reattachment on a downstream central splitter plate, showed that even though the stabilising curvature of the shear layer might delay transition, it is more likely that, even close to the point of separation, the effects of entrainment of highly turbulent fluid will be dominant. They proposed the possibility of "positive feedback", where the shear layer entrains high energy fluid from the reverse flow region which increases the turbulence in the shear layer, thus ensuring an early transition. This was mentioned in Section 2.5.2.

Figures 5.7a and 5.7b show the mean and rms component of the velocity normal to the plate for 3 degrees incidence. The damping of this rms component can be seen close to the surface in Figure 5.7b, as the profile tends to zero. This can be compared to the behaviour of the chordwise and spanwise components, shown in Figures 5.5c and 5.6 respectively. The chordwise and spanwise rms components are maintained at high values until close to the surface, a possible result of the conversion of normal velocity perturbations to chordwise and spanwise directions perturbations.

Up until this point in the investigation, the location of transition in the shear layer had been determined to be within 5% of the leading edge, but had not been accurately pinpointed. Figure 5.8 shows data obtained at high spatial resolution from a chordwise measurement plane perpendicular to the plate and close to the leading edge. The absolute dimensions of the largest of the two measurement planes was 10mm by 6.4mm containing approximately 1200 data points. Presented is the chordwise rms velocity for both high and low freestream Reynolds number cases i.e.

$0.53x10^5$ and $2.13x10^5$. It can be seen that the spreading rate of the shear layer is greater at the low Reynolds number, analogous to the effect that Reynolds number has on the thickening of a normal attached boundary layer. The onset of transition, however occurs at about the same position in both cases, as can be seen by the plots of chordwise rms velocity along the centre-line of the shear layer in Figure 5.9 (The centre-line is defined as the inflection point in the velocity profile across the shear layer and the onset of transition can be identified by the discontinuity in the chordwise gradient of the rms velocity component and is shown to occur at 2-2.5% x/c). This shows that for this range of Reynolds number the transition point is close to the leading edge and is almost independent of the local Reynolds number. However, the influence of the shear layer will reach the surface in a shorter distance at low Reynolds number (on account of the increased spreading rate) and might therefore be expected to initiate reattachment sooner. Further assessment of the dependence of the bubble length on Reynolds number is made in Section 5.6.

5.3.2 Reattachment of the Shear Layer and subsequent Relaxation of the Boundary Layer

At a low enough incidence, the bending of the shear layer will enable the flow to reattach to the surface, at some distance after transition of the shear layer. The reattachment region is highly unstable and is a dividing region between fluid that either flows upstream to form the reverse flow region or downstream to the trailing edge. The instability is derived from imbalances between fluid entrained by the shear layer and that returned in the recirculation region. Also, large scale eddy structures that develop in the shear layer will cause further instability when the shear layer bifurcates. Castro & Epik (1998) showed that energetic structures present in the shear layer are carried along into the relaxation region and change their form from "mixing layer" structures to those found in boundary layers.

At reattachment, the velocity profile displays a form unique to reattaching turbulent shear layers with an almost linear region from close to the surface to the edge of the boundary layer. Horton (1969) identified the similarity in many such profiles by analysing existing data, and subsequently proposing a universal reattachment profile based on a semi-empirical method of analysis. The resulting shape had a zero velocity gradient at the wall, a necessary parameter for flow reattachment, followed by a constant gradient to near the edge of the boundary layer. Schmidt & Mueller (1989) used results by O'Meara (1985) for comparison with Horton's universal profile (shown in Figure 2.13, Chapter 2). O'Meara's profiles were obtained very close to his estimate of the reattachment point but were much fuller in shape than Horton's universal profile would suggest, with higher velocities near the wall and no obvious tendency towards a zero slope. Schmidt & Mueller explained the difference as either the measurement location being further downstream of reattachment than estimated or distortion of the profiles by the hot-wire measurement technique used. In the present study the nearest velocity profile to reattachment was taken at approximately 3% chord downstream at 3 degrees incidence. This profile, shown in Figure 5.4c, where $x_R/c=0.47$, conforms generally to Horton's, but the inner region of near zero gradient is seen to be suppressed in height, a possible consequence of the very high turbulence in this region.

Downstream of reattachment, the newly attached boundary layer initially exhibits a very different profile to that of a conventional turbulent boundary layer. It consists of a region of steep velocity gradient near the surface, almost too thin to measure, where a new inner boundary layer is developing, and above this, a broad region of near constant velocity gradient extending to freestream conditions. During the relaxation process, the lower half of this region is accelerated by the high-energy flow being injected into it from above, but the profile retains its near-constant gradient. This confirms the results of Bradshaw & Wong (1972) who showed that the outer part of the boundary layer develops much more slowly than the inner region. More recently, Castro & Epik (1998) showed that the inner region develops no more quickly than the outer region, which controls the development of the whole flow. They showed

this relaxation process to be very slow and for the present investigation, except for very low incidence, the flow reaches the trailing edge before the boundary layer has fully relaxed.

5.3.3 Reverse Flow Region

The majority of the fluid passes downstream from reattachment, but still a considerable portion passes upstream to form the reverse flow region. The strong reverse component reaches a maximum velocity of $-0.4U_\infty$ at approximately half the bubble length. From Figure 5.3 it can be seen that the newly formed reverse flow boundary layer experiences a favourable pressure gradient which accelerates it to the maximum velocity. The fluid is also driven by the entrainment needs of the shear layer, which by continuity must be fulfilled on its inner side by the reverse flow region.

The shorter length bubbles sustain a steeper pressure gradient and thus will accelerate the flow faster than a corresponding longer bubble. Hence the same reverse flow velocity can be achieved in a shorter distance along the plate surface allowing the reverse flow velocity to be scaled for different length bubbles.

Although the majority of the fluid that forms the reverse flow region is likely to come from the splitting of the shear layer in the reattachment region, fluid will also enter this region further upstream by the movement of large eddies from the shear layer towards the wall as suggested by Simpson et al. (1981). This process is validated by the inflections seen in the profile of chordwise and spanwise rms velocity which are not present in the profile of normal rms component. As discussed in the previous section, they are caused by the conversion of the vertical velocity into components parallel to the wall as it is approached. The injection of eddies into the reverse flow region causes increased turbulence and increases chordwise intermittency. It should

be noted that profiles of this nature were not seen in the relaxation region of the flow, downstream of reattachment.

A secondary effect of the favourable pressure gradient is to stabilise the reverse flow boundary layer. Castro & Haque (1987) first highlighted evidence suggesting that the boundary layer in the reverse flow region can develop "laminar-like" features. This effect is indicated in Figure 5.2a-e, which shows a noticeable drop in turbulence intensity as the reverse flow progresses, suggesting that the boundary layer is stabilising. An enlarged view of the part of the mean velocity profiles in the reverse flow (see inset, Figure 5.4c-e) shows a reduction of the velocity gradient near the surface as the flow meets the adverse pressure gradient along the forward part of the bubble. This leaves the boundary layer more susceptible to separation.

Figure 5.10 shows the chordwise distribution of the intermittency (the percentage of time that reversed flow is occurring) of the reverse flow region measured 0.5mm from the surface. 0.5mm was chosen as sufficiently far from the surface to give a high enough data rate, necessary for resolving time history information. The distance along the plate is normalised with respect to the reattachment length, and again shows similarity between bubbles of different lengths. As the measurements were taken above the surface, the reattachment point does not occur at 50% reverse flow as would be the case at the surface. If the reattachment region is defined as where there is between 5% and 95% reverse flow, it is seen to occupy a length of $\pm 0.4x_R$ for all bubble lengths. This agrees well with previous work carried out on flow through a sudden expansion by Westphal et al. (1984) who concluded that all recirculating regions bounded by turbulent shear layers were likely to be dynamically similar. In the 1 degree incidence case, the bubble is much shallower relative to the height of the measurement location, and Figure 5.10 shows an offset towards lower intermittency in comparison to the other incidences, which is probably caused by this.

The inset time traces of velocity in Figure 5.10, taken at half bubble length, 0.5mm from the surface, show a periodic suppression of the turbulent fluctuations. This

stabilisation is associated with the favourable pressure gradient over the rear half of the bubble.

5.3.4 Secondary Separation Bubble

The stabilisation of the reverse flow in the bubble adjacent to the surface assists the formation of the secondary separation bubble. It reduces the velocity gradient adjacent to the surface, by reducing the turbulent mixing process, leaving the reverse boundary layer susceptible to separation in the adverse pressure gradient occurring over the front half of the bubble. The flow separates in a similar manner to a short separation bubble before reattaching close to the leading edge when it encounters the strong chordwise adverse pressure gradient, caused by the separation of the shear layer. Unlike the short bubble, the reattachment position is fixed by the external pressure gradient and therefore the bubble size will depend on the location of the separation point. The secondary bubble rotates in the opposite direction to the main bubble and is comparable to a corner eddy, but having a much larger influence on the main shear layer.

Figure 5.11 shows chordwise velocity profiles through the secondary separation bubble. It can be seen that the maximum velocity near the surface is only about 4% U_∞. The length of this bubble varies between 2% and 8% chord over the range of incidence and Reynolds number investigated (Section 5.6). A major effect of the secondary separation bubble is to enhance the main shear layer immediately after leading edge separation due to the opposing velocity on its inner side. This increases the velocity gradient in the shear layer with consequent influence on transition. The driving force for the secondary separation bubble is therefore not the main shear layer which opposes its rotation but entrainment at the separation of the reverse flow, together with the chordwise pressure gradient near the leading edge. The chordwise rms velocity profiles close to the surface display a peak through the secondary separation bubble, most clearly seen in Figure 5.5c (x/c = 0.031). The cause is

identical to that in the main bubble, resulting from the separated shear layer that exists above the secondary separation bubble, albeit on a much smaller scale.

5.3.5 Location of the Forward Stagnation Point

On conventional rounded aerofoils, the position of the stagnation point is expected to be dependent on incidence. However, the pressure distributions in Figure 5.3 indicate that, for the flat plate tested, the stagnation point remains at the leading edge for all incidences at which the separation bubble reattaches. To investigate this further, LDA measurements were made on a smaller plate at a Reynolds number of 0.2×10^5 over a wide range of incidence. Figure 5.12 shows the results of this study and the set-up used. Starting with the plate normal to the freestream flow, the stagnation point converges rapidly on the leading edge, along the underside of the plate, as incidence is reduced. By 20 degrees incidence, the location is as close to the leading edge as could be resolved by detailed small scale surveys. The nature of a stagnation point means that it must be balanced by equal pressures to either side to be stable. It cannot therefore exist on an infinitely sharp leading edge unless at zero incidence. Although the leading edge appears sharp it clearly must have thickness and be somewhat rounded. This enables a pressure balance for the stagnation point to exist and explains why there is no apparent movement through the first 20 degrees of incidence. The consequence is that there is no significant boundary layer developed from the stagnation point around the leading edge before separation occurs on the upper surface.

5.4 Effect of Changes in Incidence on the Thin Aerofoil Bubble

The most important effect of a change in incidence is on the length of the separation bubble. As incidence is increased, the reattachment point moves progressively rearward until at some incidence the shear layer fails to reattach at all. Considering the geometry, as the plate incidence is increased, the angle that the shear layer leaves the leading edge increases and so, assuming a given thickening rate in the shear layer, the greater the distance becomes before reattachment can occur.

Figure 5.13 shows the reattachment lengths, non-dimensionalised with respect to chord length, against plate incidence for previous investigations involving flat plate type aerofoils, together with the results from the current and preliminary investigations for the 80mm, 160mm and 700mm chord length plates.

	Authors	Reynolds number based on chord	Chord length (mm)	Measurement technique used	Profile shape
1)	Rose & Altman (1950) and McCullough & Gault (1951)	5.8×10^{6}	1524	Pitot-static probes	Double-wedge
2)	Newman & Tse (1992)	0.5×10^{6}	305	Surface tufts	Double-wedge
3)	Gault (1957)	4×10^{6}	1524	Pitot-static probes & hot-wire	Flat upper, wedge lower surface
4)	Present Investigations	1×10^{5}	80	LDA	Chamfered leading edge
		2.13×10^{5}	160	LDA	"
	(Preliminary Investigation)	9.3×10^{5}	700	LDA	"

Table 5.1 Summary of investigations for which separation bubble lengths were examined (see Figure 5.13).

Table 5.1 summarises the investigations responsible for the data presented in Figure 5.13. The tests of McCullough and Gault (1951), were a continuation of the work by Rose & Altman (1950) and utilised the same double-wedge aerofoil. Work by Newman & Tse (1992) was based on a 1/5 scale model of the section used by Rose & Altman.

The discrepancies between the previous investigations referenced are considerable and it is likely they are due to three main factors.

1. The different experimental techniques used
2. Differing plate cross sectional shapes
3. Different geometries of model relative to wind tunnel working section dimension; leading to different levels of wind tunnel constraints (discussed in Section 5.5.1)

Newman & Tse found the bubble length to be proportional to α^2 with a slope, $d x_R/c/d\alpha$, which was dependent on the rate of growth of the shear layer. The discrepancy between their results and those of Rose & Altman was attributed to probe interference in the reattaching flow (Rose & Altman's experiments used pitot-static probes to determine the bubble length). However, the surface tuft method, used by Newman & Tse, is very approximate and they estimated the accuracy of their results to be: $x_R/c \pm 0.05$ and $\alpha \pm 0.5°$.

The limitations of the various measurement techniques used have been discussed more fully in Chapter 4. It was agreed by McCullough & Gault and Rose & Altman that the quantitative values from their flow surveys (including bubble length), were uncertain due to the techniques used. Gault intended the purpose of his flow surveys to be used for illustrating general features only.

The cross section shape of the plate is important when determining bubble length because, different shapes display different pressure distributions. The ideal test case for the investigation of the thin aerofoil bubble is an infinitely thin flat plate which, at

zero incidence, has a zero pressure gradient and produces zero lift. However practically, a finite thickness is required which can result in different cross sectional interpretations. An important parameter, set by the cross section shape, is the angle of incidence at which the separation bubble first forms. This angle is difficult to determine experimentally and for the purpose of this analysis is extrapolated from the behaviour of bubble length against incidence shown in Figure 5.13.

The double-wedge aerofoil is symmetrical along the mean chord line and produces zero lift at zero incidence. However, the shape of the upper surface has two main consequences. Firstly, the angle of the upper surface to the chord line means that a positive angle of plate incidence is required before a bubble will form. i.e. approximately 2 degrees in the case of Rose & Altman, McCullough & Gault and Newman & Tse, where the wedge angle was 5.2 degrees. Secondly, the pressure distribution is non uniform along the upper surface and therefore the behaviour of the separation bubble length, x_R, against incidence will be different when x_R is $<c/2$ compared to when x_R is between c/2 and full chord length. Once the bubble reaches the change in the cross section shape at c/2, a rapid increase in bubble length is expected for further incremental increases in incidence. Both these features can be seen in Figure 5.13, with the double-wedge showing a significantly steeper rate of change of x_R with incidence once the separation bubble length is greater than c/2.

For plates with a flat upper surface and either a double-wedge lower surface (Gault) or chamfered leading edge (present investigation), a more continuous response of separation bubble length can be expected for changes in incidence.

However, at zero incidence, because of the non-symmetric cross section, the mean camber line is slightly curved and a separation bubble will be present on the upper surface. Therefore a small negative incidence is required before the bubble is eliminated. Gault was aware of this behaviour and applied a correction of 0.3 degree to his results, the incidence that he determined was required to cause the onset of bubble formation (i.e. the bubble first forms at –0.3 degrees incidence). For the

chamfered leading edges used in the present investigation, a larger correction is required, and this is found to be approximately 1 degree.

Despite this geometry effect and the levels of inaccuracy expected from the differing experimental techniques, the large discrepancies are still not fully explained. In particular, the above discussion fails to explain the differences in the present investigation which used scaled plates and the same experimental technique to determine separation bubble length. Therefore, it is concluded that the effect of tunnel constraints must be significant and this is discussed in Section 5.5.1, when the effect of changes in plate chord is investigated.

5.4.1 Pressure Recovery

Figure 5.14 shows the pressure distribution data (first shown in Figure 5.3) with the chordwise distance non-dimensionalised with respect to the separation bubble length, to show the similarity in the pressure distributions. The data collapses onto a single profile, displaying further evidence of the physical similarity between different sized bubbles. The reattachment position can now be determined relative to the pressure distribution and is found to occur near the termination of the adverse pressure gradient.

There are many differences between the thin aerofoil bubble investigated here and the short bubble, but also some similarities. The firm basis of research on short bubbles can therefore provide clues to flow mechanisms in the long bubble. Work by Crabtree (1957) and Gaster (1966) amongst others, looked at the significance of pressure gradient on the short separation bubble. They concluded that in order to overcome the chordwise positive pressure gradient and allow the separation bubble to reattach, the shear stress had to be above a certain minimum value in the turbulent entrainment region. Crabtree defined a pressure recovery factor σ (Section 2.3.2.1) for the bubble based on the static pressure coefficients at separation and reattachment

and showed that there existed a maximum value, above which the bubble could not be maintained and "bursting" would occur. This value was $\sigma \approx 0.35$. In order to calculate the values of pressure recovery factor for thin aerofoil bubbles in the present investigation, the minimum value of Cp was used in place of the value of Cp at separation, which cannot easily be determined and in any case is not relevant because separation is caused by a different process in the sharp leading edge case. The result, Figure 5.15, shows an almost constant value of pressure recovery factor of around 0.35 as incidence is increased. Analysis of the work carried out by Gault (1957) gives a similar result. This is in marked contrast to the short bubble which shows a steep linear increase of pressure recovery factor with incidence, until bursting occurs, as illustrated by Crabtree's results which are also shown in Figure 5.15. As, in the case of a sharp leading edge, σ remains constant at a value close to that which causes bursting in short bubbles, it is suggested that the turbulent shear layer is maintaining close to the maximum sustainable shear stress.

5.5 Effect of Changes in Chord Length on the Thin Aerofoil Bubble

The length of the separation bubble is ultimately controlled by the plate incidence. Regardless of the chord length, the angle of incidence will control when the separation bubble initially forms at low or even negative incidence, up until the bubble fails to reattach to the plate trailing edge at a higher incidence.

For flows involving separation bubbles, the interaction of all the forces, inertial, viscous and pressure, will be involved in shaping the flow. Therefore, when comparing two experiments, assuming geometric similarity exists, and provided the magnitude ratio of any two of the forces are the same at corresponding points in the two systems, the flow structure and behaviour should be identical for both experiments. That is to say, if the Reynolds number is the same, and the geometry is scaled for the two experiments, the structure of the separation bubbles (particularly the length) should be similar.

The large variation, seen in Figure 5.13, between experiments indicates that one or more of the conditions, which must be satisfied for physical similarity, have been violated.

It has already been stated that, for this flow involving fixed separation at the leading edge, the flow is likely to be insensitive to a change in Reynolds number. This is investigated in more detail in the Section 5.6, but it is therefore likely that the geometrical similarity is the most important parameter for comparison purposes. One geometric factor has already been shown to differ between cases studied, this is the plate taper on all or part of its length. But to obtain geometric similarity, it is not just the plate geometry that must be scaled, but also the plate dimensions relative to the wind tunnel working section dimensions. Failure to do this will result in differing amounts of tunnel constraint which has been shown to affect bubble length.

Tests by Castro & Haque (1987) on a flat plate normal to the flow with a downstream central splitter plate, showed that the reattachment length was affected by the ratio of the tunnel height to the length of the plate normal to the flow. As the tunnel height reduced (or normal plate length increased), the reattachment length decreased. Hence, increasing the level of tunnel constraint forced an earlier reattachment.

Table 5.2 shows the dimensional information of the set-up used in these referenced investigations.

	Authors	Reynolds number based on chord	Chord length (mm)	Thickness to chord ratio (%)	Tunnel height (m)	Tunnel height to chord length ratio
1)	Rose & Altman (1950) and McCullough & Gault (1951)	5.8×10^6	1524	4.2	3.05	2
2)	Newman & Tse (1992)	0.5×10^6	305	4.2	0.91	3
3)	Gault (1957)	4×10^6	1524	3.8	3.05	2
4)	Present Investigations	0.1×10^5 - 0.1×10^6	80	3.8	0.60	7.5
		0.2×10^5 - 0.6×10^6	160	3.8	0.60	3.75
	(Preliminary Investigation)	0.6×10^6 - 1.0×10^6	700	1.9	0.60	0.86

Table 5.2 Summary of dimensions in the experimental set-up for thin aerofoil bubble investigations.

The ratio of chord length to tunnel height, included in Table 5.2, shows a large variation of between 0.86 and 3.75 suggesting large differences in constraint between the cases.

For the development of the analysis of tunnel constraint, only the plates used in the course of the present research were considered.

5.5.1 Wind Tunnel Constraint

There are a number of parameters that affect the reattachment length, but for a given incidence and chord length and in the absence of freestream turbulence and strong three-dimensional effects, the most dominant is the tunnel constraint. Tunnel constraint includes solid and wake blockage, lift effect and wall boundary layer interference (discussed in Section 3.2.2). A complete discussion of tunnel constraint is given by Pankhurst & Holder (1952).

As the freestream is displaced around the plate and separation bubble, the curvature of the streamlines is constrained by the presence of the tunnel walls, which must themselves become streamlines of the flow. The flow will be modified, as illustrated in Figure 5.16. This effect can be analysed using a method images to represent the plate and the wind tunnel walls. Simple combinations of singularity elements (sources, sinks, doublets and vortices) can be used to approximate the model shape and this is adequate for models that are small compared to the wind tunnel cross section.

Solid and wake blockage change the velocity past the model owing to the model and wake partially blocking the flow. In the main investigation, because the plates were very thin and operated at low incidence, the blockage was small, producing an effective velocity increase in the order of 1% at 5 degrees (for the 160mm plate), decreasing to near zero at 0 degrees incidence. Because the change in velocity is small, no correction was made to the Reynolds number. The lift effect was thought to be of more significance because of the sensitivity that the bubble length has already showed to a change in incidence.

With no trailing vortices, the lift can be represented by a vortex of strength K, at the centre of pressure (where L/unit width = $\rho U_\infty K$). To simulate the tunnel constraint effect, mirrored vortex images are used as shown in Figure 5.17. The effect of the induced velocity from the vortex images can then be used to give an approximate

incidence correction on the original plate. The derivation of the lift effect is shown in Appendix B.

The corrections were applied to the data, shown in Figure 5.18a, and the results re-plotted in Figure 5.18b. This correction leads to the important result that by taking account of wind tunnel constraint, the separation bubble length is shown to scale with plate chord and therefore, the separation bubble length can be expressed as a function of incidence.

Before determining the relationship between bubble length and incidence, a further correction must be applied to the incidence to take account of the plate section shape. As discussed in Section 5.4, the incidence at which the thin aerofoil bubble first forms depends on the plate geometry (approximately –1 degree for the plates used in this investigation). The data shown in Figure 5.18b was corrected and by re-plotting x_R against α^2, the data was seen to conform to a linear fit, shown in Figure 5.19. This relationship agrees with the conclusions of Newman & Tse. The gradient of this line, however, will depend on the Reynolds number of the flow as discussed in the next section.

5.6 Effect of Changes in Reynolds Number on the Thin Aerofoil Bubble

Until now, because of the fixed flow separation at the leading edge and the early transition, the separation bubble process has been assumed to be a turbulent one and therefore only weakly dependent on Reynolds number. However, the secondary separation bubble is formed from a "re-laminarising" boundary layer which then separates and this is likely to be dependent on the state of the boundary layer and hence be Reynolds number dependent. Tests were carried out on the 160mm chord plate and the Reynolds number was changed by varying the freestream velocity.

Figure 5.20 shows that, for a given incidence, the length of the secondary separation bubble decreases progressively as Reynolds number is increased. This is because increasing Reynolds number causes the reverse flow boundary layer to adopt a more turbulent profile and thus become more resistant to separation close to the leading edge in the adverse pressure gradient region. This behaviour is common of all boundary layers.

Figure 5.21 shows the dependency of the main separation bubble length to a change in Reynolds number for a range of incidence and for two different chord lengths. Clearly, a variation does occur as Reynolds number rises. (This Reynolds number effect was detected because the Reynolds number range of the tests was increased relative to that used in Chapter 3.)

The reattachment length first decreases then increases again, up to a certain limit above which any further change in Reynolds number has negligible effect. This limit was around 10^5 increasing slightly as incidence was reduced because, at lower incidence, the bubble is much shallower and hence viscous effects will be intensified. In similar experiments Newman & Tse (1992) found that the reattachment length became independent of Reynolds number above about 2.5×10^5. In other types of long bubble flows such as the experiments of Castro & Haque (1987), and Ruderich & Fernholz (1986) similar limits on the effect of Reynolds number were found but no clear explanation was given.

The level of entrainment in the shear layer determines the magnitude of the reverse flow velocities, hence controlling the static pressures at the surface and the curvature of the dividing streamline towards reattachment. At low Reynolds numbers entrainment is low and therefore the reattachment length is high, assuming reattachment occurs at all. Initially as Reynolds number is increased, entrainment also increases and the bubble shortens until a minimum length is reached at which entrainment has reached its maximum i.e. the shear layer is effectively fully turbulent. Beyond this, contraction of the shear layer normal to the flow direction causes

reattachment to be delayed, as described earlier in relation to Figure 5.8. Eventually the reduction in lateral growth rate becomes negligible and the reattachment length then remains constant for further increase in Reynolds number.

5.7 Analysis of the Flow using Visualisation Techniques

The objective of the flow visualisation investigation was to reinforce the quantitative results produced using the LDA. In particular, the separation bubble length was compared using the oil streakline technique. The smoke wire technique was aimed at providing a true picture of the bubble shape and direction of the flow streamlines.

5.7.1 Smoke wire

The full description of this technique is given in Section 4.5.4.1 and the results for angles of incidence between 0-5 degrees are shown in Figures 5.22a-b. Tests were carried out at a Reynolds number of 0.3×10^5, a value lower than the majority of this experimental work. The low velocities were necessary to reduce the dispersion of the smoke filaments. Higher speeds tended to break up the filaments, causing them to become indistinct. The images presented were taken with a short exposure time, 1/10000s, and therefore give a "snapshot" of the flow to best demonstrate the flow characteristics present. They are therefore not necessarily representative of the mean flow pattern.

The main features of the flow observed are outlined below:

- As the smoke particles approach the leading edge, their path is first seen to be deflected away from the upper surface before then returning to it. This is best seen at the higher incidences (3-5 deg.) where a clear inflection point is observed at the leading edge.

- When the flow returns to the surface it shows a diffuse reattachment region, which is more clearly defined at the lower incidences (<3 deg.). Downstream of this is an indistinct region where the smoke follows a more irregular path.
- As the incidence increases, the reattachment region moves further downstream and becomes less well defined whilst there is a gradual increase in the thickness of turbulent fluid above the surface. This is characterised by a "blurred" region extending from the surface into the freestream.
- The dark region within the bubble is the reverse flow region showing little entrainment of smoke particles from the freestream. However, visible at 3 and 4 degrees is a small region of smoke close to the leading edge of the reverse flow region. This is in the vicinity of the secondary separation bubble and may have been entrained from the shear layer by the high shear seen to be present there.

The descriptions above are all consistent with the proposed model of a laminar separation followed by transition in the shear layer and a turbulent reattachment process. Figure 5.12 showed the stagnation point to be on the leading edge and this is complimented by the flow visualisation showing an inflection in the flow at the leading edge. The turbulence created by the separation bubble is passed into the freestream by lateral momentum transfer and this is in full agreement with the LDA results for the streamwise rms component of the flow. Figures 5.2a-e show the thickening region of high rms velocity downstream of the separation bubble as the incidence is increased. This compares well with the images presented.

Overall, this new adaptation of the smoke wire method easily identifies main characteristics of the flow but is not suitable for giving quantitative information, such as bubble length. The method however produced clear images which show the direction of the inviscid flow path.

5.7.2 Oil Streakline

Figures 5.23a-c show the patterns revealed by the oil streakline method at a Reynolds number of 2.13×10^5. A full explanation of this flow visualisation method is given in Section 4.5.3.3. The patterns obtained were symmetrical about the centre span line and the images presented therefore show one side of the plate only. Lines have been added to illustrate how the results were interpreted.

It is clear from the patterns that there are well defined areas of scouring, these being regions of attached flow, with a high mean velocity parallel to the surface. Conversely, in the reattachment region, where there are frequent changes in flow direction, the flow failed to scour the surface effectively. The scoured area downstream is the relaxing attached turbulent boundary layer and upstream is the reverse flow region. The line of deposit close to the leading edge is the separation of the reverse flow boundary layer that forms the secondary separation bubble.

As the incidence is increased, the reattachment region moves further rearward and widens in its chordwise extent, and the secondary separation bubble also increases in length. At low incidences, planar flow is present across the majority of the plate. As incidence increases, the bubble length becomes more and more affected by the plate junction with the wall. There is also a tendency of the reverse flow to circulate as seen by the curved lines of flow towards the mid span along the reattachment region and towards the edges along the leading edge. A small vortex (corner vortex) is set up at the junction of the wall and plate leading edge which induces cross-flow and shortens the bubble length locally, a similar effect to that caused by sweep which is discussed in Section 5.8. As the opposite edges of the aerofoil circulate in opposite directions, there is always a region of planar flow that must exist at the mid span. This region of planar flow was shown to be 60% span in the preliminary investigation (for 3 degrees incidence). The flow visualisation reveals that for the modified plate with reduced chord (increased aspect ratio), the region of planar flow has increased to 80-85% span for the same incidence. For reference, this region of planar flow is

>90% span for incidences <3 degrees and reduces to 70% for 4 and 5 degrees incidence.

The LDA results defined a mean reattachment length and further, defined a reattachment region where the flow contained between 5%-95% backflow. This was found to occupy a length of $\pm 0.4x_R$. Subjective measurements were made of the reattachment region and the secondary separation bubble length from the oil streakline method and are compared to the LDA results in Figure 5.24. The agreement between the defined reattachment region and that determined from the oil streakline is excellent. This agreement suggests that the intermittency of the flow must exceed 95% in one direction for visible scouring of the oil to occur. The length of the secondary separation bubble is consistently higher when calculated using the oil streakline results. The majority of the oil deposit located along the separation line is driven from the reverse flow region towards the leading edge by the action of the shear in the reverse flow boundary layer. As the oil deposit builds up, and the flow decelerates, there may be insufficient shear force to drive the oil as far as the true separation point. As the oil evaporates, even more shear force is required and if this is not overcome, the line revealed by the flow pattern is in fact located prior to the separation point giving an impression of a larger region. Further evidence comes from under the secondary separation bubble itself. The original brush stroke pattern when the oil was applied is unchanged, signifying very low velocities. However, overall the oil streakline method is very suitable at defining the length of a separated region of flow at these incidences.

5.8 Introduction to the Effects of Sweep on the Thin Aerofoil Bubble

5.8.1 Introduction

The previous sections have concentrated on the two-dimensional configuration i.e a plate spanning the wind tunnel entirely with the ends sealed against the tunnel walls. This section aims to investigate the thin aerofoil bubble further by introducing further three-dimensionality into the flow, this is achieved by introducing a sweep angle to the plate and by freeing one plate tip away from the influence of the tunnel wall. This is a preliminary investigation into the three-dimensional bubble and only qualitative descriptions are given of the developing flow. The objective is to provide an introduction for future investigations into the swept bubble case. A mounting system, first used by Nash (1996) for a NACA 0012 aerofoil, was modified to carry the 160mm chord flat plate and allow the incidence and the sweep angle to be varied. The span of the plate across the working section was reduced to 600mm thereby giving an unswept tip clearance of 200mm to the tunnel wall.

The flow was visualised using the oil streakline method described in Section 4.5.3.3, which was employed successfully for the two-dimensional case. The systematic approach used is illustrated in Figure 5.25 below.

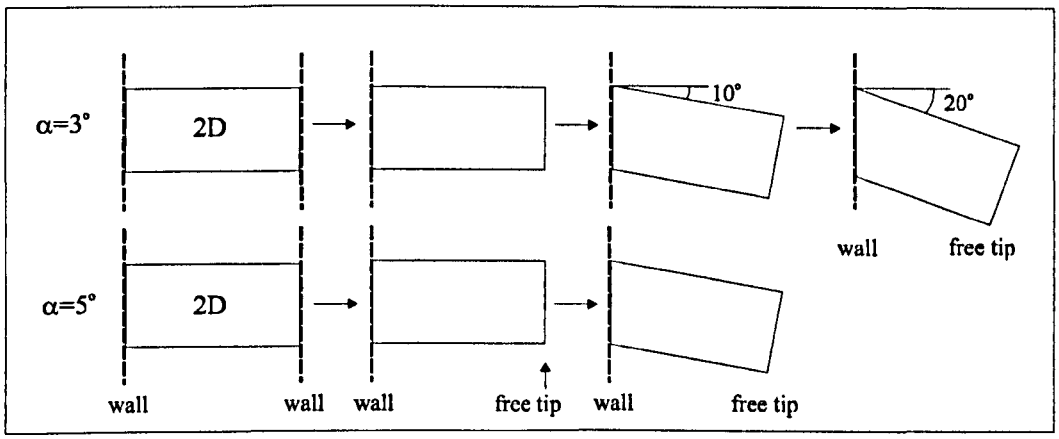

Figure 5.25 Systematic approach used to investigate sweep.

The main factors which will influence the flow pattern on a swept wing at a particular incidence are likely to include angle of sweep (Λ), leading edge radius, thickness to chord ratio, Reynolds number and the edge conditions. For a rounded aerofoil, the conditions at which flow separates from some or all of the suction surface will be driven by all the above factors. Lambourne & Pusey (1958) suggested that once the condition is reached that the flow separates along the entire leading edge, then the fundamental character of the flow will not be affected to a great extent by replacing the aerofoil with a flat plate of similar planform. Lambourne & Pusey also considered that the flow from a sharp leading edge would remain much the same over a wide range of Reynolds number, a feature confirmed from the present investigation. Therefore, in this study it is assumed that the main influences are sweep angle, incidence and end conditions.

5.8.2 Description of Flow Visualisation Results

5.8.2.1 Effect of Free Tip

Firstly, the effect on the flow pattern of creating a free tip was investigated for the unswept case. Figure 5.23b and 5.23c shows the two-dimensional case (with the plate spanning the working section) for incidences of 3 and 5 degrees. The corner vortices that form near the junction of the leading edge and the tunnel wall locally curtail the separation bubble, causing premature reattachment. The effect of introducing a free tip is shown in Figure 5.26a and Figure 5.26b for the 3 and 5 degree cases respectively.

The flow at the plate-wall junction is unaffected by the free edge condition. In contrast, at the free tip:

- the corner vortex has disappeared. There is now considerable inflow along the reattachment line and along the leading edge. The effect is enhanced as the incidence is increased to 5 degrees, a sinuous flow pattern can be seen developing in the recirculating region, indicating a spiralling motion of the flow.
- a "tip vortex" emanates along the chordwise free edge, illustrated by a scouring pattern. The vortex rotates about an axis parallel with the freestream direction, and was confirmed by holding a "spinner" probe in the wake and observing the rapid rotation. The tip vortex grows in size as the incidence is increased.
- The inflow reduces the reattachment length at the free tip more than is the case in the presence of the solid wall (seen on the opposite end of the plate) creating an asymmetry in the mean reattachment line across the span. Because there is flow, towards the mid-span, along the reattachment line, from both ends of the plate, there exists a location in the reattachment region where there is no spanwise flow component. This occurs at approximately 1/3 span (for 5 degrees incidence) from the wall and coincides with the maximum length of the separation bubble.

5.8.2.2 Effect of 10 degree Sweep Angle

The effect on the flow of a 10 degree sweep angle is shown in Figures 5.27a and Figure 5.27b for the 3 and 5 degree incidence cases respectively. The key changes are:

- The tip vortex is no longer visible on the plate surface because its axis has moved away from the plate tip.
- The increased sweep causes an overall velocity component towards the free tip. Therefore, the location in the reattachment region where there is no spanwise component moves outboard (approximately 2/3 span from the wall for the 5 degrees incidence case). This is again the spanwise location of maximum reattachment length.
- The corner vortex at the plate-wall junction is smaller and the local reattachment length is curtailed by the cross-flow. Sinuous flow now starts, in the recirculating region, close to this corner vortex and develops all the way to the maximum reattachment length. This spiralling is regarded as the onset of the process which at high sweep becomes recognisable as the rolling up of a vortex layer from the leading edge (most common in delta wing flows).
- The inflow from the free tip along the reattachment line, seen clearly at zero sweep angle, is reduced by the sweep of 10 degrees.

5.8.2.3 Effect of 20 degree Sweep Angle

Increasing the sweep to 20 degrees continues to develop the trends described above. The 3 degrees incidence case is shown in Figure 5.28. There is a noticeable increase in outward tangential flow velocity along the reattachment line and recirculating region. The sinuous profile in the recirculating region extends almost all the way to the free tip and is only counteracted by the corner vortex within a few percent span of the free tip itself. The local reattachment length remains curtailed at the free tip.

5.8.3 Summary of the Effects of Sweep

Overall, the main observations from the introduction of a free tip and a sweep angle are:

- Creating a free tip allows significant inflow along the reattachment line and causes a spiralling of the recirculating region away from the free tip. This locally reduces the reattachment length.
- A tip vortex forms along the chordwise free tip, but has no significant impact on the flow and as the sweep angle increases, its axis of rotation moves away from the plate.
- Increasing the sweep angle generates cross-flow outboard along the plate and causes a spiralling of the recirculating region, from the tunnel wall towards the free tip.
- The corner vortex at the plate-wall junction grows in size with incidence, but is reduced by an increase in sweep angle.
- The corner vortex at the free tip is not present at zero sweep, but as the sweep angle increases, it first grows in size and then shrinks as the outflow in the recirculation becomes dominant.
- The location of the maximum reattachment length is associated with the location at which the reverse flow streaklines are in a chordwise direction.
- The secondary separation line scales approximately in chordwise length with the main reattachment line for all angles of incidence and sweep tested.

5.9 Summary of the Chapter

The velocity profiles presented have shown the detailed structure of the thin aerofoil separation bubble. The external flow is accelerated over the front portion of the bubble up to a maximum velocity of approximately $1.35U_\infty$ and the reverse flow inside the bubble reaches a maximum velocity of $-0.4U_\infty$. There has been shown to be similarity in the velocity profiles of different length bubbles over the range of incidence tested.

Further similarity was shown by the pressure distribution along the plate surface. When non-dimensionalised with respect to the separation bubble length, the distributions collapse onto a single profile. A common value of pressure recovery factor has therefore been shown to exist for different length separation bubbles. This value is the same as that at which short separation are expected to burst. It is suggested that the shear layer has reached a maximum value of shear stress.

The shear layer was shown to initiate transition very close to the leading edge (2.5% x/c). The early transition is thought to be due to a number of factors including 1) the high level of shear close to the leading edge (a change of $1.5U_\infty$ over a distance of 1% chord perpendicular to the plate), and 2) the entrainment of highly turbulent fluid from the reverse flow region on the low velocity edge of the shear layer. Downstream of transition, the shear layer displays very high levels of unsteadiness (37.5% u_{rms}/U_∞).

The ordered periodic structures found prior to transition in the shear layer were not detected downstream of the separation bubble. This implies that as the structures propagate downstream, they become less distinct as the level of background turbulence increases. They are then absorbed in the overall turbulence of the shear layer before reattachment.

The reverse flow region is driven by the entrainment needs of the shear layer, which by continuity must be fulfilled on its inner side by the reverse flow. The reduction in static pressure resulting from the reverse flow helps to bend the shear layer towards the surface.

The favourable pressure gradient experienced by the reverse flow has been shown to periodically suppress the turbulent fluctuations in the reverse flow boundary layer. This boundary layer is decelerated close to the leading edge and separates. This results in the formation of the, previously undetected, *Secondary Separation Bubble* which rotates in the opposite direction to the main bubble and has a length of between 2-8% chord. (This is similar to a corner eddy found in flows over backward facing steps, but has not been measured for the case of a flat plate at incidence.).

The incidence of the plate is the main factor controlling the length of the separation bubble from its initial formation at low incidence until its failure to reattach at all. Analysis of the discrepancies in separation bubble length in previous investigations have focussed on experimental technique and the geometrical scaling of the section shape and experimental set-up. Differences between chord length and wind tunnel working section height cause different levels of wind tunnel constraint. For the current research, incidence corrections were made to the data resulting in a single profile for the behaviour of separation bubble length with incidence for three different chord lengths. In addition, when corrected for plate geometry, the thin aerofoil bubble length was shown to be proportional to the square of the incidence.

Reynolds number was shown to have a small effect on the separation bubble length, but only over a limited range of Reynolds number. The changes were due to the increasing entrainment of the shear layer and the falling growth rate of the shear layer (perpendicular to the mean flow direction) as Reynolds number rose. However, above a Reynolds number of 10^5, any further increases have negligible effect on the separation bubble length.

Analysis of the flow using visualisation techniques have confirmed the LDA results. The oil streakline results for the separation bubble length correlate well with the numerical results and the smoke wire method provides a very useful qualitative image of the inviscid flow path around the separation bubble.

Finally, the introduction of further three-dimensionality was investigated. The free tip increased inflow along the recirculating region and addition of sweep angle generated outflow along the plate. The location where the inflow and outflow balanced, resulting in chordwise flow patterns in the reverse flow, is associated with the maximum reattachment length across the span.

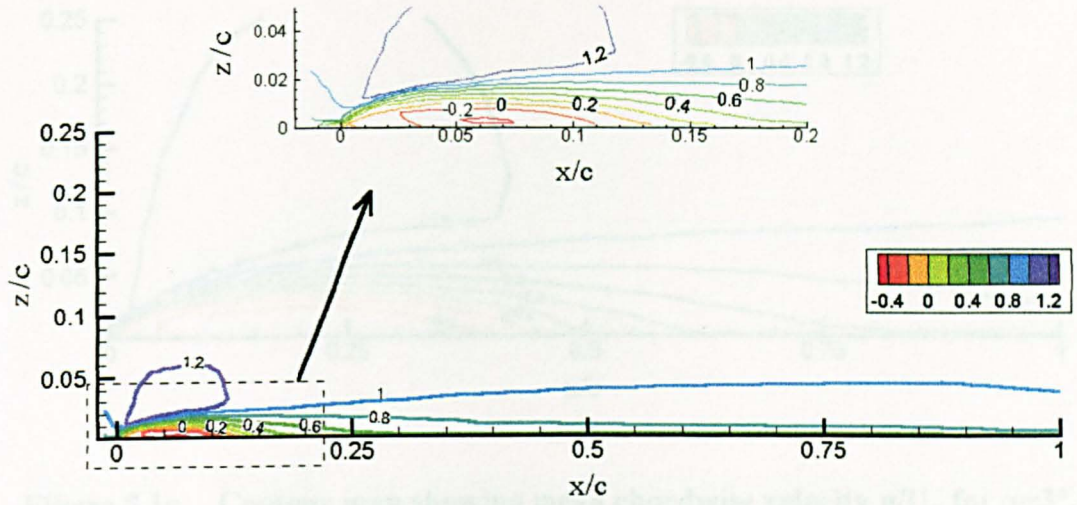

Figure 5.1a Contour map showing mean chordwise velocity u/U_∞ for α=1°, U_∞=20m/s, Re_c=2.13x10^5.

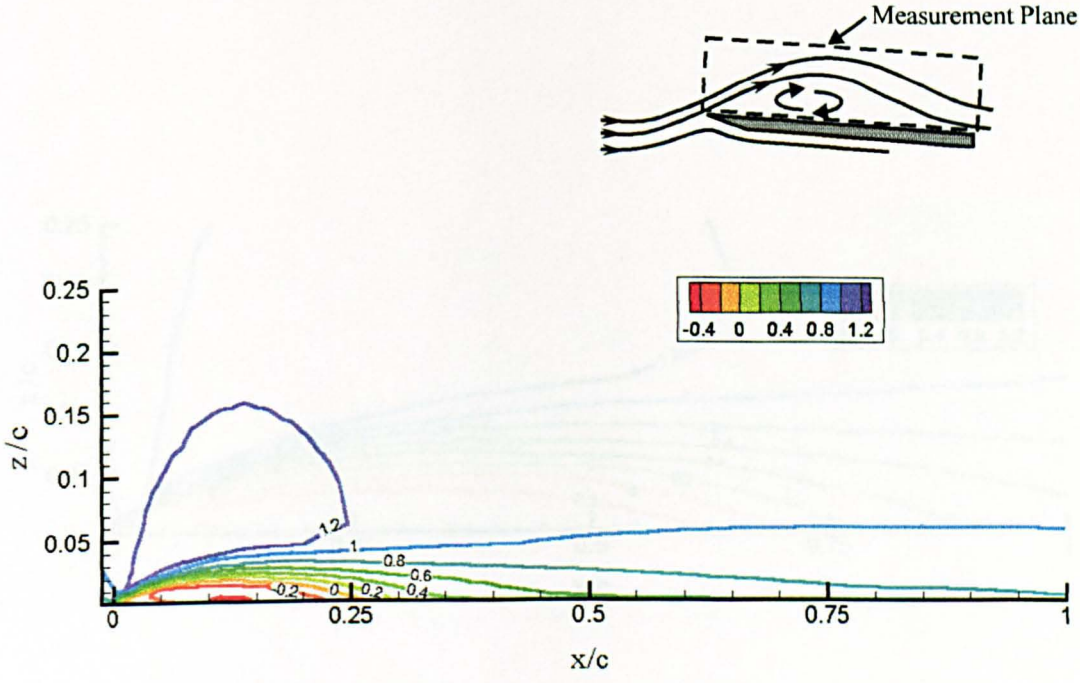

Figure 5.1b Contour map showing mean chordwise velocity u/U_∞ for α=2°, U_∞=20m/s, Re_c=2.13x10^5.

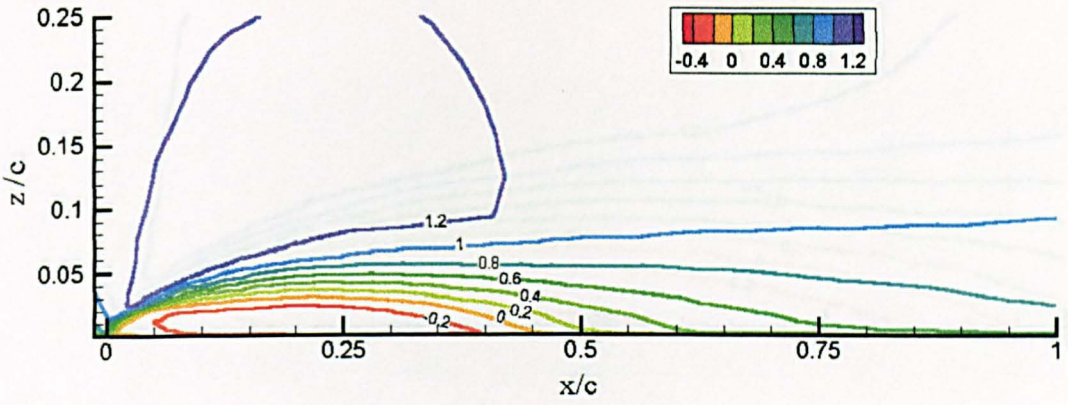

Figure 5.1c Contour map showing mean chordwise velocity u/U_∞ for $\alpha=3°$, $U_\infty=20m/s$, $Re_c=2.13x10^5$.

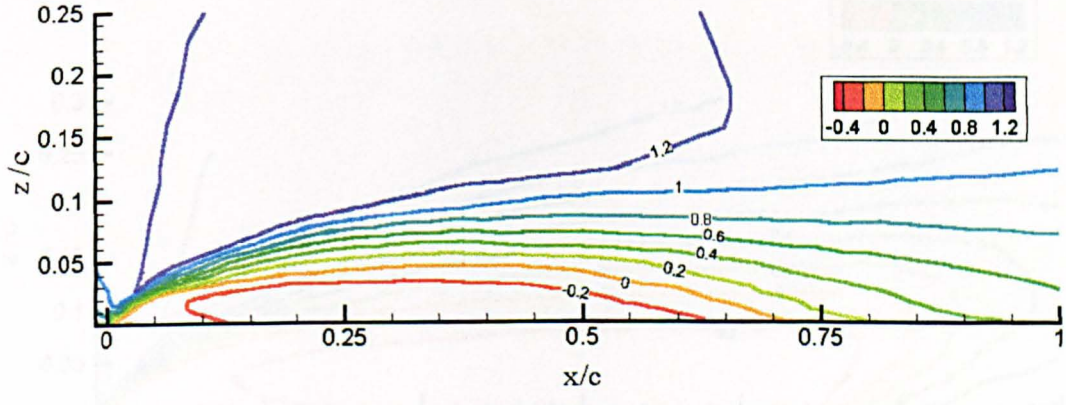

Figure 5.1d Contour map showing mean chordwise velocity u/U_∞ for $\alpha=4°$, $U_\infty=20m/s$, $Re_c=2.13x10^5$.

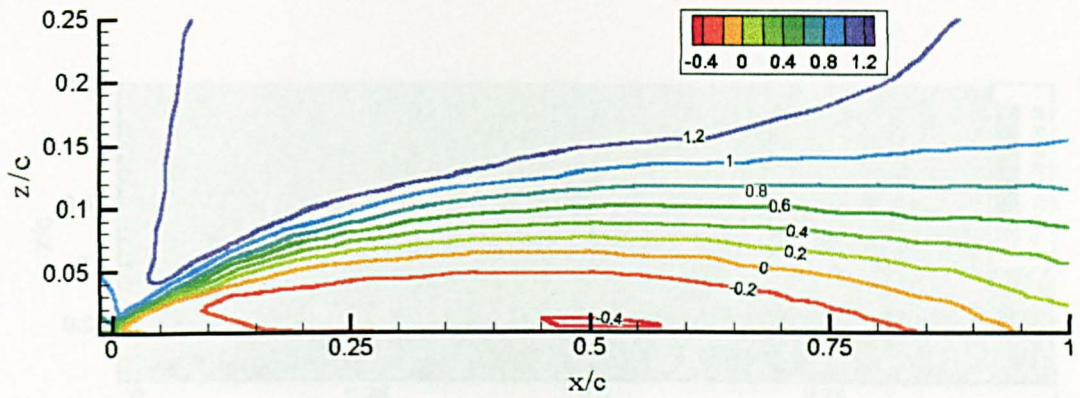

Figure 5.1e Contour map showing mean chordwise velocity u/U_∞ for α=5°, U_∞=20m/s, Re_c=2.13x10^5.

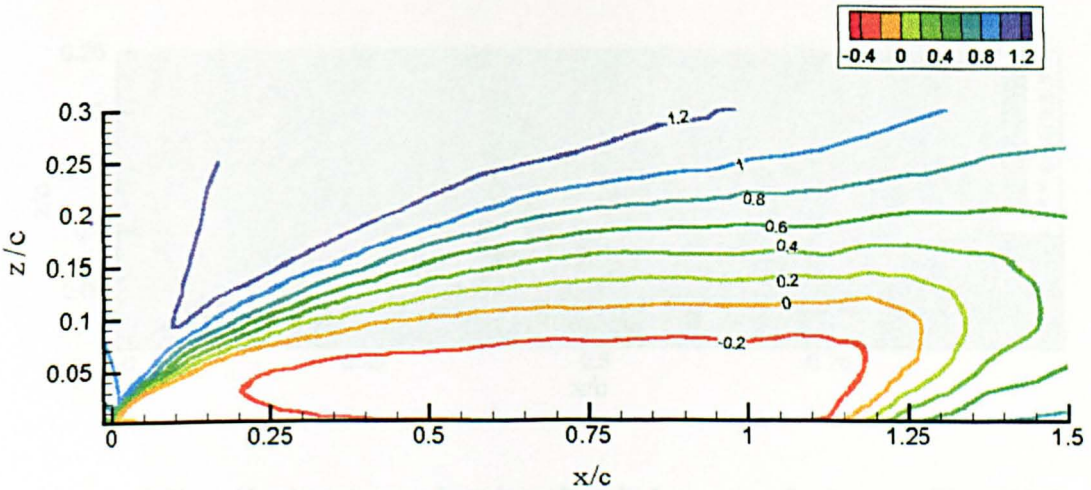

Figure 5.1f Contour map showing mean chordwise velocity u/U_∞ for α=8°, U_∞=20m/s, Re_c=2.13x10^5.

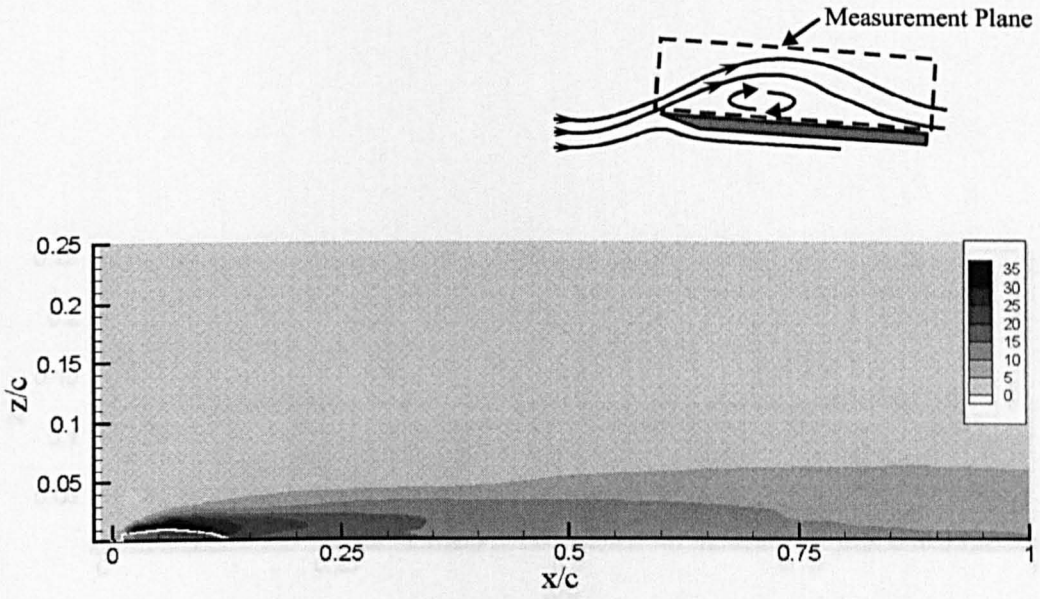

Figure 5.2a Contour map showing chordwise rms velocity u_{rms}/U_∞ (%) for $\alpha=1°$, $U_\infty=20m/s$, $Re_c=2.13x10^5$. ----, locus $u/U_\infty=0$.

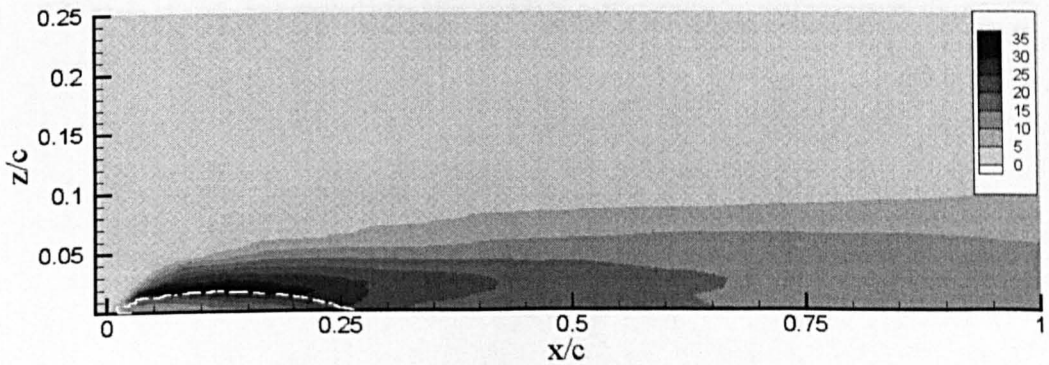

Figure 5.2b Contour map showing chordwise rms velocity u_{rms}/U_∞ (%) for $\alpha=2°$, $U_\infty=20m/s$, $Re_c=2.13x10^5$. ----, locus $u/U_\infty=0$.

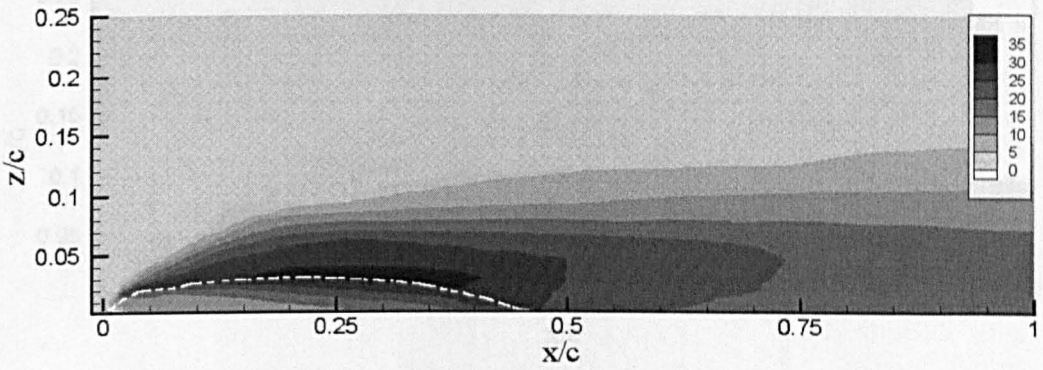

Figure 5.2c Contour map showing chordwise rms velocity u_{rms}/U_∞ (%) for $\alpha=3°$, $U_\infty=20m/s$, $Re_c=2.13x10^5$. ----, locus $u/U_\infty=0$.

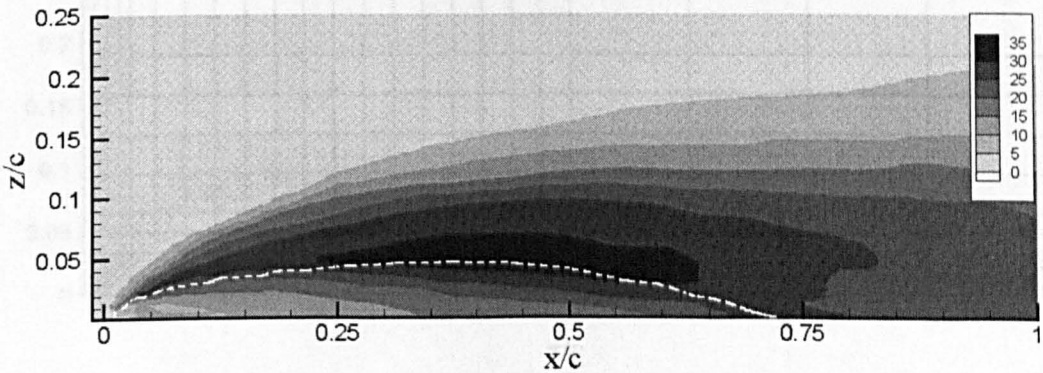

Figure 5.2d Contour map showing chordwise rms velocity u_{rms}/U_∞ (%) for $\alpha=4°$, $U_\infty=20m/s$, $Re_c=2.13x10^5$. ----, locus $u/U_\infty=0$.

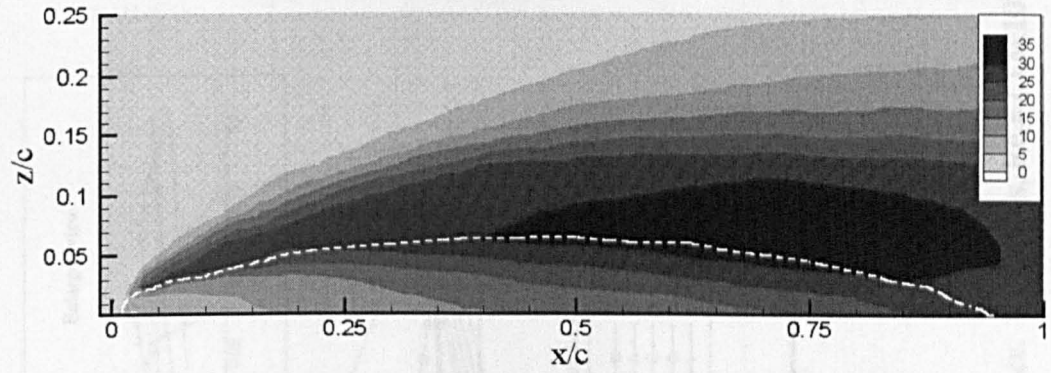

Figure 5.2e Contour map showing chordwise rms velocity u_{rms}/U_∞ (%) for $\alpha=5°$, $U_\infty=20m/s$, $Re_c=2.13x10^5$. ----, locus $u/U_\infty=0$.

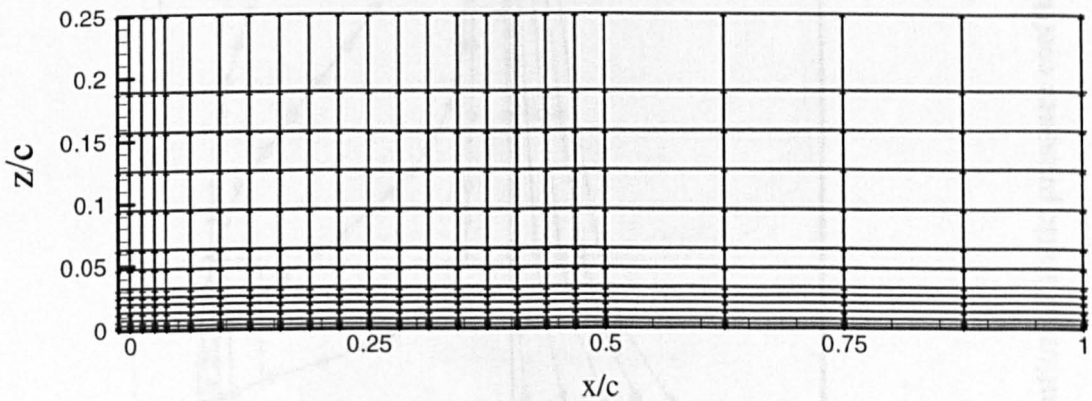

Figure 5.2f Typical graduated measurement grid used for contour mappings (not all detail shown for clarity).

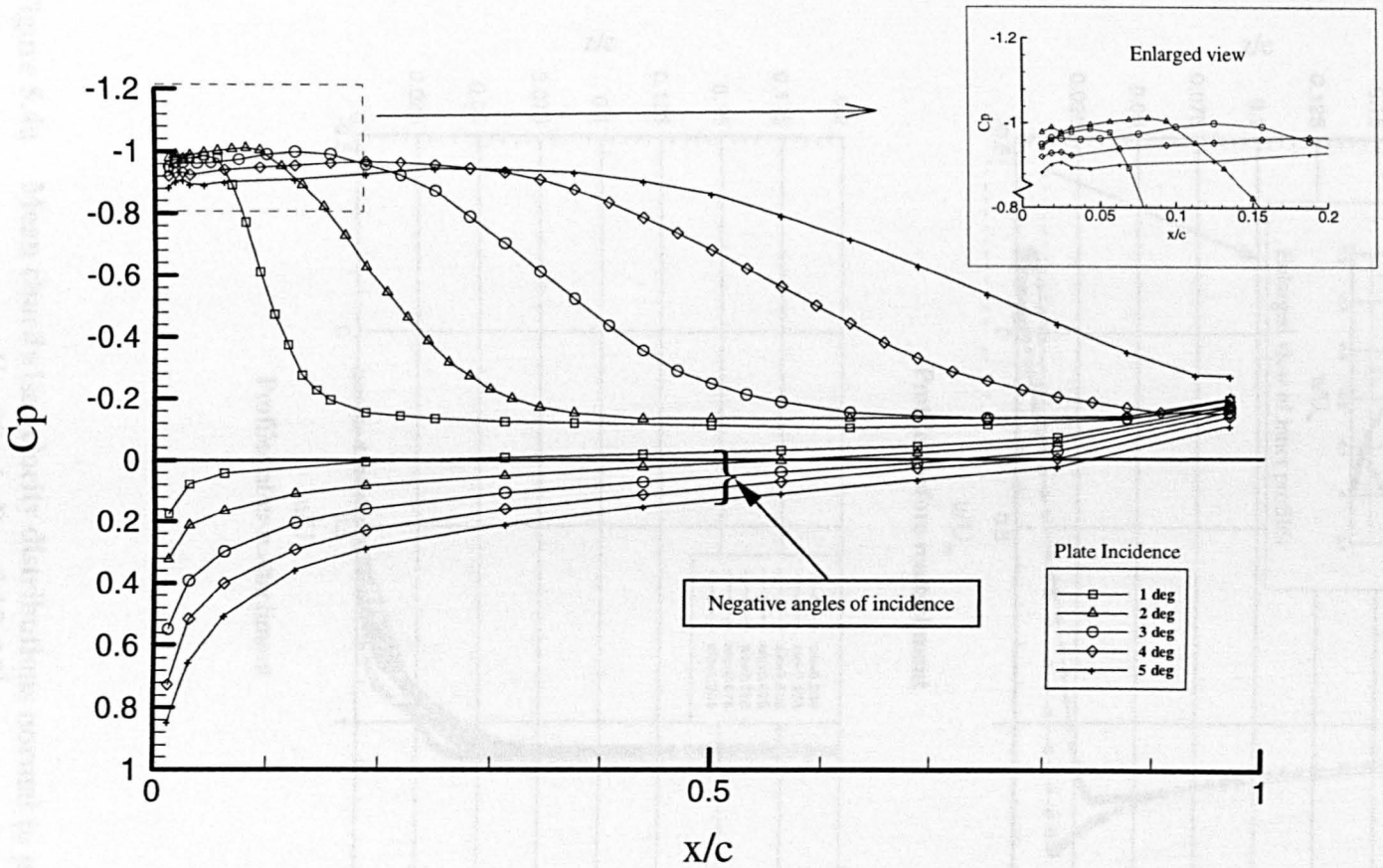

Figure 5.3 Distribution of static pressure coefficient for various angles of incidence. U_∞=20m/s, Re_c=2.13x10^5.

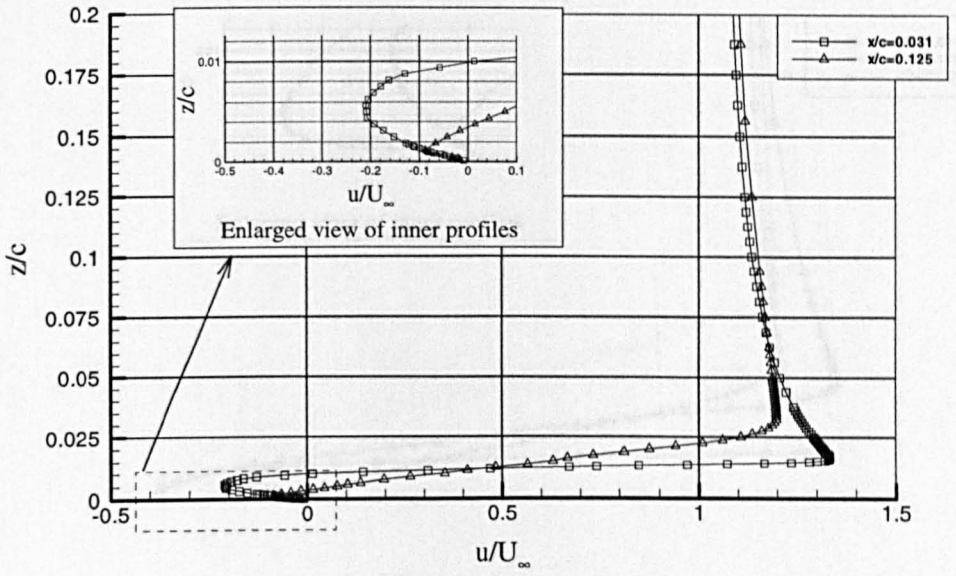

Profiles before reattachment

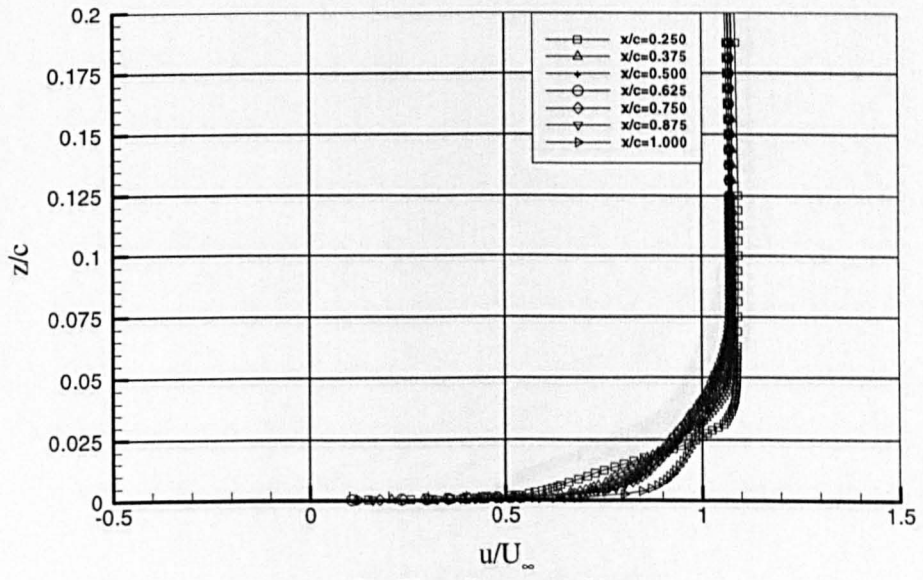

Profiles after reattachment

Figure 5.4a Mean chordwise velocity distributions normal to plate for α=1°, U_∞=20m/s, Re_c=2.13x10^5.

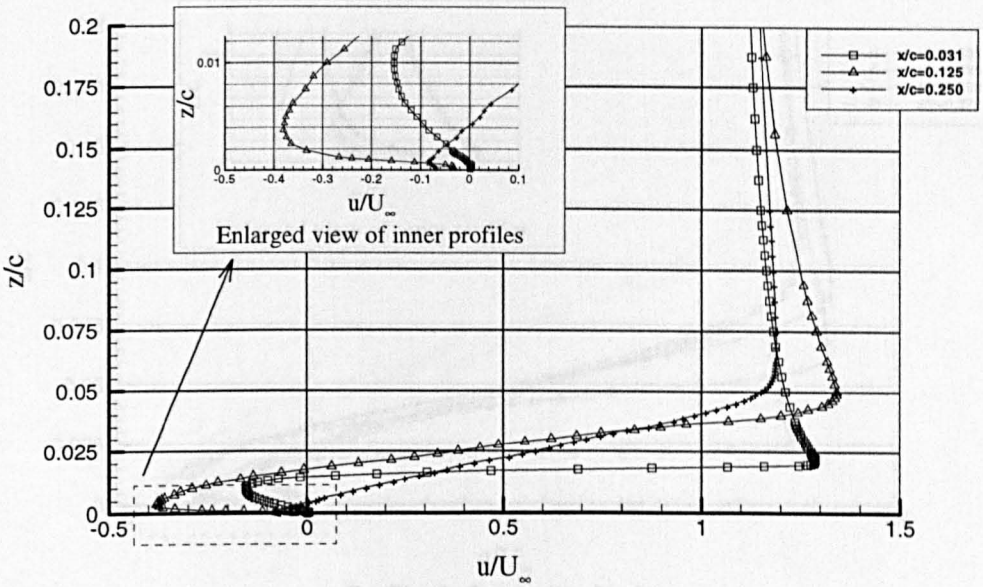

Profiles before reattachment

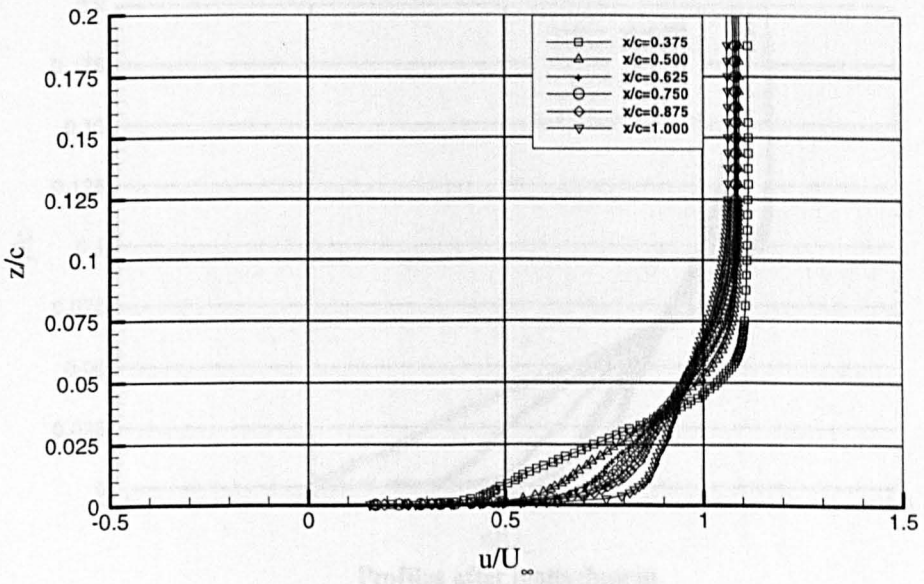

Profiles after reattachment

Figure 5.4b Mean chordwise velocity distributions normal to plate for α=2°, U_∞=20m/s, Re_c=2.13x10^5.

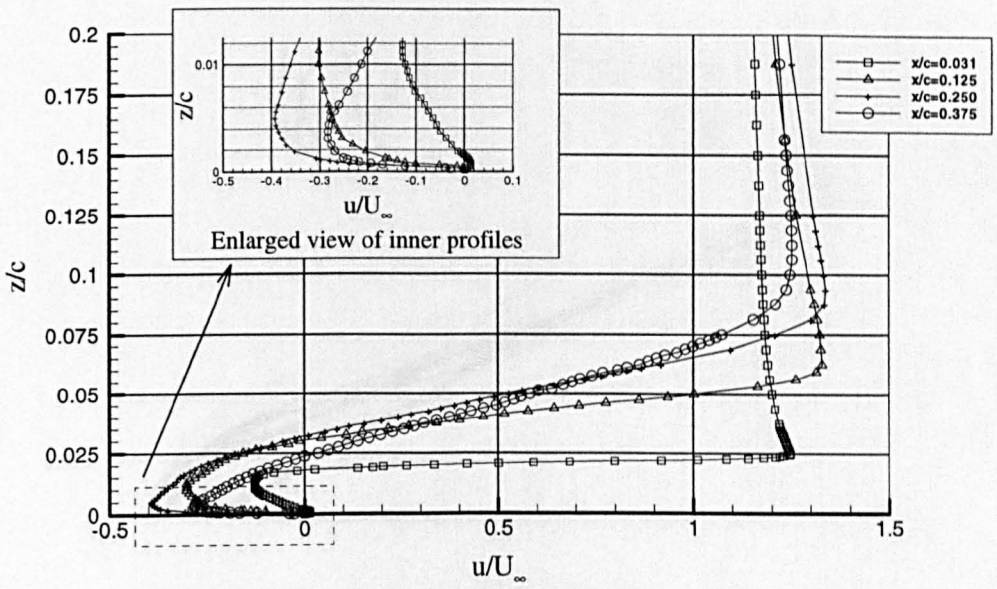

Profiles before reattachment

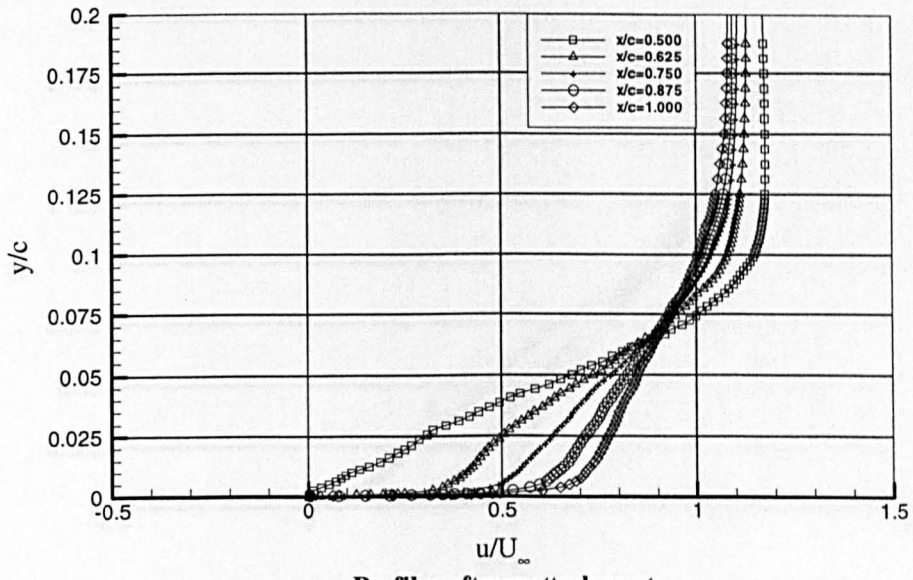

Profiles after reattachment

Figure 5.4c Mean chordwise velocity distributions normal to plate for α=3°, U_∞=20m/s, Re_c=2.13x10^5.

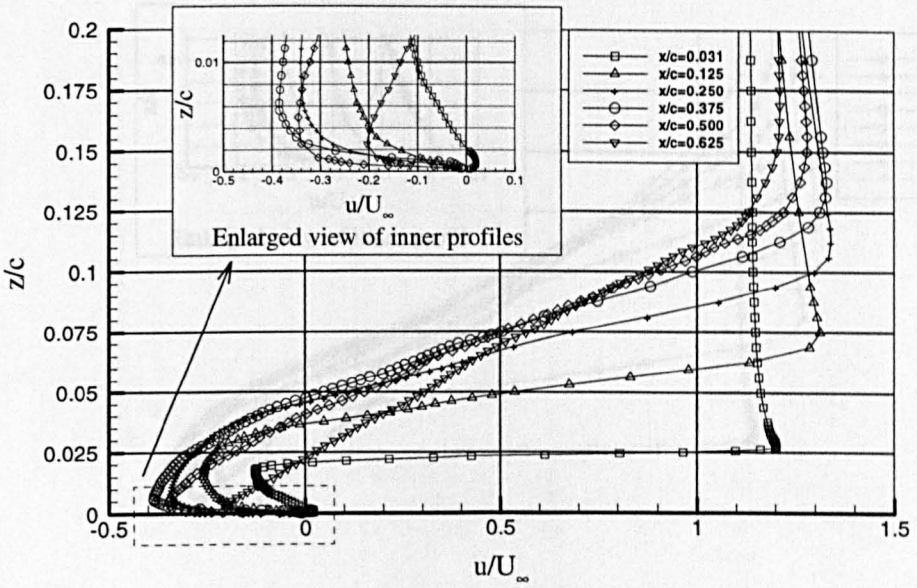

Profiles before reattachment

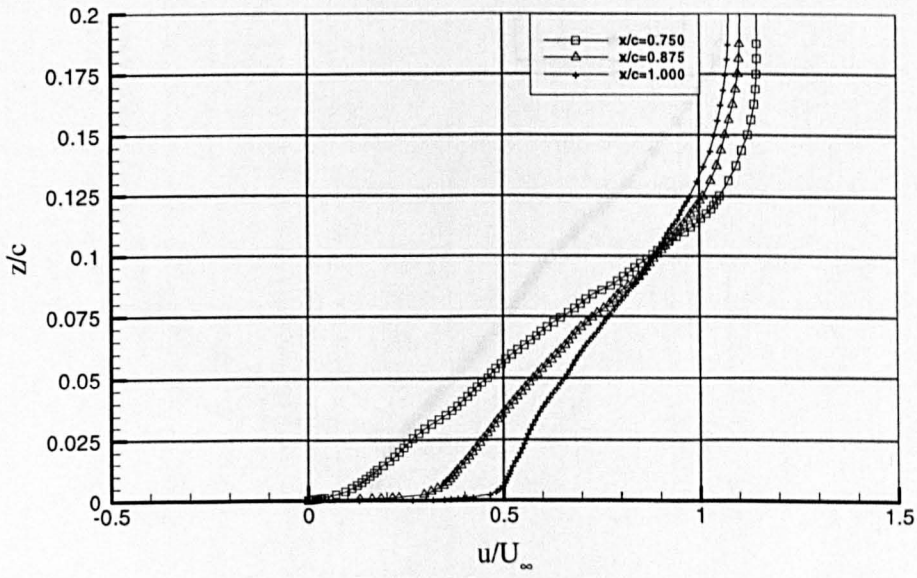

Profiles after reattachment

Figure 5.4d Mean chordwise velocity distributions normal to plate for α=4°, U_∞=20m/s, Re_c=2.13x10^5.

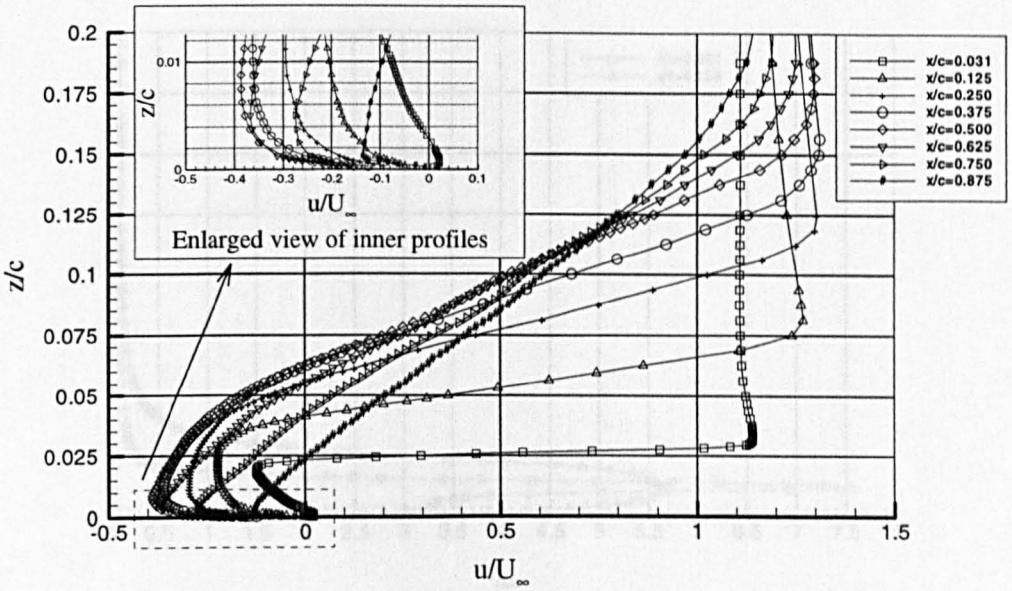

Profiles before reattachment

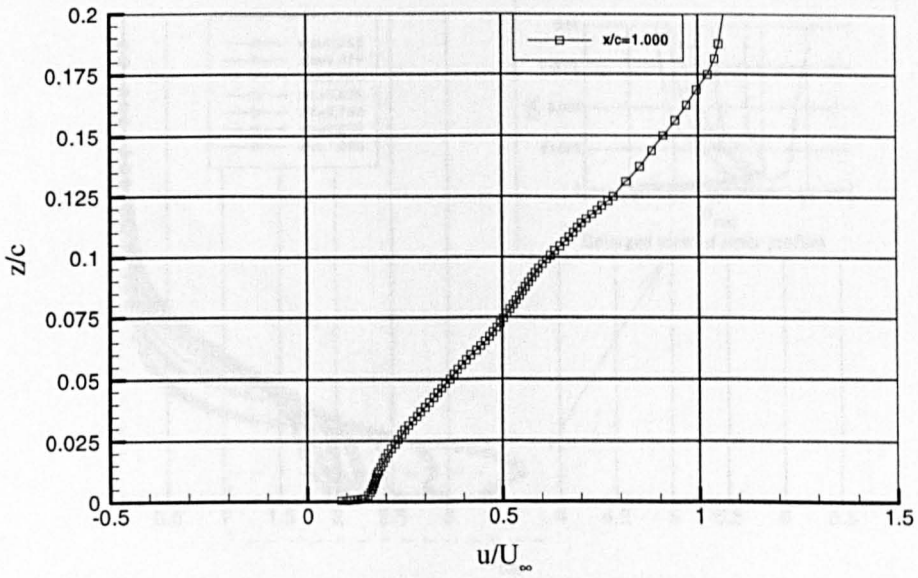

Profiles after reattachment

Figure 5.4e Mean chordwise velocity distributions normal to plate for α=5°, U_∞=20m/s, Re_c=2.13x10^5.

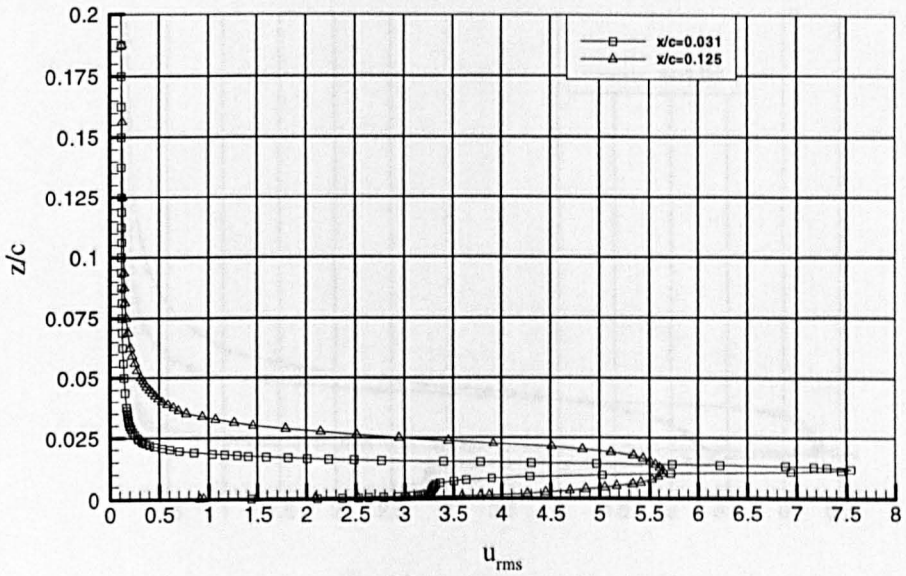

Profiles before reattachment

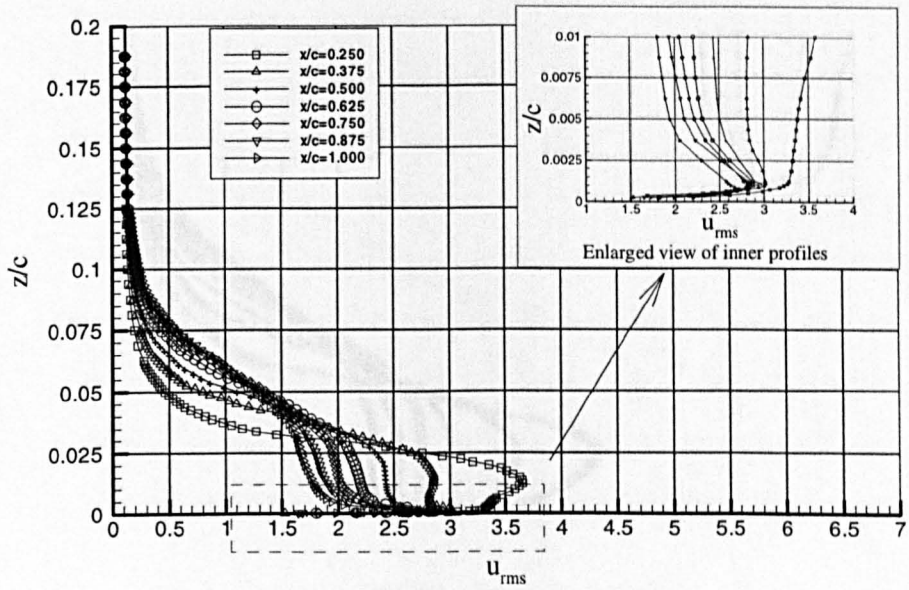

Profiles after reattachment

Figure 5.5a Chordwise rms velocity distributions (m/s) normal to plate for α=1°, U_∞=20m/s, Re_c=2.13x10^5.

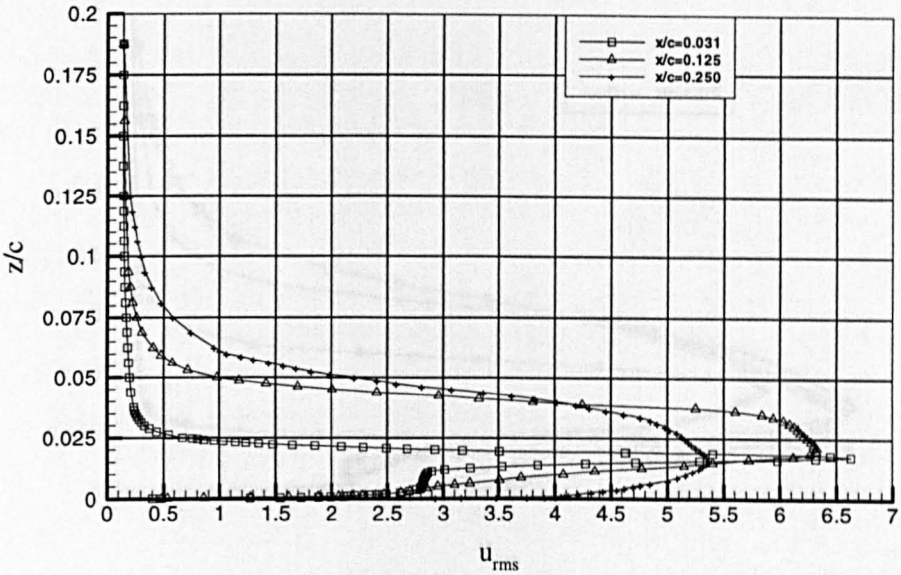

Profiles before reattachment

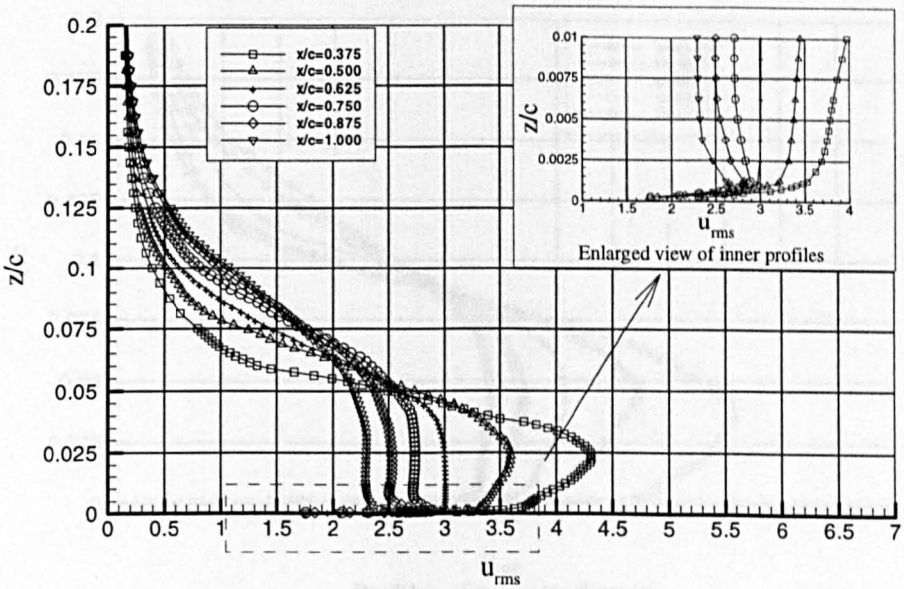

Profiles after reattachment

Figure 5.5b Chordwise rms velocity distributions (m/s) normal to plate for α=2°, U_∞=20m/s, Re_c=2.13x10^5.

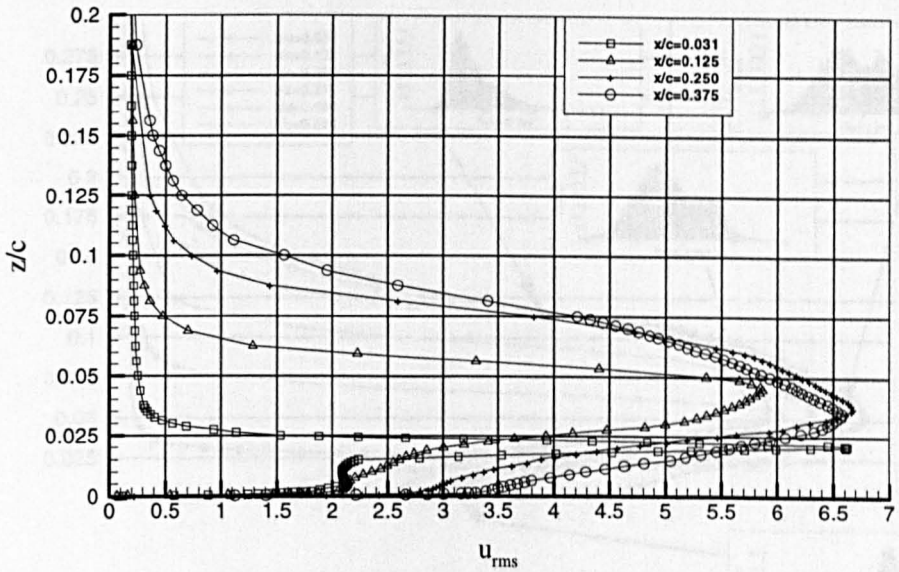

Profiles before reattachment

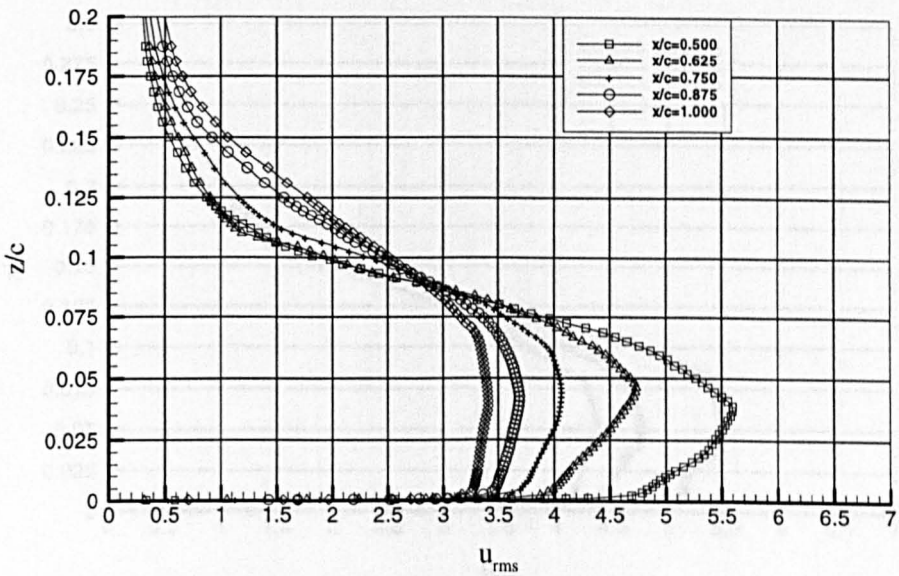

Profiles after reattachment

Figure 5.5c Chordwise rms velocity distributions (m/s) normal to plate for α=3°, U_∞=20m/s, Re_c=2.13x10^5.

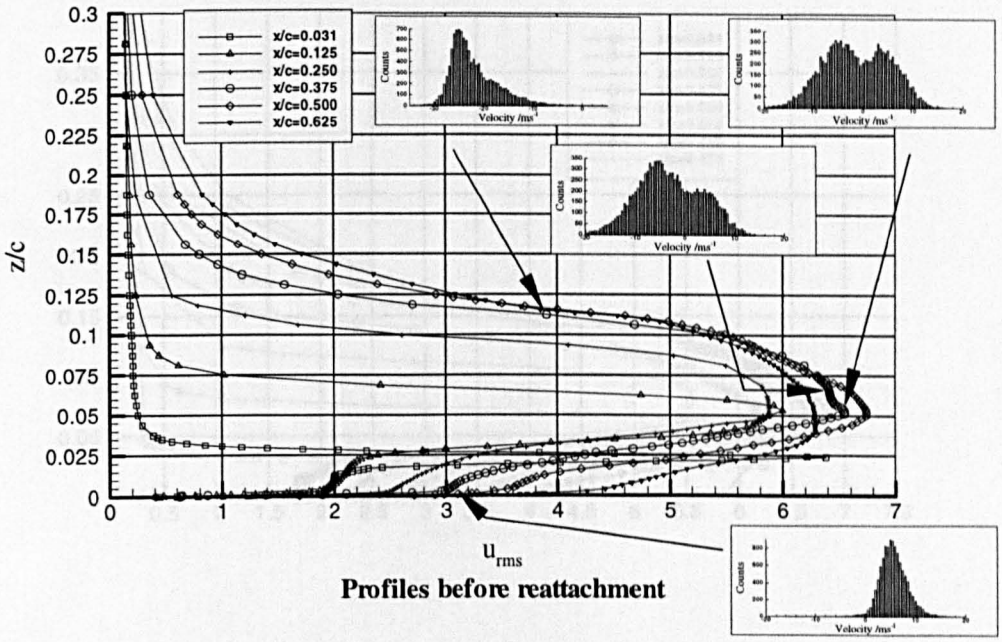

Profiles before reattachment

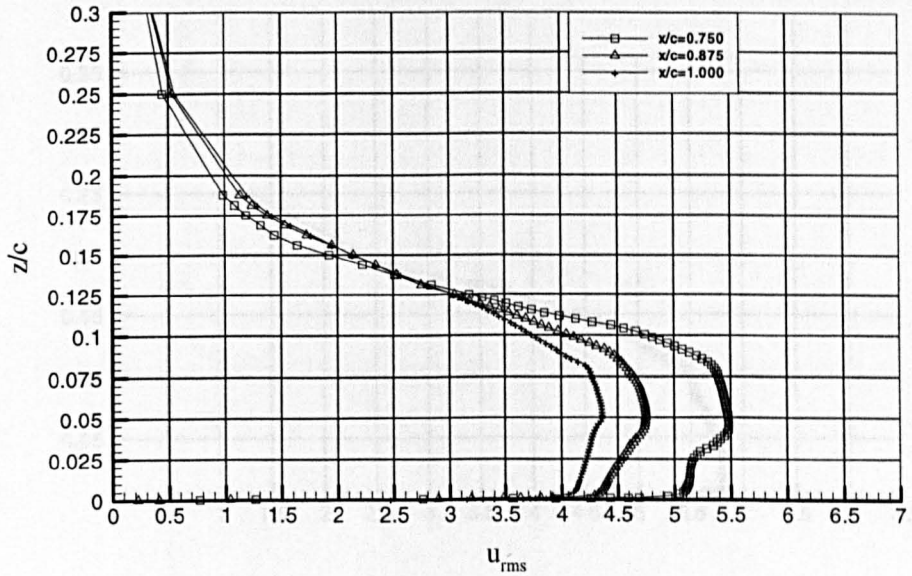

Profiles after reattachment

Figure 5.5d Chordwise rms velocity distributions (m/s) normal to plate for α=4°, U_∞=20m/s, Re_c=2.13x10^5. Includes velocity histograms.

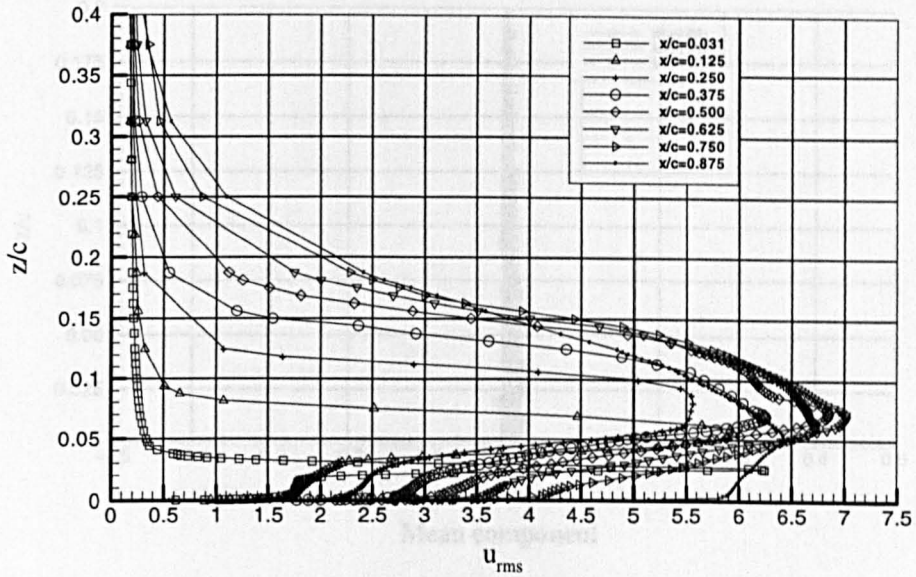

Profiles before reattachment

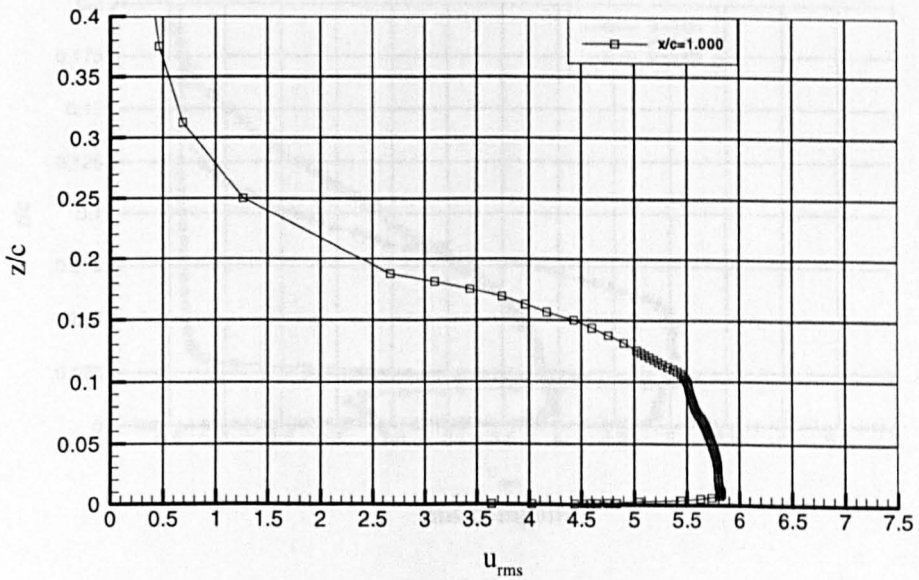

Profiles after reattachment

Figure 5.5e Chordwise rms velocity distributions (m/s) normal to plate for α=5°, U_∞=20m/s, Re_c=2.13x10^5.

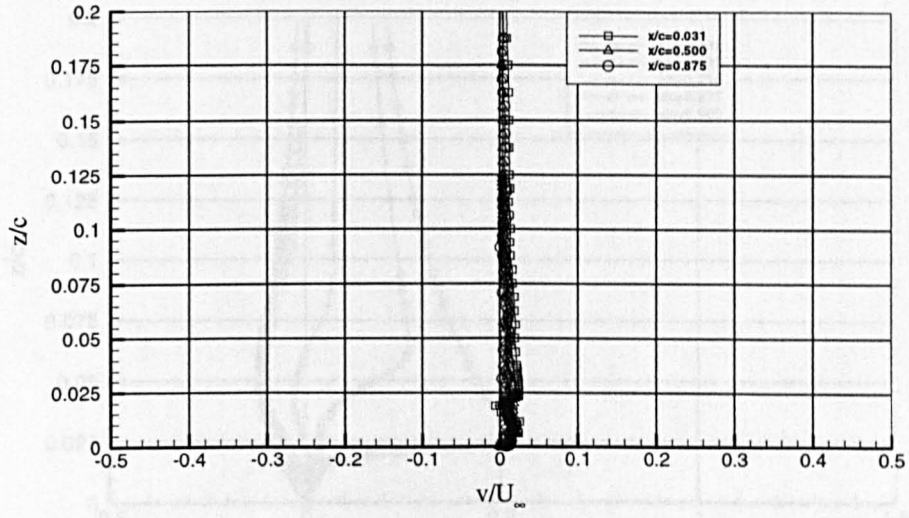

Mean component

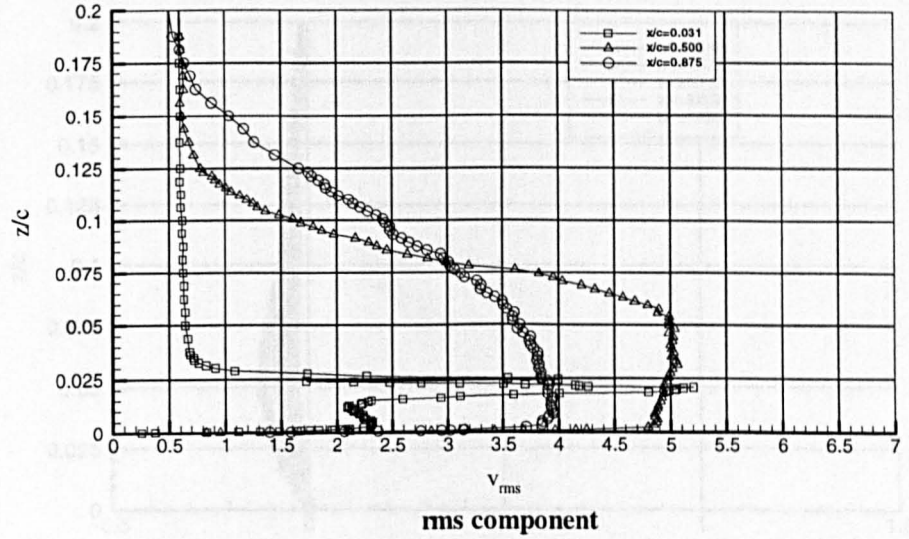

rms component

Figure 5.6 Transverse rms (m/s) and mean velocity distributions normal to plate for α=3°, U_∞=20m/s, Re_c=2.13x10^5.

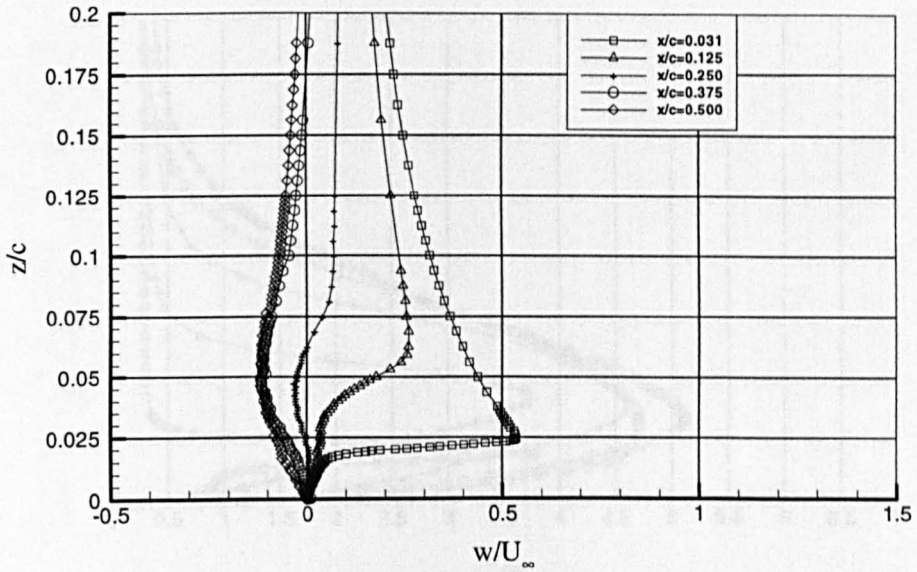

Profiles before reattachment

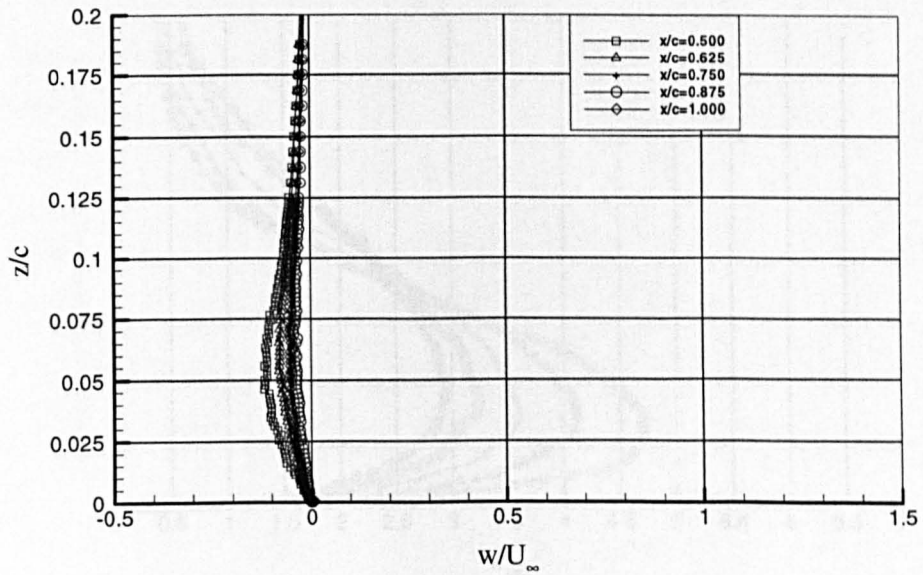

Profiles after reattachment

Figure 5.7a Mean normal velocity distributions perpendicular to plate for α=3°, U_∞=20m/s, Re_c=2.13x10^5.

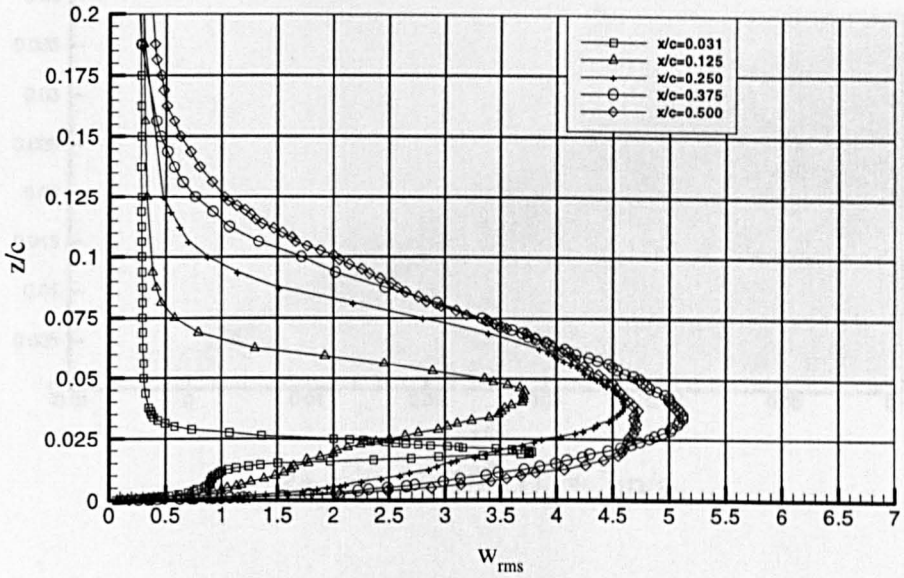

Profiles before reattachment

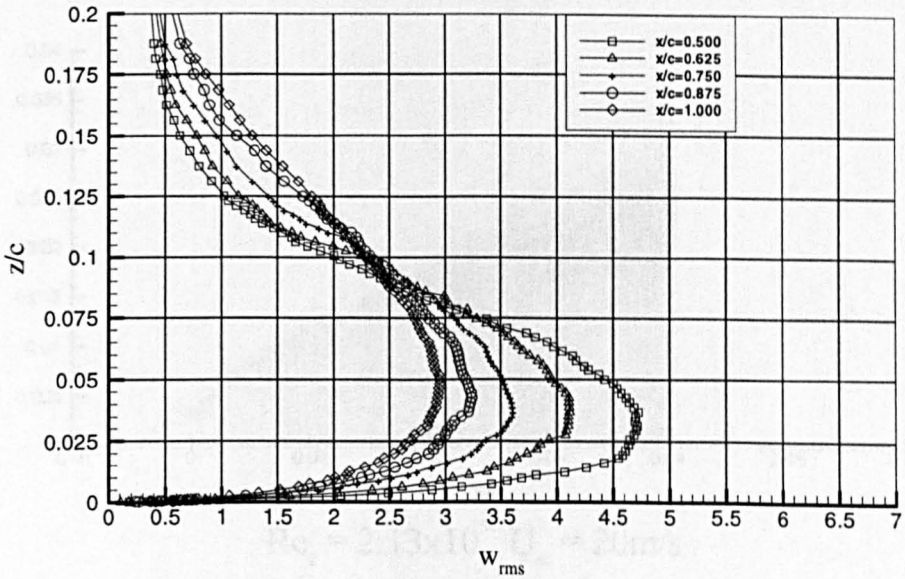

Profiles after reattachment

Figure 5.7b Normal rms velocity component (m/s) perpendicular to plate for $\alpha=3°$, $U_\infty=20m/s$, $Re_c=2.13x10^5$.

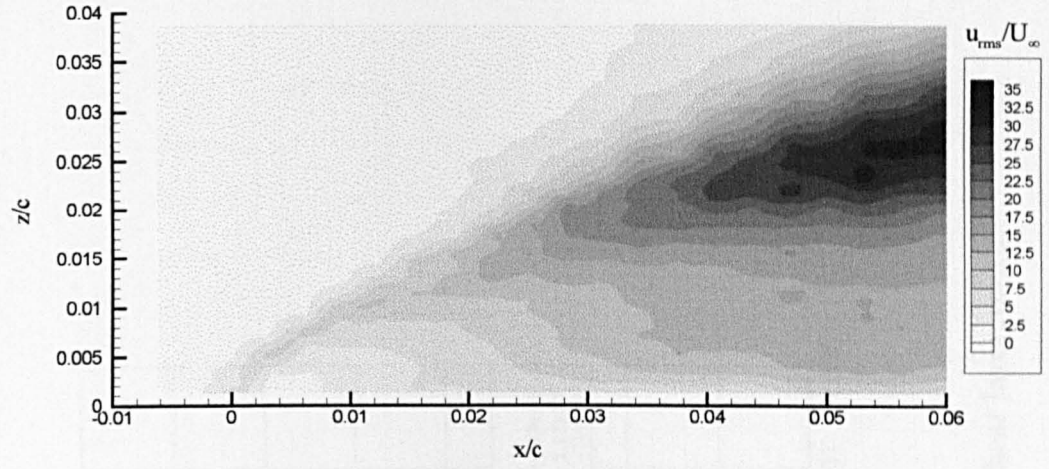

$Re_c = 0.53x10^5$, $U_\infty = 5m/s$

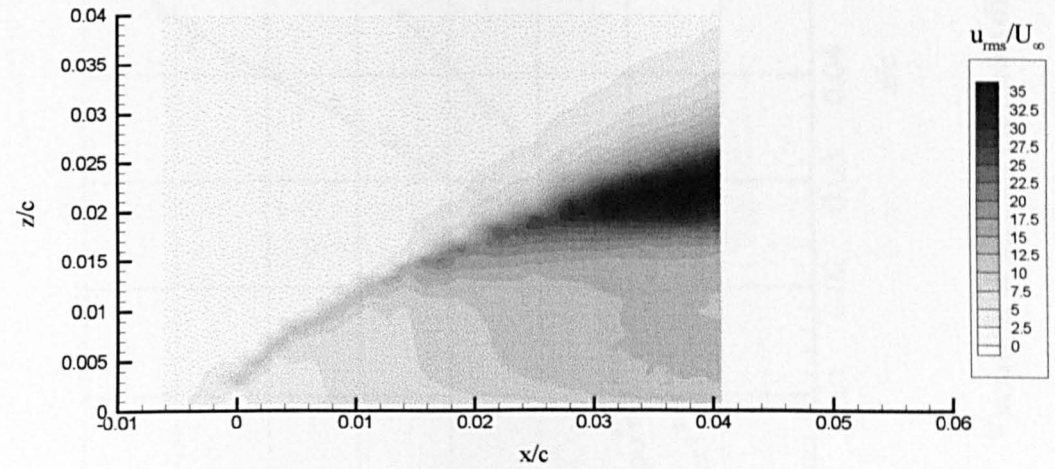

$Re_c = 2.13x10^5$, $U_\infty = 20m/s$

Figure 5.8 Contour map showing the effects of Reynolds number on the distribution of u_{rms}/U_∞ (%) near the leading edge, α=3°.

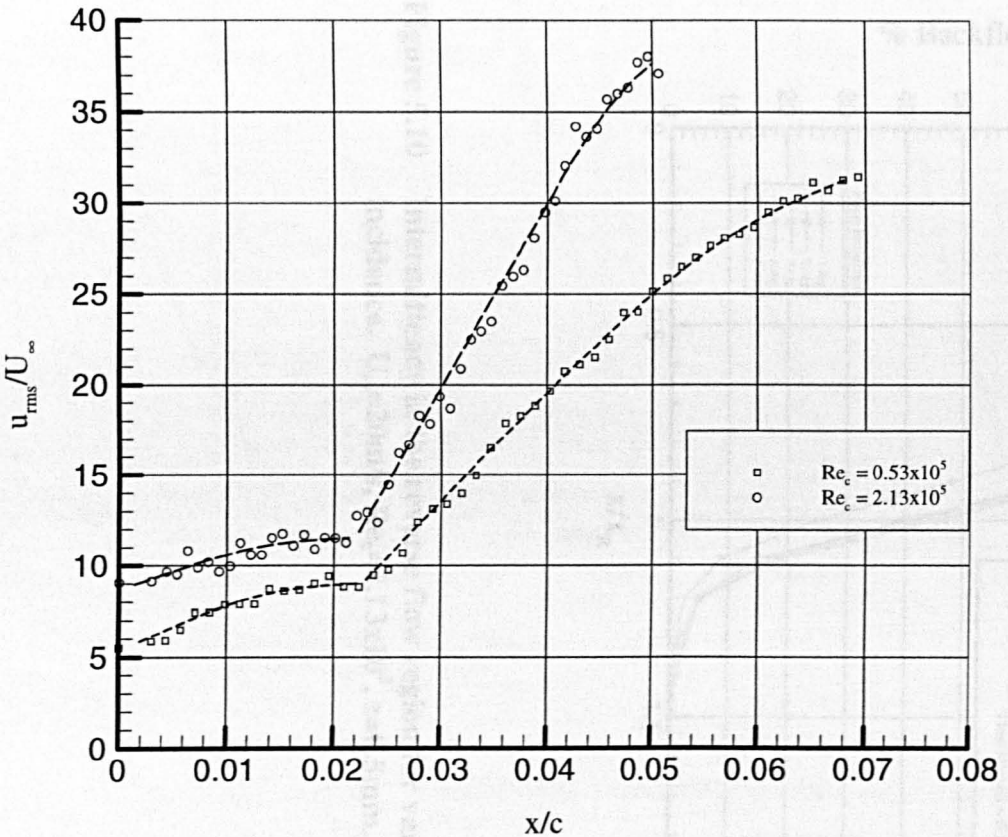

Figure 5.9 Variation of u_{rms}/U_∞ (%) with distance along the shear layer, α=3°.

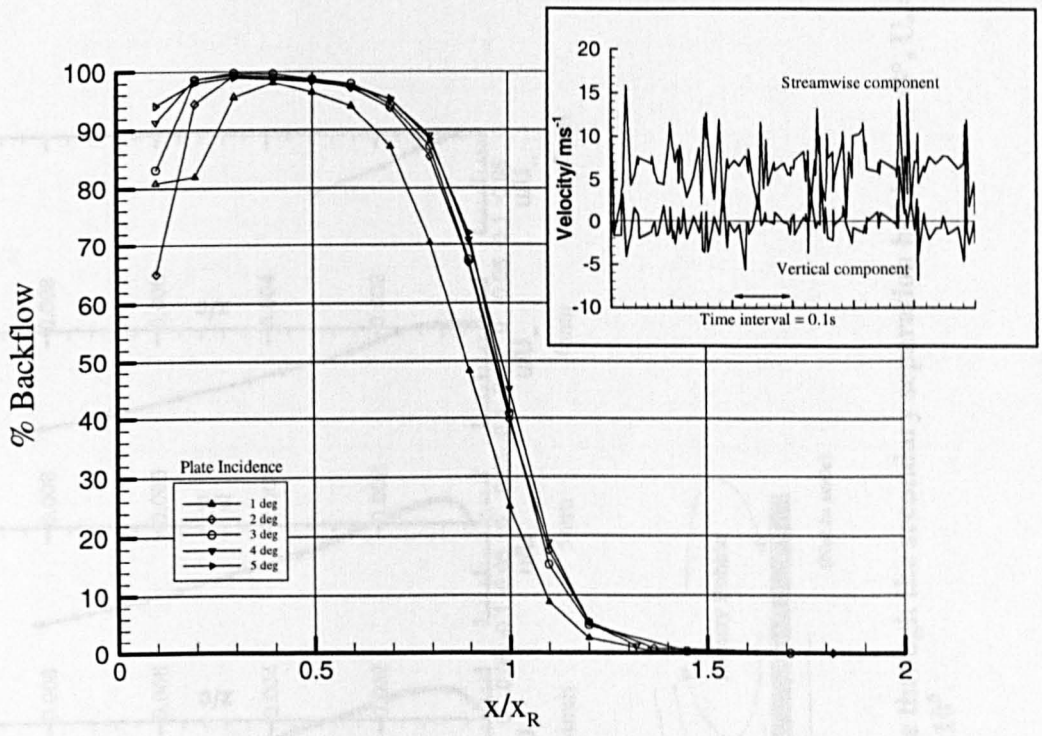

Figure 5.10 **Intermittency in the reverse flow region for various angles of incidence. U_∞=20m/s, Re_c=2.13x10^5, z=0.5mm.**

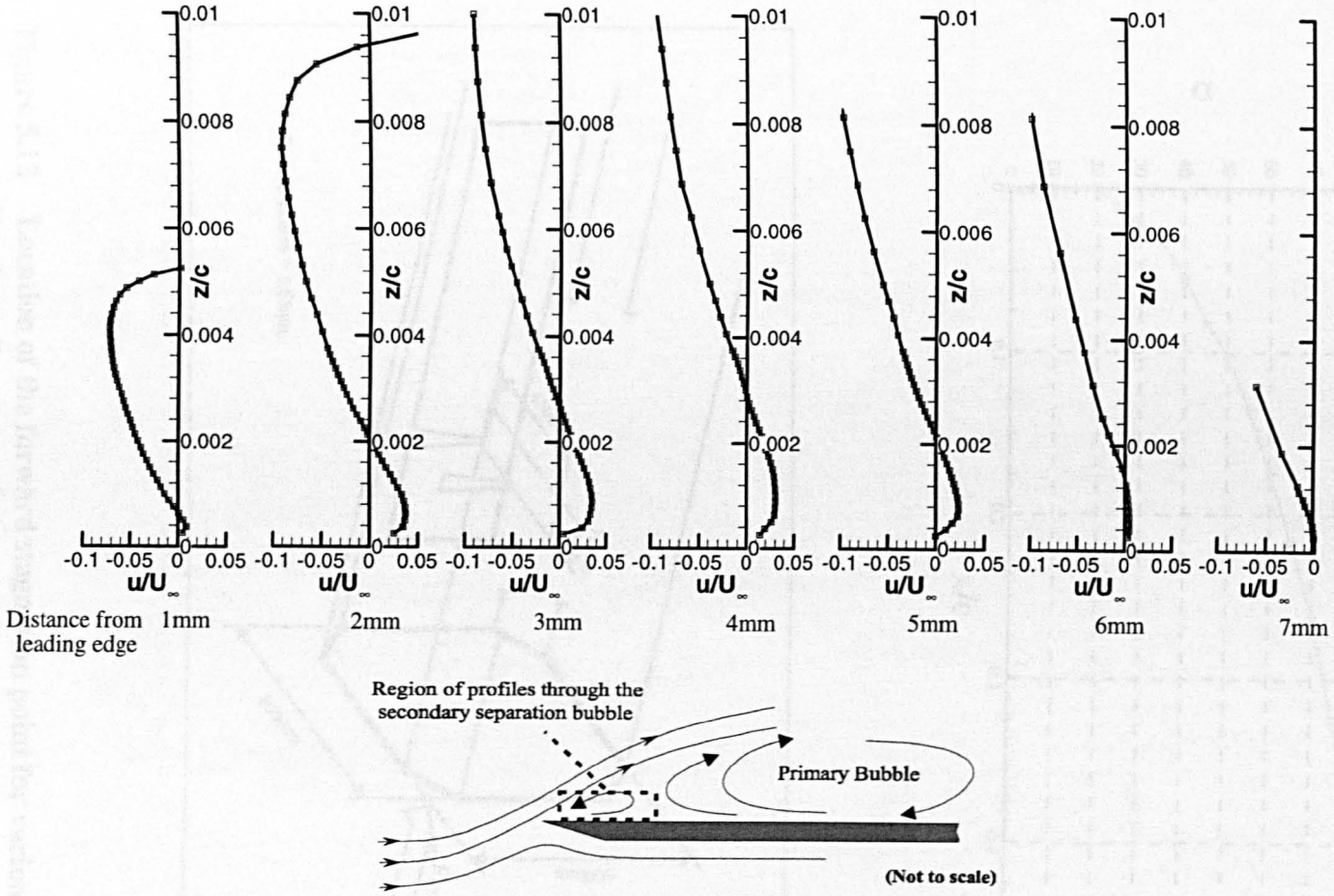

Figure 5.11 Mean chordwise velocity distributions normal to plate through the secondary separation bubble. α=3°, U_∞=20m/s, Re_c=2.13x10^5.

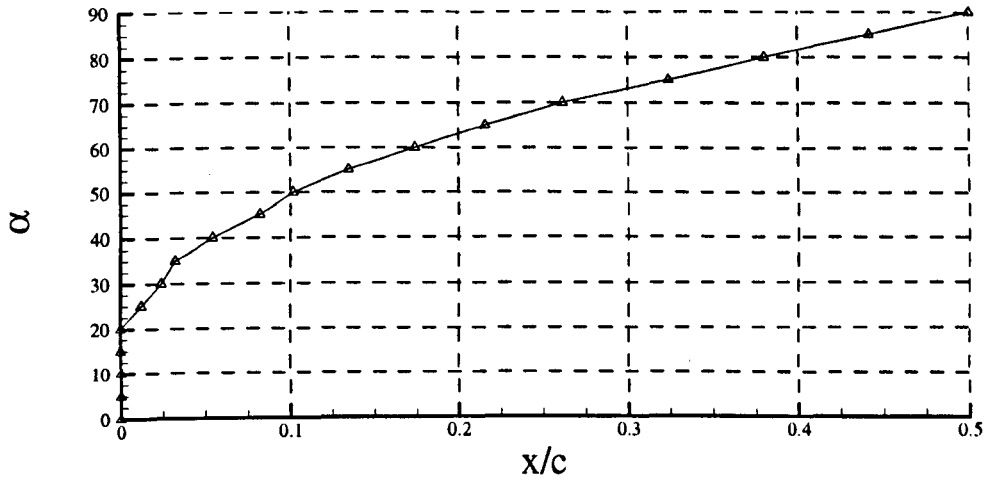

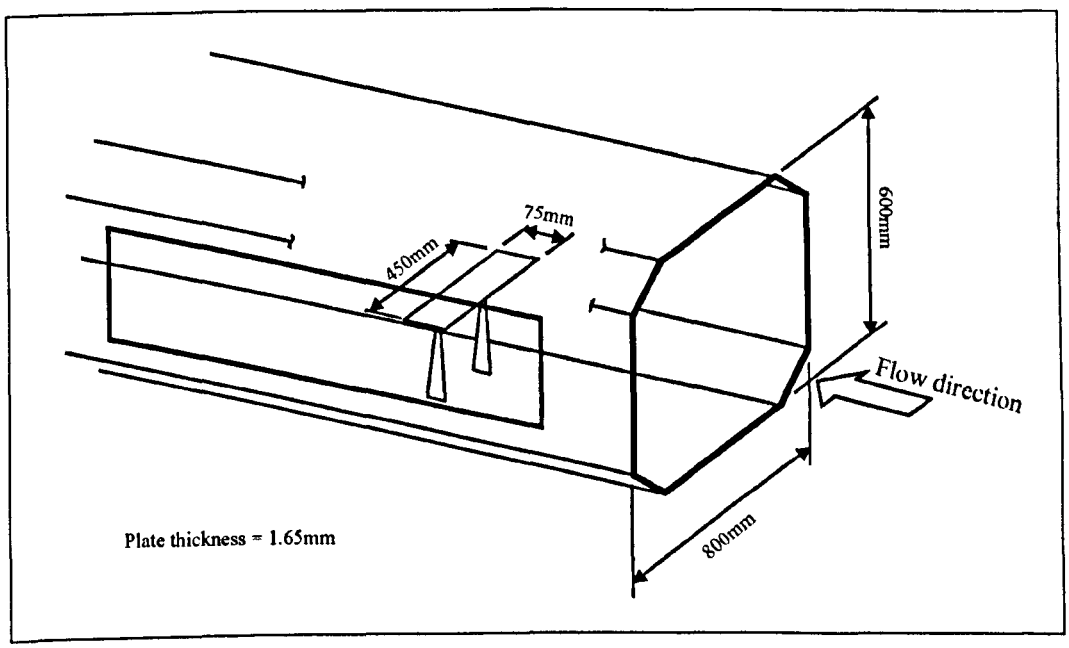

Figure 5.12 Location of the forward stagnation point for various angles of incidence. U_∞=4m/s, Re_c=0.2x10^5. Includes schematic representation of experimental set-up used to determine stagnation point location.

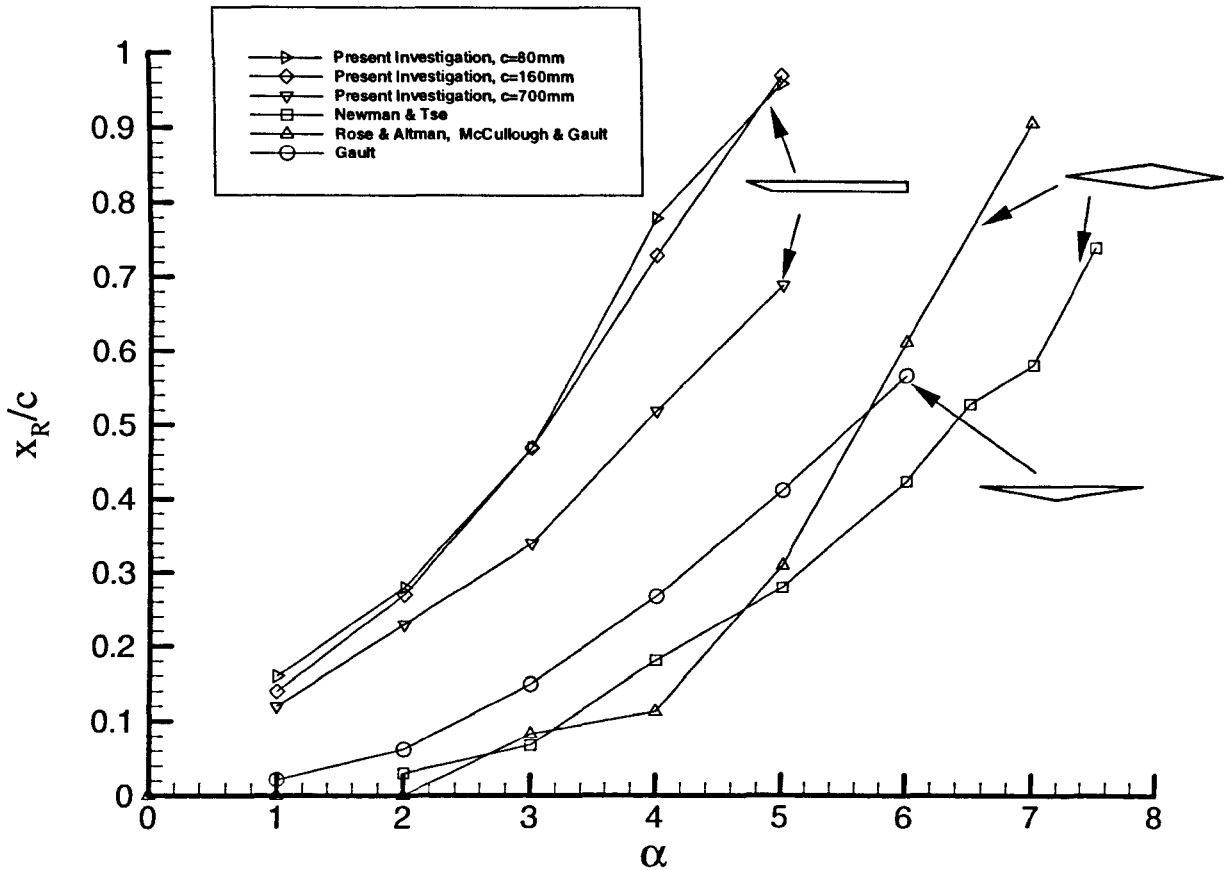

Figure 5.13 Relationship between angle of incidence and separation bubble length for all previous experiments on thin aerofoil bubbles.

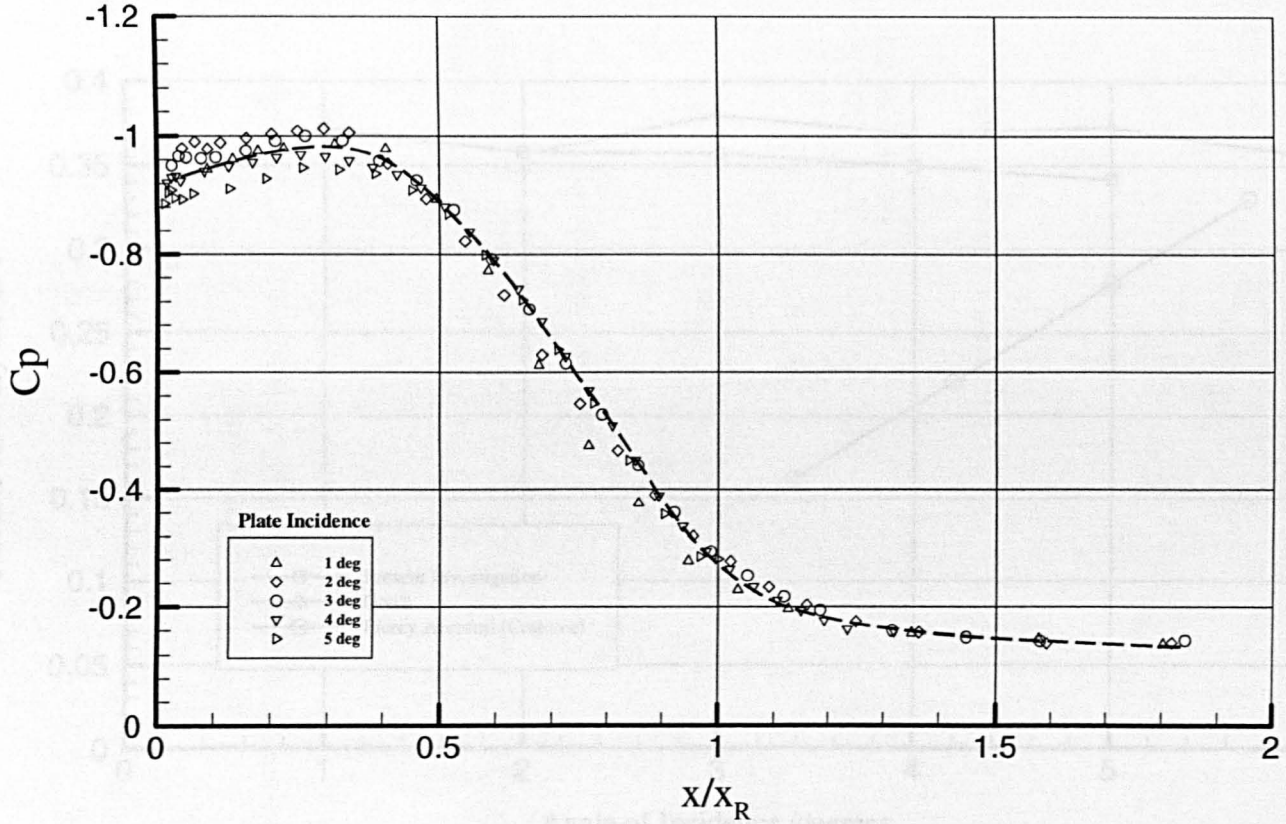

Figure 5.14 Distribution of static pressure coefficient, non-dimensionalised with respect to the reattachment length for various angles of incidence. U_∞=20m/s, Re_c=2.13x10^5.

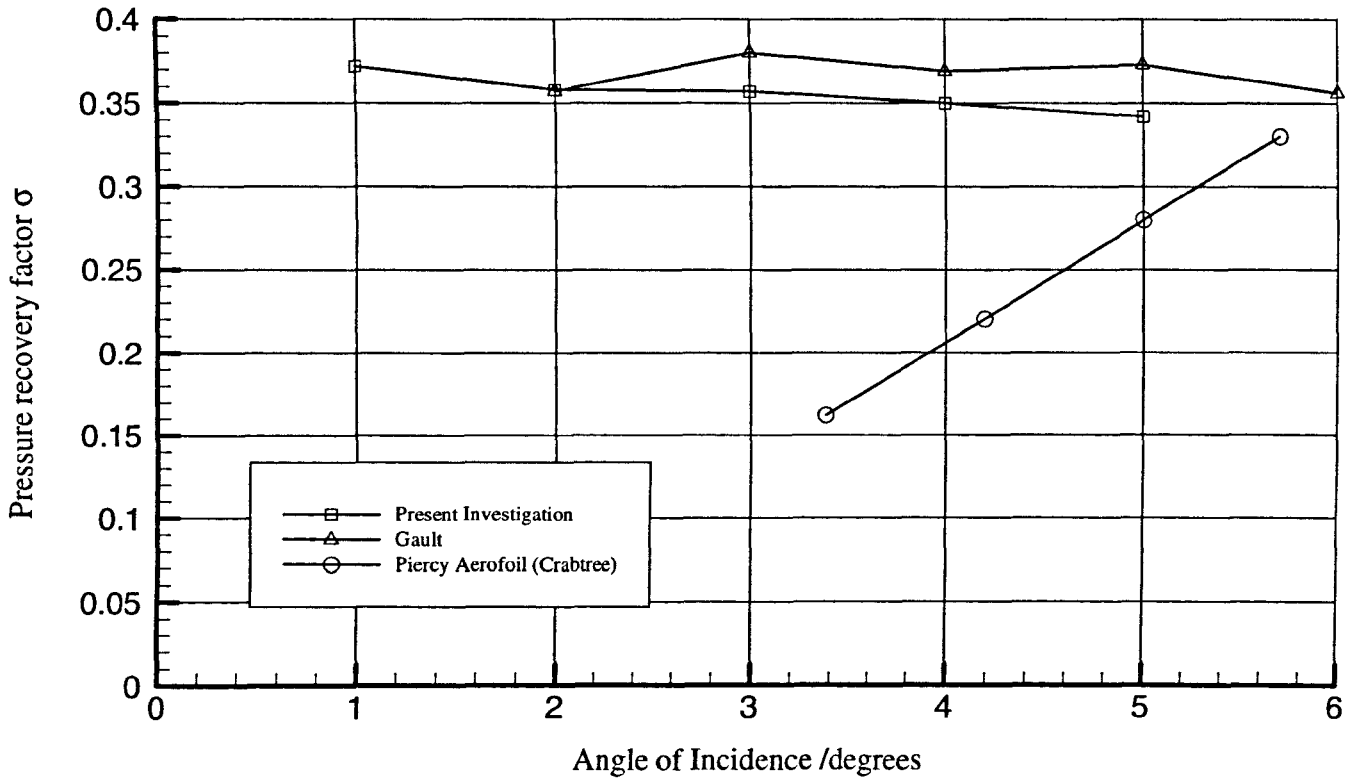

Figure 5.15 Pressure recovery factor for thin aerofoil and short bubble types.

1) No flow constraint

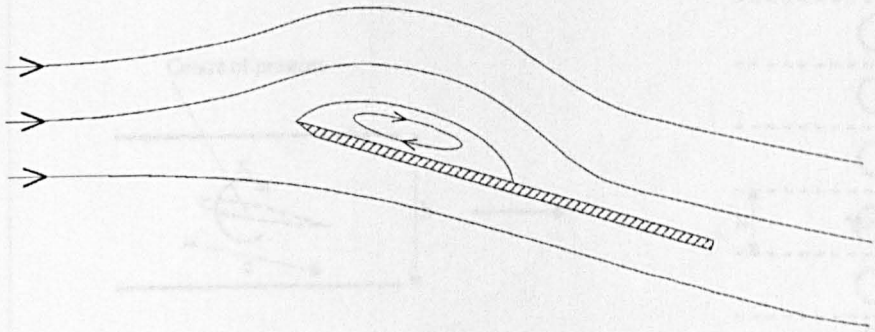

2) Wind tunnel constraint

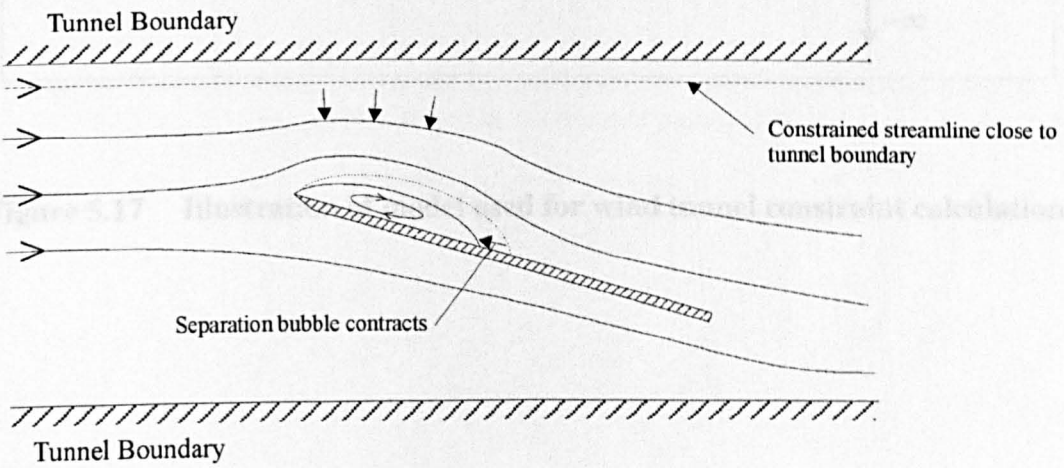

Figure 5.16 Illustration of the effect of tunnel constraint on the separation bubble.

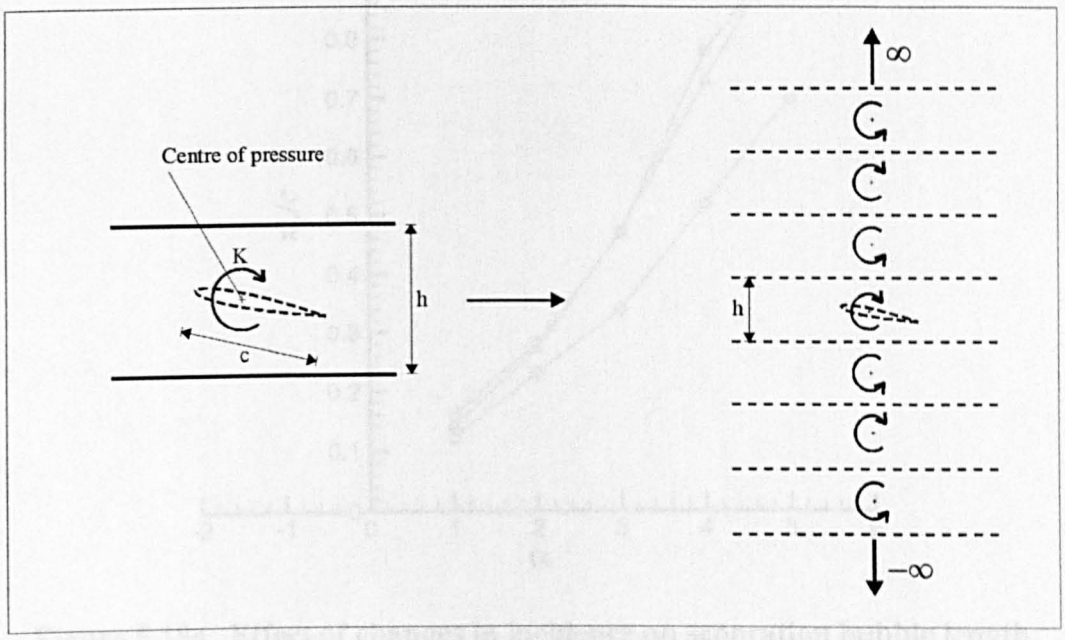

Figure 5.17 Illustration of model used for wind tunnel constraint calculation.

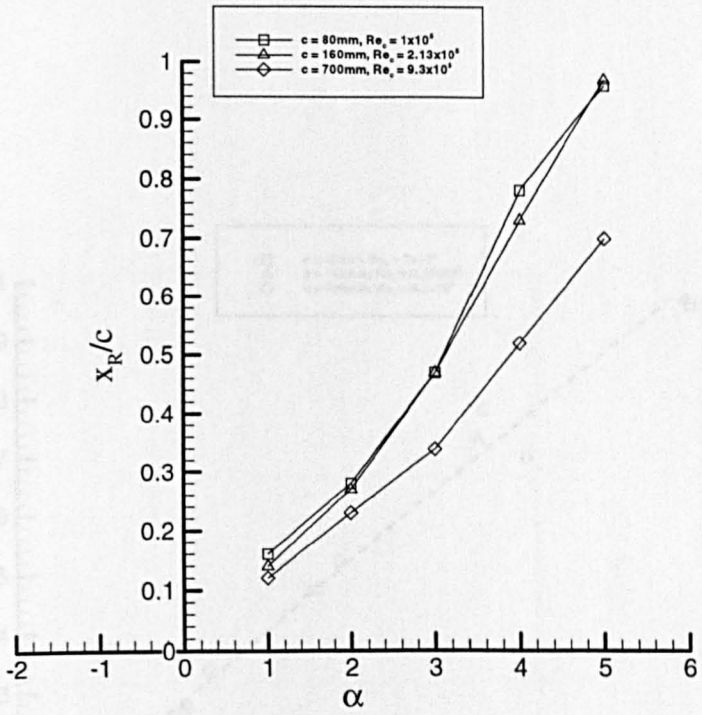

Figure 5.18a Effect of changes in incidence on separation bubble length, uncorrected for wind tunnel constraint.

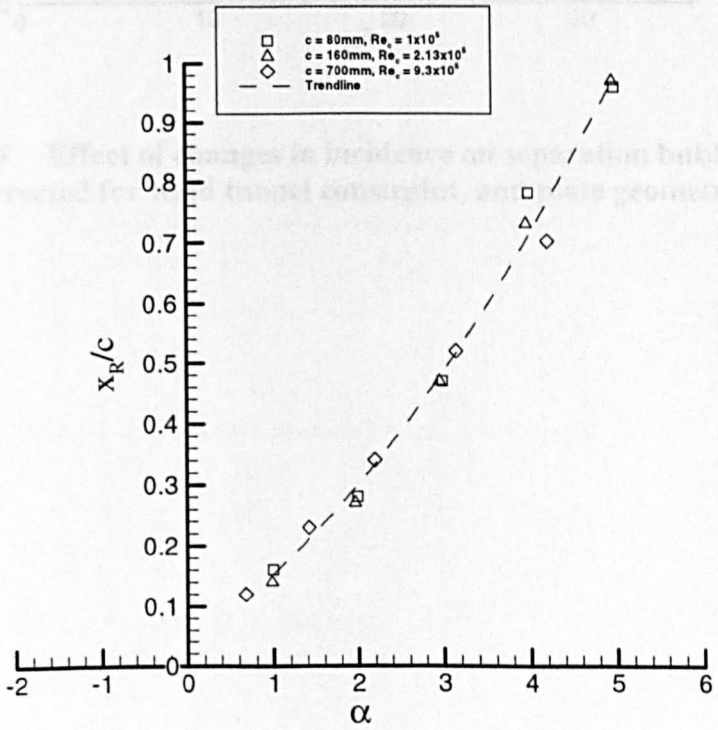

Figure 5.18b Effect of changes in incidence on separation bubble length, corrected for wind tunnel constraint.

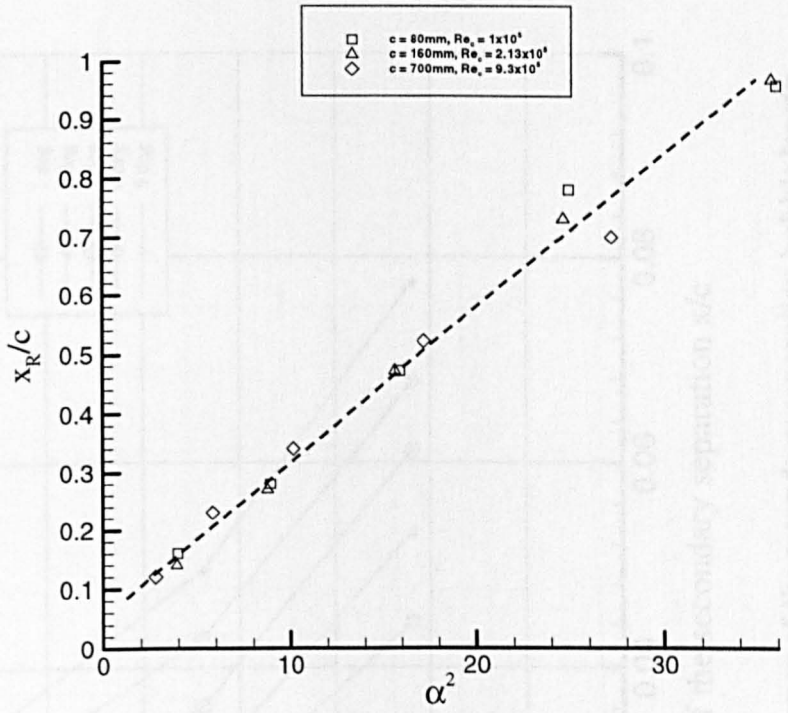

Figure 5.19 Effect of changes in incidence on separation bubble length, corrected for wind tunnel constraint, and plate geometry.

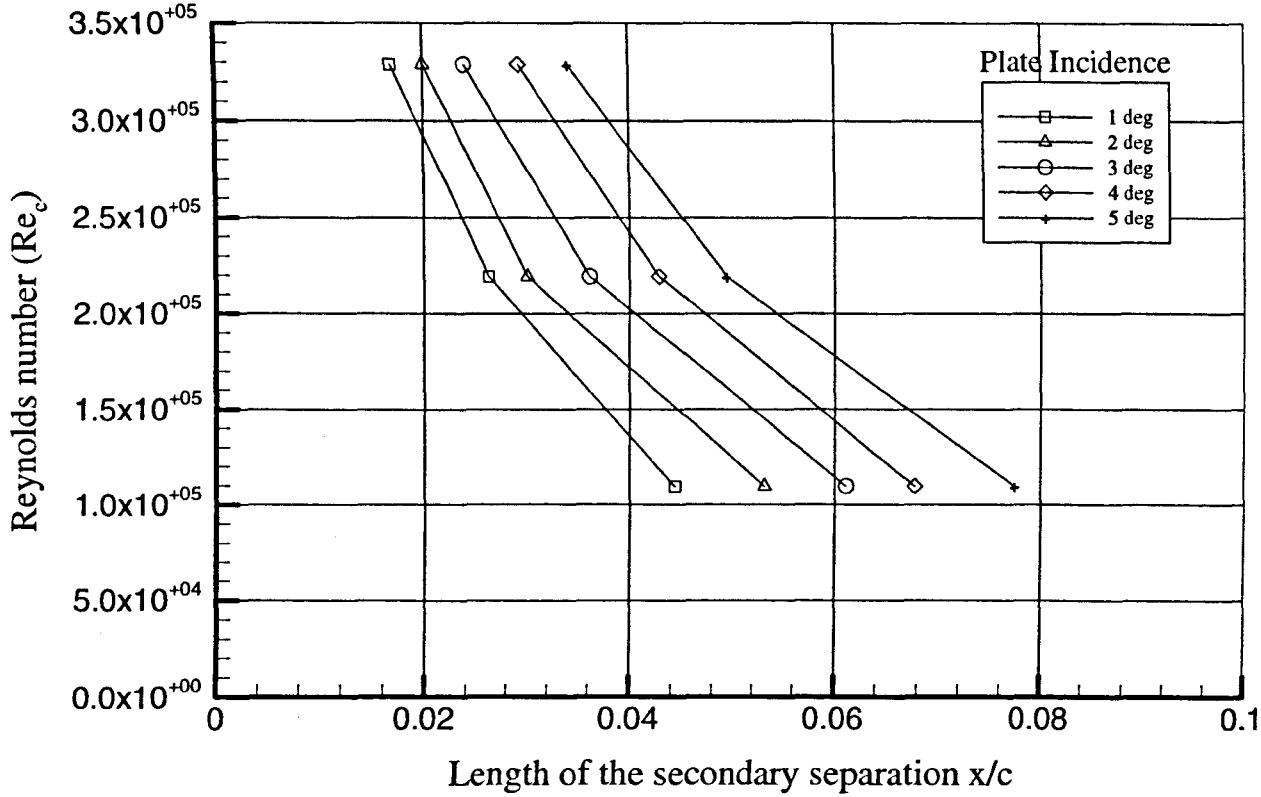

Figure 5.20 Reynolds number dependency of the secondary separation bubble length for various angles of incidence. c=160mm.

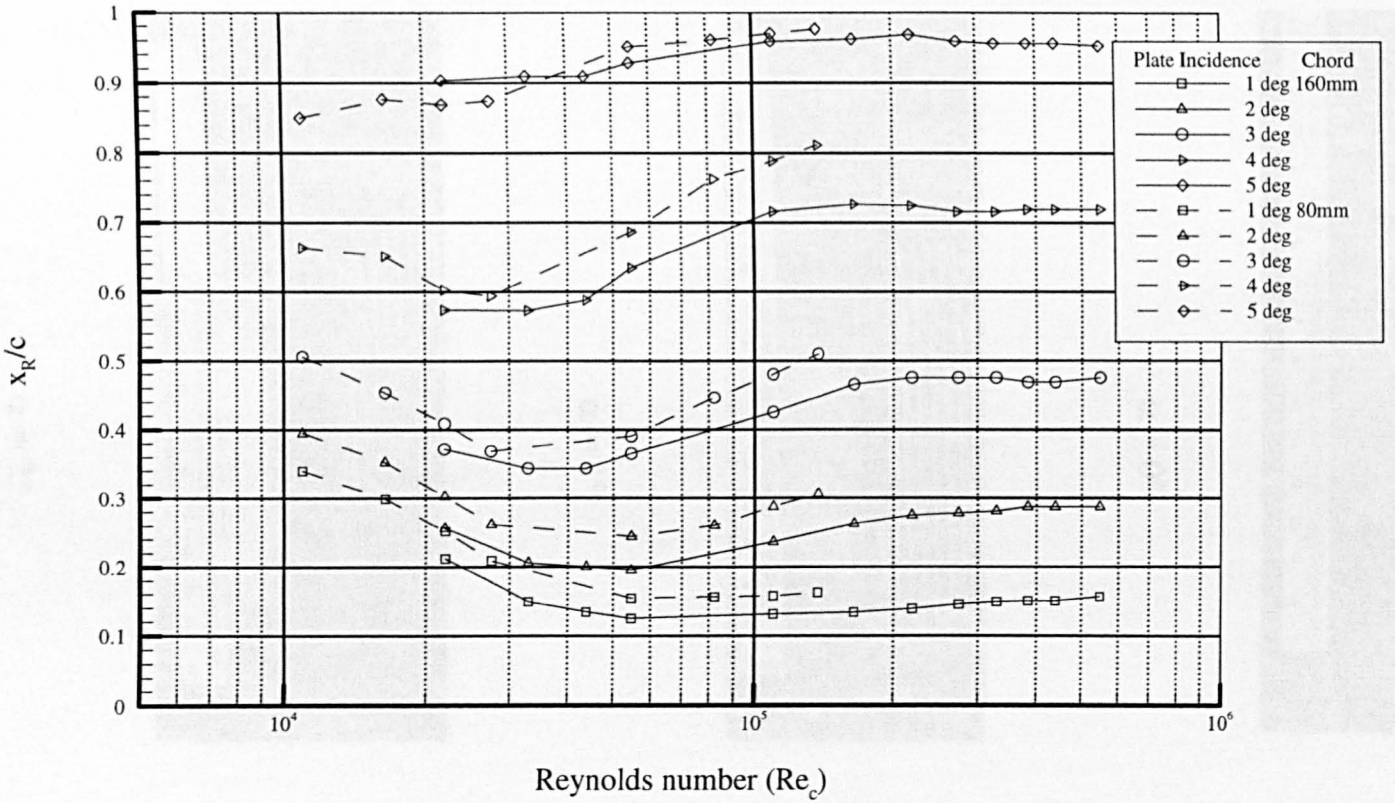

Figure 5.21 Variation in separation bubble length with Reynolds number for various angles of incidence and two different plate chords.

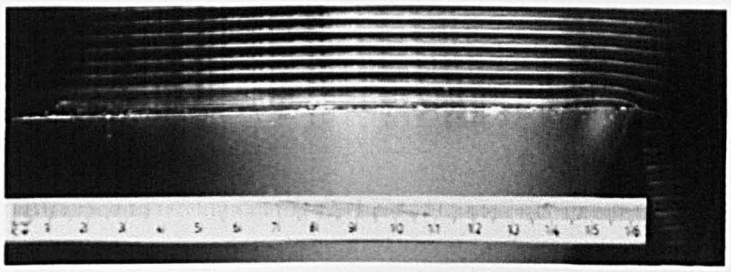

Flow direction

$\alpha = 0°$

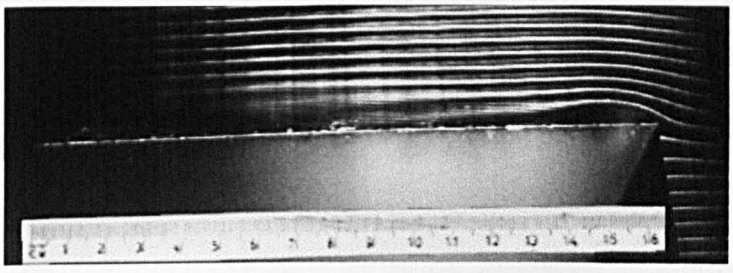

Flow direction

$\alpha = 1°$

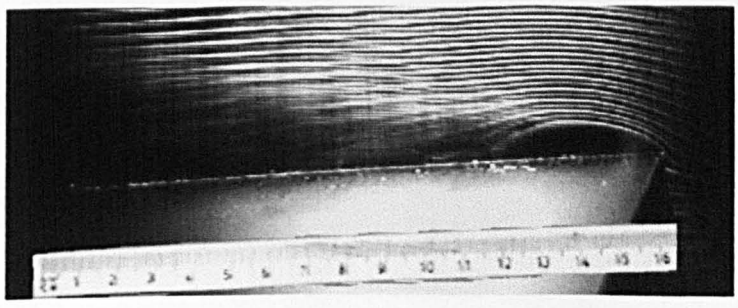

Flow direction

$\alpha = 2°$

Figure 5.22a Smoke wire visualisation of the separation bubble. α=0-2°, Re_c=0.3x10^5.

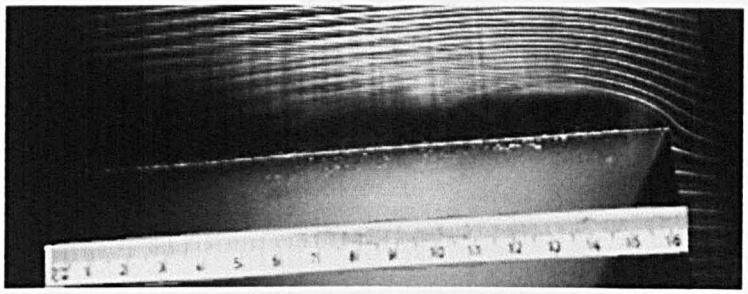

Flow direction

$\alpha = 3°$

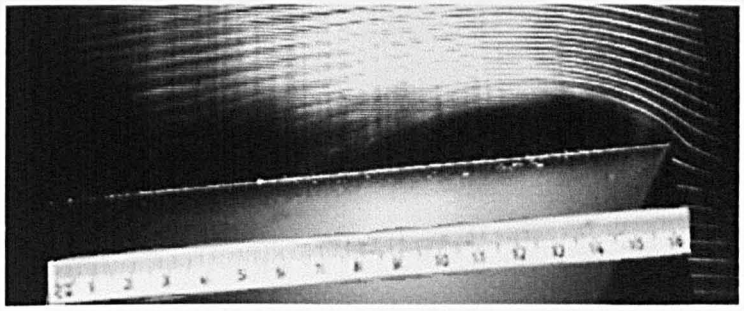

Flow direction

$\alpha = 4°$

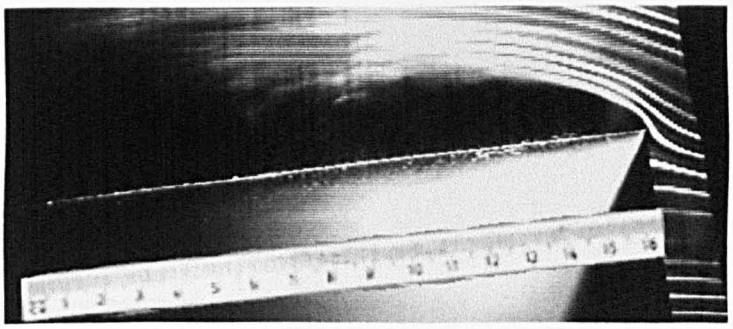

Flow direction

$\alpha = 5°$

Figure 5.22b Smoke wire visualisation of the separation bubble. α=3-5°, Re_c=0.3x10^5.

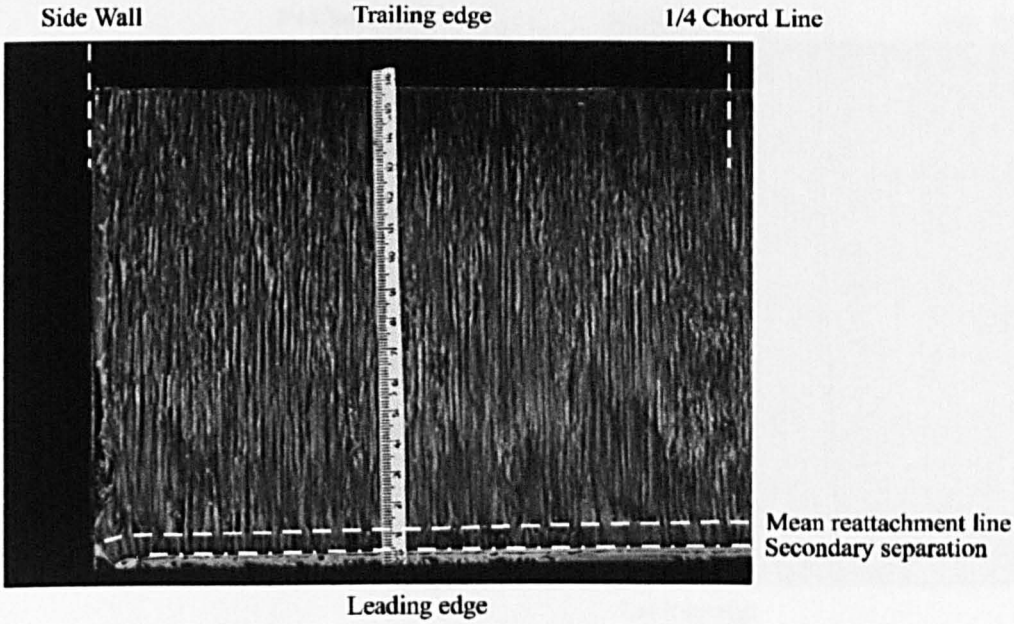

$\alpha = 0°$

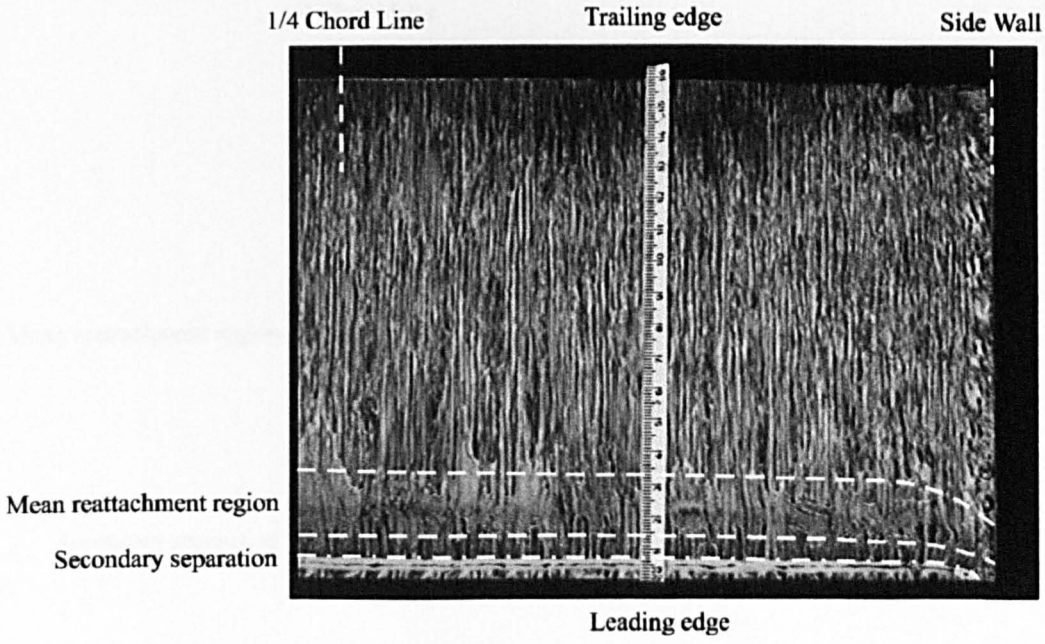

$\alpha = 1°$

Figure 5.23a Oil streakline visualisation of the separation bubble. α=0°, 1°, Re_c=2.13x10^5.

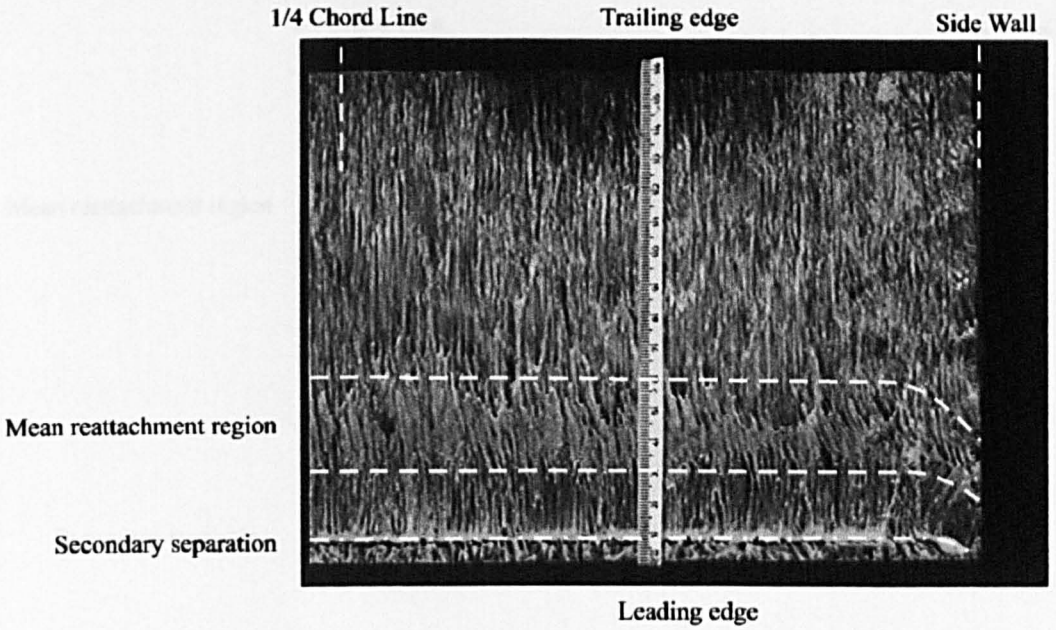

$\alpha = 2°$

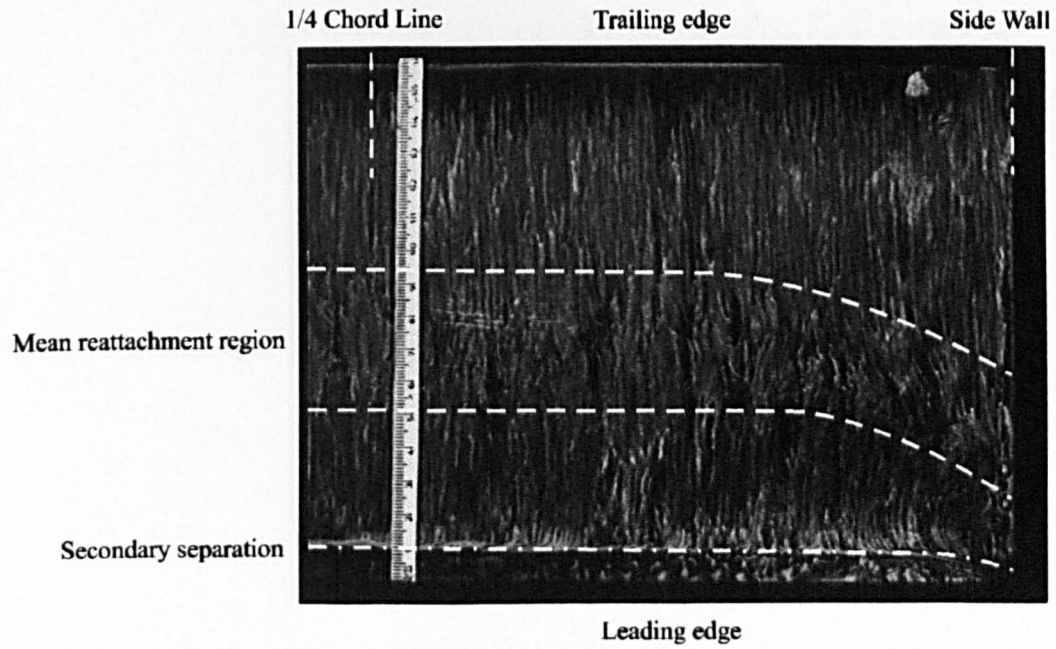

$\alpha = 3°$

Figure 5.23b Oil streakline visualisation of the separation bubble. α=2°, 3°, Re_c=2.13x10^5.

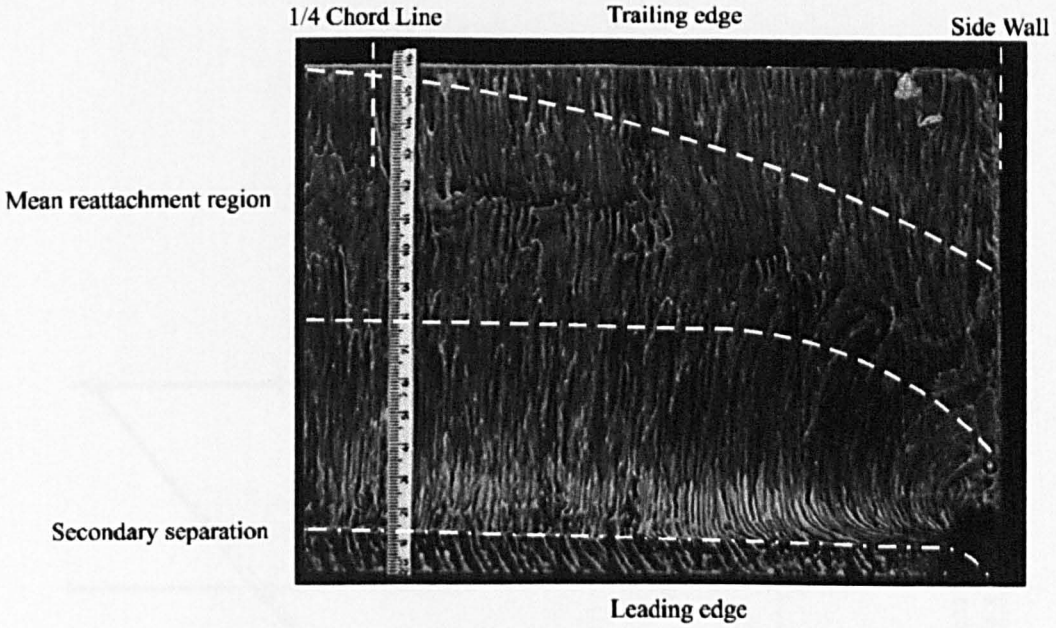

$\alpha = 4°$

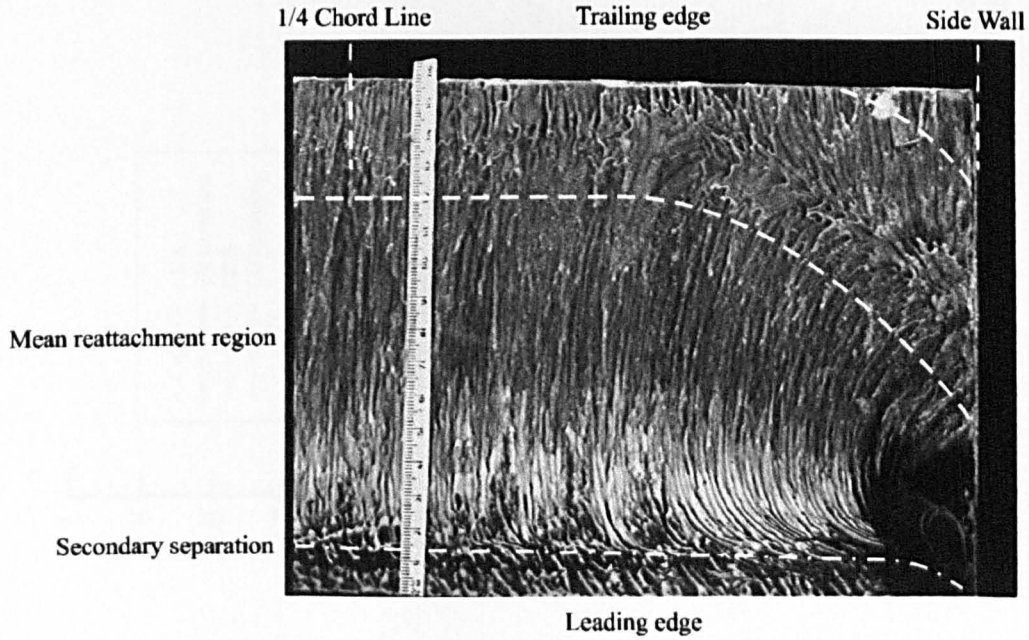

$\alpha = 5°$

Figure 5.23c Oil streakline visualisation of the separation bubble. α=4°, 5°, Re_c=2.13x10^5.

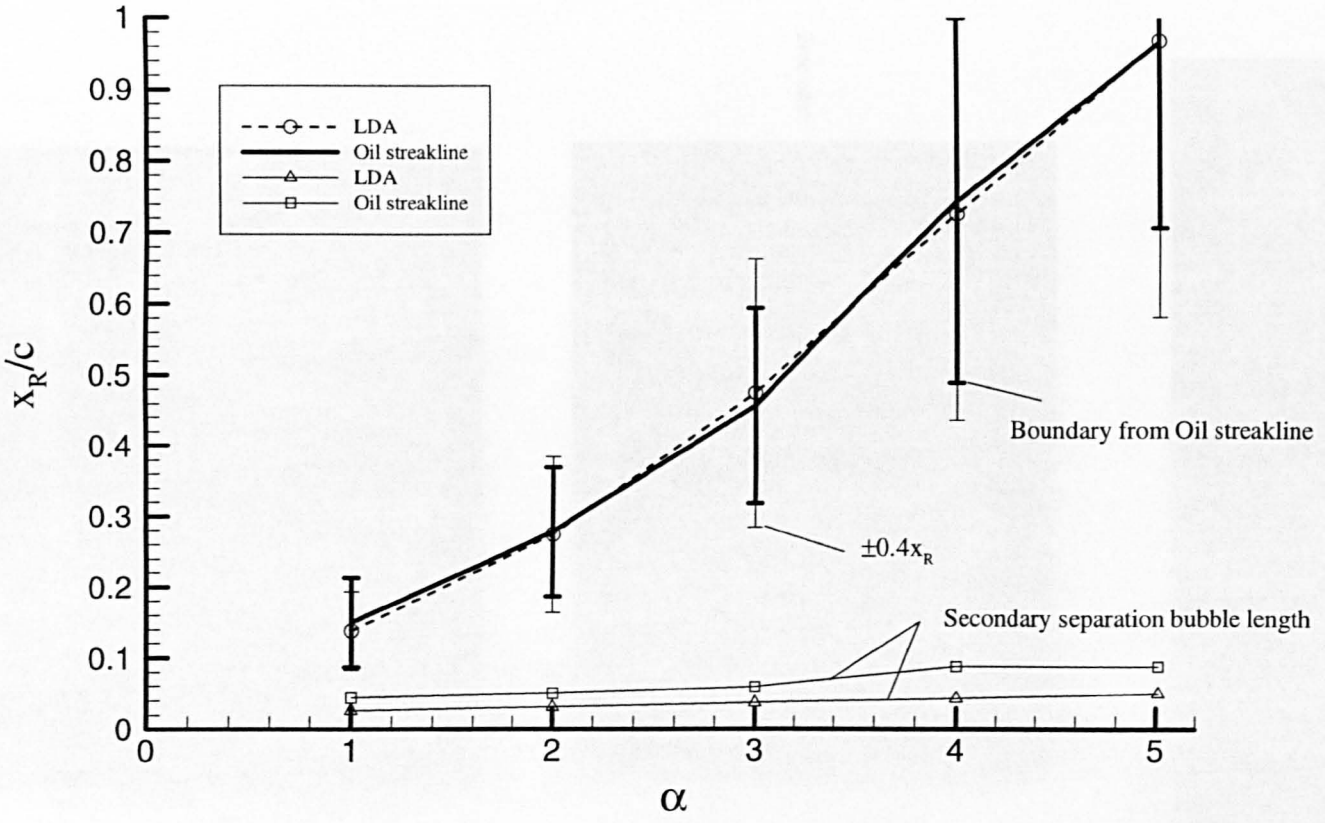

Figure 5.24 Comparison of mean separation bubble length and secondary separation bubble length using LDA and oil streakline flow visualisation techniques, $Re_c=2.13x10^5$.

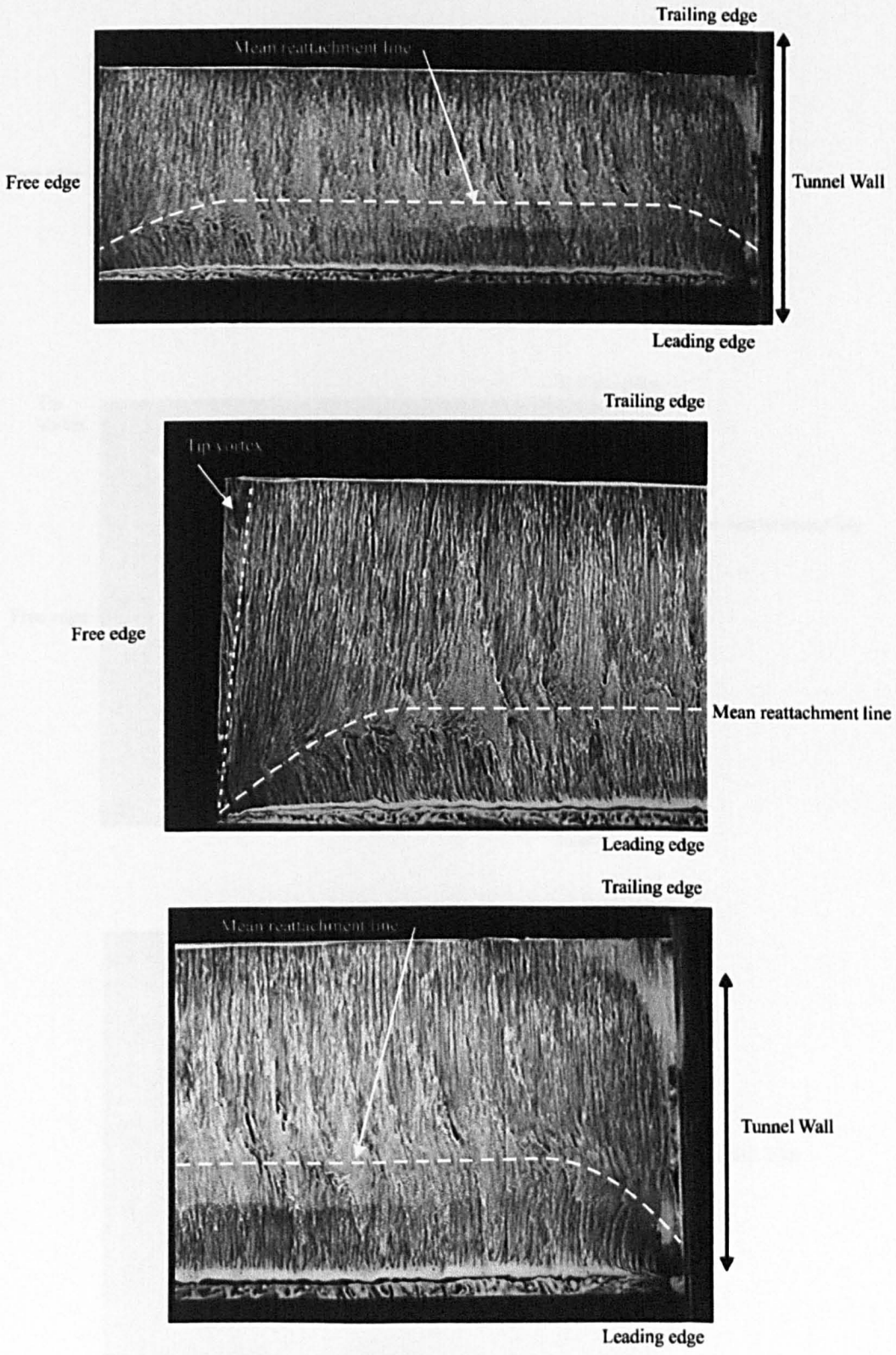

Figure 5.26a Oil streakline visualisation for α=3°, Λ=0° and Re_c=2.13x10^5.

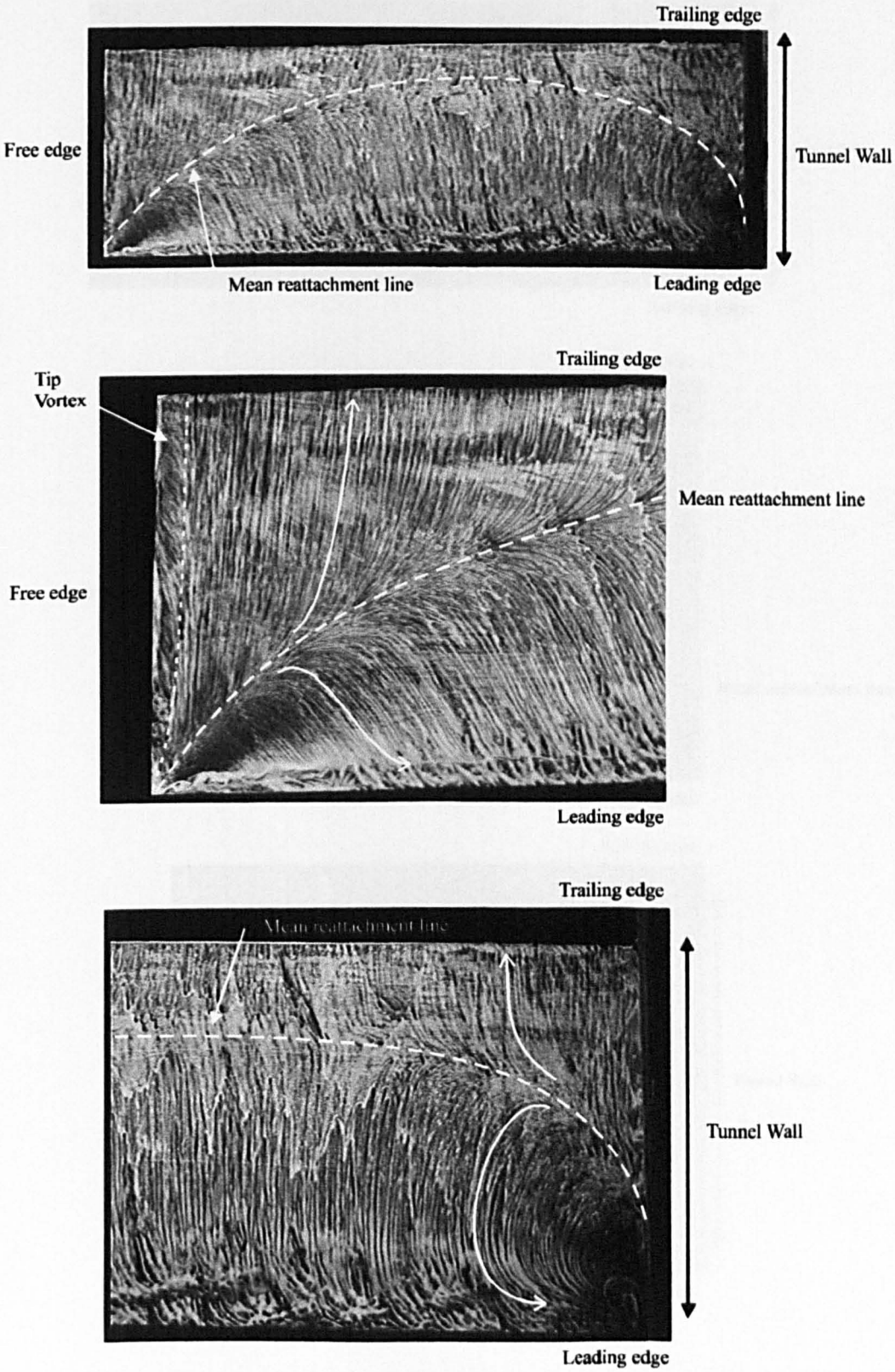

Figure 5.26b Oil streakline visualisation for α=5°, Λ=0° and Re_c=2.13x10^5.

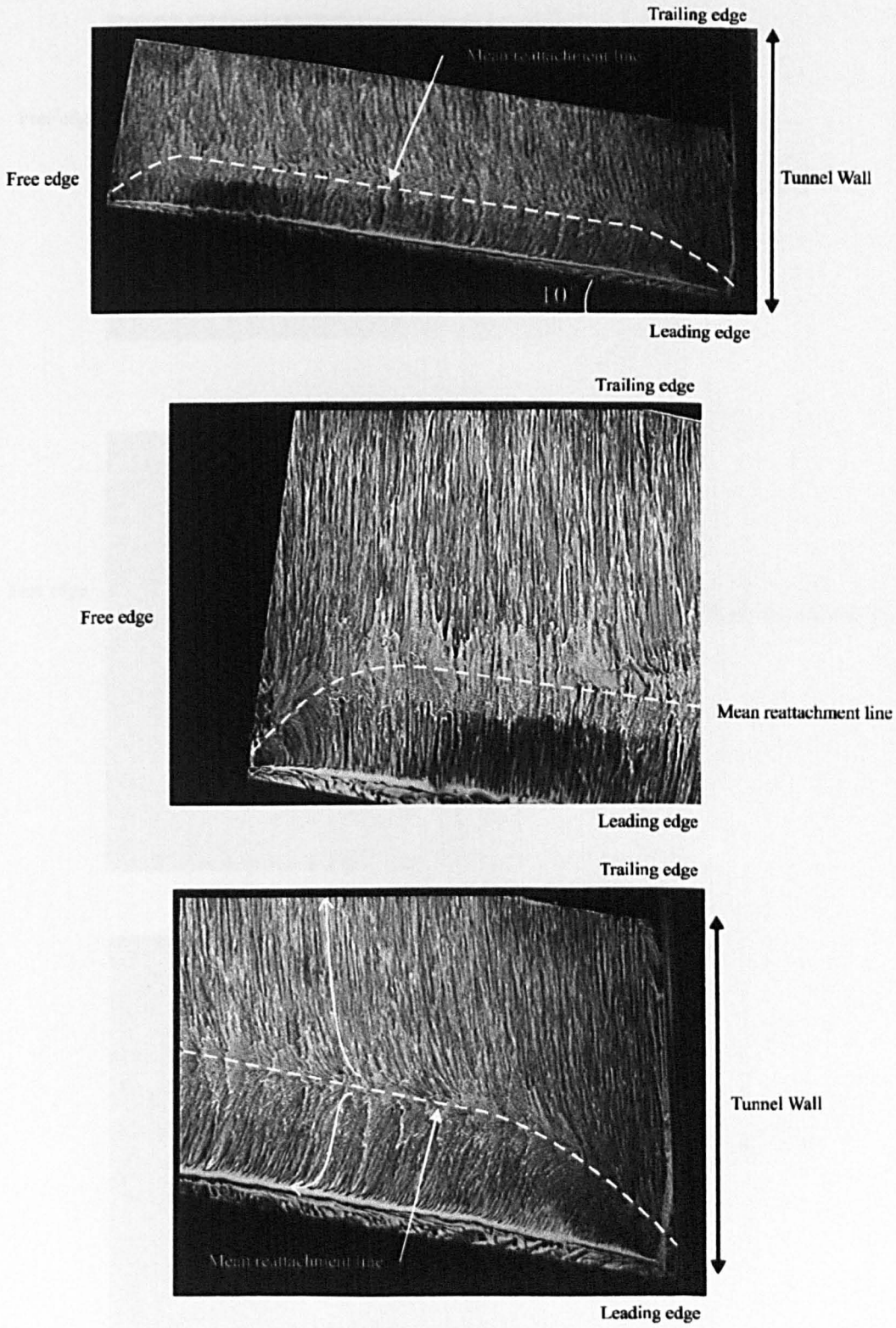

Figure 5.27a Oil streakline visualisation for α=3°, Λ=10° and Re_c=2.13x10^5.

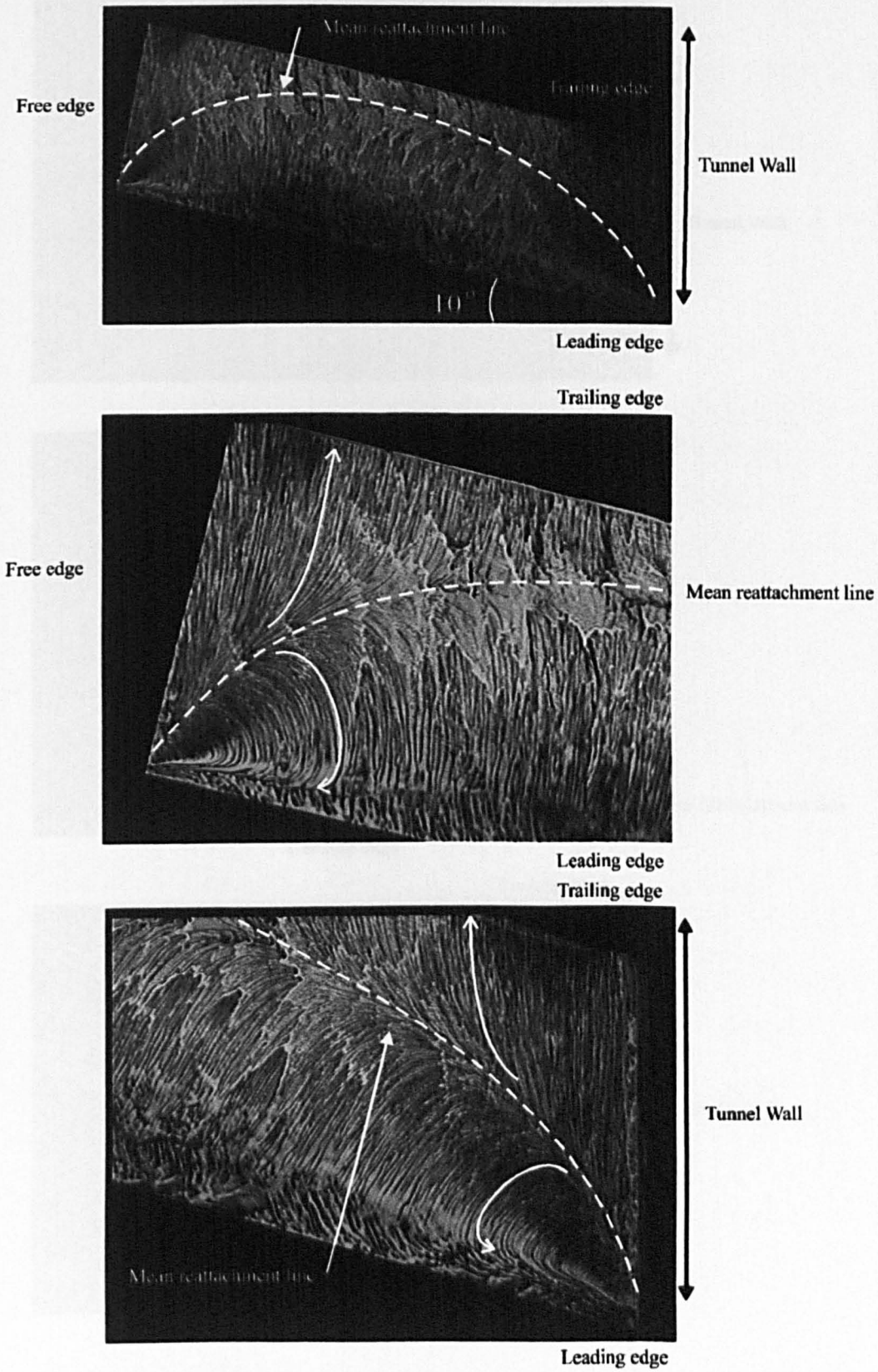

Figure 5.27b Oil streakline visualisation for α=5°, Λ=10° and Re_c=2.13x10^5.

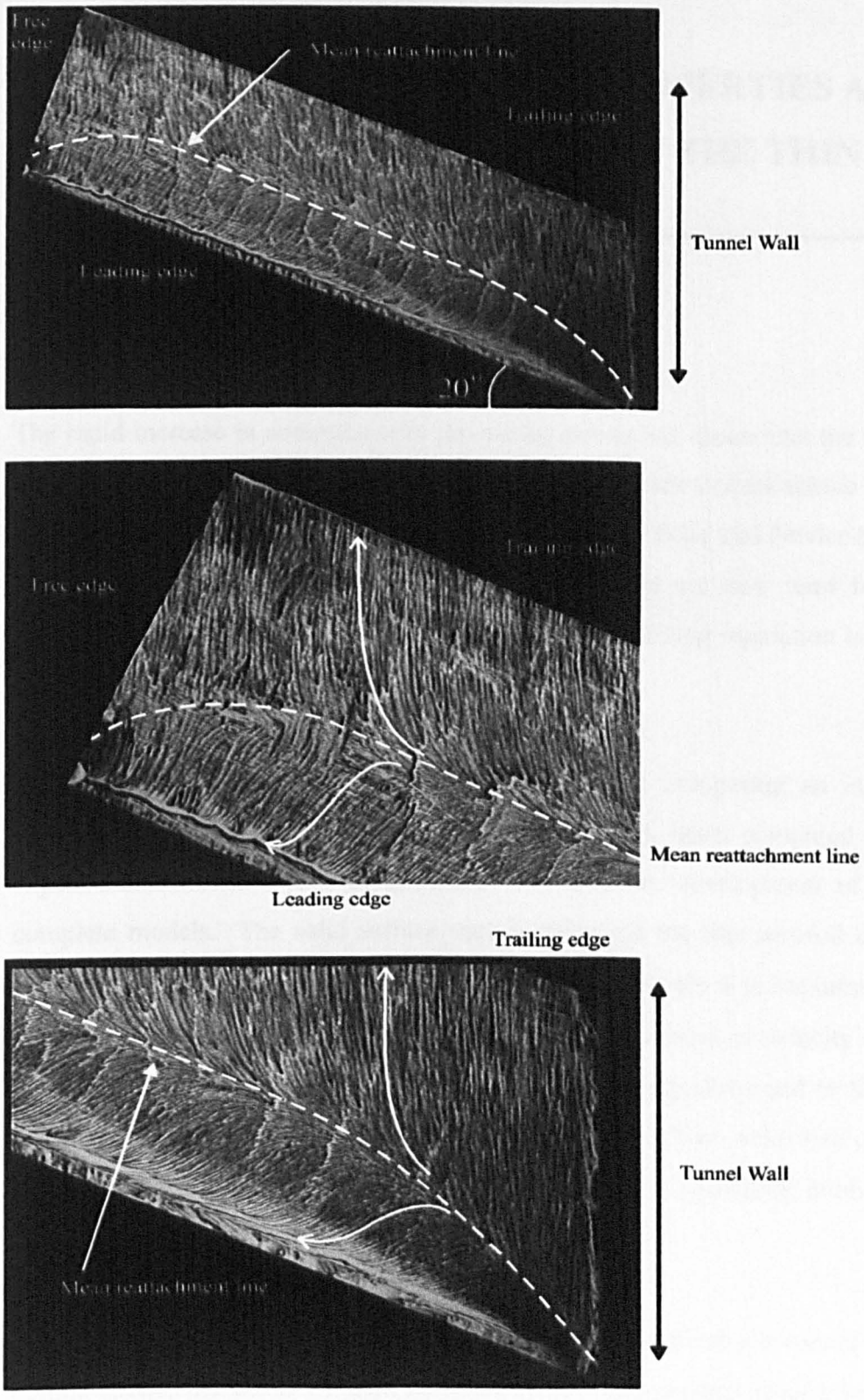

Figure 5.28 Oil streakline visualisation for α=3°, Λ=20° and Re_c=2.13x10^5.

CHAPTER 6
BOUNDARY LAYER INTEGRAL PROPERTIES AND COMPUTATIONAL MODELLING OF THE THIN AEROFOIL BUBBLE.

6.1 Introduction

The rapid increase in computational processing power has meant that the use of computational fluid dynamics (CFD) methods has become commonplace in the aerospace industry. Numerical methods, used to solve Euler and Navier-Stokes fluid dynamic equations or inviscid coupling methods are now used for the design of many types of aerofoil. However, flows involving separation bubbles are much more complex to solve.

For the thin aerofoil bubble, it was considered that computing an inviscid solution that predicted the correct pressure distribution, when compared to the experimental results would be beneficial to the future development of more complete models. The solid surface used to represent the thin aerofoil bubble was defined using the displacement thickness, δ^*, and hence it is important that this is calculated accurately. However, accurate measurement of velocity within the reverse flow region has been shown to be difficult, as discussed in Section 4.3.1. With the use of the LDA, however the reverse flow velocities can be accurately determined and the integral properties over a separation bubble can finally be ascertained.

This chapter starts by discussing in general terms the difficulty involved in the computational modelling of separation bubbles. The boundary layer properties are then calculated from the velocity data obtained earlier, and the displacement thickness is used to represent the thin aerofoil bubble. The validity of this shape

is then tested by comparing the predicted pressure distribution to the experimental results.

6.2 Introduction to the Problem of Computational Modelling of Separation Bubbles

Computational modelling of the short separation bubble has evolved from the semi-empirical methods developed in the 1960s, most notably by Horton (1969). Although in most cases the correlation between predicted and experimental results is good, there remain some cases where there is poor agreement. In general, these cases arise when incidence is high and there are significant pressure gradients.

An example of difficulty associated with computational modelling of the short separation bubble was provided by Calvert (1992). He employed a viscous-inviscid code to calculate losses in turbomachine cascades which are prone to short separation bubbles. He stated that the estimation of the transition position and the development of the turbulent boundary layer would limit the accuracy of the model. The transition position was therefore input separately. The correlation was good at most incidences but at high incidences the results became erroneous. The reason provided by Calvert was that the calculation did not take proper account of the comparatively thick turbulent boundary layer which existed downstream of reattachment of the short separation bubble.

Ripley & Pauley (1993) and Lin & Pauley (1996) modelled the short separation bubble by solving the two-dimensional incompressible Navier-Stokes equations and more recently Alam & Sandham (2000) completed a full three-dimensional simulation using the incompressible Navier–Stokes equations. The two-dimensional models only partially reproduced experimental results of the bubble structure, while the three-dimensional solution in addition resolved the

reattaching and relaxing turbulent boundary layer. Alam & Sandham stated that the two-dimensional simulations do not appear to represent adequately the characteristics of the short separation bubble.

For the task of modelling the thin aerofoil bubble, the available prediction methods are hampered by the characteristics of the flow and surface geometry which differ from those of the short separation bubble. In particular, the steep velocity gradients, large area of separated flow and the geometry around the sharp leading edge add considerable complexity to the modelling process.

For methods including Direct Numerical Simulation (DNS), Large Eddy Simulation (LES) and Reynolds-Averaged Navier-Stokes (RANS) equations, the entire flow domain must be meshed and steep velocity gradients and sharp changes in geometry captured in the mesh.

DNS methods solve the governing equations in full for every length scale, including the growth and decay of every eddy, without the need for modelling assumptions. For the thin aerofoil bubble, this method would require very dense meshes to represent the turbulence and steep velocity gradients in the flow. As a consequence, this would demand too much processing power to be practical.

Turbulence modelling techniques, such as LES and RANS, require the Navier-Stokes conservation equations to be solved approximately in every cell. Both LES, which resolves large eddies and models smaller ones and RANS equations, which models scales which are averaged out, are limited by the necessity to simulate or model some scale of turbulence and are unable to predict transition. Determining the empirical constants used in the modelling is difficult, and any errors are carried through the model. The constants are also only valid for one flow case and are often unreliable when the model is applied to a new flow case. The turbulence model would therefore not cope well with the thin aerofoil bubble flow.

Methods which do not require the meshing of the entire flow domain include panel methods, where only the surface is meshed but this does not provide a field solution. Boundary layer integration techniques solve for integral boundary layer quantities at each point on the surface and do not require the velocity profile to be evaluated.

The boundary layer integration method, which uses the external stream velocities as a calculation starting point, has been attempted for this type of flow. Jackson & Fiddes (1995) employed a weak viscous-inviscid interaction of a panel method and integrated boundary layer method to model the viscous region past a flexible sail section. A new model for the thin aerofoil bubble was employed which set the chordwise starting position and effective thickness of the turbulent boundary layer downstream of the bubble. This model gave good agreement with experimental results for short bubble lengths but the authors noted that to successfully model large bubble lengths, a fully-coupled method would be required. They proposed that modern strong-interaction methods, which now cope well with other kinds of separation, may be extended to the sharp leading edge case. A requirement of the fully-coupled method is to represent the displacement effects of the boundary layer. Unless this is done, the pressure in the leading edge bubble cannot be predicted and so good results cannot be achieved for anything but the smallest of separated regions.

This process of determining the interaction between the inviscid solution and the solutions from the boundary layer equations requires a method of coupling the two regions, which is beyond the scope of this work. A review of suitable viscous-inviscid methods for this is application is given by Lock & Williams (1987).

The detailed velocity data obtained in the main investigation provides an ideal test case to supplement computational modelling of the thin aerofoil bubble. In

addition, the data can be used to improve computational methods. For example, the integral boundary layer methods, used by Jackson & Fiddes relied on inputting the momentum thickness and shape factor of the turbulent boundary layer at reattachment. This can easily be determined from good experimental data.

6.3 Determination of Boundary Layer Integral Properties across a Thin Aerofoil Bubble

For most high Reynolds number flows, the flow-field may be divided into two distinct regions, the viscous boundary layer close to the surface and the inviscid flow outside the boundary layer. The displacement effect of the boundary layer then needs to be evaluated for the application of an inviscid flow analysis. The "effective" inviscid surface is therefore the actual body plus the displacement thickness of the boundary layer. However, to generate an inviscid solution, the flow velocity is required to be parallel to the effective surface thus satisfying the physical criterion of no flow through a solid surface. Computational methods requiring empirical inputs cannot be expected to produce good results if the inputs themselves are unreliable. One reason for this has been the difficulty in accurately determining the boundary layer integral properties for the separated flow case. Gault (1957) chose not to calculate these parameters because of their "doubtful significance". Walraevens & Cumpsty (1993) treated all the measured "negative" flow velocities in the reverse flow region as "positive". This is a common approach when using measurement techniques which are directionally ambiguous, since the size and magnitude of the reverse flow cannot be ascertained. Calvert (1994) compared a measured velocity profile through a separation bubble to a Falkner-Skan profile and confirmed the major differences to be within the low velocity region near the wall. By subsequently assuming reverse flow near the wall (a correct assumption), the value of shape factor was

increased from 7.7 to 11.6 which was closer to the value of 13 for the Falkner-Skan profile.

Schmidt & Mueller (1989) addressed the effect on the boundary layer integral properties of neglecting the reverse flow velocities in the calculations. They showed that the displacement thickness will be smaller and the momentum thickness greater relative to the case when reverse flow (negative local velocity) is calculated.

The standard expression for displacement thickness takes account of the displacement due to the separation bubble as well as the shear layer above it. This is confirmed if the displacement thickness is represented by an equivalent expression which includes the contribution of the bubble separately. For the two-dimensional bubble, the net mass flow between the surface and dividing streamline (z_D) is zero, as shown in Figure 6.1. Therefore,

$$\int_0^{z_D}\left(1-{}^{u}\!/\!_{U_{max}}\right)dz = z_D$$

and so,

$$\delta^* = z_D + \int_{z_D}^{\delta}\left(1-{}^{u}\!/\!_{U_{max}}\right)dz \equiv \int_0^{\delta}\left(1-{}^{u}\!/\!_{U_{max}}\right)dz$$

The displacement thickness is then the sum of the height of the dividing streamline plus the additional thickness as a result of the viscous shear layer contribution.

Figure 6.2 shows the calculated displacement thickness, for plate incidences of 1-5 degrees at a Reynolds number of $2.13\text{x}10^5$. The equations were applied to the velocity profiles given in Figure 5.4a-e.

The displacement thickness can be seen to grow rapidly following separation at the leading edge. A maximum thickness is then reached at about half the bubble length. The thickness then decreases as the flow reattaches and the boundary layer relaxes towards the form of a conventional turbulent boundary layer. In most cases, the displacement thickness reduces all the way to the trailing edge. However, at 1 degree incidence, when the bubble is very short, the displacement thickness can be seen to increase downstream of reattachment. This indicates that the attached boundary layer has finished relaxing and has begun to grow in the same way as a conventional turbulent boundary layer. Therefore, in most cases, the boundary layer reaches the trailing edge prior to the conventional form of a turbulent boundary layer being reached.

Figure 6.3 shows the displacement thickness, scaled with respect to the separation bubble length at each incidence. The results collapse onto a single profile showing that the bubbles are geometrically similar. This is a particularly useful result for computational modelling because the inviscid model of the thin aerofoil bubble is simplified.

Figure 6.4 shows the distribution of momentum thickness, scaled with respect to the separation bubble length at each incidence. The momentum thickness can be seen to become very slightly negative over the front half of the bubble, but soon increases rapidly over the reattachment region. Following reattachment, the growth rate reduces as the boundary layer relaxes. Results of Mangalam et al. (1985) and Hobsen et al. (1997) for a short separation bubbles show a local reduction in the momentum thickness over the separation bubble region. However, for the thin aerofoil bubble there is no attached boundary layer prior to separation and therefore no established value of momentum thickness to be reduced, hence a negative value is reached. The behaviour of both bubble types are in agreement approaching reattachment, both showing a marked increase as the shear layer rapidly thickens and reattachment first occurs.

As previously mentioned, a value of x_R/θ_R and H was used by Jackson & Fiddes in a viscous-inviscid model. The former was taken from results of Newman & Tse (1992) and determined to be $x_R/\theta_R=20$ and the latter was taken to be H=1.4, a value in the range associated with turbulent boundary layer profile. In the current work, the equivalent values were found to be $x_R/\theta_R=32$ and H=2.8. Newman & Tse acknowledged that their value may be inaccurate, but it was used for modelling in the absence of any alternative data for this type of flow. The current analysis could be used to update this model.

Figure 6.5 presents the shape factor for various angles of incidence. Again, the distance along the plate is non-dimensionalised with respect to the separation bubble length. Over the bubble region, the shape factor is very large, resulting from the small values of momentum thickness caused by the reverse flow component. However, approaching reattachment the shape factor falls steeply and tends to a value of around 1.6. This value is similar to that for a turbulent boundary layer in a zero pressure gradient. Reattachment can be seen to occur at a value of H=2.8, a value typical of that normally associated with separation or reattachment (Walraevens & Cumpsty 1993).

6.4 Computational Modelling of the Thin Aerofoil Bubble

The inviscid computation of the flow past a thin aerofoil bubble was carried out using a code developed by Dr C. B. Allen at the Department of Aerospace Engineering, Bristol University. The method is described in Allen (1997 & 1999). In order to assess the validity of the model, the predicted static pressure distribution, for 3 degrees incidence, was compared to the experimental pressure distribution, shown in Figure 5.3 (Chapter 5).

6.4.1 Initial Model used for Computational Analysis

The computational model first chosen to represent the separation bubble was based on the flat plate used for the main experimental work (160mm chord). The displacement of the inviscid flow can be assumed to be as a result of firstly, the separation bubble and secondly, the wake. Therefore, as a first approximation, only the displacement of the bubble was used to start the development of the model. The combined plate geometry and the separation bubble, represented by the height of the dividing streamline, z_D, were modelled for a plate incidence of 3 degrees.

The main limitation of the model as regards meshing arose due to the sharp edges, which gave the potential for singularities in the computational solution. To overcome this, in the computational model, the leading edge was curved with a small radius and the trailing edge was converged by tapering the lower surface to meet the upper surface, terminated by another small radius. The geometry of the initial model is shown in Figure 6.6. The pressure distribution subsequent to convergence of the model to a solution is shown in Figure 6.7.

Three key areas of the upper surface pressure distribution were chosen to assess whether the solution compared well with the experimental results:

- The minimum static pressure of the pressure plateau.
- The gradient and chordwise location of the adverse pressure gradient.
- The behaviour of the pressure gradient near the trailing edge.

As expected, the initial model showed inconsistencies in the pressure distribution. The computational results showed that the minimum pressure plateau was not a smooth profile and the average static pressure in the plateau region was more positive than the experiment results had shown. The adverse pressure gradient over the rear portion of the bubble occurred at approximately the same chordwise location as that measured experimentally, but was found to

be much steeper. In addition, the value of static pressure at the termination of the adverse pressure gradient was also found to be positive. Subsequent to this, the pressure gradient became approximately zero over the final quarter of the plate.

The uneven portions of the pressure distribution are partly as a result of discontinuities in the surface profile. The empirical values of z_D were taken from few chordwise data points and the data was splined to create the surface. Hence, regions of high curvature, such as close to the leading edge and at the end of the separation bubble, were difficult to determine smoothly. The model does not take into account the thick boundary layer over the rear half of the bubble and downstream of reattachment, hence there is a steep adverse pressure gradient at the back of the bubble.

These results only serve to confirm that the additional displacement effects of the shear layer and boundary layer downstream of reattachment must be represented in the model.

6.4.2 Improved Computational Model Including Displacement Thickness

The displacement thickness arising from the shear layer and boundary layer was added to the initial model. Consequently, the thickness of the new model at the trailing edge increased. To avoid a sudden pressure change and to simulate the viscous mixing process in the wake, the trailing edge was extended downstream by an extra quarter chord length. The revised geometry is shown in Figure 6.6. Elliptical smoothing functions were applied to the upper surface to remove discontinuities caused by the splining operation to sparse data. The circular mesh generated was mapped from the flat plate surface to 25 chord lengths away. The near surface mesh is shown in Figure 6.8 and the mesh close to the leading

edge is shown in Figure 6.9. It is important to note the smooth curvature in the mesh which is essential to avoid discontinuities in the results.

The computationally predicted pressure distribution is shown in Figure 6.10. The results show much improved agreement with the experimental results. The adverse pressure region now has an almost identical gradient and chordwise location, and downstream of this, the pressure gradients match all the way to the "real" trailing edge. The correlation of pressure distribution close to the leading edge shows a slight mismatch, but overall the agreement is very promising. Throughout the modelling process, the flow around the leading edge region was shown to be very sensitive to changes in curvature and to improve the model, a higher density of empirical data is needed in the leading edge region.

6.5 Summary of Chapter

The static pressure distribution for a separation bubble formed on a flat plate has been successfully predicted by an inviscid model. The solid surface geometry was created from empirical data using the displacement thickness and adapted locally to avoid singularities in the calculations due to discontinuous gradients in the "body" shape.

The universal profile for the displacement thickness distribution indicates that computational models for angles of incidence within the range that give an attached bubble can be easily generated.

Reliable values of the boundary layer integral properties have been calculated with the use of the LDA to resolve the reverse flow components of the flow. It is essential that the reverse flow is measured accurately because it provides a significant contribution to the total displacement thickness across the separation bubble.

The correlation validates the use of displacement thickness for a thin aerofoil bubble, hence an inviscid model of the thin aerofoil bubble can be used in confidence for computational analysis.

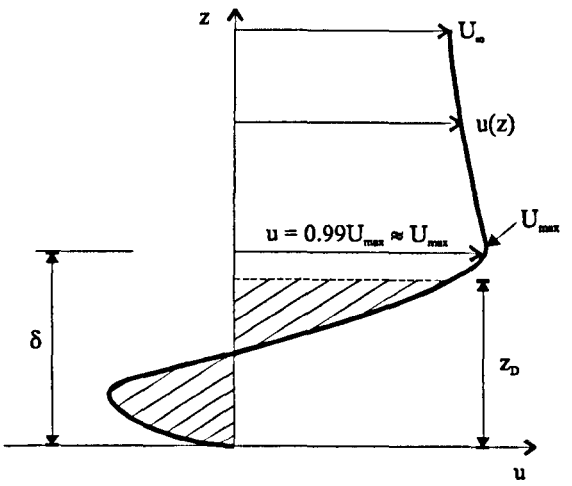

Figure 6.1 Nomenclature for separated flow velocity profile.

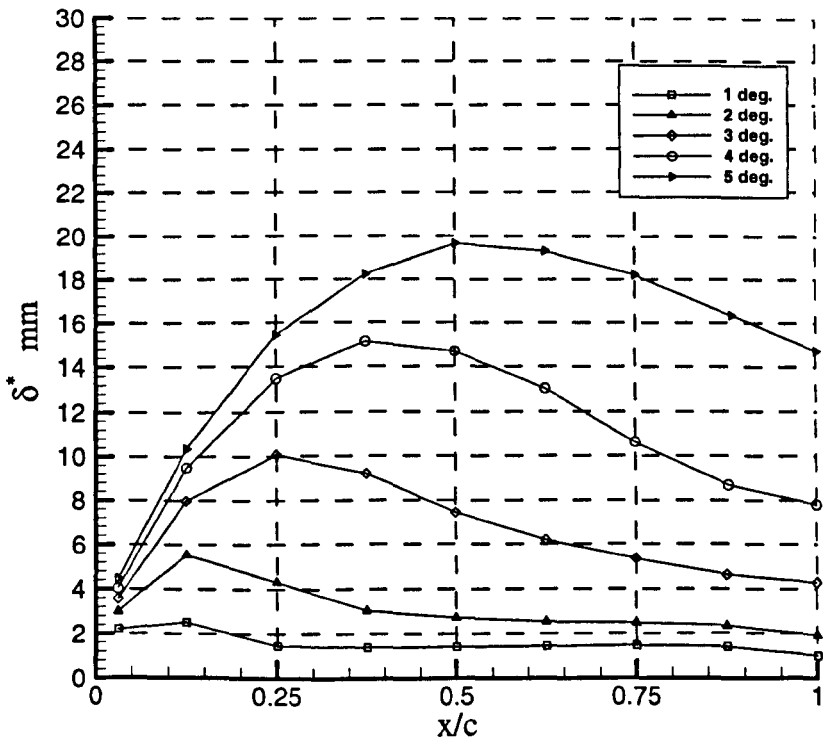

Figure 6.2 Displacement thickness distribution. α=1-5°, U_∞=20m/s, $Re_c=2.13x10^5$.

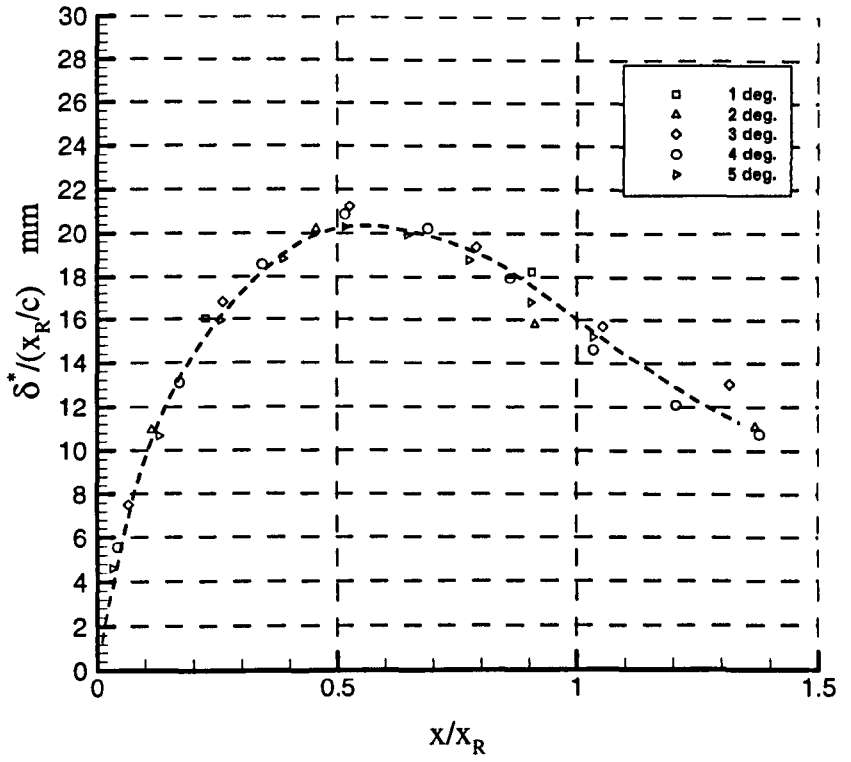

Figure 6.3 Displacement thickness distribution scaled with respect to reattachment length. α=1-5°, U_∞=20m/s, Re_c=2.13x10^5.

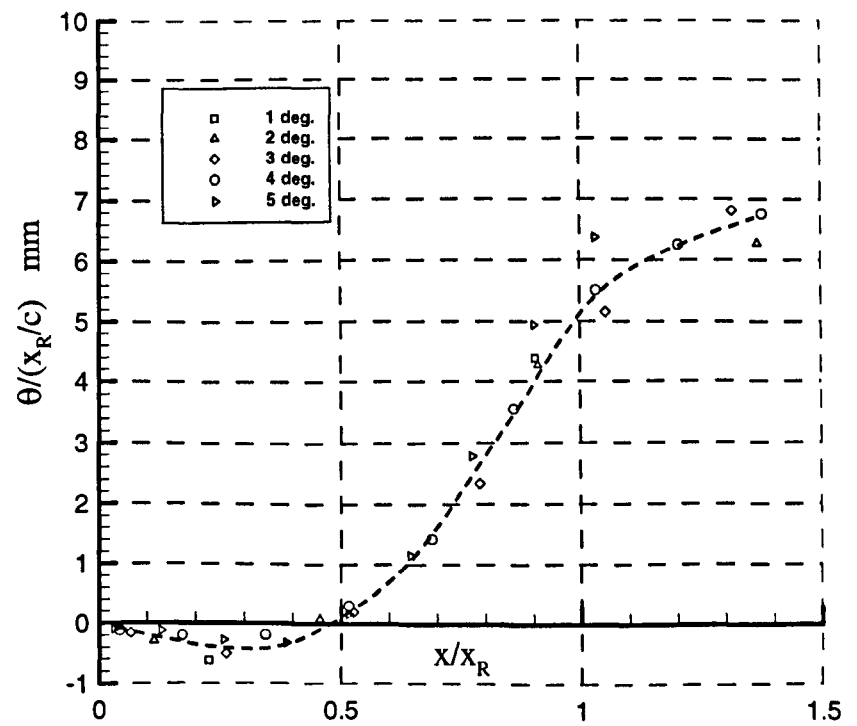

Figure 6.4 Momentum thickness distribution scaled with respect to reattachment length. α=1-5°, U_∞=20m/s, Re_c=2.13x10^5.

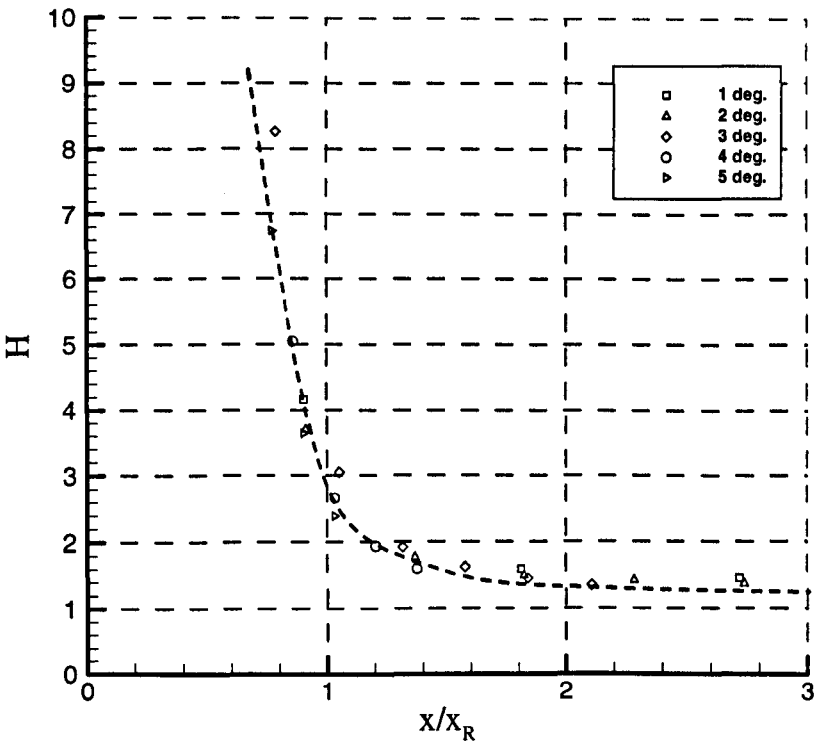

Figure 6.5 Shape factor distribution. for α=1-5°, U_∞=20m/s, Re_c=2.13x10^5.

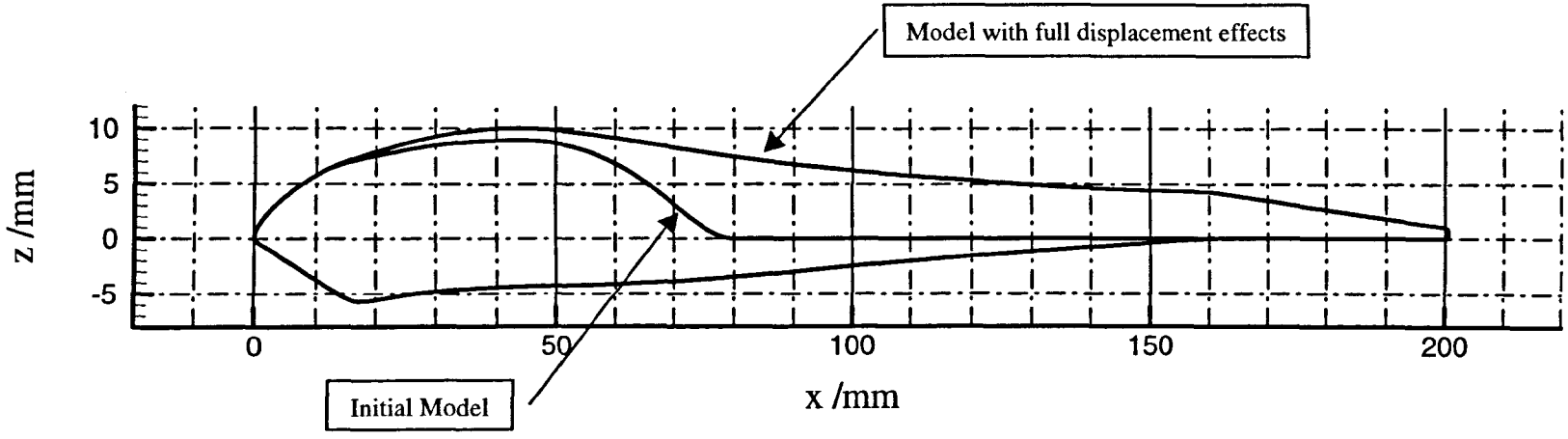

Figure 6.6 Outline of model used for numerical analysis.

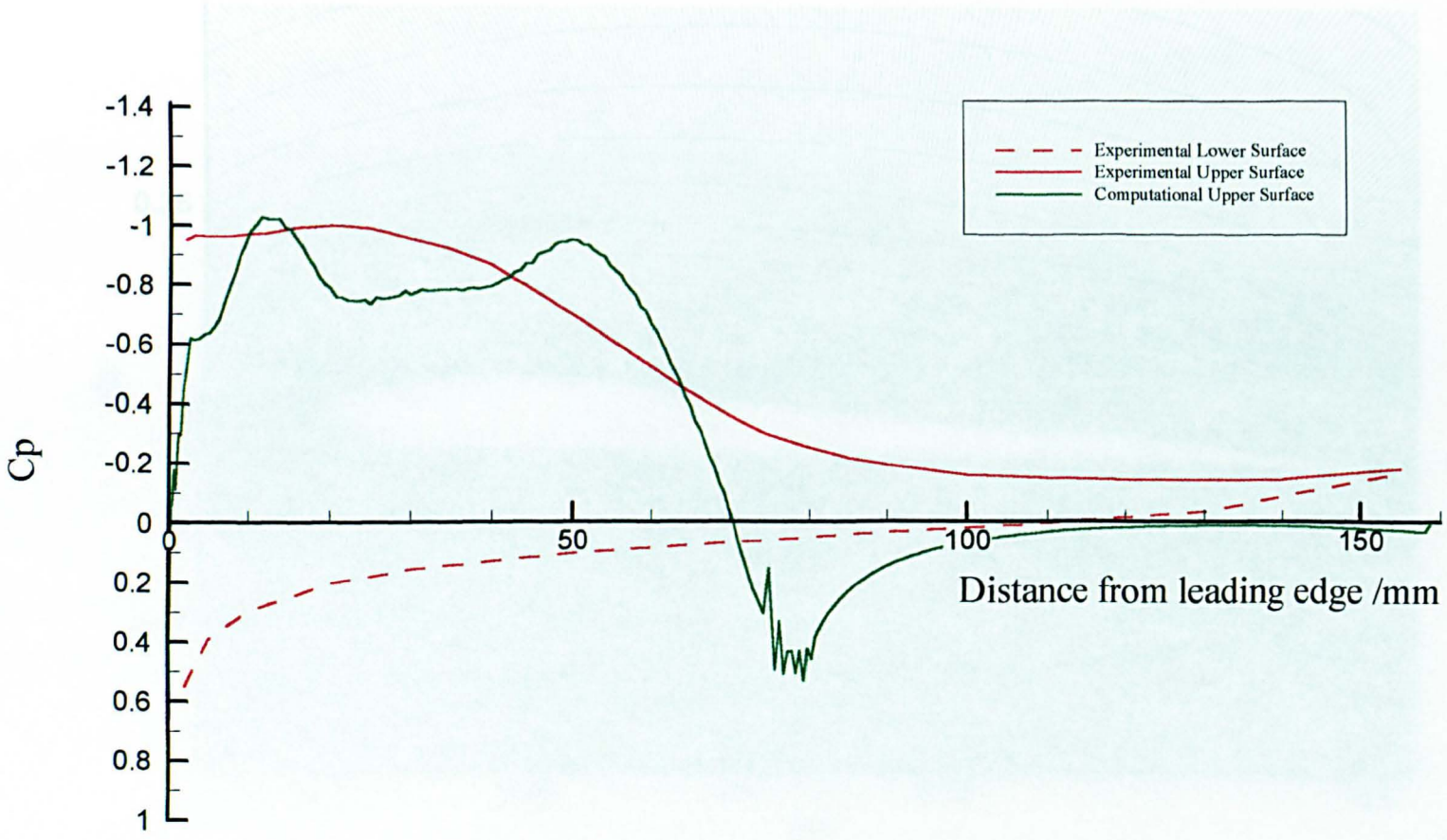

Figure 6.7 Comparison of numerical with experimental results for simplified model.

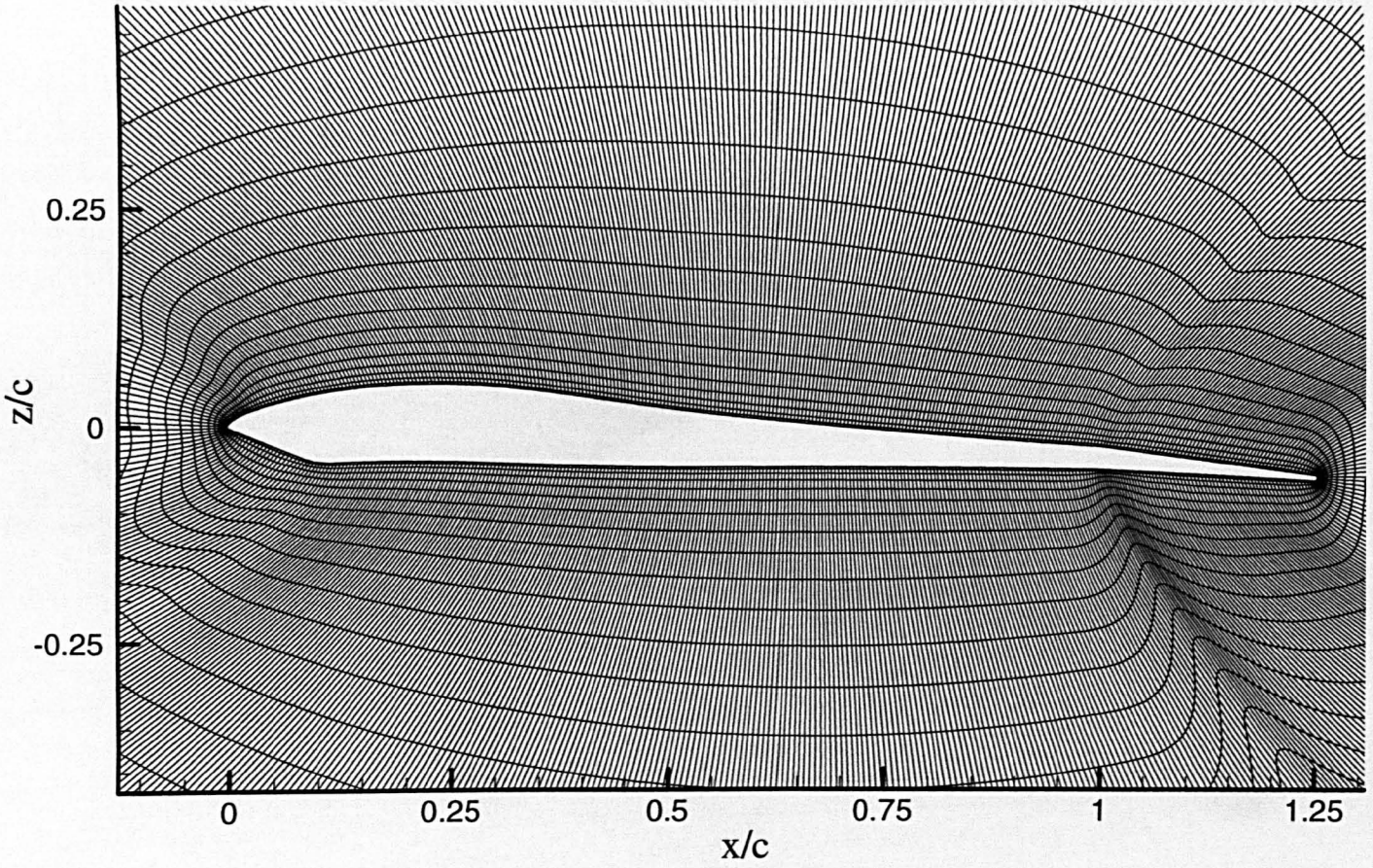

Figure 6.8 Near thin aerofoil bubble mesh, α=3°.

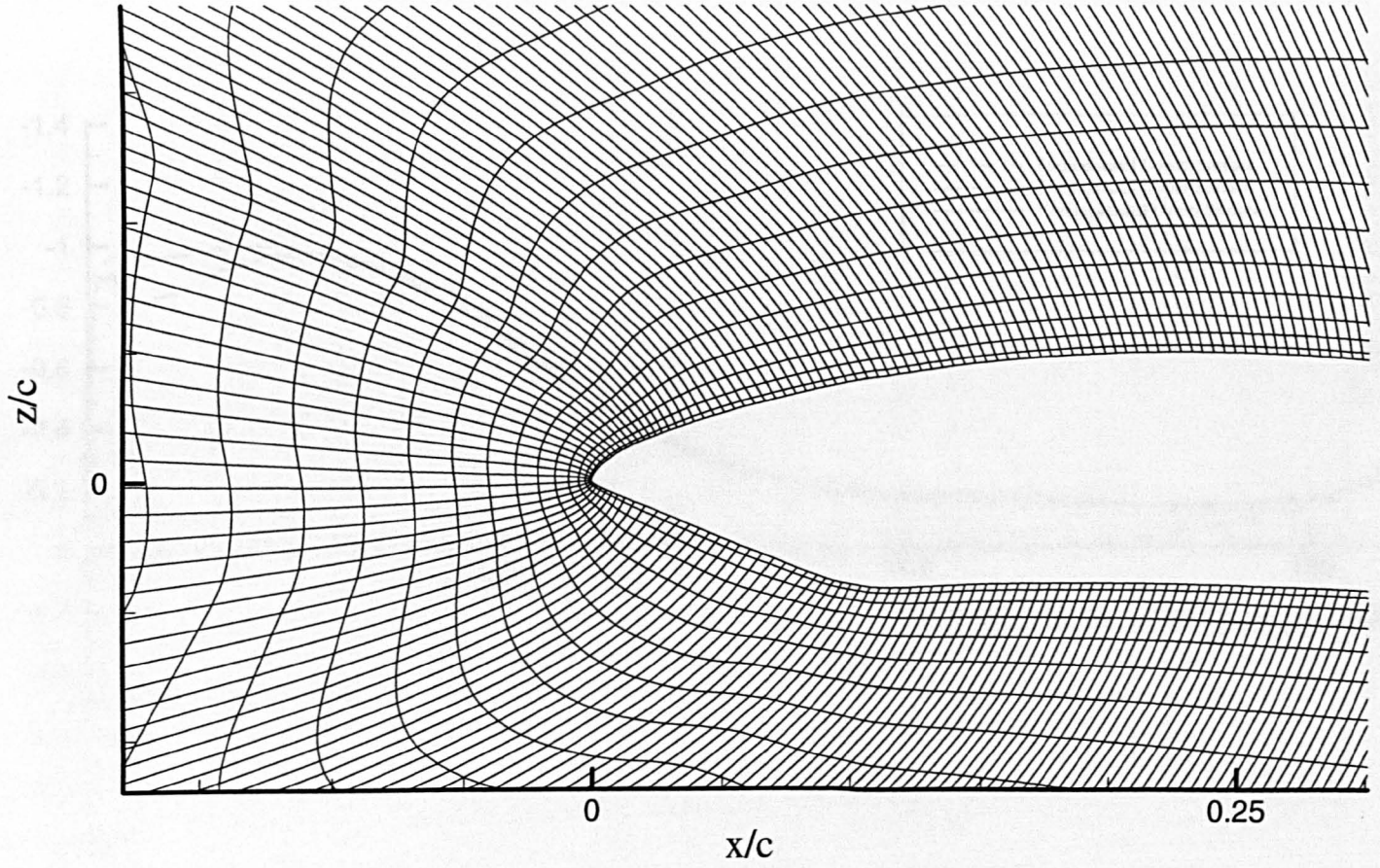

Figure 6.9 Near thin aerofoil bubble mesh showing leading edge detail, α=3°.

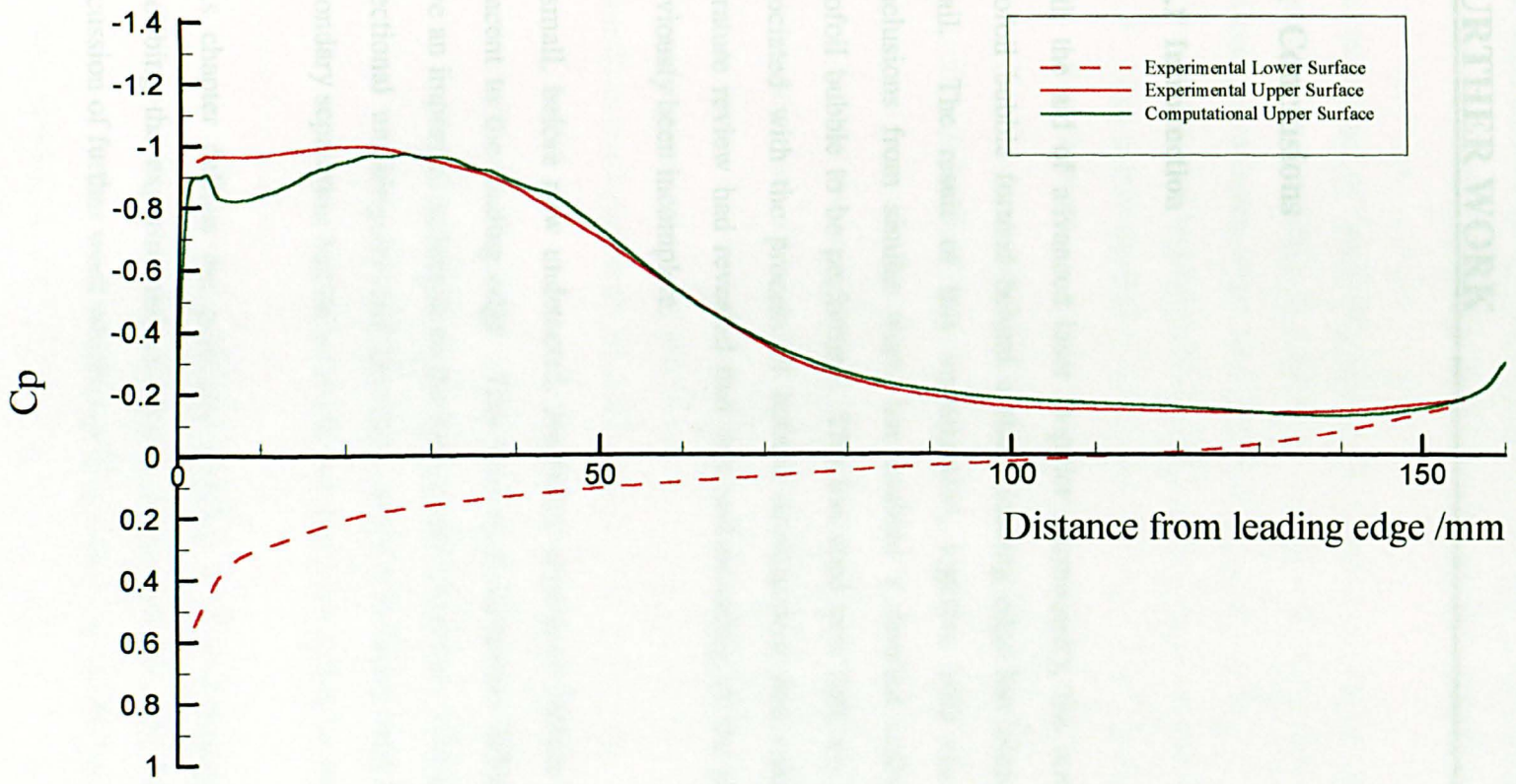

Figure 6.10 Comparison of numerical with experimental results for model including displacement effects.

CHAPTER 7
CONCLUSIONS AND RECOMMENDATIONS FOR FURTHER WORK

7.1 Conclusions

7.1.1 Introduction

With the aid of advanced laser Doppler anemometry, the structure of a thin aerofoil bubble formed behind a sharp leading edge has been investigated in detail. The result of this investigation, together with the application of conclusions from similar work, has enabled a detailed analysis of the thin aerofoil bubble to be performed. This has shed new light on the mechanisms associated with the process of bubble development and reattachment. The literature review had revealed that this understanding of the phenomenon had previously been incomplete.

A small, before now undetected, secondary separation bubble has been found adjacent to the leading edge. This secondary separation bubble is thought to have an important influence on the main bubble structure. It is the LDA, with its directional unambiguity and excellent spatial resolution, that has enabled the secondary separation bubble to be identified and measured for the first time.

This chapter defines the principal findings of this investigation, as well as describing the experimental techniques employed, and concludes with a brief discussion of further work which could be realised to complement this study.

7.1.2 Experimental Technique

The experimental set-up used, including the wind tunnel, support rig and flat plates proved very suitable for the investigation of thin aerofoil bubbles.

The technique of laser Doppler anemometry has proved itself to be very successful at providing measurements within this type of flow. The three particular advantages, which make this technique successful are:

- Directional unambiguity, vital for measuring in reverse flow regions.
- High spatial resolution, to define steep velocity gradients and small scale flow features.
- Non-intrusiveness, which ensures no probe interference in a multi-directional flow.

To complement the laser Doppler anemometer (LDA), a qualitative smoke-wire flow visualisation technique has been developed, using a twisted wire pair to produce evenly spaced smoke filaments illuminated by a laser light sheet. Unlike the plane of smoke produced by a single wire, the filaments acted as streamlines, producing high definition images of the outer flow-field.

An oil streakline technique was used to show detailed surface patterns under the thin aerofoil bubble. The reattachment region produced a distinctive pattern and comparisons of the bubble length with the LDA results showed excellent correlation.

7.1.3 Thin Aerofoil Bubble Structure

The main structure of the bubble is composed of a large recirculating region of fluid. This is bounded on the upper edge by a curved shear layer that reattaches to the plate surface downstream of the leading edge.

Shear Layer and Transition

The shear layer is initially laminar but, other than at very low Reynolds number, undergoes the start of transition close to the leading edge (2.5% x/c). There are three reasons for the early transition:

- Very high shear close to the leading edge.
- A feedback of turbulent fluid into the recirculation region which is then entrained in the shear layer, inducing unsteadiness close to the leading edge.
- Natural instability in the shear layer, prior to transition, thought to be of the Kelvin-Helmholtz type.

The inflection point in the velocity profile across the shear layer was observed from the measurements to be associated with the amplification mechanism for instability in the shear layer.

Entrainment

A key feature of the flow is the entrainment on the low-velocity edge of the shear layer. This is responsible for the reverse flow inside the bubble, the form of the pressure distribution and the curvature of the shear layer. The degree of entrainment is partly determined by the Reynolds number of the flow; this also determines the rate of thickening of the shear layer.

Reverse Flow Region

In the reverse flow boundary layer, evidence was found of periodic stabilisation due to the favourable pressure gradient over the rear half of the bubble. The favourable pressure gradient was shown to periodically suppress turbulent fluctuations in the reverse flow boundary layer.

Over the front half of the bubble the boundary layer is decelerated by an adverse pressure gradient which leaves it more susceptible to separation close to the leading edge.

Secondary Separation Bubble

The measurements revealed a small secondary separation bubble within the primary bubble, rotating in the opposite sense, immediately downstream of the leading edge. This had not previously been recognised in this type of flow.

The secondary bubble is formed by the separation of the reverse flow boundary layer. The location of the separation point is dependent on the freestream Reynolds number but the reattachment point is fixed close to the leading edge by the very steep adverse pressure gradient.

Although small in size (2-8% chord), the secondary separation bubble has the effect of increasing the velocity gradient in the shear layer close to the leading edge which encourages the shear layer to undergo early transition.

Reattachment and Relaxation of the Boundary Layer

The reattachment region is highly unstable due to imbalances between the quantity of fluid entrained by the shear layer and that returned by the reverse flow region.

Periodic unsteadiness first observed prior to transition, propagates downstream in the shear layer and is thought to be as a result of eddy structures developing. However, as the shear layer widens and the background turbulence levels increase, the periodic structures become undistinguishable in the measurements by the time the flow reattaches.

Downstream of reattachment, the boundary layer changes form towards that of a normal turbulent boundary layer profile due to the injection of high-energy fluid into the lower portion of the layer.

Stagnation Point

The stagnation point has been shown to remain attached to the leading edge, over and beyond the incidence range for which the separation bubble exists.

It was clear that no significant boundary layer develops from the stagnation point around the leading edge before separation occurs on the upper surface.

7.1.4 Effect of Changes in Incidence, Reynolds Number and Chord Length on Bubble Length

The bubble forms at low incidence, (the exact angle depending on plate leading edge geometry), and increases in length with incidence until it reaches the trailing edge. The length of the bubble is proportional to the square of the incidence.

The bubble length scales directly with changes in chord length, providing valid geometrical scaling of the experimental set-up is used. Alternatively incidence corrections can be applied to account for differing tunnel constraint which will occur if the geometrical scaling is violated.

Reynolds number has been shown to influence the bubble length. Starting at low Reynolds number, the bubble length decreases and reaches a minimum. Further increases in Reynolds number and the bubble length increases and reaches a plateau, found to be around 10^5.

- At low Reynolds number, the entrainment is low and the reattachment length high, assuming reattachment occurs at all.
- As the Reynolds number increases, the entrainment increases until it reaches a maximum. The shear layer is effectively fully turbulent and the bubble length reaches a minimum.
- Further increases in Reynolds number lead to a contraction of the shear layer, normal to the flow direction, causing the bubble length to increase.
- Eventually, the reduction in lateral growth rate becomes negligible and the bubble length remains constant for further increases in Reynolds number.

7.1.5 Similarities of Thin Aerofoil Bubbles

Different length bubbles formed by a change in incidence are similar to one another. This similarity was proven when the following properties were non-dimensionalised with respect to bubble length:

- Velocity distribution
- Static pressure distribution
- Intermittency in the reverse flow region
- Displacement thickness

This commonality of the static pressure distributions results in a single value of pressure recovery factor for all bubble lengths. This value is identical to that at which short laminar separation bubbles are shown to "burst" and it is suggested that the turbulent shear layer of the thin aerofoil bubble is maintaining close to the maximum sustainable shear stress.

7.1.6 Effect of Sweep on Bubble Structure

The investigation into the effects further three-dimensionality provides a qualitative description of how the thin aerofoil bubble structure changes as firstly, a free tip and secondly, sweep is introduced. The key behavioural changes are outlined below.

The free tip increased inflow along the recirculating region and addition of sweep angle generated outflow along the plate. The location where the inflow and outflow balanced, resulted in chordwise flow patterns in the reverse flow which is associated with the maximum reattachment length across the span.

Sinuous flow patterns develop under the bubble as sweep is increased, indicating the development of an orderly spiral flow. This flow becomes more powerful with further increases in incidence and sweep, and eventually the conical vortex will turn downstream, resulting in a flow closely resembling a delta wing vortex flow.

7.1.7 Computational Modelling of the Thin Aerofoil Bubble

An inviscid solution for the thin aerofoil bubble successfully predicted the static pressure distribution implying that the correct displacement thickness was used.

The displacement thickness can be represented by a universal profile for all angles of incidence at which the bubble reattaches. This enables inviscid solutions to be easily computed for different length bubbles, where the displacement thickness defines the solid surface.

Accurate boundary layer data is needed to provide empirical inputs for turbulence modelling and boundary layer integral techniques.

7.2 Recommendations for Further Work

This research has provided a valuable insight into the thin aerofoil bubble formed behind a sharp leading edge at incidence. Detailed velocity measurements and flow visualisation images have led to a new understanding of the mechanisms involved in the development and behaviour of the thin aerofoil bubble. The improved understanding should aid the design process in cases where existence of the thin aerofoil bubble affect performance and need to be minimised.

The results also provide a detailed test case to assist in the development and validation of numerical calculations of thin aerofoil flows. Jackson & Fiddes (1995) had identified that such a test case was not available from previous work but was necessary for further progress in the analysis of this flow regime.

Although the research provides a cohesive study into the thin aerofoil bubble, a number of avenues for further work have been opened up.

- An important area warranting further research is the elimination of the thin aerofoil bubble which would lead to reduced drag and, for example, the improved performance of a sail section. This should include an investigation of the effect of leading edge curvature on bubble length, with either modifications to the leading edge radius or the addition of "mast" sections. For thicker sections, the effect of suction or blowing should be investigated with a view to remove the reverse flow region and induce premature reattachment.

- A more advanced computational analysis, using viscous-inviscid coupling should be undertaken and correlated with the experimental data provided. This would enhance the analysis of flexible sail sections, where such bubbles

are critical to the performance. In addition, the boundary layer data should be used to improve turbulence modelling techniques.

- The introductory investigation into the effects of sweep should be extended and include rigid curved sections to better represent the shape of sail sections.

- The periodic behaviour, shown to exist in the shear layer, should be investigated further with the fundamental frequency being determined to see whether it relates to any length scales associated with the thin aerofoil bubble.

REFERENCES

ALAM, M. and **SANDHAM, N. D.** Direct numerical simulation of "short" laminar separation bubbles with turbulent reattachment. *J. Fluid Mechanics*, **403**, 223-250, 2000.

ALLEN, C. B. The effect of grid topology and density on inviscid hovering rotor solutions. *Proc Instn Mech Engrs.*, **213**, Part G, 81-95, 1999.

ALLEN, C. B. Central-difference and upwind-biased schemes for steady and unsteady Euler aerofoil computations. *Aeronautical J.*, **99**, 52-62, 1995.

ANON. User's guide- 57N10/57N14/57N25 Burst spectrum analyser, Dantec Measurement Technology, 1994.

ANON. Safex fog generator 2001, Instruction manual, Dantec Measurement Technology.

ARIE, M. and **ROUSE, H.** Experiments on two-dimensional flow over a normal wall. *J. Fluid Mechanics*, **1**, 129-141, 1956.

BANDYOPADHYAY, P. R. Instabilities and large structures in reattaching boundary layers. *AIAA J.*, **29**, 1149-1155, 1989.

BARRETT, R. V. Design and performance of a new low turbulence wind tunnel at Bristol University. *Aeronautical J.*, **88**, 86-90, 1984.

BARRETT, R. V. and **SWALES, C.** Realisation of the full potential of the laser Doppler anemometer in the analysis of complex flows. *Aeronautical J.*, **102**, 313-320, 1998.

BLASIUS, H. Grenzschichten in Flüssigkeiten mit kleiner Reibung. Z Maths Phys, **56**, English Translation, *NACA TM-1256*, 1908.

BRADSHAW, P. and **WONG, F. Y. F.** Reattachment of a turbulent shear layer. *J. Fluid Mechanics*, **52**, 113-135, 1972.

CALVERT, J. W. An inviscid-viscous method to model leading edge separation bubbles. *International Gas Turbine and Aeroengine Congress and Exposition*, The Hague, Netherlands, 1994.

CASTRO, I.P. Measurements in shear layers separating from surface mounting obstacles. *J. Wind Engng Indust. Aero.*, **7**, 253-272, 1981.

CASTRO, I. P. and **EPIK, E.** Boundary layer development after a separated region. *J. Fluid Mechanics*, **374**, 91-116, 1998.

CASTRO, I. P. and **HAQUE, A.** The structure of a turbulent shear layer bounding a separation region. *J. Fluid Mechanics*, **179**, 439-468, 1987.

CHANDRSUDA, C and **BRADSHAW, P.** Turbulent structure of a reattaching layer. *J. Fluid Mechanics*, **110**, 171-194, 1981.

CRABTREE, L. F. The formation of regions of separated flow on wing surfaces. *R&M*-3122, Aeronautical Research Council, London, 1957.

DOBNEY, D. G., HANSON, P. and **FIDDES, S. P.** The minituft surface flow visualisation method; Experience of use in the RAE 5m pressurised low-speed wind tunnel. *Aeronautical J.*, **90**, 10-17, 1986.

DOVGAL, A. V., KOZLOV, V. V. and **MICHALKE, A.** Laminar boundary layer separation: Instability and associated phenomena. *Prog Aero Sci.*, **30**, 61-94, 1994

DRAIN, L. E. The laser Doppler technique. Wiley, *ISBN 0 471 27627 8*, Great Britain, 1980.

DRAZIN, P. G. and **REID, W. H.** Hydrodynamic stability. Cambridge University press, *ISBN 0 521 22798 4*, 1981.

EUSTACE, R. M. Stabilisation of roughness particle induced turbulence using laminar flow control suction surfaces. *Ph. D. Thesis*, University of Bristol, 1999.

GASTER, M. The structure and behaviour of laminar separation bubbles. *AGARD CP*-4 Part 2, 813-854, 1966.

GAULT, D. E. An experimental investigation of regions of separated laminar flow. *NACA TN-3505*, 1955.

GAULT, D. E. An investigation at low speed of the flow over a simulated flat plate at small angles of attack using pitot static and hot-wire probes. *NACA TN-3876*, 1957.

GREENHALGH, S., CURTISS JR, H. C. and **SMITH, B.** Aerodynamic properties of a two-dimensional inextensible flexible airfoil. *AIAA J.*, **22**, 865-870, 1984.

HÄGGMARK, C. Investigations of disturbances developing in a laminar separation bubble flow. *Tech. Reports from Dept. of Mechanics*, Royal Institute of Technology, Stockholm, Sweden, 2000.

HANCOCK, P. E. Low Reynolds number two-dimensional separated and reattaching turbulent shear flow. *J. Fluid Mechanics*, **410**, 101-122, 2000.

HOBSEN, G. V., HANSEN, D. J., SCHNORENBERG, D. V. and **GROVE, D. V.** Effect of Reynolds number on separation bubbles on controlled-diffusion compressor blades in cascade. *ASME IGTI*, Stockholm, 1998.

HORTON, H. P. Laminar separation bubbles in two and three dimensional incompressible flow. *Ph. D. Thesis*, University of London, 1968.

HORTON, H. P. A semi-empirical theory for the growth and bursting of laminar separation bubbles. *ARC CP*-1073, Aeronautical Research Council, London, 1969.

HOUGHTON, E. L. and **CARPENTER, P. W.** Aerodynamics for engineering students. Fourth edition, Edward Arnold, London, *ISBN 0-340-54847-9*, 1993.

JACKSON, P. S. A simple model for elastic two-dimensional sails. *AIAA J.*, **21**, 153-155, 1983.

JACKSON, P. S. and **FIDDES, S. P.** Two-dimensional flow past flexible sail sections close to ideal incidence. *Aeronautical J.*, **99**, 217-225, 1995.

JOHNSEN, I. A. and **BULLOCK, R. O.** Aerodynamic design of axial-flow compressors. *NASA SP-36*, 1965.

JONES, B. M. Stalling. *J. Roy. Aero. Soc.*, **38**, No. 285, 741-770, 1934.

KIYA, M. and **SASAKI, K.** Structure of a turbulent separation bubble. *J. Fluid Mechanics*, **137**, 83-113, 1983.

LAMBOURNE, N. C. and **PUSEY, P. S.** Some visual observations of the effects of sweep on the low-speed flow over a sharp-edged plate at incidence. *Reports and Memoranda*, No. 3106, 1958.

LIEBECK, R. H. Laminar separation bubbles and airfoil design at low Reynolds number. *AIAA J-92-2735-CP*, 441-455, 1992.

LIN, J. C. M. and **PAULEY, L. L.** Low-Reynolds-number separation on an aerofoil. *AIAA J.*, **34**, 1570-1577, 1996.

LOCK, R. C. and **WILLIAMS, B. R.** Viscous-inviscid interaction in external aerodynamics. *Prog. Aerospace Sci.*, **24**, 51-171, 1987.

MACMANUS, D., EATON, J., BARRETT, R. V., RICKARDS, J. and **SWALES, C.** Mapping the flow field induced by a HLFC perforation using a high resolution LDV. *34th Aero. Sci. Meeting and Exhibit*, Reno, NV, 1996.

MANGALAM, S., MEYERS, J. F., DAGENHART, J. R. and **HARVEY, W. D.** A study of laminar separation bubble in the concave region of an airfoil using laser velocimetry. *Sym. on Laser Anemometry*, Miami, FL, 1985.

MASKELL, E. C. Flow separation in three dimensions. *RAE Report Aero. 2565*, 1955.

McLAUGHLIN, D. K. and **TIEDERMANN, W. G.** Biasing corrections for individual realisation of laser anemometer measurements in turbulent flows. *The Physics of Fluids,* **16**, No 12, 2082-2088, 1973.

McCULLOUGH, G. B. and **GAULT, D. E.** Examples of three representative types of airfoil stall at low speed. *NACA TN-2502*, 1951.

McGREGOR, I. Regions of localised boundary layer separation and their role in the nose-stalling of aerofoils. *Ph. D. Thesis*, Queen Mary College, University of London, 1954.

MELLING, A. and **WHITELAW, J. H.** Seeding of gas flows for laser anemometry. *DISA Information,* **No. 15**, 1973.

MOIR, I. R. M. Recent experience in the RAE 5 metre wind tunnel of a china clay method for indicating boundary layer transition. *Aeronautical J.*, **90**, 6-9, 1986.

MUELLER, T. J. The role of flow visualisation in the study of afterbody and base flows. *Experiments in Fluids*, **3**, No. 2, 61-70, 1985.

NASH, E. C. Boundary layer instability noise on aerofoils. *Ph. D. Thesis*, University of Bristol, 1996.

NEWMAN, B. G. and **LOW, H. T.** Two-dimensional impervious sails; experimental results compared with theory. *J Fluid Mechanics*, **144**, 445-446, 1984.

NEWMAN, B. G. and **TSE, M-C.** Incompressible flow past a flat plate aerofoil with leading edge separation bubble. *Aeronautical J.*, **96,** 57-64, 1992.

NORBURY, J. F. and **CRABTREE, L. F.** A simplified model of the incompressible flow past two-dimensional aerofoils with a long bubble type of flow separation. *RAE Tech. Note Aero. 2352*, 1955.

O'MEARA, M. M. An experimental investigation of the separation bubble flow field over an airfoil at low Reynolds numbers. *M. S. Thesis.* University of Notre Dame, Notre Dame, IN, 1985.

O'MEARA, M. M. and **MUELLER, T. J.** Laminar separation bubble characteristics on an airfoil at low Reynolds numbers. *AIAA J.*, **25**, 8, 1033-1041, 1987.

OWEN, P. R. and **KLANFER, L.** On the laminar boundary-layer separation from the leading edge of a thin aerofoil. *ARC CP 220*, 1953.

PANKHURST, R. C. and **HOLDER, D. W.** Wind tunnel technique. *Sir Isaac Pitman & Sons Ltd.*, London, 1952.

PAULEY, L. L., PARVIZ, M. and **REYNOLDS, W. C.** The structure of two-dimensional separation. *J Fluid Mechanics*, **220**, 397-411, 1990.

PFEIFER, H. J. Post processing of data. *VKI Lecture Series- Laser Velocimetry*, Rhode Saint Genese, Belgium, 1991.

PRANDTL, L. Über Flüssigkeitsbewegung bei sehr kleiner Reibung. *Proc III International Math. Congress*, Heidelberg, 1904.

REYNOLDS, O. On the dynamical theory of incompressible viscous fluids and the determination of the criterion. *Phil Trans Royal Soc A*, **186**, 1895.

RICKARDS, J., SWALES, C., BRAKE, C. J. and **BARRETT, R. V.** An improved alignment technique enabling cross-coupled operation of a 3D laser Doppler anemometer for small scale flow surveys. *ICIASF Conf.*, France, 1993.

RICKARDS, J., RILEY, A. J., and **SWALES, C.** Error analysis for a three-component LDA system operating in cross-coupled mode. *Engineering Report 725*, Dept. Aerospace Eng., University of Bristol, 1995.

RIPLEY, M. D. and **PAULEY, L. L.** The unsteady structure of two-dimensional steady laminar separation. *Physics of Fluids A*, **12**, 3099-3106, 1993.

ROBERTS, W. B. Calculation of laminar separation bubbles. *AIAA J.*, **18**, No. 1, 25-31, 1980.

ROSE, L. M. and **ALTMAN, J. M.** Low-speed experimental investigation of a thin, faired, double-wedge airfoil section with nose and trailing-edge flaps. *NACA TN-1934*, 1949.

ROSE, L. M. and **ALTMAN, J. M.** Low-speed investigation of the stalling of a thin, faired double-wedge airfoil with nose flap. *NACA TN-2172*, 1950.

RUDERICH, R. and **FERNHOLZ, H. H.** An experimental investigation of a turbulent shear layer with separation, reverse flow and reattachment. *J. Fluid Mechanics*, **163**, 283-322, 1986.

SAVAGE, S. B. An approximate analysis for reattaching turbulent shear layers in two-dimensional incompressible flow. *Report Ae-3*, McGill University, 1960.

SCHMIDT, G. S. and **MUELLER, T. J.** Analysis of low Reynolds number separation bubbles using semiempirical methods. *AIAA J.*, **27** No. 8, 993-1001, 1989.

SIMPSON, R. L. Two-dimensional turbulent separated flow. *AIAA J.*, **25**, No. 6, 775-777, 1987.

SIMPSON, R. L., CHEW, Y-T. and **SHIVAPRASAD, B. G.** The structure of a separating turbulent boundary layer. *J. Fluid Mechanics*, **113**, 23-90, 1981.

SWALES, C. Advanced LDA techniques for measurement of 3D boundary layer velocity on a helicopter rotor. *Ph. D. Thesis*, University of Bristol, 1994.

SWALES, C., RICKARDS, J., BRAKE, C. J. and **BARRETT, R. V.** Derivation of a global velocity transformation matrix for three-dimensional laser Doppler anemometers. *Engineering Report 462*, Dept. Aerospace Eng., University of Bristol, 1992.

SUGIMATO, T. and **SATO, J.** Aerodynamic characteristics of two-dimensional membrane aerofoils. *Trans Jap Soc Aero and Space Sciences*, **34**, 88-100, 1991.

TAN, A. C. N. and **AULD, D. J.** Study of laminar separation bubbles at low Reynolds number under various conditions. *Eleventh Australian Fluid Mechanics Conference*, University of Tasmania, Hobart, Australia, 1992.

TANI, I. Low-speed flows involving bubble separations. *Progress in Aero. Sci.*, **5**, 70-103, 1964.

THWAITES, B. Approximate calculation of the laminar boundary layer. *Aero. Quart.*, **1**, 245-280, 1949.

WALLIS, R. A. Boundary layer transition at the leading edge of thin wings and its effect on general nose separation. *ICAS Second Congress*, Zurich, 1960.

WALRAEVENS, R. E. and **CUMPSTY, N. A.** Leading edge separation bubbles on turbomachine blades. *International Gas Turbine and Aeroengine Congress and Exposition*, Cincinnati, Ohio, 1993.

WARD, J. W. The behaviour and effects of laminar separation bubbles on aerofoils in incompressible flow. *J. Roy. Aero. Soc.*, **67**, 783-790, 1963.

WEIBUST, E., BERTELRUD, A. and **RIDDER, S. O.** Experimental investigation of laminar separation bubbles and comparison with theory. *Journal of Aircraft,* **24**, No. 5, 291-297, 1987.

WESTPHAL, R. V., EATON, J. K. and **JOHNSTON, J. P.** Experimental study of flow reattachment in a single sided sudden expansion. *NASA CR*-3765, 1984.

WYNGAARD, J. C.,TENNEKES, H., LUMLEY, J. L. and **MARGOLIS, D. P.** Structure of turbulence in a curved mixing layer. *Physics of Fluids*, **11**, No. 6, 1251-1253, 1968.

YOUNG, A. D. and **HORTON, H. P.** Some results of investigations of separation bubbles. *AGARD C.P.*, **4**, 779-811, 1966.

Papers Produced During the Course of this Research

CROMPTON, M. J. Experimental investigation of laminar flow separation bubbles on thin aerofoils with sharp leading edges. Year 1- Progress report. *Engineering Report 97-04,* Dept. Aerospace Eng., University of Bristol, 1997.

CROMPTON, M. J. and **BARRETT, R. V.** Investigation of the separation bubble formed behind the sharp leading edge of a flat plate at incidence. *Proc Instn Mech Engrs.*, **214**, Part G, 157-176, 2000.

Appendix A – Chordwise Location of Pressure Tappings

Chordwise location of static pressure tappings for the flat plate used in the Preliminary Investigation (Chapter 3). Chord length = 700mm.

Static Pressure tapping No.	Distance from leading edge /mm	x/c
1	10	0.014
2	15	0.021
3	20	0.029
4	25	0.036
5	30	0.043
6	40	0.057
7	50	0.071
8	60	0.086
9	70	0.100
10	80	0.114
11	90	0.129
12	100	0.143
13	110	0.157
14	120	0.171
15	130	0.186
16	140	0.200
17	150	0.214
18	160	0.229
19	180	0.257
20	200	0.286
21	220	0.314
22	240	0.343
23	260	0.371
24	280	0.400
25	300	0.429
26	320	0.457
27	340	0.486
28	360	0.514
29	400	0.571
30	440	0.629
31	480	0.686
32	520	0.743
33	560	0.800
34	600	0.857
35	640	0.914

Appendix B – Tunnel Constraint Corrections

2-Dimensional case: It can be assumed that there are no trailing vortices and the lift can be represented by a vortex of strength K at the centre of pressure where,

$$L/_{unitwidth} = \rho UK.$$

Thus,

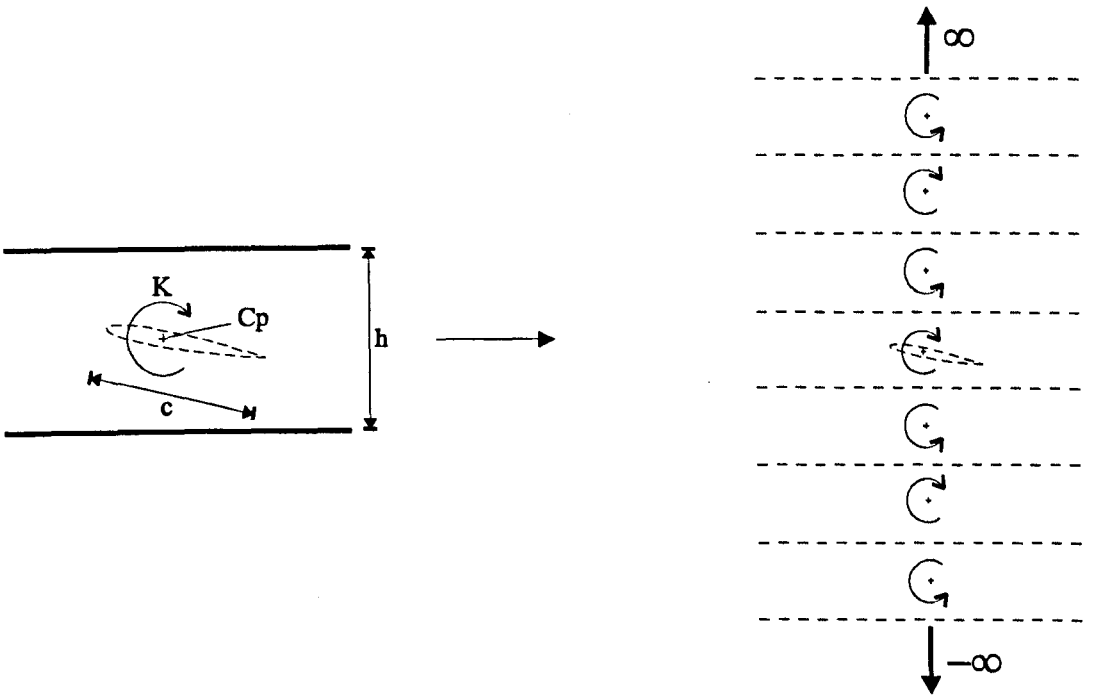

Consider the first pair of images. The velocity induced by a vortex at distance r,

$$v' = \frac{K}{2\pi r}$$

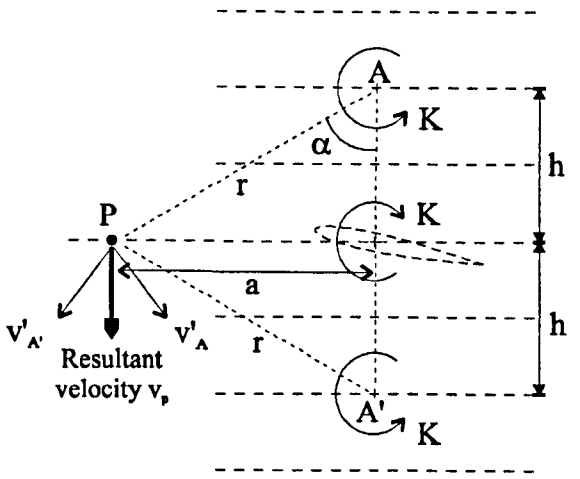

Lateral velocity induced at P by vortices at A and A' $= 2v' \sin\alpha$

$$= \frac{2K}{2\pi r}\frac{a}{r}$$

$$= \frac{Ka}{\pi\left(a^2 + h^2\right)}$$

The next pair of vortices have an opposite effect, but weaker in magnitude. This continues to an infinite distance away from the central vortex.
Therefore, the overall effect is:

$$v_P = \frac{Ka}{\pi}\left(\frac{1}{a^2 + h^2} - \frac{1}{a^2 + (2h)^2} + \frac{1}{a^2 + (3h)^2} \cdots\cdots\right)$$

Thus there is an induced lateral velocity field due to the images.

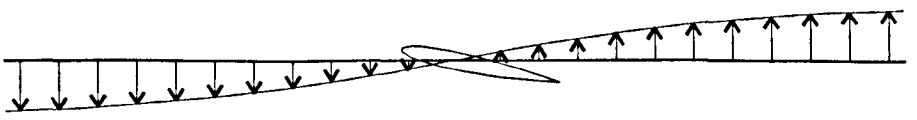

This is superimposed on the free air lateral velocity field due to the bound vortex,

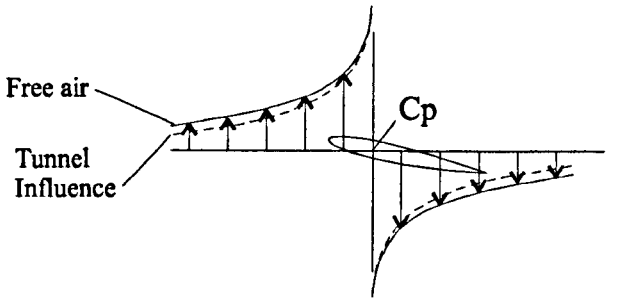

The induced velocity field is equivalent to a curvature of the flow,

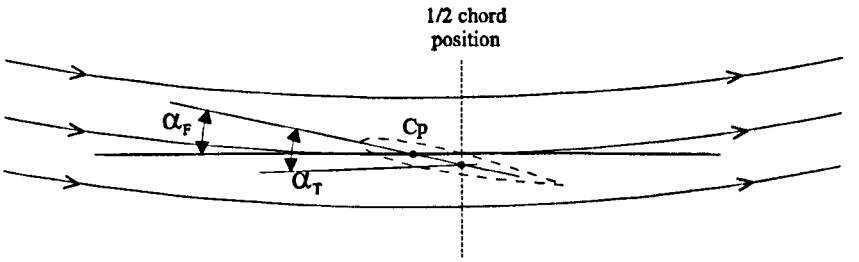

The effect of this is two fold:

- There is an effective camber given to the wing. (Considered as a straightening of the curved flow and a bending of the aerofoil in unison).
- There is an effective increase of incidence. Ahead of the centre of pressure, the incidence is reduced; Behind the centre of pressure, the incidence is increased. On average (as at ½ chord position) the incidence is increased from α_F to α_T.

Camber is defined as $\gamma = y/c$

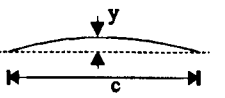

The induced camber is an arc of equal but opposite curvature to the induced velocity field.

Analysis of the induced velocity field gives, to a 1st-order,

$$\Delta\gamma = \gamma_F - \gamma_T = \frac{\pi}{192}\left(\frac{c}{h}\right)^2 C_{L_T}$$

From this we can find the incidence correction. $\Delta\alpha$ is the angle between tangents to the induced camber line at the centre of pressure and the ½ chord positions.

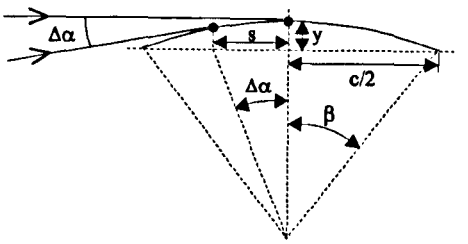

$$\frac{\Delta\alpha}{\beta} = \frac{s}{c/2} \qquad \Delta\alpha = \beta \, s/c/2$$

For small angles: $\beta = c/2/R$ $\therefore$ $\Delta\alpha = s/R$

and $R^2 = (c/2)^2 + (R-y)^2$ $\qquad R = \dfrac{c^2}{8\Delta y}$

$$\Delta\alpha = \frac{s}{R} = \frac{8s\Delta y}{c^2} = 8\frac{\Delta y}{c}\frac{s}{c}$$

$$\Delta\alpha = 8\Delta\gamma \, s/c$$

$$\underline{\Delta\alpha = \frac{8\pi}{192}\left(\frac{c}{h}\right)^2 C_{L_T}\frac{s}{c}}$$

C_{L_T} was determined from the results of Newman & Tse (1992) and the location of the centre of pressure was determined from the static pressure distributions (see Appendix C).

Appendix C – Determination of Centre of Pressure

In order to calculate the centre of pressure from the static pressure distributions, the approximation below can be employed. The static pressure profiles are shown in Figure 5.3.

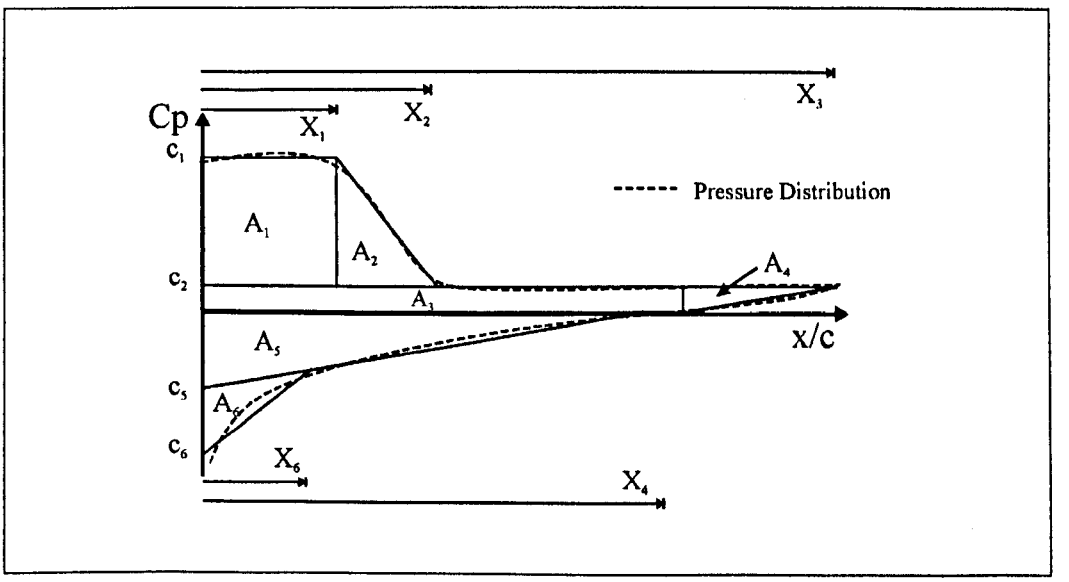

The Centre of Pressure for the top surface is given by:

$$X_{cp} = \frac{A_1.X_1/2 + A_2.\left(X_1 + (X_2 - X_1)/3\right) + A_3.X_4/2 + A_4.\left(X_4 + (X_3 - X_4)/3\right) + A_5.X_4/3 + A_6.X_6/3}{(A_1 + A_2 + A_3 + A_4 + A_5 + A_6)}$$

Using approximate values determined from Figure 5.3, This following results were calculated:

α	Centre of Pressure (x/c)
1	0.20
2	0.21
3	0.25
4	0.34
5	0.40